LEVEL II

(12)

AD A108973

DTIC
S ELECTE
DEC 3 0 1981
E

Proceedings of the NITINOL Heat Engine Conference

Edited by: David M. Goldstein
Leo J. McNamara

26-27 September 1978

Silver Spring, Maryland

Sponsored by:

U.S. Naval Surface Weapons Center

U.S. Department of Energy

81 12 23 079

REPORT DOCUMENTATION PAGE	READ INSTRUCTIONS BEFORE COMPLETING FORM	
1. REPORT NUMBER NSWC/MP-79-441	2 GOVT ACCESSION NO. AD-A100 973	3. RECIPIENT'S CATALOG NUMBER
4. TITLE (and Subtitle) Proceedings of the NITINOL Heat Engine Conference, 26-27 September 1978, Silver Spring, MD. Sponsored by U.S. Naval Surface Weapons Center and U.S. Department of Energy	5. TYPE OF REPORT & PERIOD COVERED Final: 26-27 September 1978	
	6. PERFORMING ORG. REPORT NUMBER	
7. AUTHOR(s) Editors: David M. Goldstein Leo J. McNamara	8. CONTRACT OR GRANT NUMBER(s) DOE-ET-78-I-05-5919, updated by DOE-DE-AI05-78-OR05919	
9. PERFORMING ORGANIZATION NAME AND ADDRESS Naval Surface Weapons Center White Oak Silver Spring, MD 20910	10. PROGRAM ELEMENT, PROJECT, TASK AREA & WORK UNIT NUMBERS 0;	
11. CONTROLLING OFFICE NAME AND ADDRESS	12. REPORT DATE 27 September 1978	
	13. NUMBER OF PAGES 261	
14. MONITORING AGENCY NAME & ADDRESS(if different from Controlling Office) U.S. Department of Energy Ofc. of Assistant Secretary for Fossil Energy 1000 Independence Ave., S.W. Washington, D.C. 20585	15. SECURITY CLASS. (of this report) UNCLASSIFIED	
	15a. DECLASSIFICATION/DOWNGRADING SCHEDULE	

16. DISTRIBUTION STATEMENT (of this Report)

Approved for public release, distribution unlimited.

17. DISTRIBUTION STATEMENT (of the abstract entered in Block 20, if different from Report)

18. SUPPLEMENTARY NOTES

19. KEY WORDS (Continue on reverse side if necessary and identify by block number)

NITINOL
Heat Engines
Shape Memory Effect
Shape Memory Alloys

Energy Conversion

20. ABSTRACT (Continue on reverse side if necessary and identify by block number)

A Conference on NITINOL Heat Engines was held at NSWC on 26-27 September 1978. Twelve technical papers were tape-recorded and reduced to these Proceedings. The Conference technical sessions were: Overview of Low Grade Energy Utilization, NITINOL Heat Engines, Engine Performance Efficiency and Thermodynamics, and NITINOL Alloys.

Engine efficiencies were reasonably estimated to range up to 4% absolute,

DD FORM 1473 JAN 73   EDITION OF 1 NOV 65 IS OBSOLETE
S/N 0102-LF-014-6601

411563

or ≤ 30% of Carnot (maximum) efficiency, although some were estimated higher. Output estimates ranged from a few watts to a kw per kilogram of NITINOL alloy.

Engine performance data and new designs up to 25 HP were presented during the sessions. The thermodynamics of NITINOL Heat Engines was examined from the viewpoints of both theory and application. Tests on NITINOL wire in simulations of various Heat Engine cycles are reported on, as well as the "training" (bi-stable memory) phenomenon. Progress on preparation of NITINOL alloys by powder metallurgy techniques is discussed, as well as X-ray diffraction studies of the shape memory transformation.

Separately, inventors displayed 8 different working engines. Engine output of these models was estimated to be under 10 watts for each.

MP 79-441

FOREWORD

The potential of shape memory effect (SME) alloys as the working element of useful energy converters has excited a great many researchers. NITINOL[1] has been the alloy used in most demonstration Heat Engines built to date. It was fitting, therefore, that the U.S. Naval Surface Weapons Center (NSWC), at which NITINOL was invented, hosted the first conference on this subject. A second conference will be held in Leuven, Belgium in August 1982, at Katholieke Universiteit.

The U.S. Department of Energy (DOE) provided funds, and NSWC provided technical assistance, to support development of Heat Engines. Mr. Marvin E. Gunn, Jr. of the Division of Power Systems was Program Manager for DOE under Interagency Agreement DOE ET-78-1-05-5919, subsequently updated by DOE DE-AI05-78OR05919. Mr. David M. Goldstein was Program Manager for NSWC.

The purpose of the Conference was threefold:

   * to review the state of the art,

   * to indicate the direction of current and proposed
research, and

   * to provide a forum for the exchange of information.

The Conference opened with introductory remarks followed by an Overview of Low Grade Energy Utilization. Congressional, DOE, and Navy viewpoints on this subject were given by the respective representatives: for Congress, Dr. John Andelin of the House Committee on Science and Technology, and Dr. David Claridge of the Office of Technology Assessment; for DOE, Mr. Marvin Gunn, Jr.; and for Navy, B. Sobers of the Navy Energy and Natural Resources R&D Office. These presentations are not included in these Proceedings, which are limited to NITINOL-related technical material.

----

[1]NITINOL alloys are based on the compound TiNi. They exhibit a shape memory phenomenon due to an austenite $\rightleftarrows$ martensite phase transformation. Specifically, if deformed in the martensite phase, they will recover their prior shape upon reheating into the austenite temperature range. The increased modulus of the austenite enables useful work to be done by the warmed alloy, above that used to deform the cold metal. This shape memory capability is exploited in the NITINOL Heat Engine.

Fourteen technical papers were presented. One by Mr. J.T. Gibbs, on Stirling Cycle NITINOL Engine, was scheduled but not presented. Neither Dr. H. Mohamed's (now known as Dr. H. Mohamed Tawancy) paper on Recovery Stresses, which Mr. R. Banks delivered, nor the paper Mr. C. Raymond gave, which contained numerous innovative designs, is included in the Proceedings.

The Conference was organized in much less than the normal working time allowance for a conference at this Center. Due to this short time, the authors were given the option of using their recorded presentations to prepare the papers for publication in these Proceedings. Although the papers were reviewed for clarity, there has been no peer review for technical accuracy. The data and viewpoints are the authors' own, and are offered to the community as their best input and not necessarily their oral delivery at the Conference.

Eight different prototype engines, all working, were displayed by 7 inventors. Several of these prototypes were subsequently shown on television in the U.S. and Britain. During the intervening evening of the two-day Conference, a social buffet allowed Conference participants to interchange information to mutual advantage.

The success of this Conference was in great measure due to the dedicated effort of several people: Mrs. Joy White foremost and Mrs. Deanna Zook, Messrs. George Schmitz, Scott Hoover, and Ernie Inman. Our appreciation extends to other NSWC staffers who participated in the Conference, Engine Demonstrations, and Reception.

Finally, it is appropriate to recognize the efforts of Mr. David Goldstein in organizing this Conference.

JACK DIXON
By direction

PREFACE

Over 2/3 of the thermal energy available in the U.S. is rejected as waste heat. Creating economically viable Heat Engines--using this low grade (less than 100°C) heat energy--would clearly serve the national interest. In recognition of this, the U.S. Department of Energy supported research in engine design, construction, and efficiency determination. DOE's agreement with the Navy provided for a coordination center, information interchange, and an enhanced supply of NITINOL alloy for workers in the Heat Engine field.

The Navy has its own potentially valuable uses for NITINOL engines, for example: helping to reduce petroleum energy dependence, and providing power sources for remote locations as well as for emergency use at sea.

Aside from helping to conserve power, any significant increase in NITINOL use will also benefit the Navy in another way. A larger market for NITINOL will lower its cost and remove some of the restrictions on its supply. This would enhance its use in ship construction, where it is now being introduced in tube and pipe couplings. These couplings--now being evaluated in new Navy destroyers--provide for weld-free, high-pressure connections, using the same shape memory phenomenon as for Heat Engines. A joint market in both Heat Engines and couplings is of interest to the Navy, since it can utilize both devices in large quantities.

In sum, NITINOL's total return on investment to the Navy is potentially very attractive.

The variety of model NITINOL engines constructed in the U.S. and abroad has long since dissipated the question of whether these engines would work. Their designs generally suggest that they can be scaled in size to provide greater than 1 kilowatt of power. The remaining question is economic: comparing NITINOL engines with other low temperature regime energy converters.

We can assume that the energy cost (of waste heat or solar energy) is negligible for organic Rankine engines, photovoltaics, and NITINOL Heat Engines. A comparison of their installed costs per kw is:

Energy Converter Type	Cost/kw
Rankine	$400-$600[1]
Photovoltaic	$10,000[2]
NITINOL	$600[3]

For comparison, nuclear power is $1000/kw.

If NITINOL engines can use the low grade heat now being wasted, they will be a boon to the nation. As shown above, these engines have potential and should be further investigated. The authors of the following papers are pioneers in this effort.

---

[1] Assumes annual production of 10,000 to 20,000 units. If production is just a few engines, cost would be about $2000-$4000 per kw. Costs are projected from 1973 data, allowing 100% for inflation. U.S. Office of Technology Assessment, Application of Solar Technology to Today's Energy Needs, V. 1, June 1978, pp. 346, 354.

[2] Assumes optimal conditions of "noon on a sunny day." W. Mossberg, "Many Experts Say Solar Electric Cells Too Costly Now, Have a Bright Future," Wall Street Journal, 19 Dec 1979.

[3] The $600 per kw assumes a power output of 1/2 kw per kilogram (250 watts/lb) of NITINOL. The output of NITINOL Heat Engines has been estimated at up to 1 kw per kg. Measured values of up to 0.3 kw per kg (150w per lb) are reported in these Proceedings. A kg of NITINOL wire of 1/2 mm (0.020 inch) diameter costs about $1200 to produce in laboratory size lots. In commercial production lots of 10,000 kg per year, $200 per kg is reasonable to expect. NITINOL costs are assumed to be 2/3 of total engine cost.

CONTENTS

ILLUSTRATIONS

ILLUSTRATIONS (Cont.)

ILLUSTRATIONS (Cont.)

ILLUSTRATIONS (Cont.)

ILLUSTRATIONS (Cont.)

ILLUSTRATIONS (Cont.)

ILLUSTRATIONS (Cont.)

TABLES

THE BANKS ENGINE: PAST, PRESENT, AND FUTURE

Ridgway Banks
Lawrence Berkeley Laboratory
University of California

It is certainly a pleasure to be at this conference which is, among other things, the first official convocation of NITINOL engine inventors and developers in history. We are an odd lot, I suppose, but with certain strong points in common: we're generally stubborn as hell, and tend to have very patient women, and water-stains on every pair of shoes we own. We also share, I think, a strong belief in the potential contributions these machines may make to the development of untapped energy resources, worldwide. I think you will find that, in many cases, the work on display here today is the product of individuals working very much on their own...solving our common problems, and willing to share their solutions in using this amazing material.

Now, in my case, when I was given my first piece of NITINOL in 1973, I had already been lobbying for development of a solid-state heat engine for some time, but not one based on NITINOL, which I had never heard of. I planned to use bimetallic working elements. I knew the bimetallics would be extremely inefficient. But--when I analyzed the cost of using high-temperature (above the boiling point) thermal energy, which requires concentrating collectors, and the cost of conversion at temperatures you can get pretty cheaply with flat-plate collectors--I was convinced that the low-temperature regime was the way to go, because I am just naive enough to believe that getting something is better than getting nothing. What I had in mind was a little heat engine which could provide a few watts of auxiliary power to pump water or charge batteries for a blackout. I wasn't trying to compete with Con Edison with these things at all. I knew they would be small and relatively inefficient. But at that time solar energy was just getting off the ground, in the public sense, and, at the time I became aware of it, solar energy's main practical impact was confined to oxidizing the finish on people's cars as they sat out in the parking lot. I felt we could do something more interesting than that.

When I got my first piece of NITINOL, it came with a printed sheet of instructions from the Edmund Scientific Company. It was a little experimenters' kit. I looked at the wire. I read the instructions, and I didn't believe them. I just had no place in my thinking for a material that had these characteristics. I wasn't in a position to go through the annealing procedures, either, so it was a matter of days before I did the obvious, classical experiment: I cooled the wire, bent it, and stuck it in the company coffee pot. Now this little experiment has been repeated on the average a dozen times a day for over five and a half years, and I still get excited when it works. Luckily, it always works.

I have a movie which goes back to within a couple hours of the first running of the first engine, so I think I'll show that now, and just talk as it procedes.

(Film begins)...This is the first Edmund wire, on my first experimental apparatus: a wooden stick. This shot shows the crankshaft of the first engine; it is a simple coaxial eccentric system. In the early days of running this machine, we were aware of only the Shape Memory response that took place on heating NITINOL wires. So this film doesn't allude to the fact that we found, after several thousand cycles, that they begin to change shape automatically on cooling as well. Only recently I measured the amount of <u>work</u> the wires in the original engine can do on cooling, and it turns out to be perhaps an additional 20% compared to the work done on heating...This was taken the first day the engine ran. There are twenty loops of NITINOL wire (we doubled the number the following November because--just at the time of the first press conference--the temperature of the hot-water heaters at LBL was lowered to conserve energy). (See Fig. 1.)

Query from the audience: Is this the first time it ran in front of a camera, or the first time it ran?

RB: This is within two hours of the first time it ran. Professor McMillan* (who is incidentally responsible for the name originally given to this machine) came to see it just after it first ran, and he suggested we call the photographers.

This shot shows the engine driving a small generator to light a tiny light bulb...Now we are on the laboratory roof running the engine with a solar collector. It is going to do the same trick with the light bulb. (Fig. 2.) This took place on an overcast day in November--the sun didn't come out until about 11:30 a.m....By 2:00 p.m. the water in this primitive collector (which is just a black vinyl sheet draped in a styrofoam-lined box, with empty fluorescent light tubes floating on the surface) got hot enough to run the engine and light the bulb.

This is engine no. 2, an attempt to boost the power output of NITINOL wires in the flexural mode sufficiently to impress the funding agencies in Washington. This machine develops considerable torque (you can't stop it at the hub with your bare hands) but there are tremendous friction losses, and so on, and a great problem in timing. You see, those are four synchronized wheels, each of which has to be hung independently from shafts which can't pass through the journals that support the wheels beneath it. And if it's not properly timed, you lose all the mechanical advantage on opening and closing. It ran, and it was helpful; it certainly showed me the limitations of the wheel approach. This is Dave Johnson's first engine...and this is Dave Johnson. I had the privilege of bringing this machine, and the next one you'll see, on a coast-to-coast tour which climaxed with some of the top management of the Foxboro Company watching these things in fascination as the room they were standing in filled up with water. Executives were literally ankle-deep and didn't complain at all.

This is Dave's Opus 5, otherwise known as the Flintstone Car engine. A differential pulley mechanism isn't used on this one. Instead, the ratio is supplied by gears, so that the wheel on one end turns faster than the one on the other end, as you will see...(Film ends.)

Query from the audience: This is not the kind of thing for which you ask for the Carnot efficiency, is it?

---

*Edwin M. McMillan, Nobel Laureate, and former Director of Lawrence Berkeley Laboratory

RB: We would love to say you don't <u>have</u> to, but that is not true. Certainly, the role of these low-grade heat engines is recovering energy now wasted, but, in any practical installation, you have to look at the <u>cost</u> of pumping water, or the cost of solar collectors. So Carnot efficiencies are a real issue, to be addressed with respect to competing technologies. It has taken a long time to develop the experimental approaches that give valid efficiency figures. You cannot isolate certain aspects of the material and treat others as passive. You have to calculate the latent heat of transformation (anomalously high in this material) plus specific heat across the cycle with respect to stress levels and displacement for a given cycle. And you never see the optimal work output in a wire that hasn't been in an engine and acquired pretty complete "training," as we call it. Of course, to get the money to build the engines, you have to talk about Carnot and the efficiency of the NITINOL conversion, so there is a loop here.

Now, with my second engine, I became pretty convinced that the mechanical configuration of the wheel, and maybe also the use of NITINOL wires in the mode of flexure, was impractical, and I began looking at wires in tension. The reasoning here is that, if you have a member in tension, the whole cross section is working for you; while if you have a member in flexure (theoretically, at least), only the outside and the inside of the bend are putting out maximum work. While this isn't necessarily the case in NITINOL, I accept it on principle, because thinner wires in tension have produced the highest work output, per unit mass of NITINOL, so far recorded. And so I proceeded to think about this. I was convinced (and it has been pretty conclusively shown elsewhere) that the mechanical cycle for wires in tension had to be something a little special. If I simply used a crankshaft as in my first wheel-type engine, with wires in tension radially disposed from the crank to the outer rim of the wheel, I was sure they would break. The reason is that the kinematics of the crank cycle makes a lousy match to the way heat enters and transforms a NITINOL wire. The leverage on a typical crank (a bicycle pedal, for instance) increases sinusoidally from zero at top dead center, to a maximum at 90 degrees. However, when heat enters a NITINOL wire, you have an exponentially <u>diminishing</u> volume of material transformed, per unit time, with the greatest proportion transformed right the beginning of the cycle. In fact, in a 20 mil NITINOL wire in tension, you get an absolutely azing jolt of force. The instantaneous recovery stresses are sufficient to permanently deform the wire--to introduce irreversible shape change--if the wires are not free to act on the mechanical system. This problem is compounded by the effects of shock-loading. To avoid these stress concentrations in the wire, what I needed to do was somehow find a cycle which somewhat mimicked the behavior of NITINOL wires during transformation. I essentially needed to let the NITINOL design its own engine cycle (Fig. 3).

This machine is called the "Cam-Track" NITINOL engine. The tracks in question are these kidney-shaped features that go around the ends of the tank in this cutaway view. The NITINOL wires are longitudinal, in tension, and they ride between trolleys which, in turn, ride along the tracks. The "cam" aspect of the tracks means they mostly do not run parallel to each other. They are supported by standoffs from the ends of the tanks. Varying the lengths of the standoffs makes it possible to vary the slope of the tracks with respect to the ends of the tank, and to each other. As the NITINOL wires dip into the semi-cylindrical hot water tank, the trolleys are at a point where the tracks are just beginning to converge. The pull exerted by the NITINOL wires as they contract drives the trolleys down along the slope, which is the power stroke of the engine. Mechanical force is transmitted through a linkage to advance the next set of NITINOL wires into the hot tank. The "compression" stroke (actually elongation, in our case) takes place in the cold bath around the outside of the hot tank. There, force is applied (through the power takeoff linkage) to drive the trolleys forward along the tracks as they <u>diverge</u>, with a secondary, or resultant, force acting on the NITINOL wires to deform them axially. The tracks are made of brass, so that altering the lengths of the supporting standoffs made it possible to actually tune them somewhat--to change the slope at

various points in the cycle. By fiddling around with the curve of the tracks, I was able to find a reproducible mechanical cycle--in which the wires could be repeatedly stretched and recover without permanent damage. Lo and behold, it turned out to be a pretty close approximation of an exponential decay curve. This engine ran, but never up to expectation--I was hoping to see half a horsepower, and we certainly never got that. It was never fully debugged, either, but it did give me confidence that wire breakage problems--encountered in other machines using NITINOL wires in tension--could be overcome. We did, in fact, have some breakage, but only at the ends of wires, at the holders, where the wires passed around a somewhat tight radius which probably introduced a complex strain field at that point. But we did not encounter breakage along the working length of the wire elements.

By the time I had figured out what the problem with this machine probably is, and how to improve its performance, I had already moved ahead in terms of design criteria for a practical engine. While the Cam Track made me optimistic about being able to use NITINOL wires efficiently, it still has the basic drawbacks of the original engine prototype in regard to parasitic losses. Too many moving parts. Too much energy lost in hydrodynamic drag--you are always moving those wires through water. Incidentally, I believe in using a liquid heat transfer medium for thermal uniformity, because if a part of a NITINOL wire is in the process of transforming--or, say, is still cold--it will naturally take up locally the complete load of the other parts of the wire that have been transformed. So it is important, in my view, to maintain thermal uniformity throughout the length of a working element. But I wanted to see if I could use wires in tension in a simple device--mechanically very simple--and also cut down on the hydraulic losses. And this is where I went (Slide.)

This is my latest machine, which I call the "Model M." It is simply a reworking of the old Newcomen "Walking Beam" steam engine. You have the wire elements at the front, with hot and cold water tanks below. The beams oscillate the wires between hot and cold baths, but while they are heated and cooled, the wires do not move. Work developed at the wire is also taken off through the beams. This thing really works. It has probably ten times the power of the original wheel prototype, with slightly less NITINOL wire in there. Less volume of NITINOL.

Query from the audience: What is the power of this gadget?

RB: Don't know. Haven't measured it. If you want a "fingertip-dynamometer" measurement, I would say around 20 watts. But the point is that now, for the first time, I can see kilowatts. I can see scaling up without more moving parts. This machine, in its rather quaint embodiment, represents all the moving parts you would need for a very powerful installation. You just plug in more wires; make it longer. Size is no problem: in solar, for example, you have already committed a long low area for your collectors. You could make a long low machine and stick it behind the collectors. There are 88 wires, 15 inches long, in tension. Displacement at the wires is very small, but amplified through the lever system. Between wire and power takeoff motion is very slight--just a slight oscillation. Lots of force, but not much displacement.

Query from the audience: At what strain levels does that machine run?

RB: This is running at about 3.5 percent strain, which I feel is safe. But recently I am beginning to feel that maybe 6.5 percent is safe--if you ask nicely.

This thing has just been through preliminary tests, to find out if it works, and I have seen it run at about 80 cycles per minute. The present setup is limited by the fact that heating and cooling equipment consists of a $19 coffee urn and a 27-year old refrigerator. So the machine operates well at the beginning of a run, then the hot and cold water supplies collapse and generalized entropy sets in. As I say, what tickles me about this machine is that I think it has the hydraulic and mechanical losses reduced to a minimum, and allows me to think of an installation which would work on a practical scale. I also think realistic efficiency measurements can be made on it.

Let me say that I hope we will, in the course of these meetings, really confront the issue of efficiency. I hope anyone who has made measurements will talk about them, even if there isn't general agreement. You are aware that a big part of the problem we face in this approach to low-temperature energy conversion is that we are trying to promote a relatively unresearched 6-year old technology. That's in direct competition with Rankine-cycle turbines which have been around for decades--and the competition is way up on the learning curve. Turbine designs are now relatively sophisticated, while we are still at the level of the devices displayed this noon. Which is absolutely where we should be. I have a strong prejudice in dealing with an unresearched entity--be it an engine or a carrot growing in your garden. You don't pull a carrot up by the roots every week to find out how it is doing. It has got to have a little time to develop before it's mature. Same with an engine. I hope we will be seeing it mature somewhat before long, but for the time being we are where we ought to be, although we must confront the efficiency question.

Question: Any idea what Carnot efficiency we should aim for? In other words, how far above and below the transformation temperature should the water baths be?

RB: Okay, that is quite a complex question. Let me treat it superficially first. We decided, in our program, to simply assign ourselves a goal of minimum conversion efficiency. We picked the number three--which we have already exceeded--because, in certain low-temperature applications, 3% conversion efficiency is competitive with existing technologies, particularly in Ocean Thermal Energy Conversion. OTEC plants are being designed with target efficiencies of 2-3% in mind. OTEC researchers can still foresee an economical operation because there are spinoff in food production and other byproducts, in addition to basic energy conversion. The ocean represents vast solar collector, heat storage, and heat sink systems. So the normal rather high-cost components of the typical solar array are already present. In principle all you have to pay for is the pumps. The major problem one has with conversion of ocean thermal energy is not the efficiency of the process, but the cost and maintenance requirements of the heat exchangers needed in the conventional turbine approaches. Vast areas of heat exchangers are not only in contact with the sea water but also subject to corrosion and biofouling on the ocean side and to attack by the working fluid (particularly if it is ammonia) should it come into contact with water, on the other side. And heat exchanger walls have to be kept reasonably thin, or thermal impedances become so great that systematic conversion efficiencies are further reduced below an acceptable limit. Now, NITINOL is noncorrosive, can directly contact an aggressive environment, and is dynamic. It changes shape with every cycle, so it should be a rotten environment for marine growth. I wouldn't want to live there...cycling up and down 20°C, sixty times a minute, on a moving substrate. This may eliminate the scaling problem as well.

The more complicated side of your question is this: we don't really know--I certainly don't know--what NITINOL is yet. I know where it starts, how much force it takes to deform it, how much energy it puts out, and so on. But I don't know what a fully stabilized piece of optimized alloy will do, and for how long. In other words, I see a "double" memory developing in the wires in the original engine, and I am able to measure a potential energy output that

might be realized from those wires on cooling...but where is that going to stop? It doesn't exist at all in a naive wire; there is no double memory. Then, what happens to the transformation temperatures as a result of cycling...to the thermal hysteresis? Will it get bigger or smaller? What happens to the wire on the crystalline level? Certain favorably-oriented domans obviously become dominant as you break the wires in. Are they doing all the work? With the generation of defects there is work hardening, but where are the defects localized? My unsophisticated observation is that not only do wires not degrade with repeated cycling in engines (at least on the order of twenty-five million cycles)-they in fact improve. I have seen speed of operation increase about 50% in the original engine at the same temperatures, which does not take into account hydrodynamic losses. So probably the energy output, per cycle, of the NITINOL has more than doubled in five years of intermittent operation. Apparently engines do a certain amount of cold working on these wires that seems to optimize them. What if you strapped a metallurgist to the engine and let him work on the problem too? The wires are extremely history-dependent. Every aspect of their performance changes with cycling. I don't know.

Question: Where do you get the wire?

RB: The actual physical wire used in my machines was commercially produced by the Titanium Metals Corporation of America, also known as TIMET or TMCA, which no longer produces it. As far as I know, NITINOL wire is not yet quite available, commercially. Well, maybe some people would disagree.

Question: That means this is the end of this work?

RB: No, it is the beginning of a new way.

Question: Is it available or not, commercially?

David Goldstein: Wire drawn to a specific transition temperature is not commercially available. The Naval Surface Weapons Center, which is not a commercial producer, is producing the alloy in 10 pound melts. NSWC draws wire and provides it to a specific transition temperature.

Currently one major commercial firm, TMCA, is accepting orders for the alloy to a specified composition. TMCA will break ingots down to two inches or some other size, but does not guarantee transition temperatures. Another firm, Reactive Metals, Inc., can also produce the alloy.

NSWC has placed orders with both firms for ingots. These materials will be final processed at NSWC to ensure material uniformity. They will then be supplied as wire or strip to various people approved by the Department of Energy. In this way the engine builders will have uniform NITINOLs to work with.

Question: We at MIT would like to experiment. How would we get the wire--from DOE, you, or TMCA? How do the three fit together?

DG: You should write directly to NSWC--to me or our NITINOL Technology Center.

Question: Where is TMCA?

DG: Henderson, Nevada. Please call me for the names of the people to contact there.

Question: If we ask you for some wire or sheets, we don't really have to go to TMCA?

DG: No. I might add: The last talks tomorrow afternoon will refer to a somewhat new and possibly successful process of producing NITINOL.

Question: I am still confused about whether the conversion efficiency of these engines is limited by the transition temperature range.

RB: Yes. That is the Second Law nature of the beast.* You have to have a ΔT, a specified ΔT, in order to make them run. The original wheel engine runs on a temperature difference of $9^{o}C$ between the baths. To have a high Carnot efficiency, you would like that way up around incandescence, but, in fact, the heat available for these purposes is around ambient.

Question: In the applications we're talking about, isn't horsepower more important than fraction of Carnot efficiency?

RB: Yes, except that the efficiencies will determine how many solar collectors you need, or how many pumping horsepower you lose in your ocean or geothermal installation. A really tiny conversion efficiency here couldn't compete with that of organic fluid Rankine-cycle turbines. That's the real competition. We really have to beat those costs, and I believe a reasonable installation's costs can be very competitive. One further point: In solar thermal electric conversion, the push now is almost entirely to the central-receiver "power tower" concept. There, focussing mirrors--heliostats--drive the temperatures up, focus them on a central boiler, and get high efficiencies with a steam turbine. The concept looks good on paper, but has one serious limitation nobody seems to talk about. When the sun goes down, the conventional or nuclear plant turns on, because you can't store steam. There is nothing easier to store than hot water. It beats batteries, and everything else. A good low-temperature energy conversion approach--and I don't even care whether it's NITINOL--could be the basis of solar electricity generating plants that will work 24 hours a day. We suddenly get into base load territory, whereas before the most optimistic place for solar energy conversion was during the peak load sunny hours of the day. Very, very serious consideration, I think. Thank you.

---

*Editorial note: From the vantage of six months' time elapsed since the NITINOL Heat Engine Conference and present struggles with this transcript, I would strongly disqualify my answer to this question. (RMB)
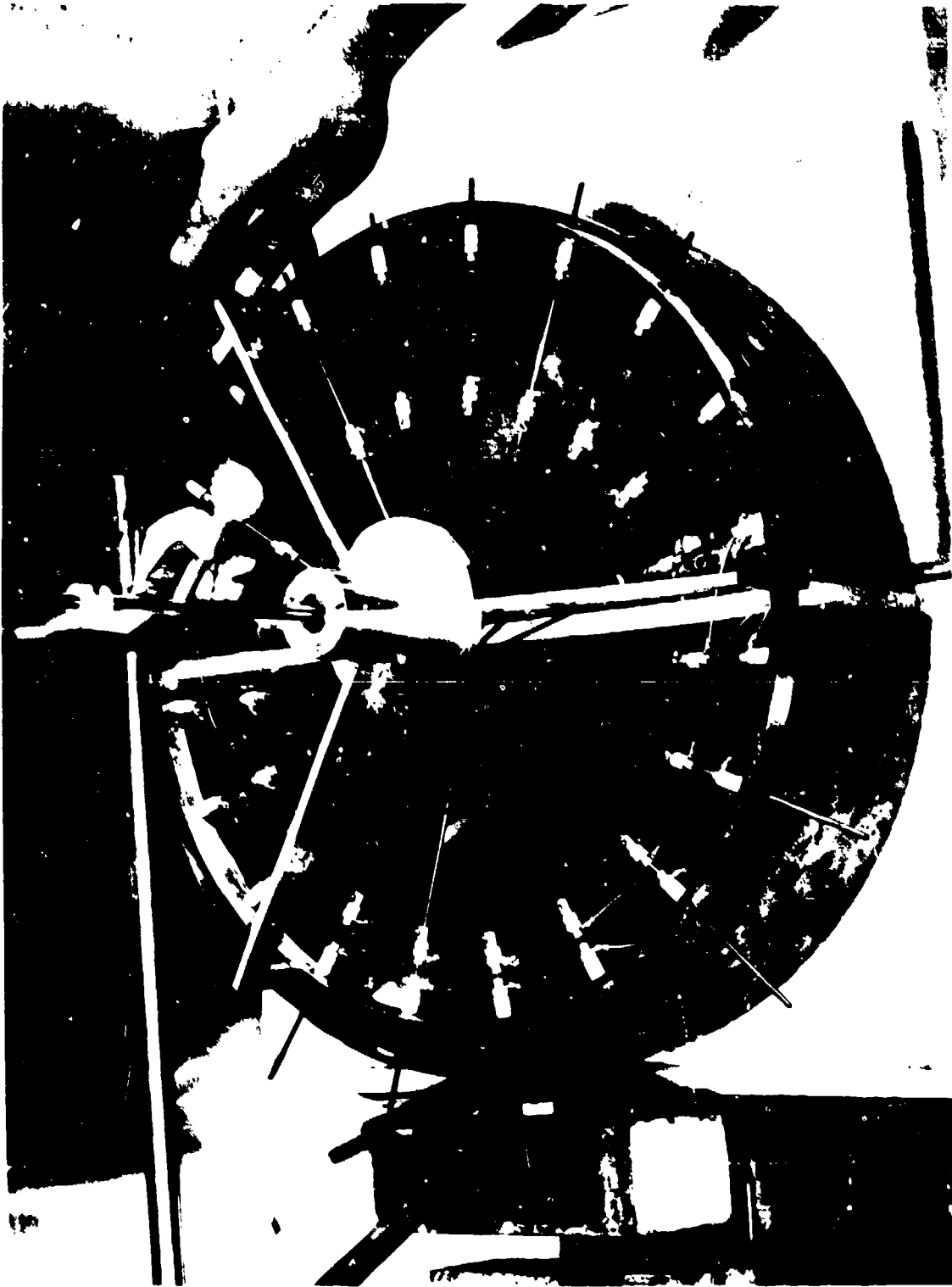
FIGURE 1   THE ORIGINAL LAWRENCE BERKELEY LABORATORY PROTOTYPE NITINOL ENGINE
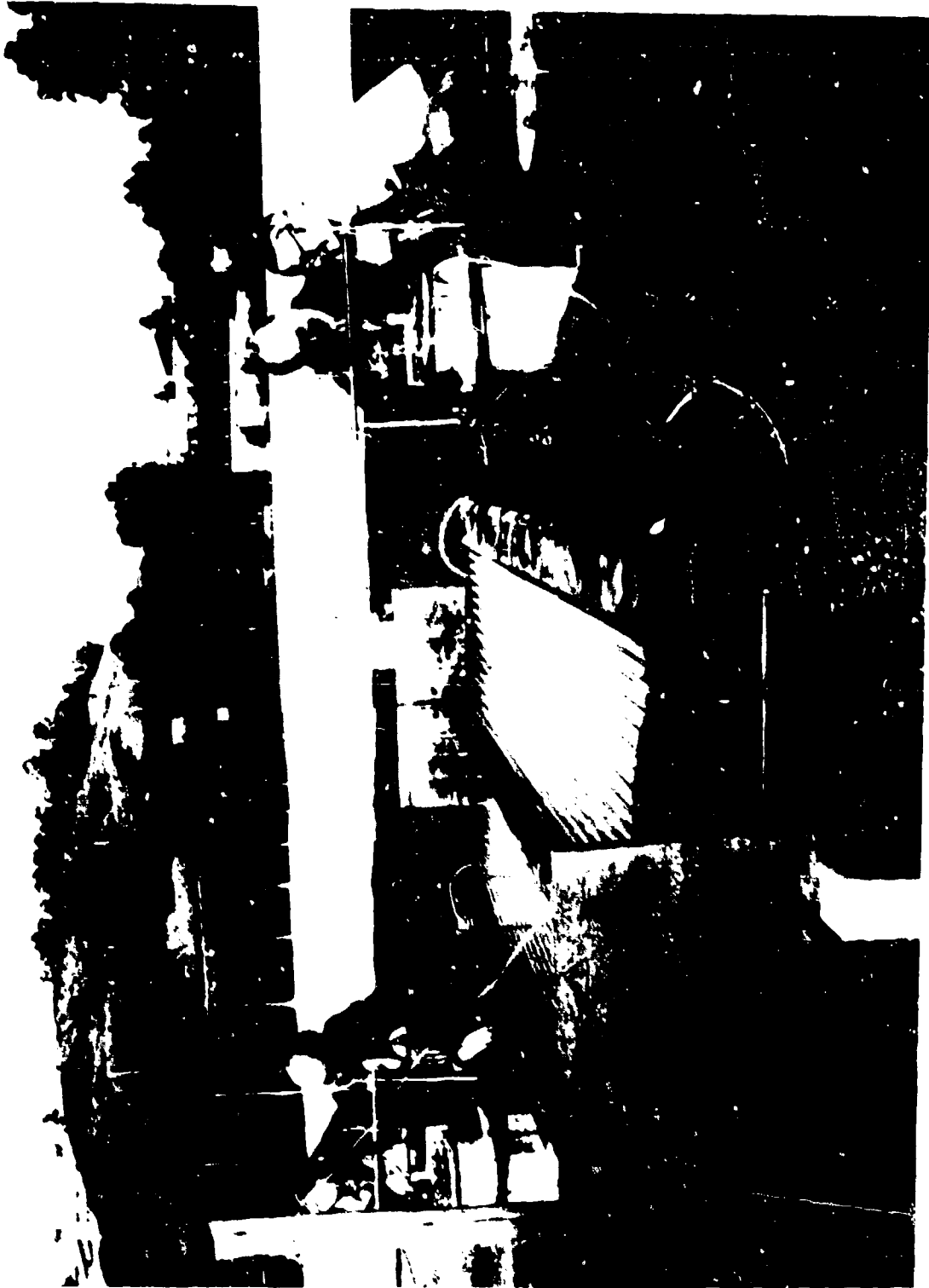
FIGURE 2   THE FIRST CONVERSION OF SOLAR ENERGY TO MECHANICAL WORK

XBL 767 3131
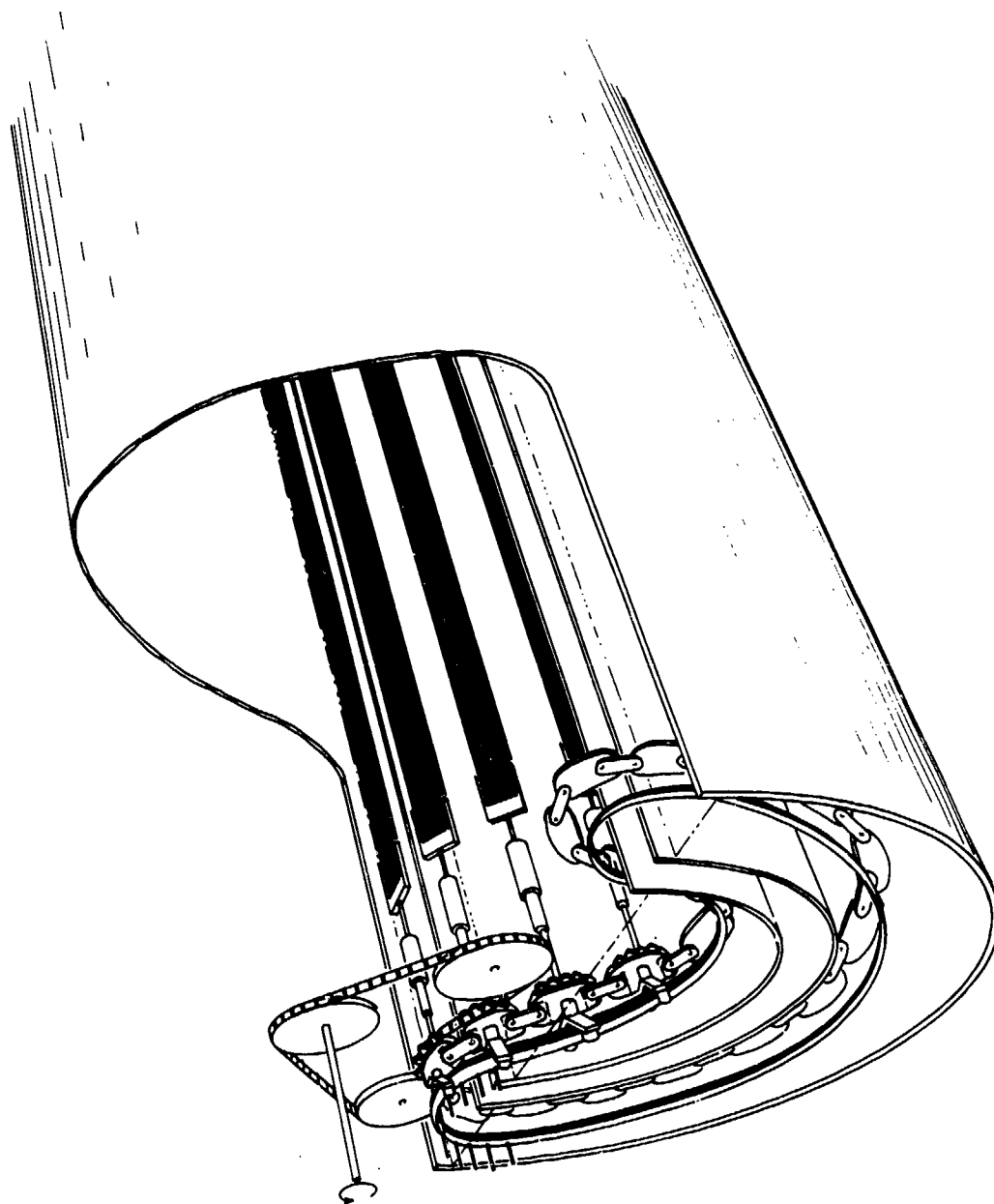
FIGURE 3   CUTAWAY VIEW OF THE "CAM-TRACK" NITINOL ENGINE

ONE HORSEPOWER THERMOTURBINE NITINOL ENGINE

W. S. Ginell, J. L. McNichols
McDonnell Douglas Astronautics Company
Huntington Beach, CA

J. S. Cory
Cory Laboratories
Escondido, CA

The earliest patent on the concept of thermal-to-mechanical energy conversion using NITINOL was issued to Buehler and Goldstein in 1968 (Reference 1). During the ten years since the patent was issued, a variety of small model engines of different designs has been built and operated--engines that demonstrated conclusively the technical feasibility of cyclic thermal energy conversion using NITINOL. Some engines were built as curiosities--devices that rotated or oscillated and attracted attention--but little else. Many of these were designed empirically, and they operated only because a large enough quantity of NITINOL was used to overcome design defects that were unsuspected at that time. Other investigators designed and built operable engines on the basis of the then-known physical properties of NITINOL. These were capable of producing small amounts of power--fractions to tens of watts. To our knowledge, operating engines of larger power output have not been demonstrated at this time.* Such demonstrations are vitally important in furthering the development of NITINOL heat engine technology to the commercial level.

The NITINOL Heat Engine program at McDonnell Douglas Astronautics Company is directed toward this goal. The program is sponsored by the Department of Energy with Marvin Gunn of the Fossil Fuel Utilization Division as the technical program manager. Work on this effort was initiated officially on September 28, 1978 and therefore we have little in the way of results that can be presented.

The objectives of the program are: first, to design, construct, and operate a reliable NITINOL heat engine that will deliver practical amounts of power, about one horsepower; and second, to demonstrate that engine performance parameters can be predicted. I will describe

---

[1] Buehler, W. J. and Goldstein, D. M., "Conversion of Heat to Mechanical Energy," U. S. Patent 3,403,238, Sept. 1968.

* We recognize, however, that the details of such efforts could be considered proprietary because of the tremendous commercial potential of NITINOL engines. Design and performance information exchange under these circumstances understandably would be restricted. We hope that one result of this conference would be enhanced communication among active workers in the field, primarily in the area of fundamental information, so that progress in our understanding of the behavior of NITINOL can be accelerated.

first the engine type that we have selected and its advantages. This will be followed by a qualitative description of the engine configuration and the procedure to be used for engine design.

One class of small model engines that was built and tested extensively is known as the thermoturbine. Essentially, it is a variation of the well-known differential pulley mechanical design. The general turbine configuration which uses the thermal expansion and contraction of an endless, normal-metal belt was patented by Lee in 1967 (Reference 2). A similar engine design using NITINOL was patented by A. D. Johnson in 1977 and is shown schematically in Figure 1 (Reference 3).

A continuous loop of NITINOL wire or a NITINOL helix is guided by idlers through cold and hot water baths and over the differential pulleys which are of different diameters. One pulley serves as an expander (or turbine) and extracts power from the rotating loop because tension in the loop on the hot side is greater than tension on the cold side. The expander pulley is connected mechanically to a compressor (or pump) pulley that does work on the loop. Because the work performed by the loop on the expander exceeds the work performed by the compressor on the loop, a net work output results.

Operating NITINOL turbines have also been built by Raymond and by Cory (Reference 4). A number of engine variations was devised and constructed using NITINOL helixes or wire, different methods of coupling the expander and compressor pulleys, and variations in heat source-sink configurations. One engine built by Cory (Figure 2) used a close-wound helix (3mm OD) , and the expander-compressor pulleys were of the same diameter but were geared to run at different speeds. The engine, when operated between 343K (70°C) and 278K (5°C), attained a speed of 2500 rpm and produced about 0.5 W of power.

The thermoturbine engine configuration using NITINOL in the form of an endless helix has a number of major advantages: bearing loads are all radial and therefore well-developed, inexpensive bearings can be used; heat capacity losses ($Cp \Delta T$) are small because only the relatively small NITINOL working material mass need be thermally cycled rather than a large support structure; heating and cooling of the NITINOL helix are uniform and reproducible because the helix enters and leaves the water reservoirs axially; extremely accurate machining of the mechanical structure is not required because of the greater compliance of a helix in torsion relative to that of a wire in tension (limitation of maximum material strain required); high power densities and high cycle rates possible; and the NITINOL elements cycle continuously rather than intermittently (as in an oscillating engine).

The thermoturbine engine that will be built in the McDonnell Douglas program will be a scaled-up version of the small, dual-diameter pulley design. Scale-up to a one horsepower size will be accomplished through a series-parallel mechanical arrangement of the simple design. The large and small diameter pulleys will be replaced by large and small diameter rollers which will carry 104 helixes in parallel. Each closed helix will cycle through twelve alternate hot and

---

[2] Lee, L., "Motor," U. S. Patent 3,303,642, Feb. 1967.

[3] Johnson, A. D., "Memory Alloy Heat Engine and Method of Operation "U. S. Patent 4,055,955, Nov. 1977.

[4] Cory, J. S., "Thermomechanical Behavior of NITINOL," This Conference, Paper pp. 7-1 through 7-17.

cold water reservoirs in series before returning to the starting point. Figure 3 shows an end view of an engine module which consists of two unit cells in series. A unit cell contains one large and one small diameter roller and one hot and one cold water reservoir. Unit cell rollers are coupled to each other mechanically and the total output power appears at a single shaft. Figure 4 illustrates the parallel arrangement of elements on the rollers. Notice that each roller has both a large and small diameter end. This corresponds to a direct, mechanical coupling between the driver (turbine) and driven (pump) roller and results in a zero power transmission loss. The rollers will have a webbed structure to minimize helix slippage. Water flow through the troughs will be countercurrent so that the ΔT over which each parallel helix operates will be the same.

Initially, an engine module will be built and instrumented to measure cold and hot forces, hot and cold reservoir temperatures, helix cycle speed, module output speed and torque as functions of temperature, ΔT, module speed and number of cycles. The module will be equipped with only ten helixes, and module performance will be compared with predictions to establish the existence of synergistic effects. Because helix properties and therefore engine operating parameters will change with number of operational cycles, helixes will be removed from the module periodically and their properties measured. This will facilitate correlations between element property and engine performance.

The full size engine will consist of twelve unit cells in series and 104 NITINOL helixes in parallel. Present calculations based on NITINOL wire properties (0.020 inches diameter) indicate that a mass of 1.3 kilograms will be required and the engine speed will be about 480 rpm for a $\Delta T = 60^\circ C$. NITINOL wire for this program will be supplied by Mr. Goldstein of NSWC.

Although small NITINOL heat engines have been built and have operated, their efficiencies, specific power, and total power have been low, and attempts to produce engines of practical size have not been successful, as yet. Invention of practical machines that use NITINOL efficiently for thermal to mechanical energy conversion requires first a detailed knowledge of the engineering thermodynamics of the alloy, and detailed engine design equations. Needed are: (1) reliable equation of state data in terms of the variables force, length, and temperature to identify and provide a quantitative description of possible thermodynamic paths; and (2) information on heat flow and energy dissipation associated with these paths.

Recently, extensive measurements of the force-length-temperature (FLT) behavior of NITINOL helixes have been reported (References 4,5,6) from which the form of the equation of state has been deduced. Because of the thermodynamically irreversible nature of the Joule effect in NITINOL (internal entropy generation), the equation of state exhibits hysteresis. This results in a state equation that describes a bounded volume in FLT state space, and all possible

[5]Cory, J. S., "NITINOL Thermodynamic State Surfaces," Journal of Energy, Vol. 2, No. 5, 1978, pp 257,258.

[6]McNichols, J. L., Jr., and Cory, J. S., "NITINOL Heat Engines for Economical Conversion of Low Grade Thermal Energy," Proc. 13th Interdisp. Energy Conversion Eng. Conf., Aug. 1978, pp 1998-2004.

thermodynamic paths lie on uniquely defined surfaces within that volume (Reference 5). Figure 5 illustrates schematically one pair of surfaces and a hypothetical thermoturbine thermodynamic cycle. Details of NITINOL state surfaces, their properties, and uses will be found in Reference 4.

To determine the heat flow associated with a given path or cycle, the irreversible thermodynamics for NITINOL processes has been formulated and has been used to estimate specific work and thermodynamic efficiencies for the thermoturbine cycle (Reference 6).

The empirical state equation determination procedure used previously will be used as the design tool for the one-horsepower thermoturbine engine. State surfaces for the specific NITINOL alloy to be used will be determined experimentally. A thermodynamic cycle optimized for power will be derived on the basis of heat source and sink temperatures, desired output power and speed and limitations inherent in the specific NITINOL alloy to be used. These will depend on alloy composition and processing and cycling history. This information will define the mechanical dimensions of the engine module. Predictions of module performance will be made as functions of operating parameters. Iterations on the engine design will be performed following comparison between engine module performance data and predictions. The close agreement between the actual small thermoturbine engine performance and the performance predicted on the basis of experimentally measured state surface data has given us confidence in this empirical engineering data approach to NITINOL heat engine design.

In summary, we have undertaken the design, construction, and testing of a one-horsepower NITINOL engine. The mechanical configuration will be a thermoturbine design with a series-parallel arrangement of NITINOL helixes that are cycled through hot and cold water reservoirs. The engine will be designed on the basis of an experimentally measured equation of state for the specific NITINOL alloy supplied by the NSWC NITINOL Technology Center. Successful completion of the engine tests will provide conclusive evidence of the viability of the empirical engineering data approach to engine design and the technical feasibility of low temperature energy conversion using practical-sized NITINOL heat engines.

---

[5] See footnote 5 on page 2-3.

[4] See footnote 4 on page 2-2.

[6] See footnote 6 on page 2-3.
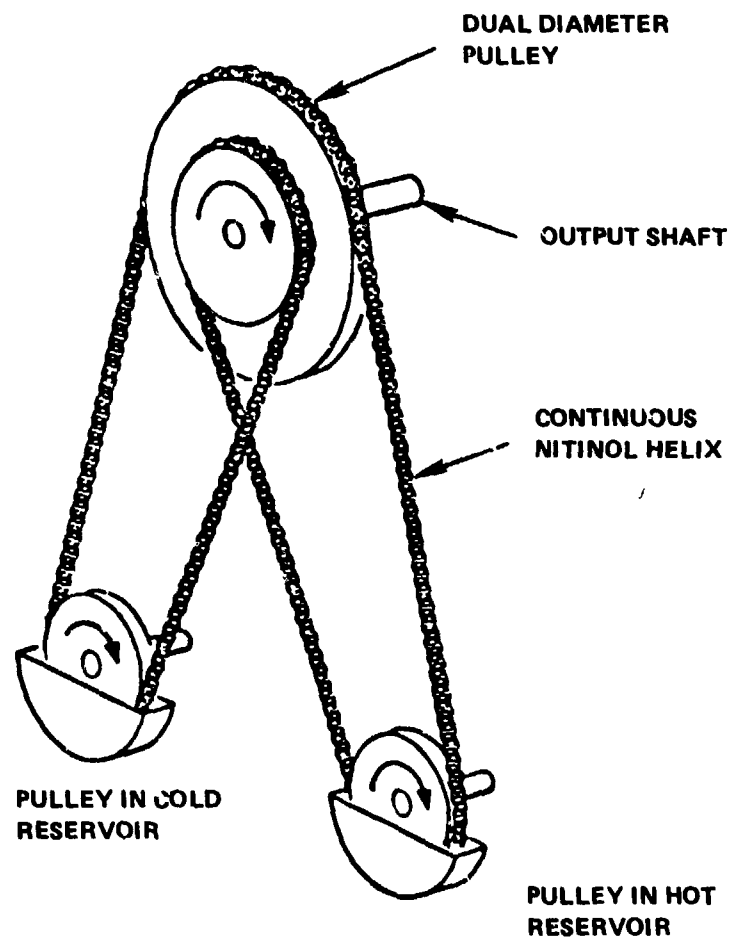
FIGURE 1 DIFFERENTIAL PULLEY THERMOTURBINE ENGINE (AFTER JOHNSON)
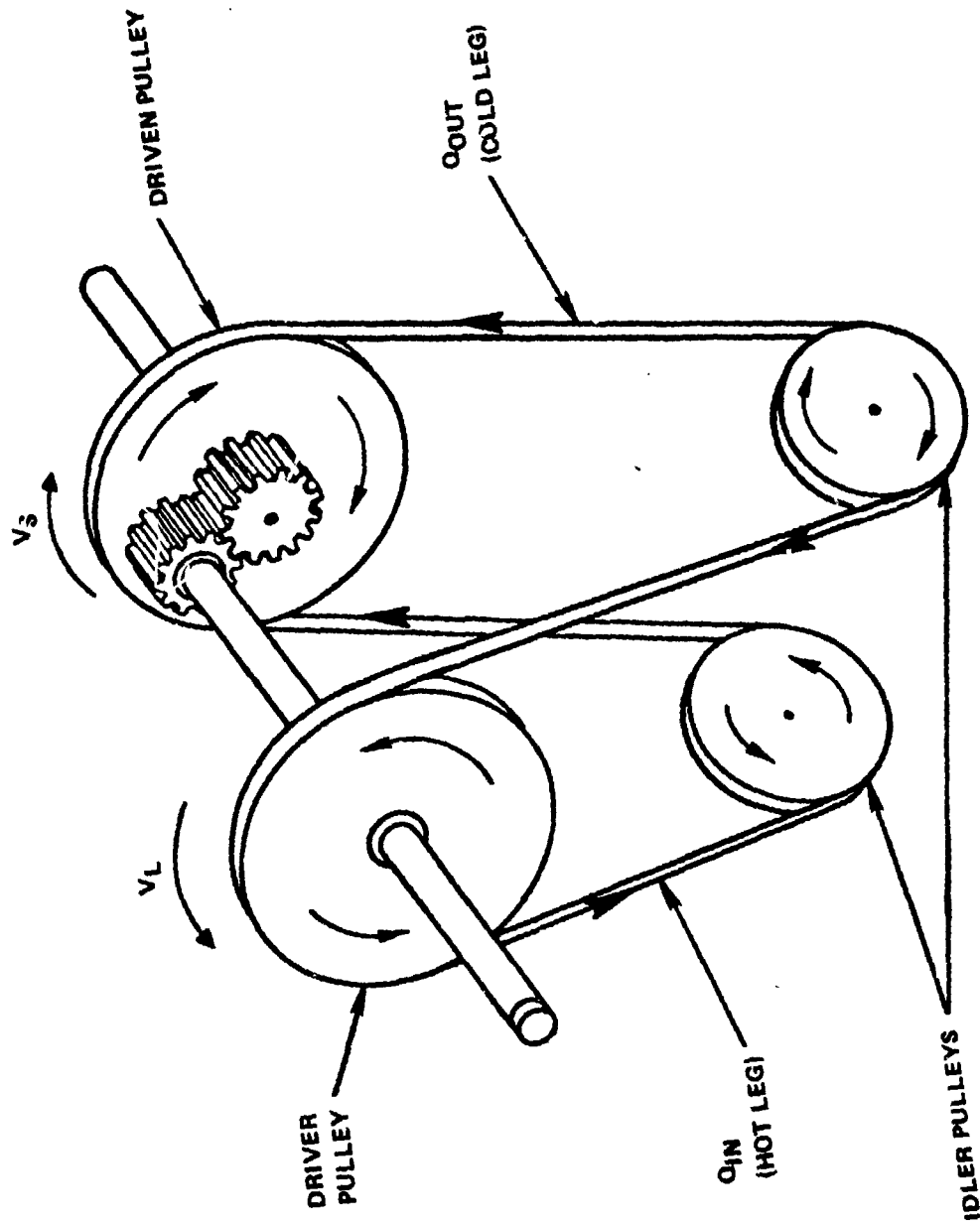
FIGURE 2 GEAR-COUPLED THERMOTURBINE ENGINE
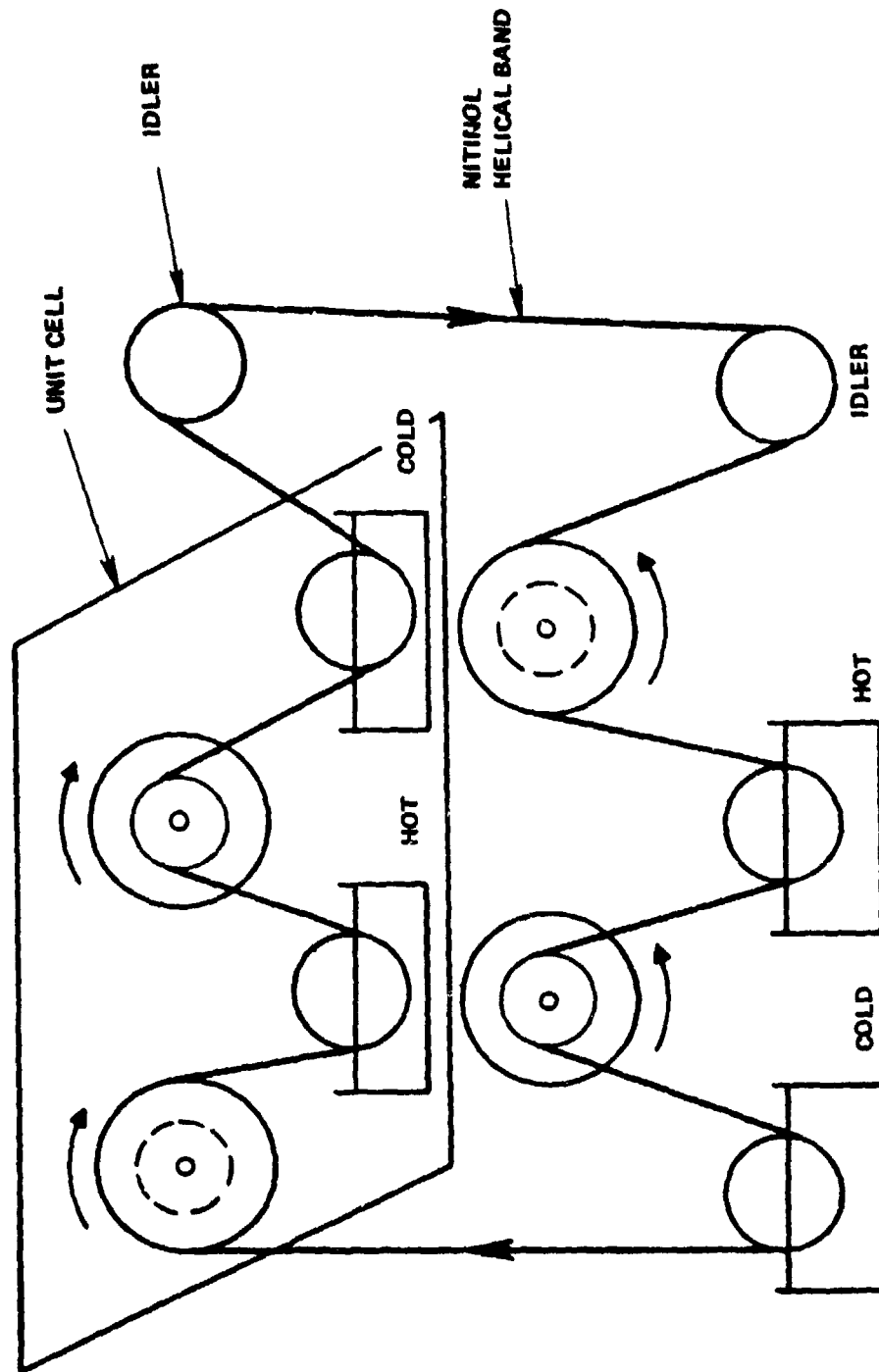
FIGURE 3 NITINOL ENGINE MODULE - END VIEW SCHEMATIC
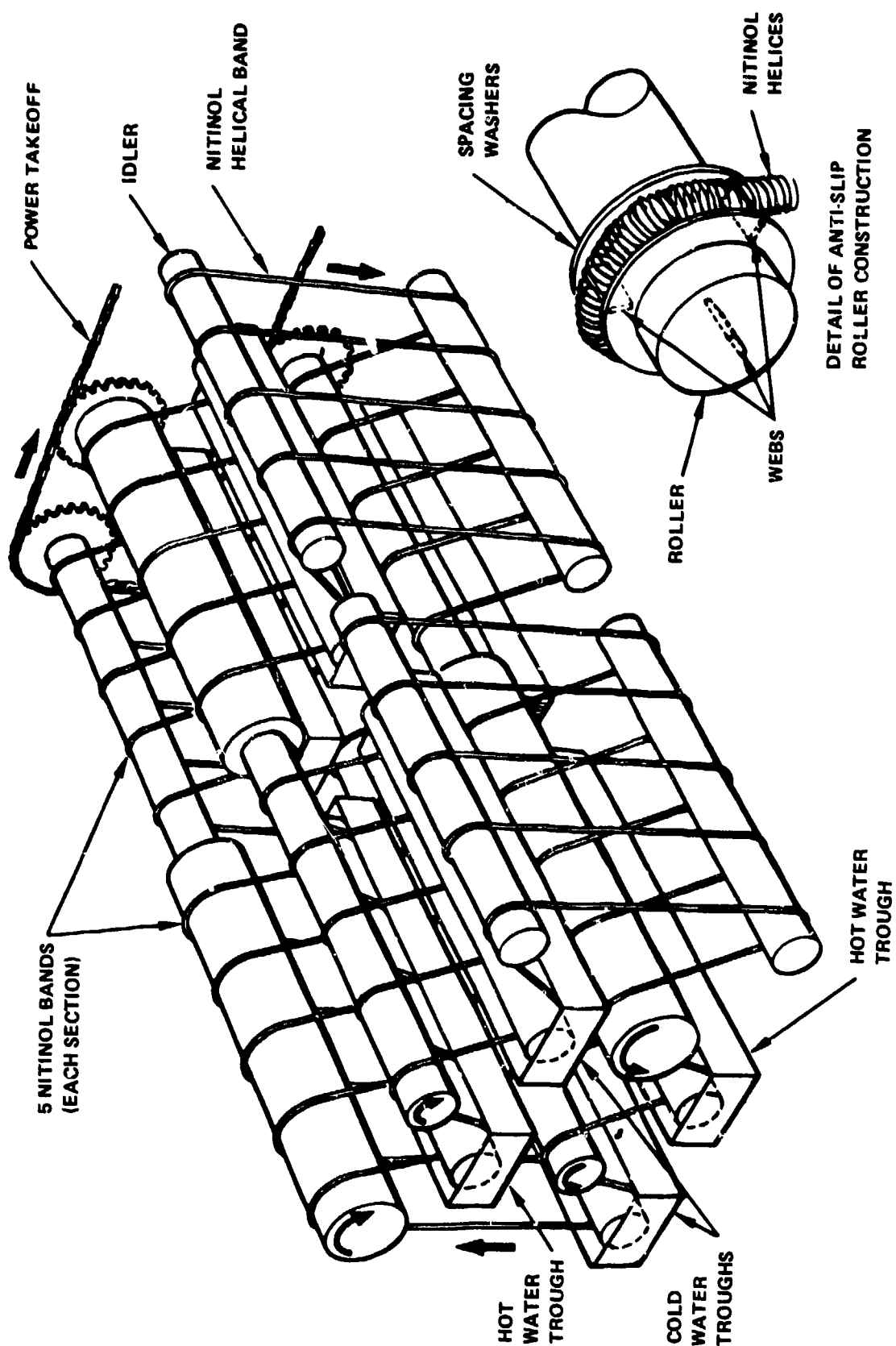
FIGURE 4   NITINOL ENGINE MODULE
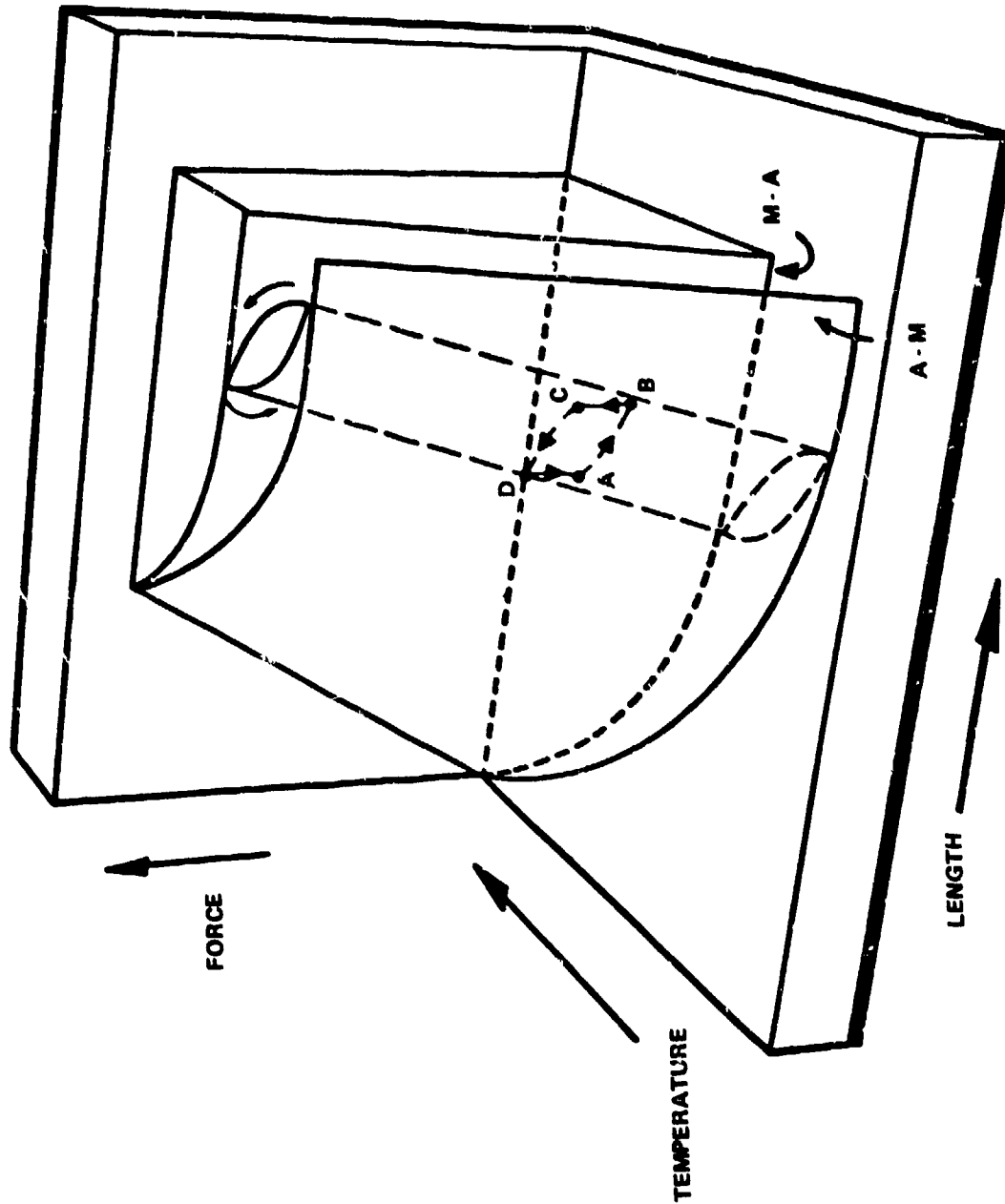
FIGURE 5 QUALITATIVE SHAPE OF NITINOL STATE SURFACES

AM – BOUNDARY SURFACE FOR AUSTENITE-MARTENSITE PHASE TRANSFORMATION
MA – BOUNDARY SURFACE FOR MARTENSITE-AUSTENITE PHASE TRANSFORMATION
SHOWN CONNECTING THE BOUNDARY SURFACES IN ONE PAIR OF AN INFINITE NUMBER
OF TRANSITION SURFACES ON WHICH IS TRACED A HYPOTHETICAL TURBINE ENGINE
CYCLE. LEGS AB AND CD ARE ISOFORCE; LEGS BC AND DA ARE ISOLENGTH.

REFERENCES

1. Buehler, W. J. and Goldstein, D. M., "Conversion of Heat to Mechanical Energy," U. S. Patent 3,403,238, Sept. 1968.

2. Lee, L., "Motor," U. S. Patent 3,303,642, Feb. 1967.

3. Johnson, A. D., "Memory Alloy Heat Engine and Method of Operation, " U. S. Patent 4,055,955, Nov. 1977.

4. Cory, J. S., "Thermomechanical Behavior of NITINOL," This Conference, Paper pp. 7-1 through 7-17.

5. Cory, J. S., "NITINOL Thermodynamic State Surfaces," Journal of Energy, Vol. 2, No. 5, 1978, pp 257, 258.

6. McNichols, J. L., Jr., and Cory, J. S., "NITINOL Heat Engines for Economical Conversion of Low Grade Thermal Energy," Proc. 13th Interdisp. Energy Conversion Eng. Conf., Aug. 1978, pp 1998-2004.

NITINOL BELT ENGINE

Dante J. Sandoval

The 55 NITINOL alloy is the active element employed in this engine to convert heat directly and instantaneously into mechanical energy. This engine of simple construction is basically comprised of two pulleys of dissimilar diameter and a belt of NITINOL alloy that fits around such pulleys. Means for heating and cooling the NITINOL belt and for power transmission are also provided.

Fig. 1 illustrates the basic NITINOL belt engine. Pulley 14, or "strain wheel," is a free wheel with a radius that gives the NITINOL belt the selected strain curvature. Pulley 16, or "power wheel," serves both as heat sink or cooling wheel, and as power transmission wheel by means of its shaft (17). The power wheel is substantially larger than the strain wheel to present a large area for heat dissipation, good traction, and small losses from bending the NITINOL belt around it.

The principle of operation of this engine consists of the work produced by a portion of the NITINOL belt while trying to recover its original shape when stimulated by heat at the strain wheel. To produce any work, the NITINOL belt should have a preset shape that is straight, convex, or with a curvature radius substantially greater than the radius of the strain wheel.

In operation, the NITINOL belt is pliantly strained around the strain wheel. A heat source (18)--such as a flame, steam, a hot water jet, or concentrated sun rays--is applied upon the belt between Points 20 and A. The stimulated portion of the belt between these points will try to recover its original shape. In doing so, that portion generates a moment of force F about a fulcrum located at Point 20, which is the last point of contact between the strain wheel and the belt (Fig. 2).

Such a moment of force has a lever arm with a length equivalent to the straight line (M) from Point 20 to the last heated point between Points 20 and A, and generates another moment of force Fr about the center of the strain wheel that is transmitted as a torque to the power wheel by the belt. This torque sets into motion the NITINOL belt and both the strain and power wheels, when the heat source is applied. When in motion, any portion of the belt entering Point A is stimulated by the heat source, becoming itself a part of the lever arm (M). Any advancement of the belt into Point A withdraws the same amount of belt from Point 20 towards a cooling region at the wheel (16).

A cooling fluid (22), such as water, is placed in a container (24) for faster cooling of the belt, making it possible to increase the rate of heat application, thus increasing the power output of the engine. Spokes or gears (26) can be used on the power wheel for transmission of power.

The present engine has a gear at the power wheel connected to a fly wheel mechanism to smooth out the jerking due to hot spots or irregularities in the NITINOL belt and variations in the heat source. Other physical parameters of this engine are the following:

Nylon Strain Wheel Radius	1.175"
Nylon Strain Wheel Width	0.875"
Aluminum Power Wheel Radius	2.656"
Aluminum Power Wheel Width	0.875"
NITINOL Belt Perimeter	22.000"
NITINOL Belt Width	.500"
NITINOL Belt Thickness	0.050"
NITINOL Belt Radius	3.500"
NITINOL Belt TTR	110-140°F

BELT CONSTRUCTION

The belt for this engine was made from a strip of 55-NITINOL alloy, 22" long, 0.5" wide, 0.050" thick, and TTR 110-140°F. Both ends were squared, fine ground, and placed in the jaws of a 3/4" band saw welder with a setting for "medium" current.

The welding was done in a regular air atmosphere; the burrs were ground off, and the weld was annealed in the same machine, as is done with regular band saws after welding. The belt was then placed for 15 minutes in a kitchen oven heated at 550°F, where it adopted a circular shape, and was then taken out to cool in the air.

When cool, the belt was placed in water at 32°F and turned inside out to become a belt with a convex shape. Then it was installed slightly loose around the strain and power wheels for operation.

The strain given to the NITINOL belt is expressed as:

$$S = S_p + S_b = \frac{\nu}{2r_p + \nu} + \frac{\nu}{2r_b + \nu}$$

where: ν = belt thickness

r_p = radius of strain wheel

r_b = radius of belt shape curvature

S_p = strain of belt from a straight line to the strain wheel curvature

S_b = strain of belt from its shape curvature to a straight line

S_b = Zero for a belt with a straight shape

S_b = Negative for a belt with a concave shape

S_b = Positive for a belt with a convex shape

BELT PROBLEMS

The NITINOL belt has a tendency to adopt an outward-channeled shape when subjected to excessive heat or stress at the strain wheel. This channeling effect causes the edges of the belt to crack in many places, thus breaking at any point in a very short time.

On the occasions when the belt broke, the original convex shape given to it was completely lost by adopting a concave shape, sometimes with a curvature radius smaller than its periphery curvature radius. The welded ends of the belt hold very well and break only when a defective weld is made; otherwise the belt may break at other points.

The most favorable conditions for belt endurance are the use of low temperature steam and a strain of 2 to 2.5%. The present engine belt has a cumulative time of about 6 hours without breaking.

ENGINE PERFORMANCE

The engine was tested with two strain wheels of different diameter, keeping all other parameters constant (Fig. 3).

CONSTANT PARAMETERS

Power Wheel	5.312" diam.
NITINOL Belt	22" x 0.5" x 0.050"
Cooling Water	32°F
Heat Source	200°F Steam Jet 0.125" from Belt
Steam Rate	7 Grams per Minute
Fly Wheel Mechanism	Connected
Point of Steam Application	5° from Point A
NITINOL Belt Return Temperature	70°F

VARIABLES

Strain Wheel	2.48" diam.
Strain Wheel	1.5" diam.

Belt Strain for 2.48" diam. Strain Wheel:

$$S_p = \frac{0.050}{2 \times 1.24 + 0.050} = 0.020$$

$$S_b = \frac{0.050}{2 \times 3.5 + 0.050} = 0.007$$

$$S = S_p + S_b = 0.020 + 0.007 = 0.027 = 2.7\%$$

Belt Strain for 1.5" diam. Strain Wheel:

$$S_p = 0.032 \qquad\qquad S_b = 0.007$$

$$S = S_p + S_b = 0.032 + 0.007 = 0.039 = 3.9\%$$

ENGINE EFFICIENCY

It was difficult to measure with reasonable accuracy the net energy input to the NITINOL belt during operation. Therefore, only to have a reference point, it was assumed that the power input was the energy required to raise the temperature of the working NITINOL in one second from 70°F to its upper TTR of 140°F. This assumption introduces the error of different amounts of heat absorbed by the belt at different speeds. This error was not accounted for in input calculations.

Specific heat for NITINOL was taken as 0.111 BTU/lb/°F., density .234 lb/cu. in. The power output of this engine was determined from the measured speed-torque developed by the engine at its power wheel.

Fig. 4 graphically represents these parameters.

APPLICATIONS FOR THIS ENGINE

The present engine prototype has been built only to demonstrate the feasibility of using NITINOL as a solid state energy converter. No effort has been made to optimize its performance or efficiency.

To simplify its construction and assembly, the engine has no bearings in its wheels, and the wheel shafts are held only by one end, all of which introduces large friction losses into the system. Thus, it is reasonable to expect a good deal of improvement in a well-constructed and engineered engine of this type.

There are many immediate and practical applications for this engine, such as:

Solar Tracking Systems
Backup Blower for Heating and Cooling
Waste Heat Recuperators
High Torque Actuators
Heat Motors
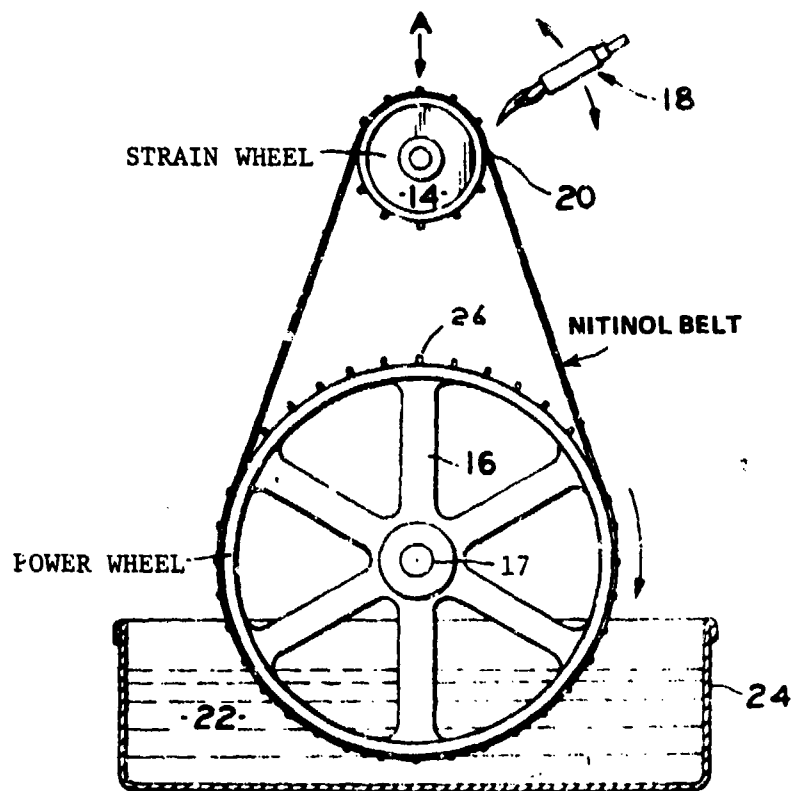
FIGURE 1   BASIC NITINOL BELT ENGINE
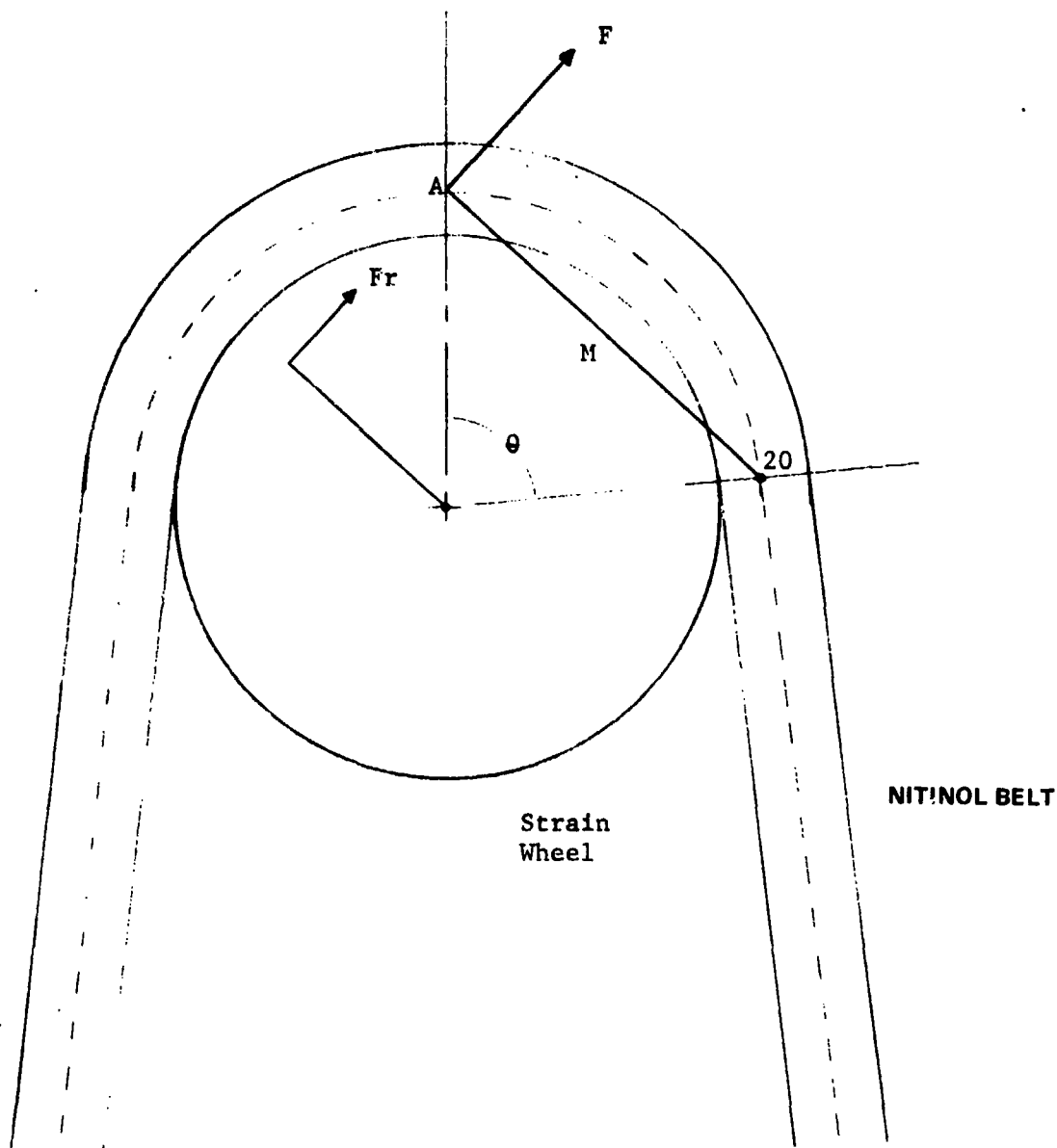
FIGURE 2   BELT STIMULATION AND TORQUE SYSTEM
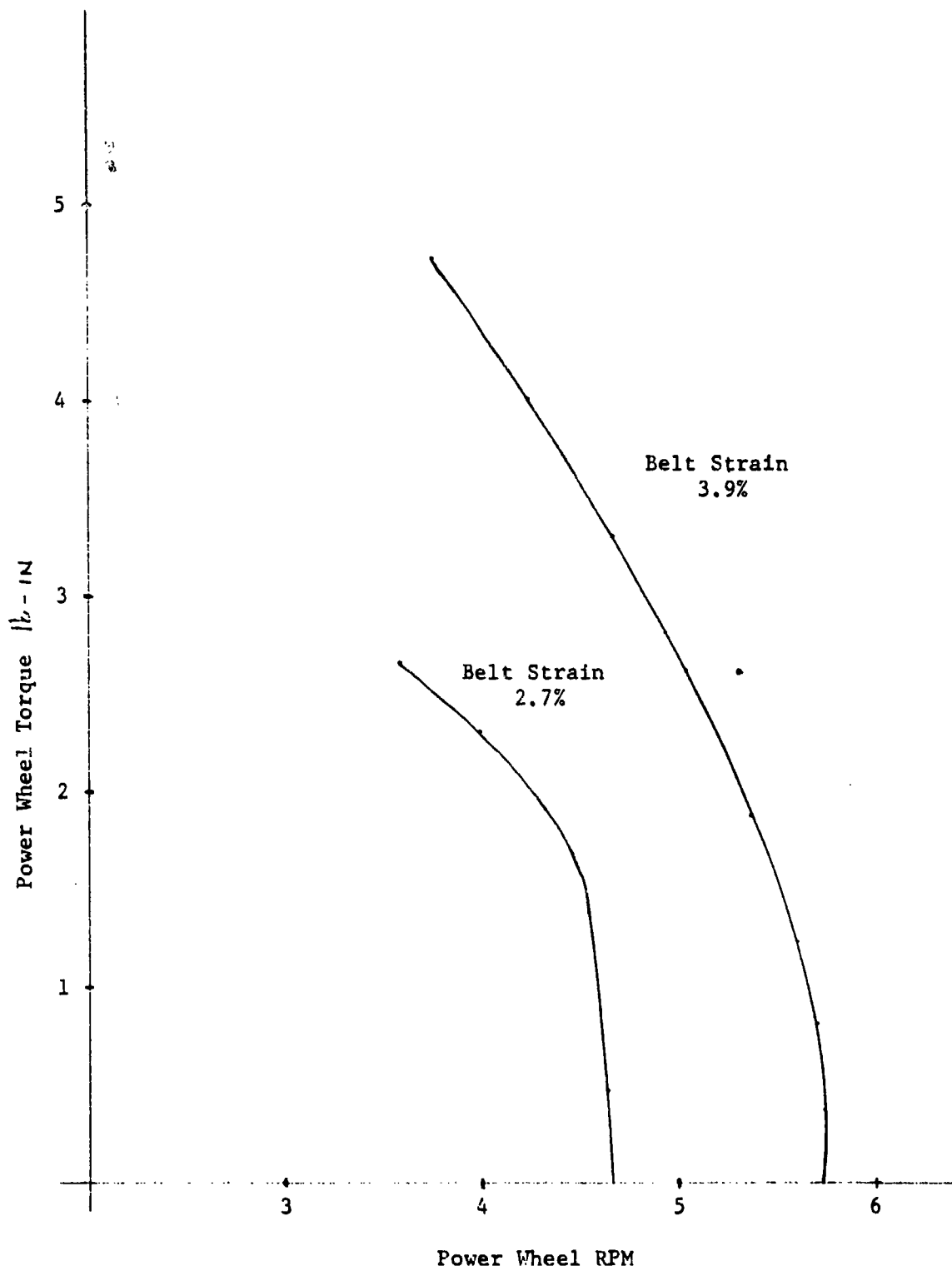
FIGURE 3   ENGINE PERFORMANCE FOR STRAIN WHEELS
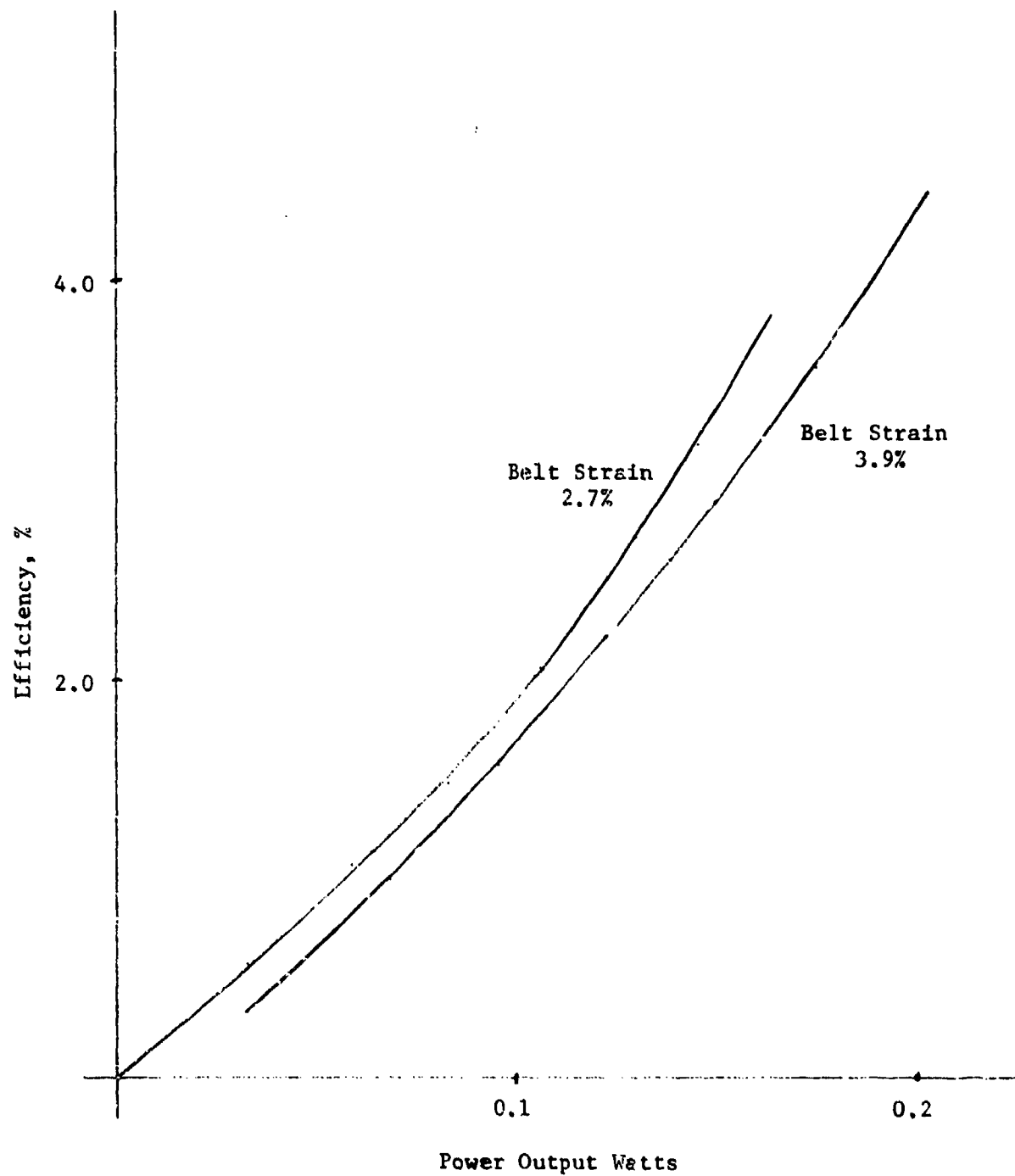
FIGURE 4   EFFICIENCY AND POWER FOR 2 STRAIN WHEELS

SOME ENGINEERING PARAMETERS FOR A NITINOL ENGINE DESIGN

P. A. Hochstein
Quantex Engineering, Incorporated
Warren, MI

INTRODUCTION

The author has been involved in NITINOL Heat Engine (NHE) design since 1974, when the first rotary vane, bending mode machine was built and tested at the General Motors Technical Center.

G.M. showed little interest in further NHE development, and work in this area was terminated until mid 1975, when Quantex Engineering Inc. was formed. The firm is primarily involved in developing electronic testing systems for the automotive industry, and NHE development proceeds as finances and time permit.

Liaison with Pringle and Assoc., a Detroit based engineering design company, has allowed us to design, build, and test various engine designs, while exploring advanced concepts with computer modeling of motor dynamics and heat exchange mechanisms.

TEST FACILITY

Our NITINOL engine testing facility is designed to supply measured quantities of hot and cold water to motors under test, while recording engine performance parameters on an electronic dynamometer (Fig. 1) with variable (resistive) loading.

Engine speed, torque, and power are electronically derived from a 4 pole A.C. brushless generator which is driven by means of a toothed belt.

The dynamometer is presently being modified to allow constant speed or constant torque operation by means of feedback control.

Two 55 gal. insulated drums supply hot and cold media (normally water). Electric heating (6 KW) temperature controllers and a stirring system permit operation up to 195^OF. A 2 H.P. refrigeration compressor allows us to operate the cold water tank down to approx. 35^OF. Continuous, rapid agitation of the cold water minimizes ice formation on the evaporator coils.

Separate variable delivery pumps dispense water to the engine through flow meters. Cavitation in the hot water delivery pumps limits the max. operating temperature to 195^OF.

No effort has been made to optimize the thermal efficiency of any of our NHE models, and no water recirculation is used.

ENGINE DESCRIPTIONS

1. BENDING MODE TYPE

Our first NHE models were of a "pancake" design (Fig. 2). These motors typically contained 150 gms. of NITINOL in the form of vanes, attached to an offset central hub. Operating in simple cantilever bending mode, these engines typically developed 10 to 20 watts of ~ower at a maximum speed of 70 rpm (36 vanes of .03 x .5 x 4 in. NITINOL). While impressive from an output power/energy density standpoint, these machines consume a prodigious amount of water which must be carefully aimed at an angle to the vanes. Separating hot and cold regions is difficult, and water recovery virtually impossible.

In retrospect, these engines are relatively unsophisticated and inefficient. However, they develop respectable power, very reliably from an extremely simple design at relatively low strain levels (<1.5%).

2. TORSIONAL VANE TYPE

More recently, we have concentrated on torsional vane engines with similar flow-through "pancake" housings.

For the most successful of these designs (Fig. 3), the actual motor has 24 NITINOL strips rigidly attached to a central hub. The free end of each strip or vane is held in a movable clamp which can place each strip in torsion along the major (attachment) axis of the element. The hub and strips are free to rotate about the center shaft, and in doing so, move through four quadrants. The quadrants being alternately sprayed with hot and cold heat exchange media (normally water).

As a NITINOL vane moves through a "cold" quadrant, it is cooled below its M_f temperature, and is concurrently torsionally strained (wound up) by a circumferential cam. When the strained element moves into the "hot" quadrant, it is now heated above its A_f temperature and forcibly recovers its unstrained shape. While unstraining, the element does work on the cam, and is moved along to the next quadrant. Obviously, each NITINOL element goes through two complete heat exchange cycles per engine revolution.

Fig. 4 shows the detail of the cam follower mechanism and provisions for lateral motion of each NITINOL clamp (7) as the element shortens during torsion. Motor housing (5), circumferential ring (10), and the hub are fabricated of Celcon AF (a 25% glass-filled acetal copolymer), which exhibits low thermal conductivity and excellent mechanical properties in a severe (boiling water) environment.

Fig. 5 diagrams the function of the sinusoidal, circumferential cam and the relationship of cam amplitude to NITINOL element torsion. Preload and working shear strain for the elements are naturally a function of cam shape. Cams have been developed for several strain levels by a numerically controlled milling machine, and are easily changed.

Pertinent engine specifications are outlined in Table 1, along with typical motor performance values.

These disk shaped motors can obviously be stacked, and the flow-through design simplifies media separation. Polycarbonate shields separate the quadrants on the test fixture. Water carry-over between adjacent quadrants at high (>100 rpm) engine speeds precludes efficient media separation at the output of the motor. An untested design of an air pressure screen to forcibly shed water from vanes between quadrants may solve this problem.

As may be determined from the motor performance figures, internal engine friction is excessively high with respect to net output power. Very high localized cam follower bearing loads on the cam surface are partly responsible. One early cam was ruined during extended operation. The primary cause of high running friction is the "scuffing component" of cam follower bearing motion on the curved cam surface.

Some relatively important conclusions may be drawn from life test data shown in Fig. 6. When operated at shear strain levels below 0.7% (26 ksi), no long term degradation of the torsional elements was apparent. At 1% shear strain, which yielded the performance data in Table 1, one small (1/16") crack developed at the edge of a NITINOL vane after approx. 10 hours of running time (nom. 10^5 cycles at an average speed of 100 rpm). The vane edges show excessive roughness, and were installed "as sheared" after a 5 min., 950°F anneal. Proper edge finishing should extend the "no failure" strain to over 1%.

Fig. 7 shows measured power and torque output for the torsional vane engine described above.

STRESS LIMITING

Torsional NHE are high compliance low stress machines, therefore desirable from a machine design standpoint. However, the intrinsic limitation of half the usable energy density relative to tensile machines has inevitably pointed most NITINOL engine developers to wires or bands in tension.

A shortage of useful NITINOL material has hampered our work in this area; however, some preliminary experimental test results will be discussed.

Ten samples of .015 in. dia. NITINOL wire (V 4547) TTR 180°/210°F were tested conventionally at constant tensile strain. Surprisingly, peak stresses on the order of 75 ksi were measured at 3.5% strain. Fig. 8 shows a typical work diagram after 15 cycles (adjusting for strain hysteresis). It seemed impossible to obtain repeatable, consistent results at strain levels > 1.5%.

The Lawrence Berkeley Laboratory apparently draws the same conclusions.[1]

Repeated annealing and recycling to "optimal" 4-5% strain levels only caused further consternation at the excessive creep --- albeit at spectacular recovery stresses. Transient stresses in excess of 93 ksi were measured when the 10 in. long 0.015 in. dia. wires were submerged in a 300°F silicone oil bath.

To limit the high peak stresses, we equipped several wires with series helical compression springs. Obviously, the spring allows the NITINOL wire to begin shape recovery at relatively low stress. As the spring compressed the stress level may be controlled by the spring rate (F=KL). Work is therefore stored in the spring.

While only preliminary experiments have been conducted, it seems that NITINOL exhibits a "safe operating area" wherein the material may be repeatably cycled to given strain and stress limits without degradation (or property change).

[1] Banks, R., Hernandez, P., and Norgren, D., "NITINOL Engine Project Test Bed," NSF/RANN/SE/AG-550/FR-75/2 (1975)

A publication by J. S. Cory[2] sheds light on this subject, and does much to clarify the mass of seemingly unrelated NITINOL property data.

The Cory Force Length Temperature (FLT) state surfaces which bound equilibrium FLT space probably exclude the shaded area shown in Fig. 8. Only at relatively low stresses (on the MA surface) can the NITINOL exist in equilibrium at relatively high strains. The limiting stress is the yield stress of about 70 ksi at 1% strain.

ENGINE DESIGN WITH STRESS LIMITING

We have done some preliminary design calculations on a multi-h.p. NITINOL heat engine using stress-limited wires in tension.

Stress limiting with helical springs offers several advantages:

1. Equalizes (compensates) for slight variations in element length in a multiwire engine.

2. Permits the engine to be stalled --- without overstressing elements.

3. Allows groups of elements to be used in tandem while sharing loads.

4. Allows for time delay in reaching transition temperatures in groups of elements.

A schematic design for an engine capable of an estimated 25 h.p. when fully loaded (10^4 NITINOL wires 12 in. long x .02 dia.) is shown in Figs. 9a-9i.

Fig. 9i shows the basic NITINOL element/spring stress limiting mechanism. Work is now under way to effectively cold head the attachment ends (Item 1) onto NITINOL wire of 0.015-0.030 in. dia. Cold working the complete wire element and annealing "in situ" may offer some advantage, as early samples show weakness at the flared ends.

The use of master - slave hydraulics (Fig 9d, item 1 and Fig. 9g, item 1) to translate the axial motion of the NITINOL wire "packets" into radial motion offers the added advantage of reduced cam follower loads (Fig. 9g, item 2).

A 5:1 area ratio on the cylinders increases cam displacement proportionately.

Alternate wire carriers (Fig. 9i) communicate with cam follower pistons on either the upper (3) or lower (4) cam in Fig. 9c. Each wire "packet" (Fig. 9e, item 5) rotates circumferentially in its own water tight compartment which commutates through alternate hot and cold quadrants.

The overall size of a 25 h.p. engine (Figs. 9a, 9b) is expected to be approx. 30 in. in dia. by 36 in. high.

---

[2] Cory, J. S., "Engineering Design Data and Correlations for NITINOL Devices" D.O.E. EC-77-X-01-4111.
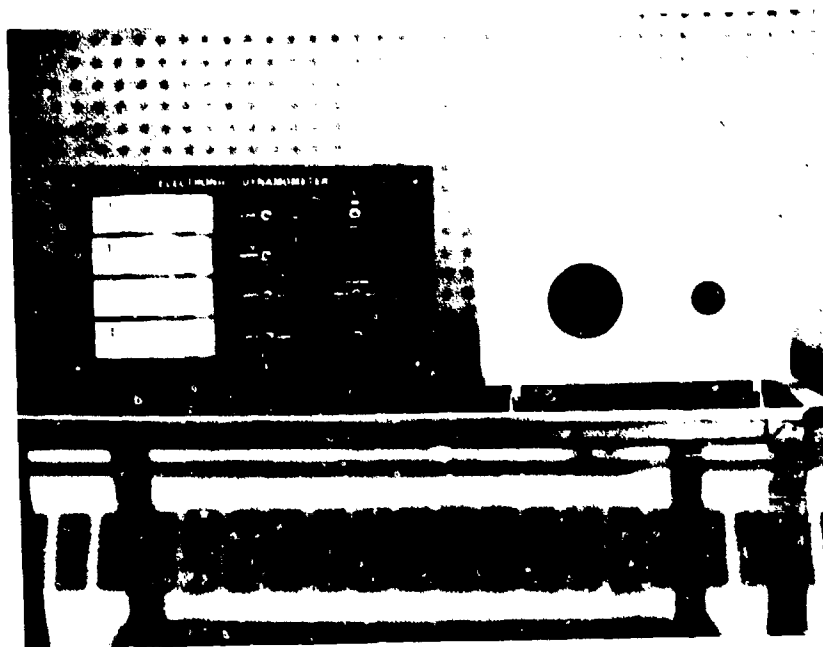
FIGURE 1   ELECTRONIC DYNAMOMETER AND LOAD BANK FOR
NITINOL MOTOR TEST FACILITY
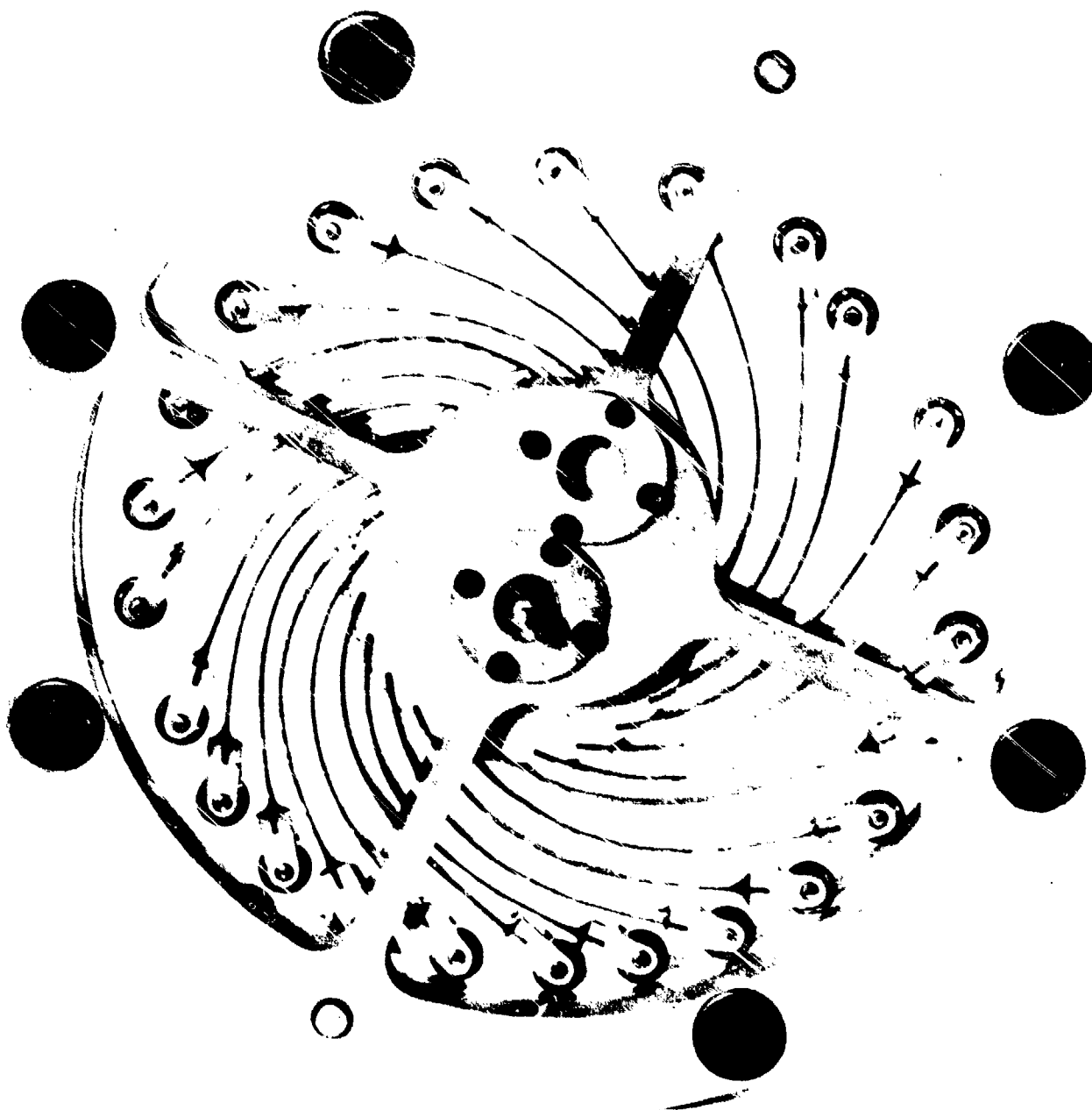
FIGURE 2   BENDING MODE NITINOL HEAT ENGINE (1975) NOM. 12 W OUTPUT
SHOWING SECONDARY MEMORY (TRAINING)
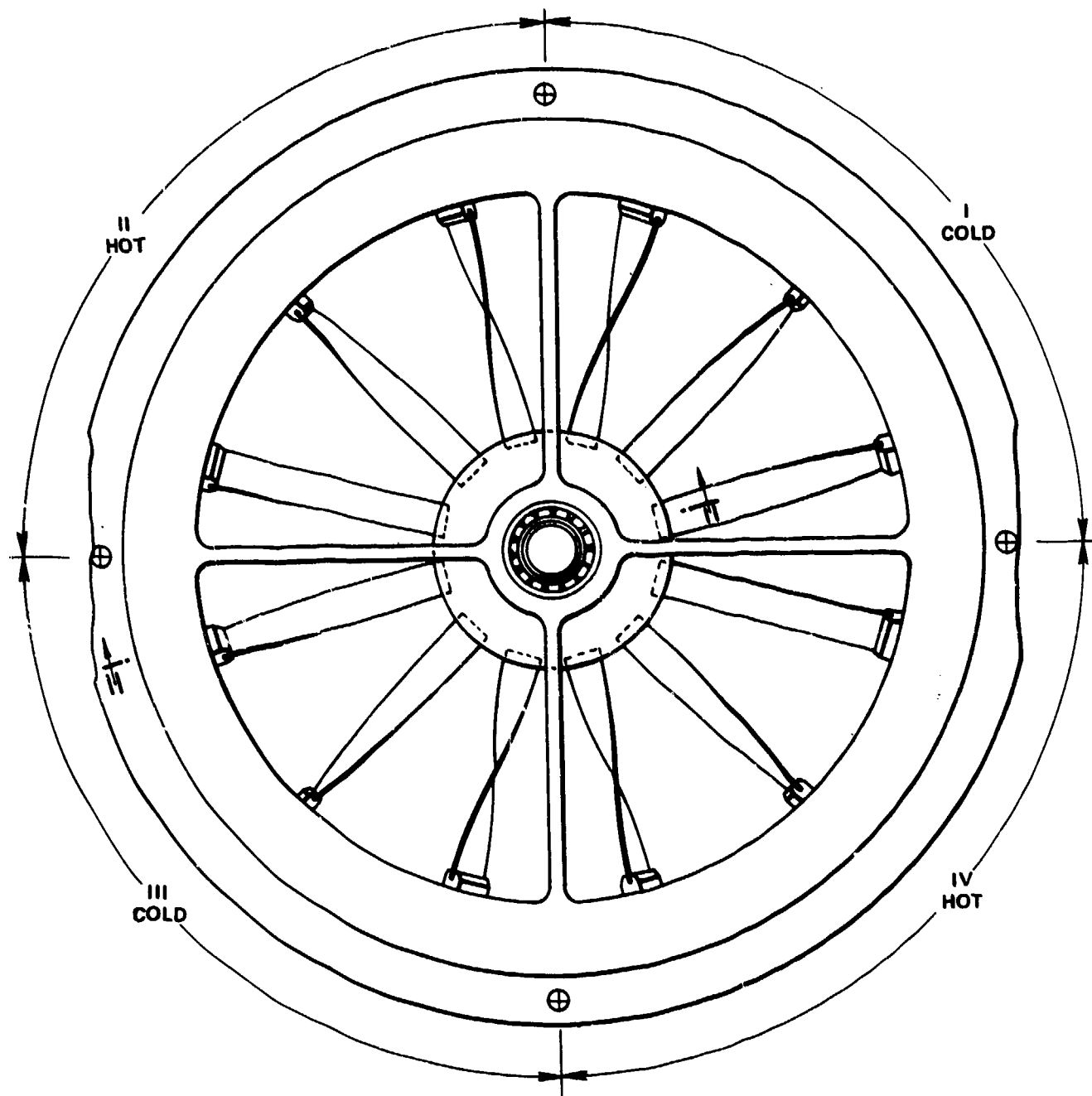
FIGURE 3 PLAN VIEW OF ROTARY THERMAL ENERGY CONVERTER

FIGURE 4   RADIAL THERMAL ENERGY CONVERTER
            SECTION THRU OUTER RIM — SHOWING CAM DETAIL
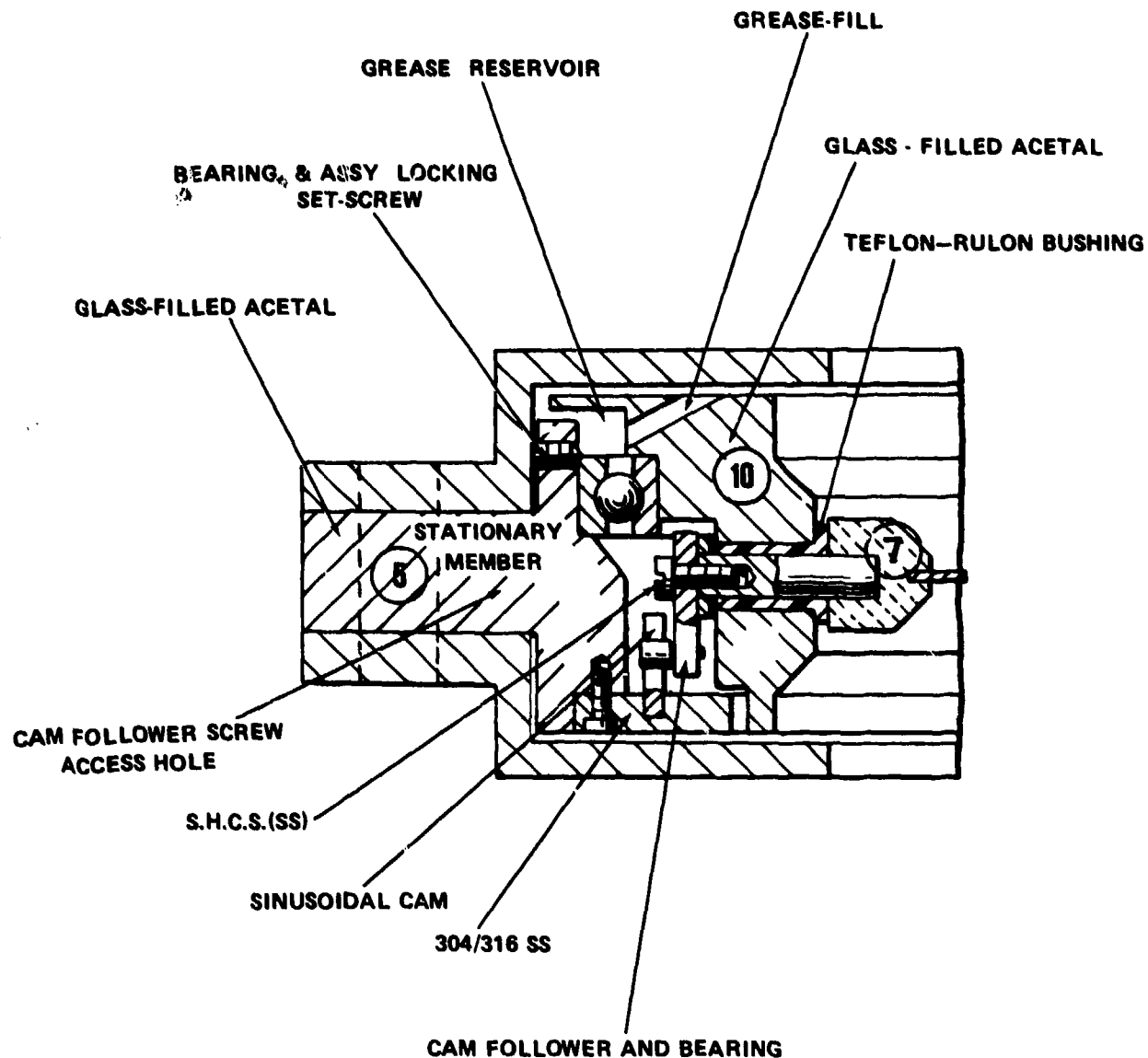
- BEARING LOCATION AT TOP AVOIDS WATER SEEPING INTO BEARING
- REMOVABLE CAM — FOR CHANGING % TORSION OR CHANGING PHASE
- INDIVIDUALLY ADJUSTABLE CAM FOLLOWERS
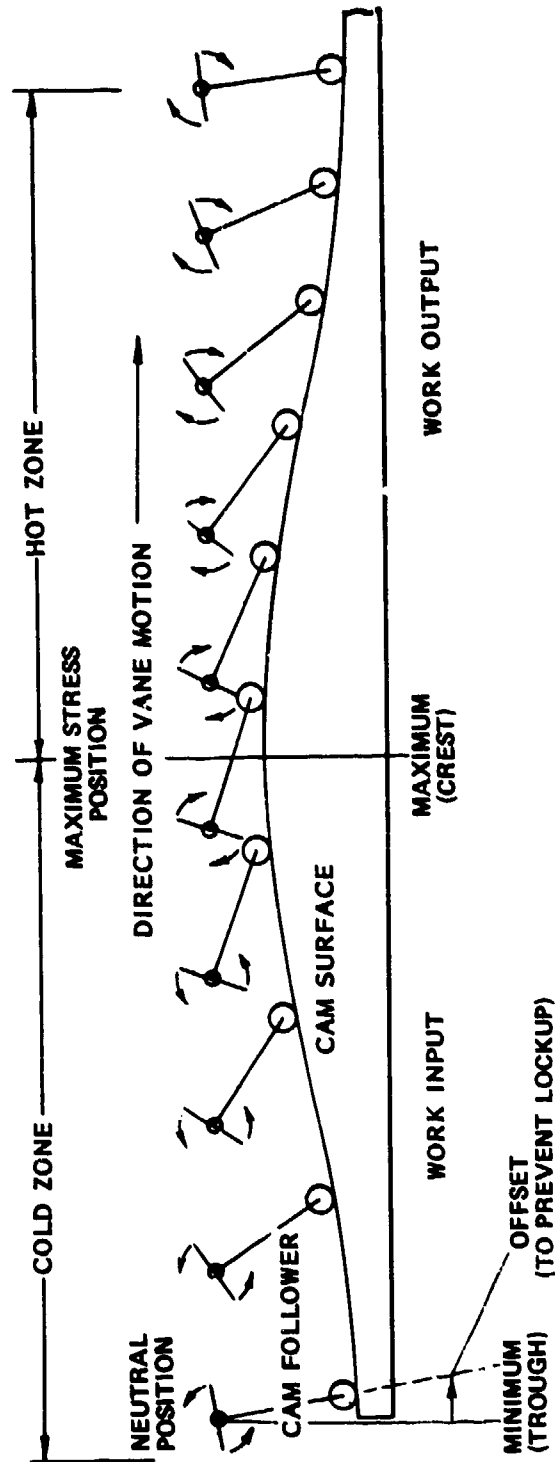
FIGURE 5   EDGE VIEW OF 'UNROLLED' ROTARY THERMAL CONVERTER – SHOWING MOTION OF THERMOELASTIC SHAPE MEMORY ELEMENT VANES THROUGH CYCLICAL STRAINING AND UNSTRAINING (POWER) CYCLES
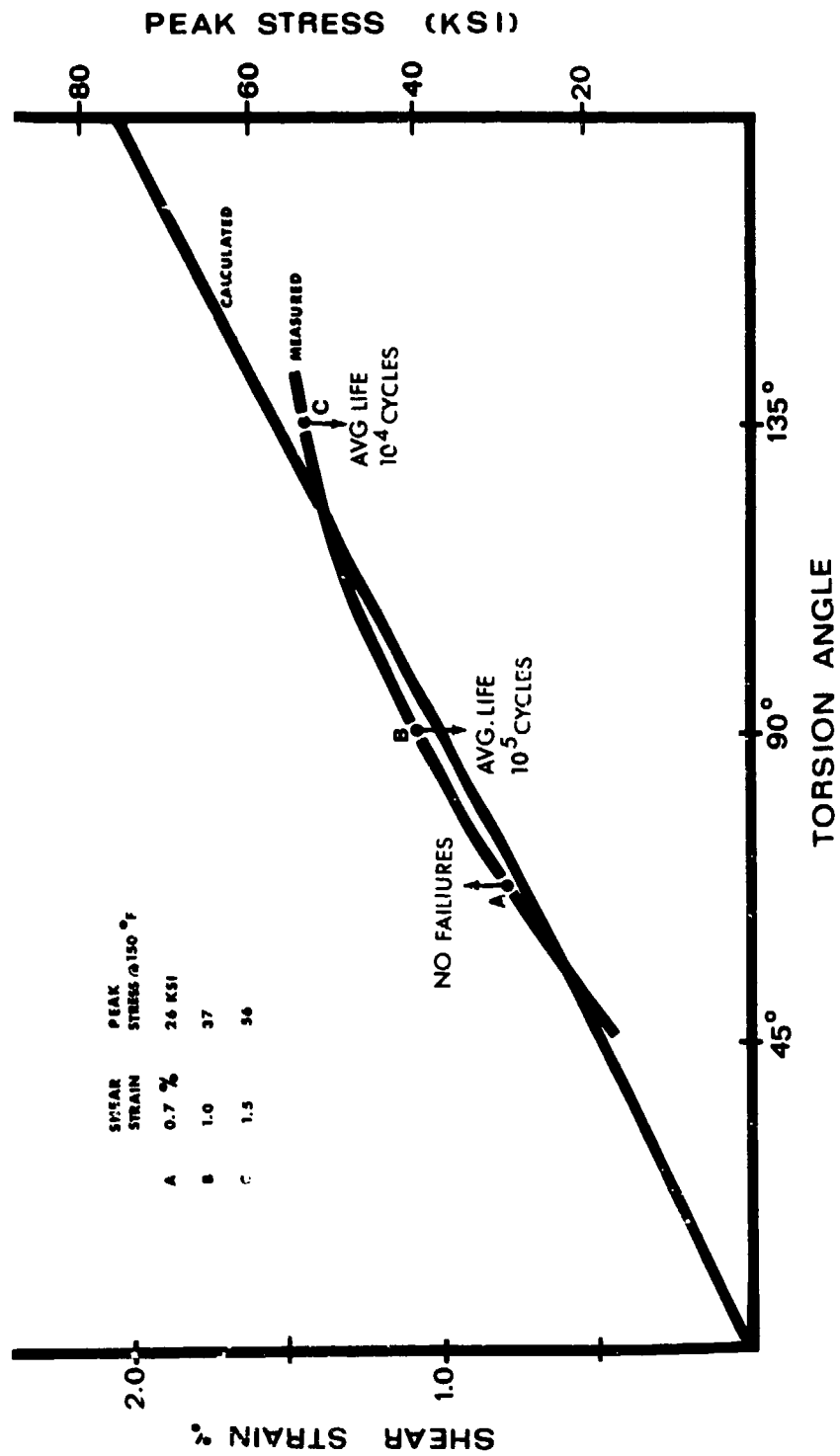
FIGURE 6   TORSIONAL VANE NITINOL HEAT ENGINE MK I
ACTIVE ELEMENTS: 24 2.0 in x .38 in x .012 in V4072
TRR 60/80°F NITINOL MAT'L.
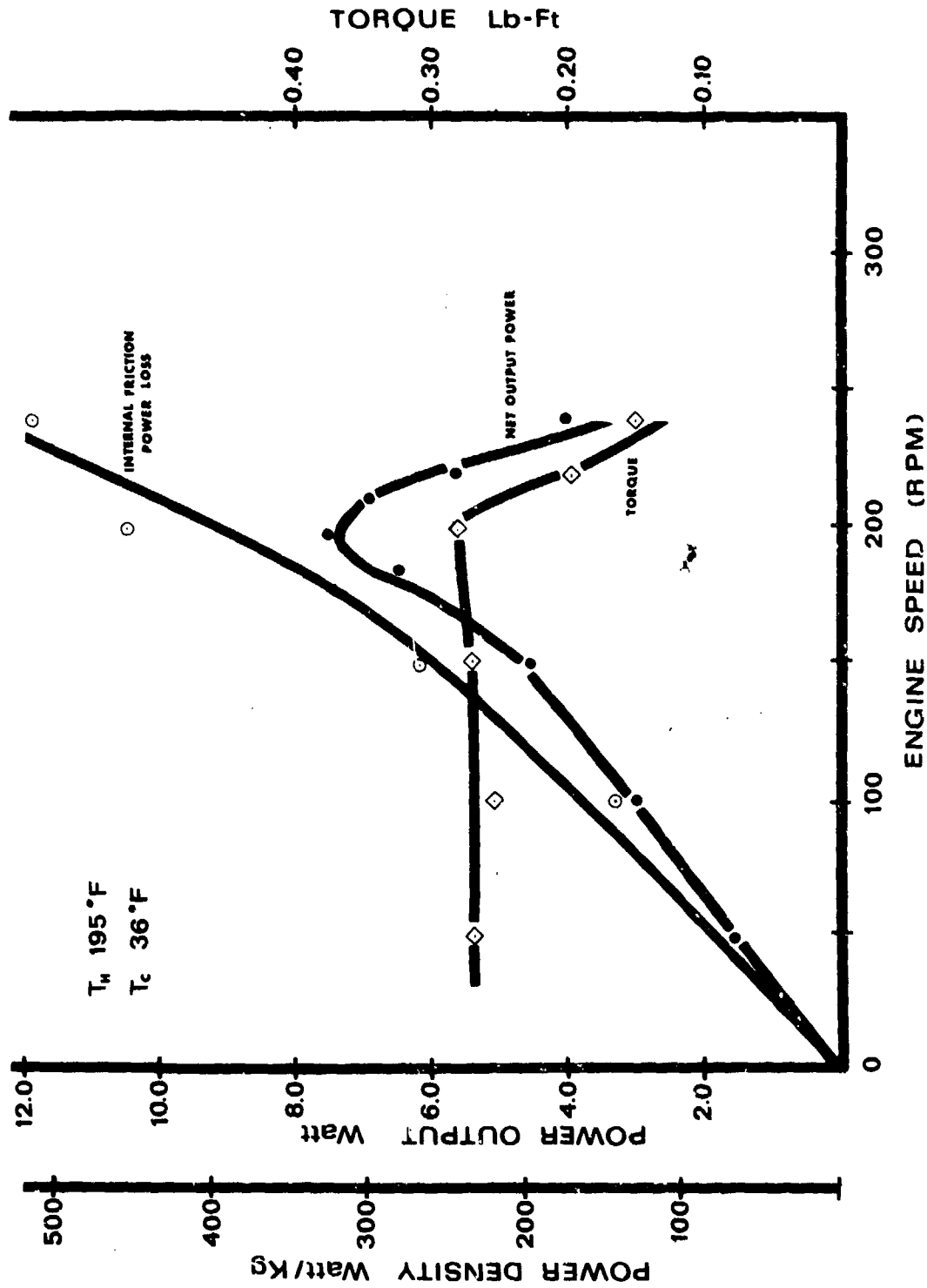
FIGURE 7   TORSIONAL VANE NITINOL HEAT ENGINE — 24 ELEMENT
23 gm V4072 MATERIAL
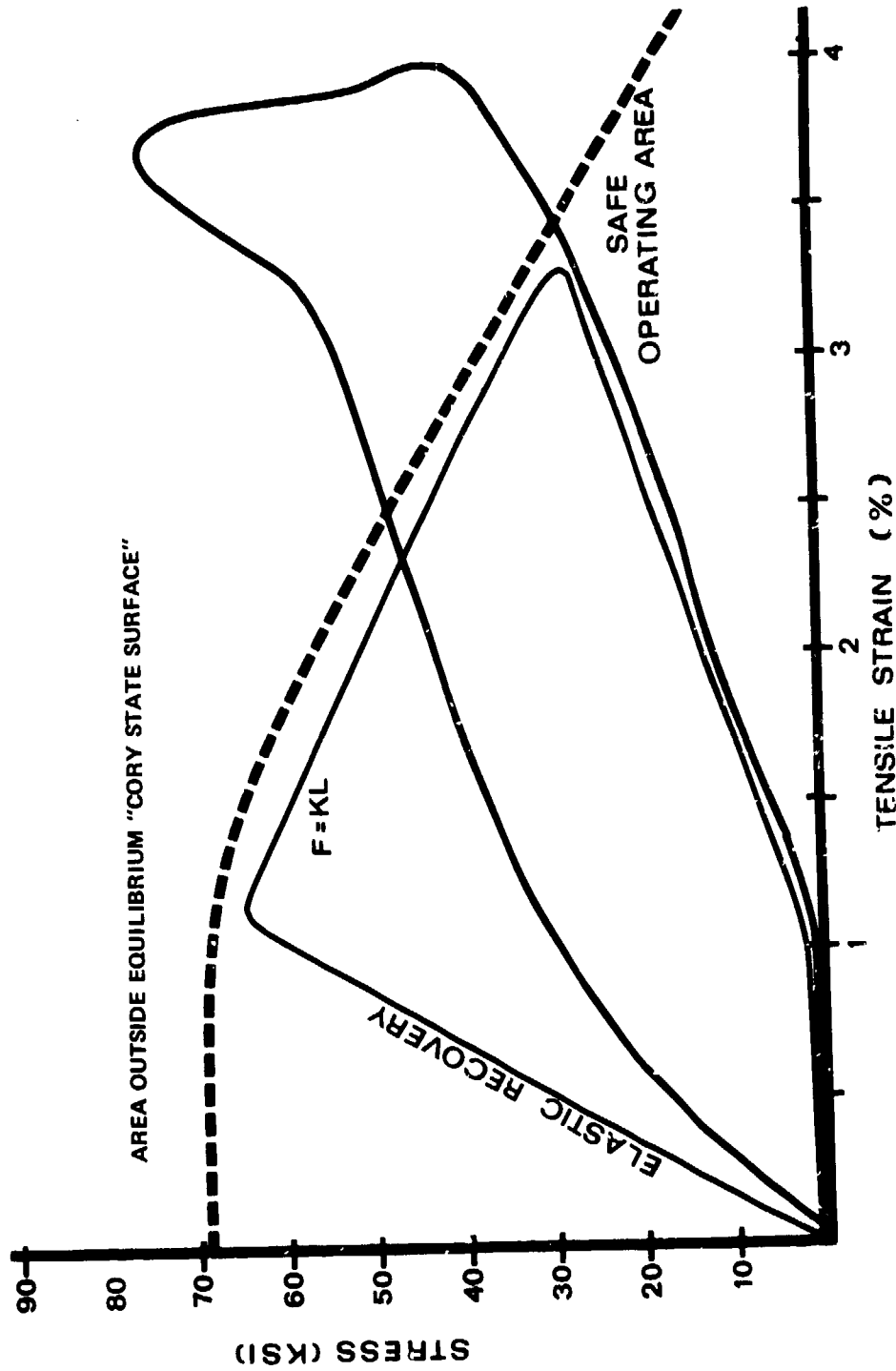
FIGURE 8   PROPOSED SAFE OPERATING AREA FOR NITINOL
STRESS LIMITING WITH SPRINGS
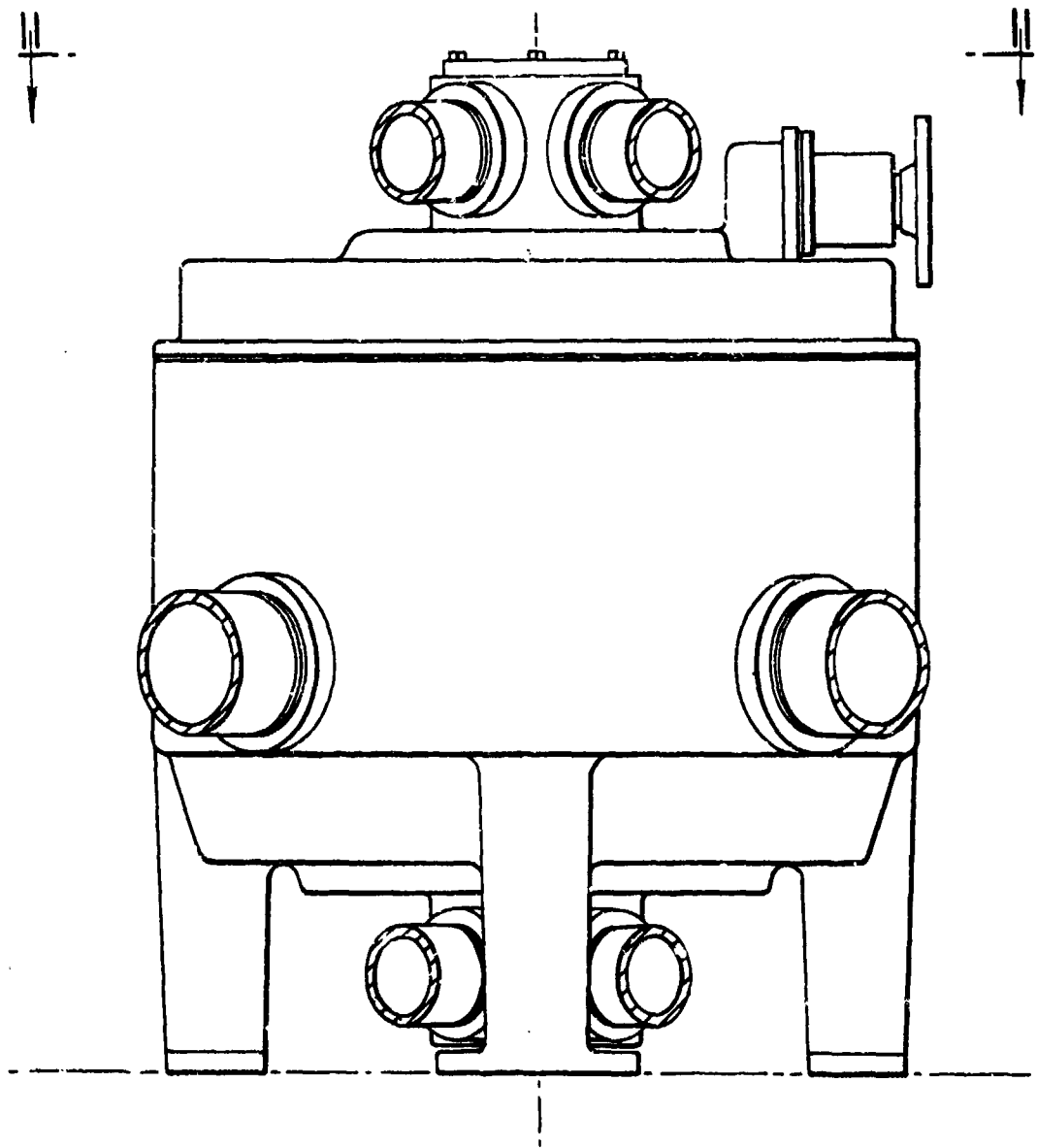
FIGURE 9a ROTARY THERMAL ENERGY CONVERTER
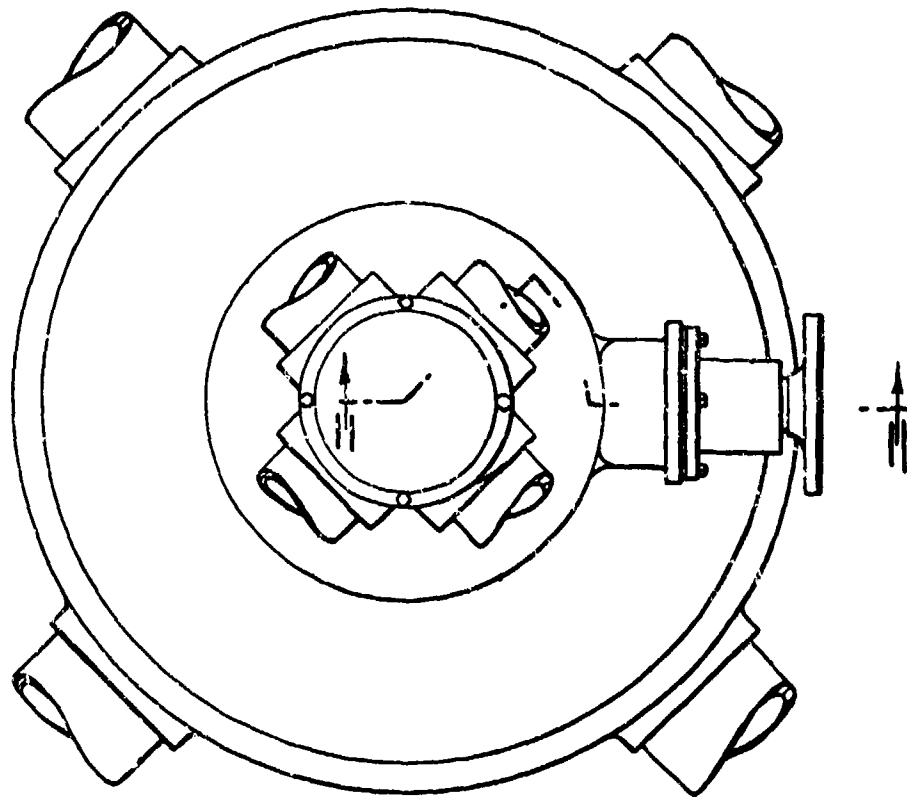
FIGURE 9b ROTARY THERMAL ENERGY CONVERTER
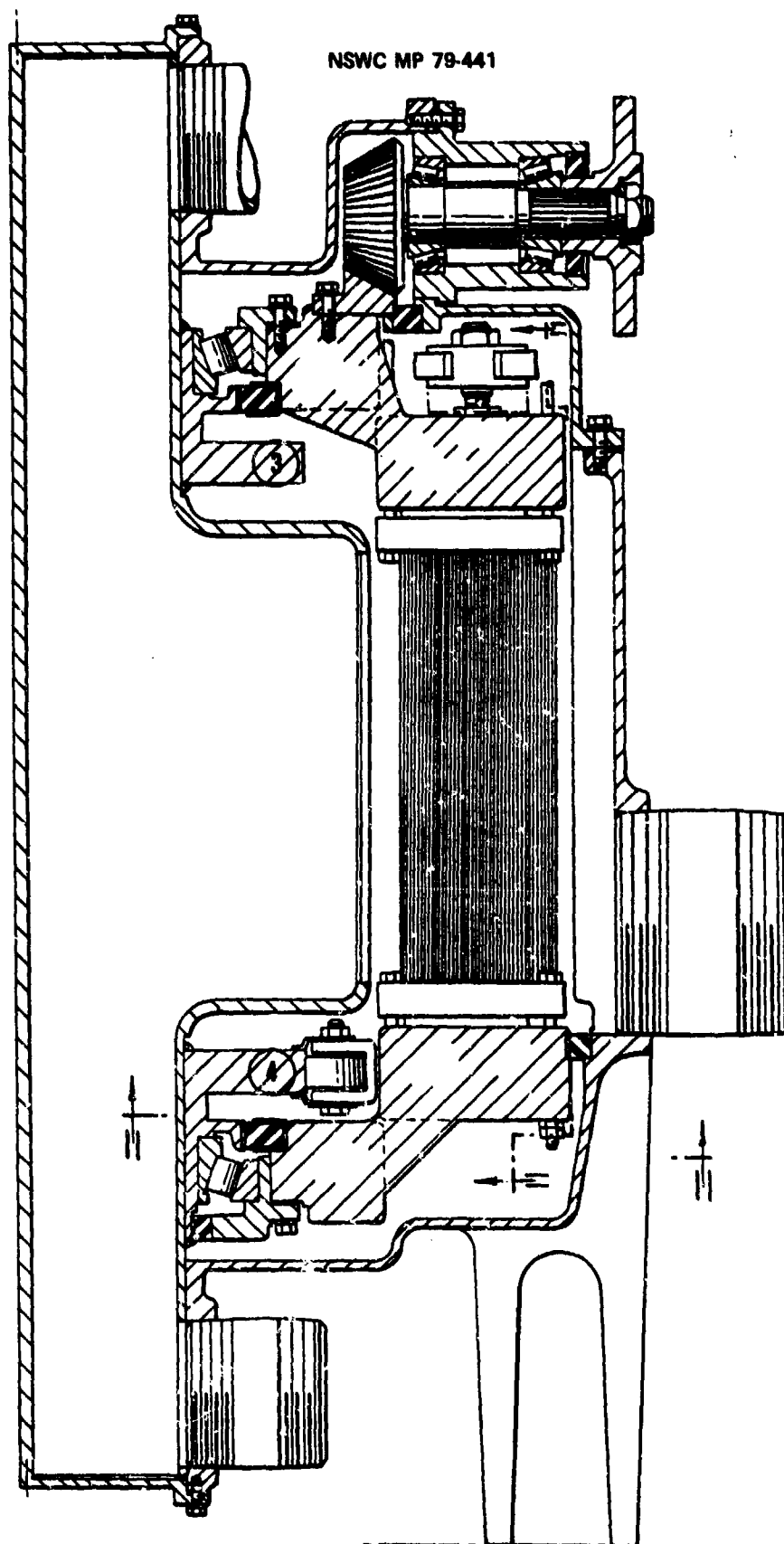
FIGURE 9c   ROTARY THERMAL ENERGY CONVERTER
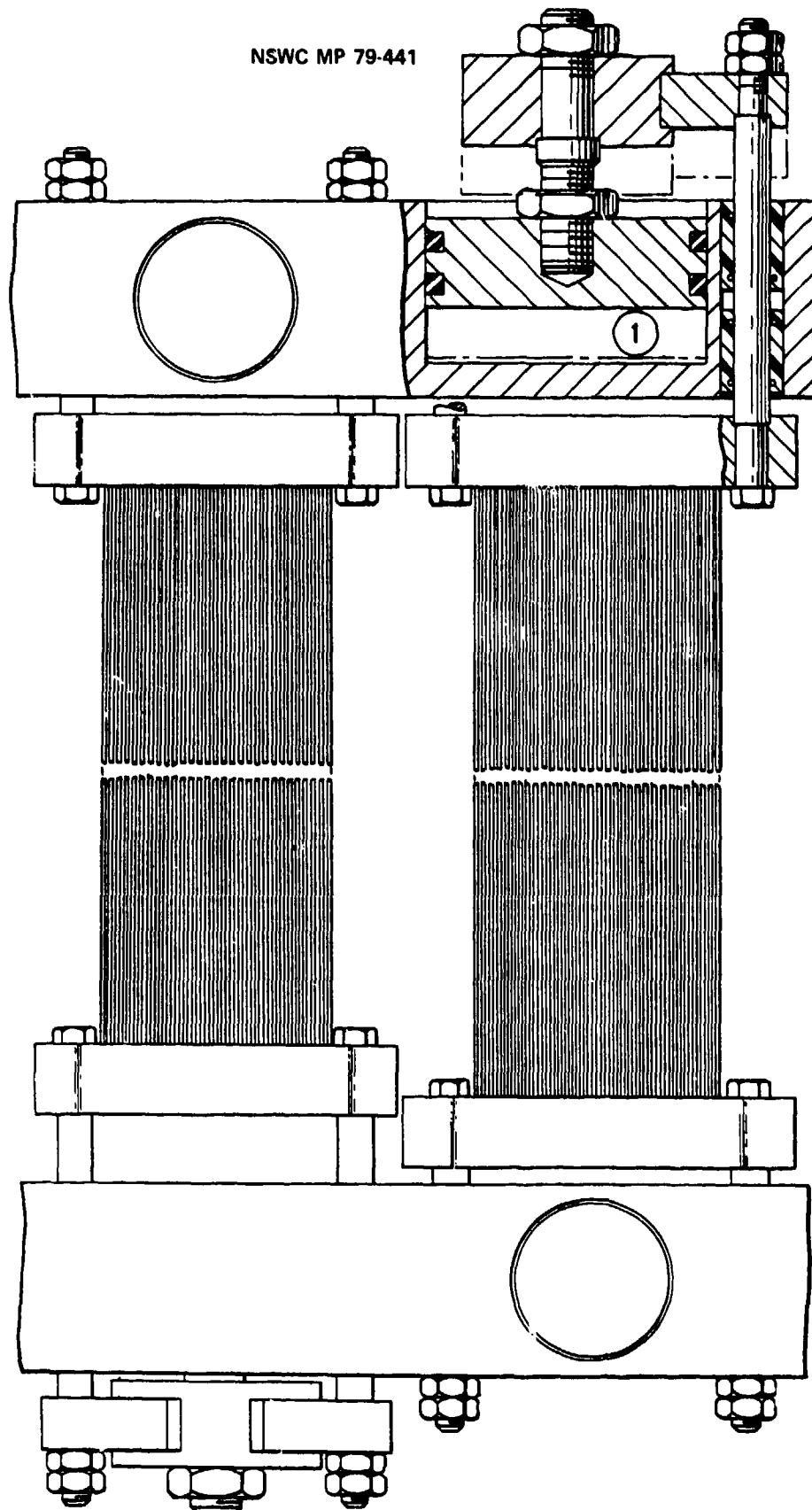
FIGURE 9d   ROTARY THERMAL ENERGY CONVERTER
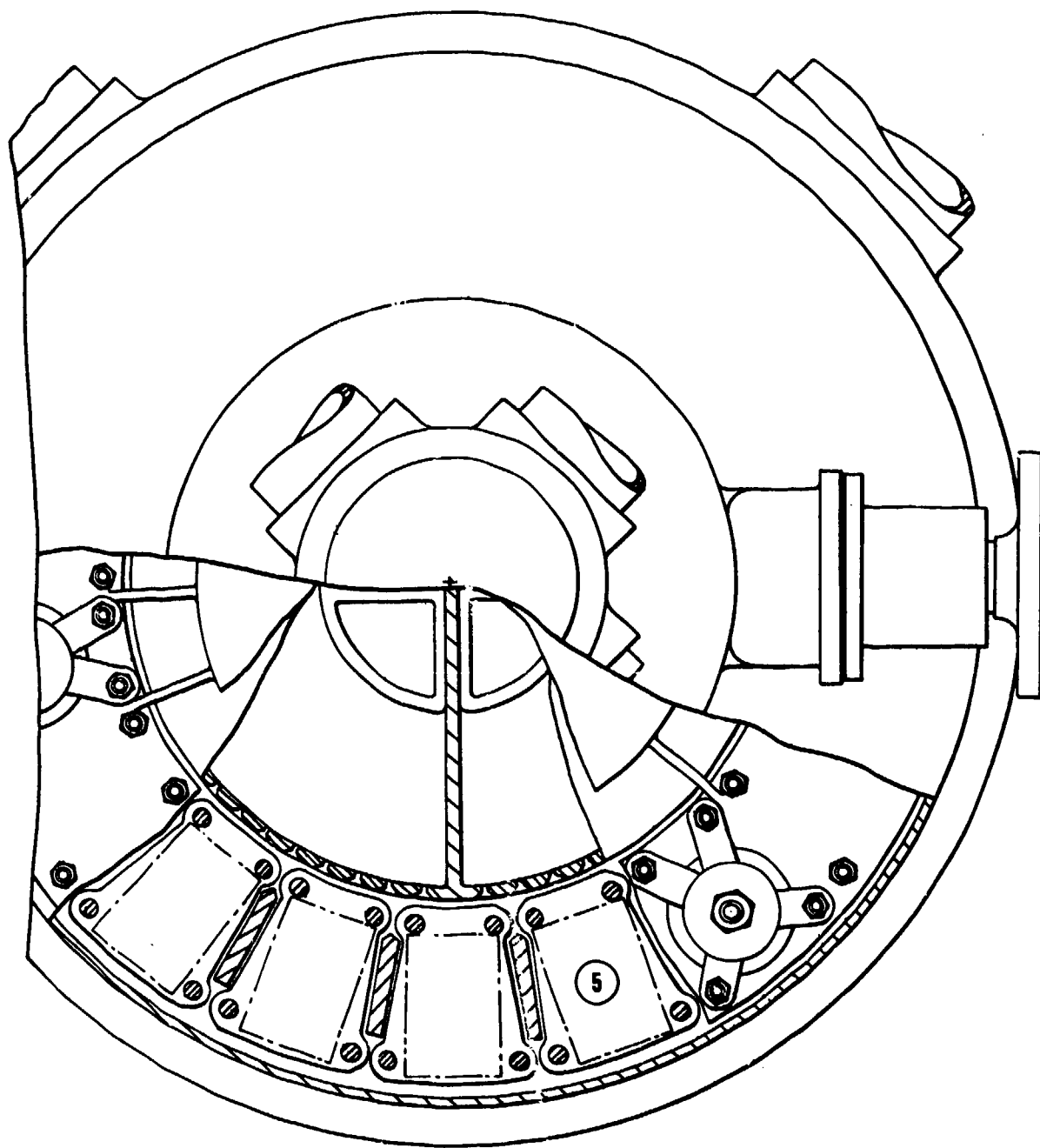
FIGURE 9a ROTARY THERMAL ENERGY CONVERTER
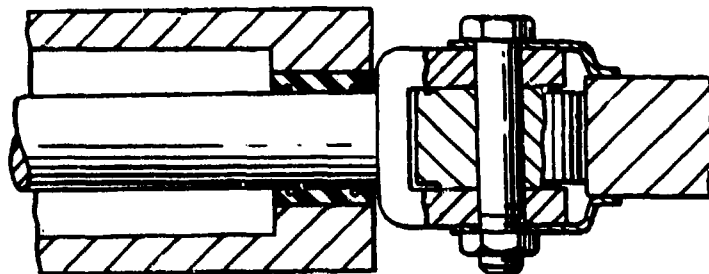
FIGURE 9f   ROTARY THERMAL ENERGY CONVERTER
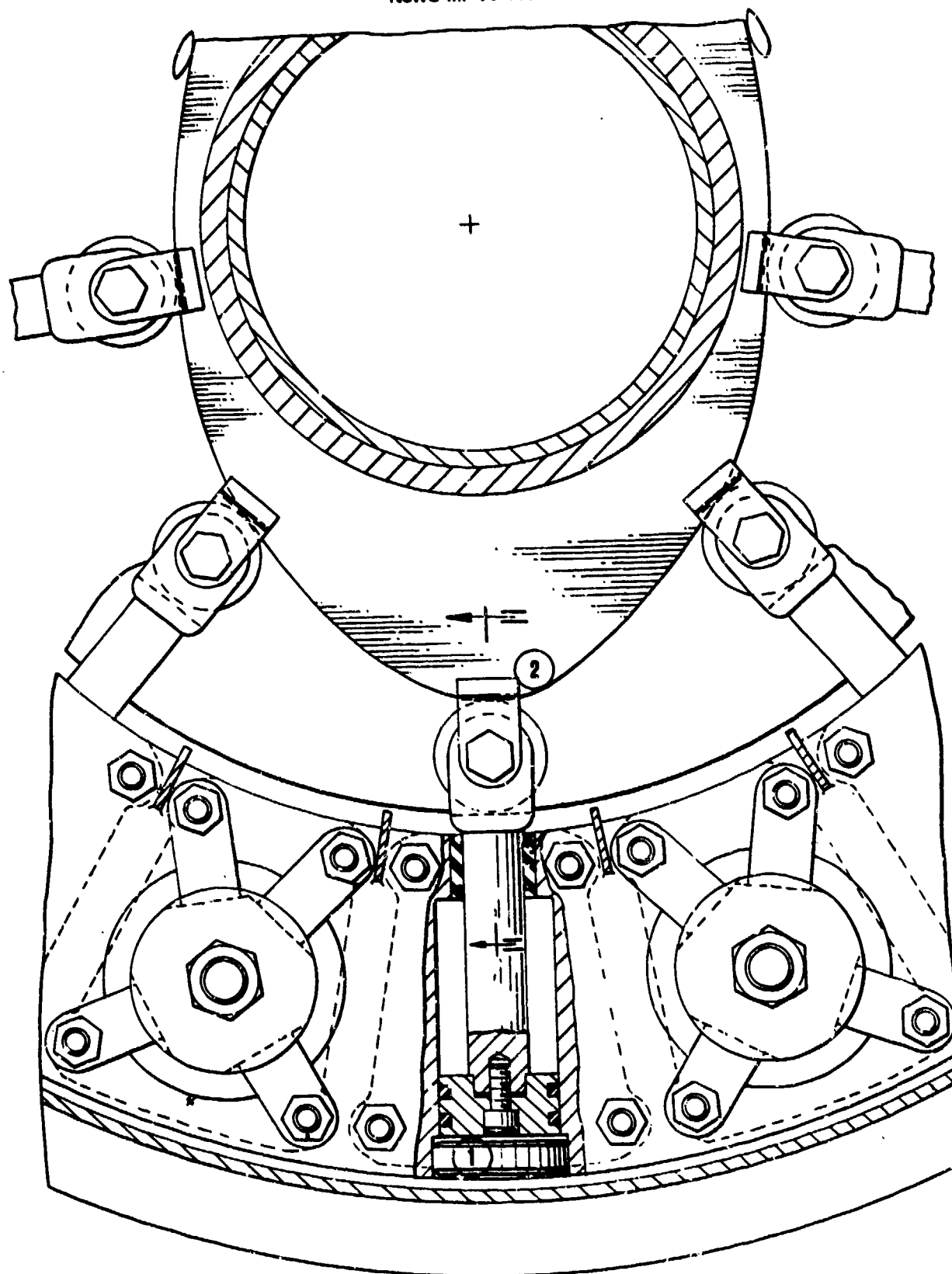
FIGURE 9g   ROTARY THERMAL ENERGY CONVERTER
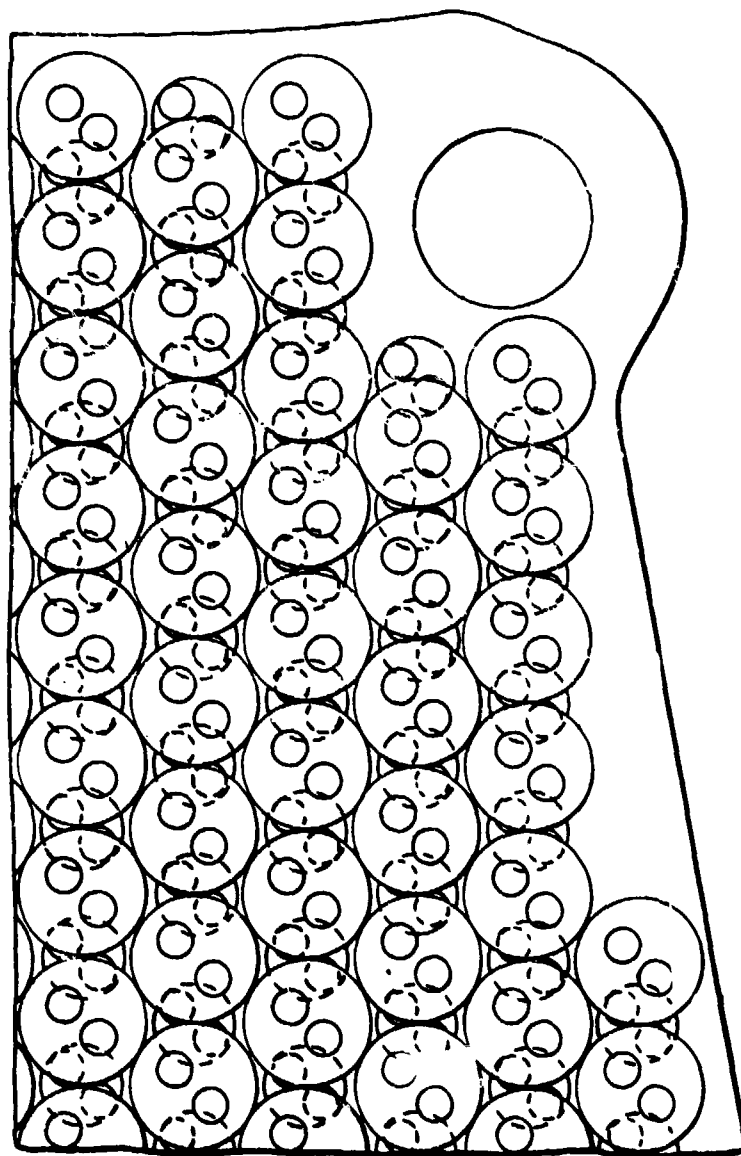
FIGURE 9h ROTARY THERMAL ENERGY CONVERTER
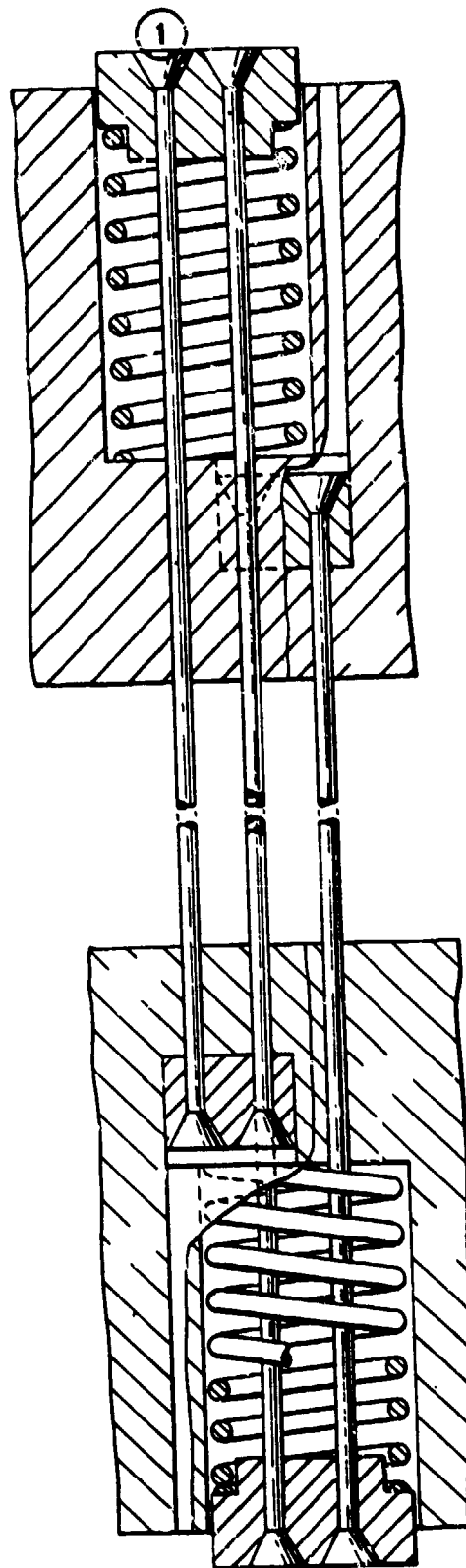
FIGURE 9i   ROTARY THERMAL ENERGY CONVERTER

TABLE 1 TORSIONAL VANE NITINOL HEAT ENGINE MK 1

SPECIFICATIONS

Size: 9.25" Dia. x 1.75" High

Construction: Glass Filled Acetal Copolymer

Number of Thermal Cycles: 2 Per Revolution
(2 Cycle Sinusoidal Cam)

Active Elements: 24 NITINOL Vanes
V 4072 TTR 60°/80°F (15°/27°C)
2.00" x 0.38" x 0.012"

Total NITINOL Mass: 23 GMS. (0.8 oz)

Thermal Media: Water

PERFORMANCE

Cold Water Inlet Temp.: 36°F (2°C) Nom. 1 GPM

Hot Water Inlet Temp.: 195°F (88°C) Nom. 2.2 GPM

Maximum N.L. Engine Speed: 240 RPM

Frictional Power Loss: Nom. 12 Watts (at 240 RPM)

Maximum Engine Output: 7.6 Watts (at 198 RPM)

Nom. Power Density: 300 Watts/Kg

AN ANALYSIS OF FACTORS AFFECTING THE EFFICIENCY OF THE SOLID-STATE ENGINE*†

Dr. A. A. Golestaneh

ARGONNE NATIONAL LABORATORY
Argonne, Illinois

ABSTRACT

We discuss the main factors that affect the energy output which accompanies the shape recovery associated with the martensitic transformation in shape-memory alloys. We describe an experimental solid-state (SS) engine made with the Ni-Ti (NITINOL) shape-memory alloy, and discuss the efficiency of such an engine. We also derive and discuss some physical insights obtained from the thermodynamic treatment of the martensitic transformation, and some limitations on the efficiency of the SS engine.

†Editor's Note: There may be some differences of opinion about certain points in this article.

I. · INTRODUCTION

The shape-recovery phenomenon (SRP), which occurs as a result of certain martensitic transformations in the shape-memory (SM) alloys, has received serious attention from industry.[1] The main applications of the SRP are in control devices, medical instruments, and the production of mechanical work from low thermal energy sources (such as industrial waste heat). The solid-state (SS) engine is a heat-mechanical energy converter based on the SRP, in which SM elements are subjected to a "cooling and deforming-heating" cycle. Several prototype SS engines with various kinematical arrangements have already been reported in the literature.[2] However, these engines are in an early demonstrative stage and are far from acceptable for industrial or domestic purposes in terms of reproducible performance, endurance, and efficiency, all of which are related to the mechanism of the martensitic phase change in SM alloys. Clearly, materials parameters (composition, impurities, grain size and orientation, etc.) as well as external parameters (such as temperature, applied stress, mode of material deformation, and cooling and heating rates) play important roles in such a device. The Carnot efficiency of this engine achieves a maximum of 20% if the temperatures of the cold reservoir (CR) and hot reservoir (HR) are $T_L \backsim 20\text{-}24^{\circ}C$ and $T_H \leq 100^{\circ}C$, respectively. The efficiency η, of the shape-recovery (SR) cycle was first estimated by Ahler[3], who used a phenomenological approach to deduce a value of $\backsim 5\%$. Later, estimates of 10-16% were reported by several authors[4-6]. However, recent experimental and theoretical studies have shown that the earlier estimate of 5% is, in fact, correct.[7,8] Despite this numerical disagreement, the work of these authors shows that η is proportional to the latent heat ΔH of the

---

[1] Many authors have studied various aspects of the shape-memory alloys. See, for instance, Shape Memory Effects in Alloys, edited by J. Perkins (Plenum Press, New York, 1975), and New Aspects of Martensitic Transformation, edited by Kobe, supplement to Trans. Jpn. Inst. Met., Vol. 17 (1976).

[2] See, for instance, R. Banks and M. Wahlig, Technical Report LBL-5293, Lawrence Berkeley Laboratory (1976); and A. D. Johnson, IECEC 75 Record No. 759082, p. 530 (1974).

[3] M. Ahler, Scripta Met. 9, 71 (1975).

[4] H. C. Tong and C. M. Wayman, Met. Trans. 6A, 29 (1975). See also C. M. Wayman and H. C. Tong, Scripta Met. 9, 737 (1975) and 10, 1129 (1976).

[5] B. Cunningham and K. H. B. Ashbee, Acta Met. 25, 1315 (1977).

[6] A. A. Golestaneh, J. Appl. Phys. 49 (3), 1241 (1978). A somewhat different treatment was used in this paper, as we will explain in more detail in the present paper.

[7] P. Wollants, M. DeBonte, L. Delaey, and J. R. Roos, Z. Metalikde, Part I, p. 147, Bd 70 (1979) H.3 and Part II, p. 298, Bd 70 (1979) H.5.

[8] A. A. Golestaneh, "Martensitic Phase Transformation in Shape Memory Alloys," Proceedings of International Conference on Martensitic Transformation (ICOMAT - 79) at Massachusetts Institute of Technology, Boston, MA, June 24, 1979, pp. 679-692.

See also Golestaneh, "Energetic Shape Recovery Associated with Martensitic Transformation in Shape Memory Alloy," Acta Metallurgica, in press.

martensitic reactions in SM alloys. Mohamed,[9] however, states that the value of η increases as ΔH decreases. This is incorrect, as will be shown subsequently. In fact, the purpose of the present article is to analyze the essential factors which contribute to, as well as limit, the energetic SRP and the value of η. We also derive some physical insights from the thermodynamic formalism applied to these martensitic reactions.

II. BACKGROUND

A. DESCRIPTION OF THE SR CYCLE

We will first describe the operation of a very small engine we constructed for laboratory tests.[10] The engine (Figure 1a), has two units fixed side by side on the shaft (a larger number of units may also be used). Each unit (Figure 1b) contains four 1-mm-dia wire elements made of a NITINOL alloy; this number can also be increased. Each element is "trained" to have a curved shape[11] and is fixed by one end to a floating ring (FR), while the other end is connected to a spoke (or ring) fixed on the engine shaft. The shaft is positioned horizontally so that about half the elements are in the HR (a water bath with T_H = 45-99°C) at any given time, while the other elements are in the CR (the air in this case, with $T_L \simeq 24°C$). The NITINOL elements used here have the SR critical temperature T_C = $33 \pm 7°C$; their structure at $T < T_C$ is mainly β'' martensite, which is a mixture of stress-induced martensite (SIM or β') and quench-induced martensite (QIM or γ'). In the martensite phase, the wires are soft and thus can be easily deformed. As soon as the elements are heated in the HR, they undergo SR and push the FR upward and off center; the weight of the FR deforms the elements which are in the CR. The gravity torque created by the off-center FR then pushes the shape-recovered elements out of the HR and replaces them by the newly deformed elements. The rotary motion continues as long as the HR has $T_H > T_C$ and the CR has $T_L < T_C$.

Effectively, the SR cycle in any SS engine consists of two stages: In Stage I, the SM element is deformed to a suitable degree (by tension, compression, bending, or torsion), typically with 2-3% strain, in the CR with temperature $T_L < T_C$. Because of the strain energy input W_i combined with the quenching process, the parent phase→martensite (P→M) reaction occurs; the parent phase, or β, transforms partly to β' with the release of the latent heat $\Delta H\beta\beta'$ and partly to γ' with the released $\Delta H\gamma'\beta$, or simply ΔH (Reference 12). In Stage II, the deformed element is rapidly heated to $T_H > T_C$ in the HR; hence the M→P transformation takes place and the element recovers its original shape by absorbing ΔH and $\Delta H\beta'\beta$ from the HR. The SR can be complete or partial, depending on T_H, the resistance stress σ_r and the uniformity of the material structure (which affects the spread ΔT_C) (Reference 13). In an SS engine, of course, it is necessary to have a complete ("closed") SR cycle.

---

[9] H. A. Mohamed, J. Mater. Sci. 14, 1339 (1979).

[10] The engine described here operates at ∼40 r/min and generates 5 mW of power. Engines with different geometries have also been constructed; for instance, see Reference 5, and the article by R. Banks in Shape Memory Effects in Alloys (Reference 1).

[11] The process of "training" the SM element into a given shape essentially consists of annealing the element (kept constrained in the desired shape) at a temperature T for a time t. Both T and t depend on the SM alloy composition and geometry.

[12] A detailed description of the latent heat $\Delta H_{\gamma'\beta}$ and $\Delta H_{\beta'\beta}$ is in Reference 8.

[13] In the present work we exclude the effects of element geometry and other material parameters which affect the heat exchange rate and kinetics of the SRP.

Experiments show that the most effective SR force is obtained when the SM elements are subjected to very rapid cooling and heating. Also, even though the martensitic reaction is massive, under an applied load the reaction period t_r is finite and depends on the engine load and the values of T_H- T_C and T_C- T_L (partly because of the heat exchange rates and partly because of the ΔT_C range[14] seen in Figure 2).

B. EFFICIENCY OF THE CLOSED SR CYCLE

As stated earlier, the efficiency η of the SR cycle has been evaluated by several authors[3-7,9], but these evaluations have certain shortcomings which are discussed in Reference 8. We will therefore consider the recent evaluation in Reference 8, the result of which is

$$\eta = \lambda \alpha h \ X + (1 + \alpha)h^{-1}, \tag{1a}$$

where
α is the fraction of the SIM which, in transforming to the P phase, causes the SRP;

$$X = T_H - T_L;$$

the characteristic temperature h is defined as

$$h - c^{-1} \Delta H \tag{1b}$$

where c is the average specific heat of the M and P phases, and ΔH is the latent heat of the stress-induced M→P transformation;

and

$$\lambda = 1 - \alpha'/\alpha, \tag{1c}$$

with α' defined by the expression

$$W_i = \alpha' \rho \Delta H, \tag{1d}$$

where ρ is the mass per unit volume of the material and W_i is the strain energy input required to deform the SM element in the CR.

In what follows we will analyze the factors that affect the energy output of the SRP and the efficiency η given by Equation (1a). From this analysis we derive some physical insights associated with the martensitic reactions in the SM alloys.

---

[14] The kinematics of the SRP will be presented in a separate article.

[3] See footnote 3 on page 5-2.

[4] See footnote 4 on page 5-2.

[5] See footnote 5 on page 5-2.

[6] See footnote 6 on page 5-2.

[7] See footnote 7 on page 5-2.

[9] See footnote 9 on page 5-2.

III. FACTORS THAT AFFECT THE SRP

A. FEATURES OF THE ENERGETIC SRP

An important question is how the SRP in an SM element can produce mechanical energy. In answering this question, briefly recall several points known from the previous work:[15]

1. The SRP is associated solely with the SIM or β'. However, recent work shows[13,8] that the QIM or γ' plays an important role in producing the SR energy output. We will discuss this point in more detail below.

2. The martensite phase in the SM alloy is essentially an admixture of γ' and β', denoted by β'' and defined as

$$\beta''(A,B) = A\gamma' + B\beta', \qquad (2)$$

where the fractional parameters A and B (with $A + B = 1$) depend on temperature T and stress σ. Thus, the martensitic transformation takes place as schematically shown by the lines $T_L CD$ and $T_L T_H D$ in Figure 3, i.e., via the following channels:

$$B\beta' \to B\beta \qquad (3a)$$

$$A\gamma' \to \begin{cases} A'\beta & (3b) \\ (A - A')\beta' \to (A - A')\beta, & (3c) \end{cases}$$

where $(A - A')$ represents the fraction of the γ' martensite that, under constant strain and the combined influence of T and σ, is transformed first to β' and then to β as shown schematically in Figure 4. This fraction $(A - A')$ of γ' which transforms via channel (3c) depends not only on T and σ, but also on the geometry of the deformed specimen.

3. The M→P transformation in SM alloys is an admixture of first- and second-order transformations and is accompanied by a small fractional volume change, about 0.1%. This fraction, associated with the γ' martensite, is equivalent to a strain $\epsilon = 0.1\%$ in a uniaxial specimen.

---

[15]A. A. Golestaneh, The Shape-recovery Phenomenon in Shape-memory Alloys, with Particular Reference to the NITINOL System--Review and Recommendations, Argonne National Laboratory Special Report (August 1978).

[13]See footnote 13 on page 5-3.

See footnote 8 on page 5-2.

4.   In an isothermal reaction, there is a temperature T_C below which no SR can occur, and in practice T_C is not necessarily equal to the martensitic transition temperature T_O, since T_C increases with the applied stress. However, for present purposes we may consider $T_C \not\approx T_O$, and T_O may be expressed[13] as

$$T_O = \frac{1}{4}(M_s + M_f + A_s + A_f).$$ (4)

In practice (Figure 2), both T_O and T_C have spreads ($\pm \Delta T_O$ and $\pm \Delta T_C$, respectively). Because of the spread ΔT_O, internal friction, and motion of defects, the martensitic reaction depends not only on T, σ, and ϵ, but also on time[14].

5.   The latent heat of the $\beta' \rightarrow \beta$ transformation, $\Delta H_{\beta'\beta}$, is larger than that of the $\gamma' \rightarrow \beta$ transformation, $\Delta H_{\gamma'\beta}$. In fact, it is found[13,7,8] that the difference,

$$\delta(\Delta H) = \Delta H_{\beta'\beta} - \Delta H_{\gamma'\beta},$$ (5)

is responsible for the mechanical energy output of the SRP. From the evaluation of the free energy for a closed SR cycle, in accordance with reactions (3a) to (3c), the factor α in the efficiency formula (1a) has been derived[8] as

$$\alpha = (A - A')\frac{\delta(\Delta H)}{\Delta H}.$$ (6)

6.   Finally, an important feature of the SM materials (particularly NITINOL alloys) is that in the absence of residual strain and stress in these alloys, the M structure is soft and pliable, whereas the P phase exhibits much greater elasticity and strength.[16]   In a uniaxial specimen, the SR strength is defined as[8]

$$\Sigma(T_H, T_L, \Delta\epsilon) = \sigma_r(T_a, \epsilon_r) - \sigma_i(T_L, \epsilon_i).$$ (7)

---

[13] See footnote 13 on page 5-3.

[14] See footnote 14 on page 5-4.

[7] See footnote 7 on page 5-2.

[8] See footnote 8 on page 5-2.

[16] The transient stress data are obtained as follows: (a) Strain the specimen, surrounded by a water bath at temperature T_L, to a fixed value; (b) change the water temperature rapidly from T_L to T_H while keeping the specimen constrained under constant strain; and (c) measure the stress change due to the change $T_H - T_L$.

Here σ_i is the stress required to produce a strain ε_i in a long and thin specimen at temperature $T_a < T_C$, and σ_r is the stress that the specimen can support while recovering the strain ε_r, at temperature $T_a > T_C$ and $\Delta\varepsilon = \varepsilon_r - \varepsilon_i$. For a closed SR, $\varepsilon_r = \varepsilon_i \equiv \varepsilon$. From a series of isothermal tensile tests such as those in Figure 5, we have deduced the Σ values shown in Figure 6. We find that the Σ data obtained in this way agree well with those obtained by the so-called transient stress test shown in Figure 7 (Reference 16).

B. SR FORCE AND EQUATION OF STATE

Many authors have used an equation of the Clausius-Clapeyron (CC) type to express the SR strength in terms of the parameters T, σ, and ε. This is possible, but only within certain temperature and strain ranges.[17] This matter has been studied in detail elsewhere;[8] the essential points are described briefly here. We first note that the energy output of the SR in an element (or in an SS engine), denoted by W, is given as[18]

$$W(T_H, \sigma_r) = \alpha_7 \Delta H + W_i(T_L, \sigma_i). \tag{8}$$

Here $\alpha_0 \Delta H$ is given by Equation (1d). Figure 6 shows that for a closed SR (i.e., $|\bar{\varepsilon}_r| = |\bar{\varepsilon}_i| \equiv \varepsilon$) we can write

$$W \, \mathscr{F} \, \Sigma\varepsilon \tag{9}$$

$$W_i = \sigma_i \varepsilon \tag{10}$$

(where we have neglected the small elastic strain energy terms). In this case the energy-balance equation (8) gives

$$\Sigma = \frac{\rho \Delta H}{\varepsilon_i} \alpha(T_H, T_C) \quad \text{for} \quad A_s < T_H < A_f. \tag{11a}$$

if we assume $\sigma_r = 0$ (zero SR), then Eq. (11a) will have the form

$$\sigma_i = \frac{\rho \Delta H}{\varepsilon_i} \alpha'(T_L, T_C) \quad \text{for} \quad M_f \leq T_L \leq M_f. \tag{11b}$$

Both Eqs. (11a) and (11b) are identical in form with the CC equations. At a given ε, we find that Σ and σ_i vary logarithmically or nearly linearly with respect to T, as shown, for instance,

---

[16] See footnote 16 on page 5-6.

[17] A more detailed comment on the work of Reference 9 is given by A. A. Golestaneh, "Comments on the Thermal Efficiency of an Ideal Shape-Recovery Cycle," Scripta Met., V. 14, August, 1980, pp. 845-848.

[8] See footnote 8 on page 5-2.

in Figure 8 where the zero point of the stress is taken to be $\alpha(T = T_C)$. Thus, it can be shown experimentally that within a certain ϵ and T range the CC equation is applicable; from Equations (11) and (1c), we have

$$\alpha = \ln \frac{T_H}{T_C} \approx \frac{X_H}{T_C},$$

(12a)

$$\alpha' = -\ln \frac{T_L}{T_C} \approx \frac{|X_L|}{T_C},$$

(12b)

and

$$\lambda = 1 - \frac{|X_L|}{X_H},$$

(12c)

where $X_H = T_H - T_C$ and $X_L = T_L - T_C$. We note that the ϵ and T ranges within which Equations (11a) to (12c) are valid depend on the nature of the SM alloy and structural conditions, particularly the internal stresses. For instance, for annealed binary alloys with T_C between 30 and 50°C, the above ranges are $\epsilon \approx 0.015$ to 0.035, $X_H \approx 0$ to 70, and $X_L \approx 0$ to -15°C, as seen, for example, in Figure 8. Note that the magnitudes of Σ and σ_i also depend on the material structural condition, and may change with, say, annealing of the specimen.

A few points about Equations (11): First, significantly, if the material had a sharp T_C value, then Equation (11b) would have been a continuation of Equation (11a), as seen in Figure 8. However, in practice there is a discontinuity between these equations in the range $2\Delta T_C$. Second, σ_r appears rapidly (Figures 7 and 9) as the temperature of the specimen is shifted from T_L to T_H, and Equation (11a) gives the peak value of σ_r - σ_i. The time required to attain the peak value depends on the material composition, impurity content, and structural condition.[14] The magnitude of Σ remains constant as long as T_H is constant (Figure 9). Σ is kept constant, the element absorbs $\Delta H_{\beta'\beta}$ from the HR. The difference between $\Delta H_{\beta'\beta}$ and ΔH, i.e., $\delta(\Delta H)$, depends on σ_r. Making use of Equations (8) to (12a), we find that

$$\Sigma = \frac{(A - A')}{\epsilon} \delta(\Delta H) - \sigma_i.$$

(13)

To obtain a correct result from Equation (13) for $\epsilon = 0$, we must take into account the elastic strain energy terms that were neglected in Equations (9) and (10). This leads to

$$(A - A')\delta(\Delta H) = \frac{\Delta E}{2} \epsilon^2 \theta(\epsilon_e - \epsilon) + \Sigma\epsilon \, \theta(\epsilon - \epsilon_e)$$

(14)

14
See footnote 14 on page 5-4.

where ΔE is the change in the Young's modulus of the specimen during the $M \rightarrow P$ reaction, ε_e is the elastic strain energy, and

$$\theta(\varepsilon_e - \varepsilon) = \begin{cases} 1 & \text{for } \varepsilon \leq \varepsilon_e \\ 0 & \text{for } \varepsilon > \varepsilon_e . \end{cases}$$

Another byproduct of our formalism is that by combining Equations (12a) and (11a), we obtain a quantity Z defined as

$$Z \equiv \frac{\Delta H}{T_C} = \frac{\Sigma_C}{\rho X_H} . \tag{15a}$$

But according to Figure 8, Σ is a linear function of X_H; that is, we can write $\Sigma = k X_H$ in which k is the slope of the line (Σ_H, T) in Figure 8. Substituting this Σ expression into Equation (15a) gives

$$Z \equiv \frac{\Delta H}{T_C} = \frac{k\varepsilon}{\rho X_H} , \tag{15b}$$

which is valid only within the ε range in which the CC equation is acceptable. In Reference 7, the authors stated that Z is a constant. However, as we see from Equation (15b), Z is not a constant, but depends on ε.

C. FACTORS AFFECTING THE SR EFFICIENCY η

The efficiency η depends on four factors: $X = T_H - T_L$, h, α, and λ. In an economical SS engine, T_H equals $T_{C_{or}}$ and T_L equals $T_{C_{oi}}$. On the other hand, the maximum efficiency, η_m, is found to be[7]

$$\eta_m \leq \frac{\lambda h}{T_C + h} . \tag{16}$$

This expression indicates that in the temperature range of interest ($X_H \leq 75$ and $X_L \leq -15°C$ for our NITINOL alloy), η_m is nearly independent of $X = T_H - T_L$. Equation (16) also shows the explicit effect of T_C on η_m. Note that for $\lambda = 1$, η_m is the Carnot efficiency of an engine which works between two temperatures $T_C + h$ and T_C. The influences of the above parameters are discussed in more detail below.

---

[7] See footnote 7 on page 5-2.

1. *The critical temperature* T_C: First we recall that the maximum SR strength Σ corresponds to a case in which $T_H > T_C$ and $T_L < T_C$, as can be deduced from Figure 9. One can also conclude from Figure 9 that a cyclic SR with $T_L > T_C$ cannot have any energy output, particularly if T_C has large spread $\pm \Delta T_C$. These considerations and Equation (11a) indicate that for an effective use of the SR strength, we must be able to prepare an SM material with a T_C which has the smallest possible spread, defined as $2\Delta T_C = T_C{}^+ - T_C{}^-$ where the upper and lower limits are close to the A_s and A_f temperatures, respectively. It is known that T_C and ΔT_C depend on the material composition, impurities, crystal defects, etc. In the case of binary NITINOL alloys, T_C is very sensitive to the alloy composition. Better control of T_C can apparently be obtained by introducing a small amount of a third element (Zr, Al, Cu, Fe, etc.) into the NITINOL alloy. However, at the present time, little quantitative information exists on the variation of T_C with material composition and impurity content. As far as the material structure is concerned, we know that, for instance, in a thin wire specimen with a given grain density, T_C varies inversely with the wire diameter d (Figure 2). Figure 2 also shows that the spread of T_C increases with the wire diameter. This may be expected, since the degree of structural uniformity is expected to increase as d is decreased. Another factor that affects T_C is residual stress: In practice, T_C increases with residual stresses which can be produced during the heat treatment or as a result of incomplete martensitic transformation. This can be explained from the relationship

$$T_{C\sigma} = T_C\left(1 + \frac{W_i}{\rho\Delta H}\right),\tag{17}$$

which is obtained by combining Equations (10) and (11), and assuming W_i to be the energy stored in the specimen as a result of internal stresses. Indeed, we have noticed that the T_C of the SM elements in the SS engine increases by a few degrees after a few thousand SR cyclic operations. To remedy this, these elements must be annealed occasionally in order to recover their initial T_C.

2. *The characteristic temperature* h: According to definition (1b), h is the ratio of ΔH over c. Since c varies little, h and, in turn, η_m [Equation (15)] depend on ΔH. For the NITINOL alloy mentioned above, $h \approx 20°C$ or $\Delta H \approx 2$ cal/g. Hence to increase η_m, it is desirable to find an SM alloy that has a larger h or ΔH value than the currently available alloys. This conclusion agrees with the results of all previous studies except Mohamed.[9] He has stated that the efficiency η increases if ΔH decreases. This is in error because, if it were true, then $\Delta H = 0$ should lead to maximum efficiency; this is meaningless, however, since no transformation can occur if $\Delta H = 0$. The reason for Mohamed's conclusion is that he overlooked the fact that the energy released by the SRP is proportional to ΔH, as shown at length in Reference 17.

3. *The parameter* λ: As noted in Section III. B, expressions (10) to (12c) are derived from the ϵ and T ranges in which the CC equation is valid. For our NITINOL specimen, in the temperature range $X_L = -15°C$ to $X_H = 70°C$, Equation (12c) gives $\lambda = 0.84$. It is also possible to evaluate λ in terms of the SR strength: To do this, we use Equations (7) to (12c), and write

$$\lambda = \frac{\gamma - 2}{\gamma - 1}\tag{18}$$

---

[9] See footnote 9 on page 5-2.

[17] See footnote 17 on page 5-7.

where $\gamma = \sigma_r/\sigma_i$. We now see that λ depends to some degree on the mode of material deformation. For instance, according to Figure 5's tensile test data, in the temperature range of interest and $\varepsilon \not\approx 2$ to 3%, we find $\gamma \not\approx 3.5$; thus Equation (18) gives $\lambda = 0.6$. On the other hand, for the same specimen in the bending mode (Figure 9) under the same ε and T, we find $\gamma \not\approx 7$, for which Equation (18) gives $\lambda \not\approx 0.83$ the same value obtained from Equation (12c). It is difficult at this time to explain why γ is smaller for the SR in the tension mode than for that in the bending mode. We are now in the process of verifying these results by refining the experimental technique by which the stress and strain values are determined for the uniaxial wire specimens. In any case, our investigation indicates that in the above ε and T ranges, λ cannot exceed 0.85. We note that in the previous work referred to, with the exception of References 7 and 8, the authors have neglected the deformation energy W_i, Equation (1d), and therefore λ does not appear in their efficiency formulas.

IV.   MAXIMUM EFFICIENCY OF THE SS ENGINE

For most practical purposes, the SS engine must work between an HR with temperature $T_H \not\approx 50\text{-}100^\circ C$ and a CR with $T_L \not\approx 20\text{-}24^\circ C$. Within this temperature range, the NITINOL SM alloy should have a critical temperature

$$T_C = (T_L \, T_H)^{1/2} \tag{19}$$

as given in Reference 6, or $T_C = 1/2(T_L + T_H)$. If we assume the latter choice, the maximum efficiency η_m of the engine, according to Equation (16), depends on h, λ, and T_C. For our NITINOL alloy, $T_C = 306 \pm 7$ K and h - 20-24; using these data and the maximum λ value of 0.85 given above, Equation (16) gives $\eta_m = 5\text{-}7\%$. This is, however, an ideal value. For $T_L \not\approx 297$ K and $T_H = 360$ K and our NITINOL alloy, Equations (1a) and (12) yield $\eta \not\approx 4\%$. We conclude that to increase η_m, we would need a ternary NITINOL or other SM alloy with $h > 20\text{-}24^\circ C$. Of course, if such an alloy is found, its usefulness will depend on such factors as preparation cost, fatigue endurance, and corrosion resistance in hot water.

---

[7] See footnote 7 on page 5-2.

[8] See footnote 8 on page 5-2.

[6] See footnote 6 on page 5-2.
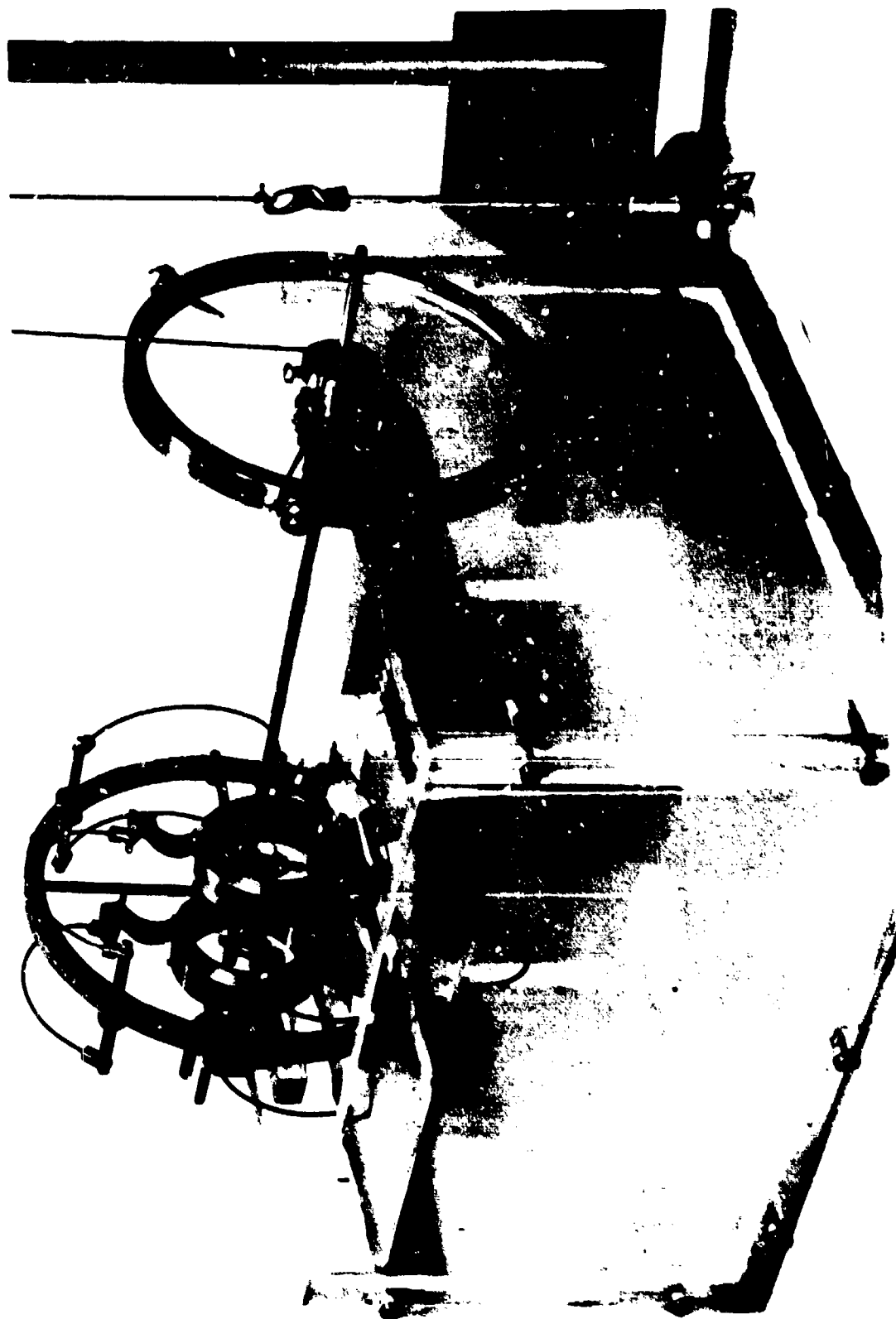
FIGURE 1(a)   SOLID-STATE ENGINE MADE WITH NITINOL WIRES, OPERATING WITH HOT RESERVOIR (WATER) AT 40-75°C AND COLD RESERVOIR (AIR) AT 23°C. TOTAL WEIGHT (INCLUDING FLYWHEEL), 420 kg. WEIGHT OF NITINOL WIRES, 3 g. MAX. TORQUE, 1200 g. cm. MAX. SPEED, 39 r/min.   THERMOMECHANICAL ENERGY OUTPUT, 4.7%.
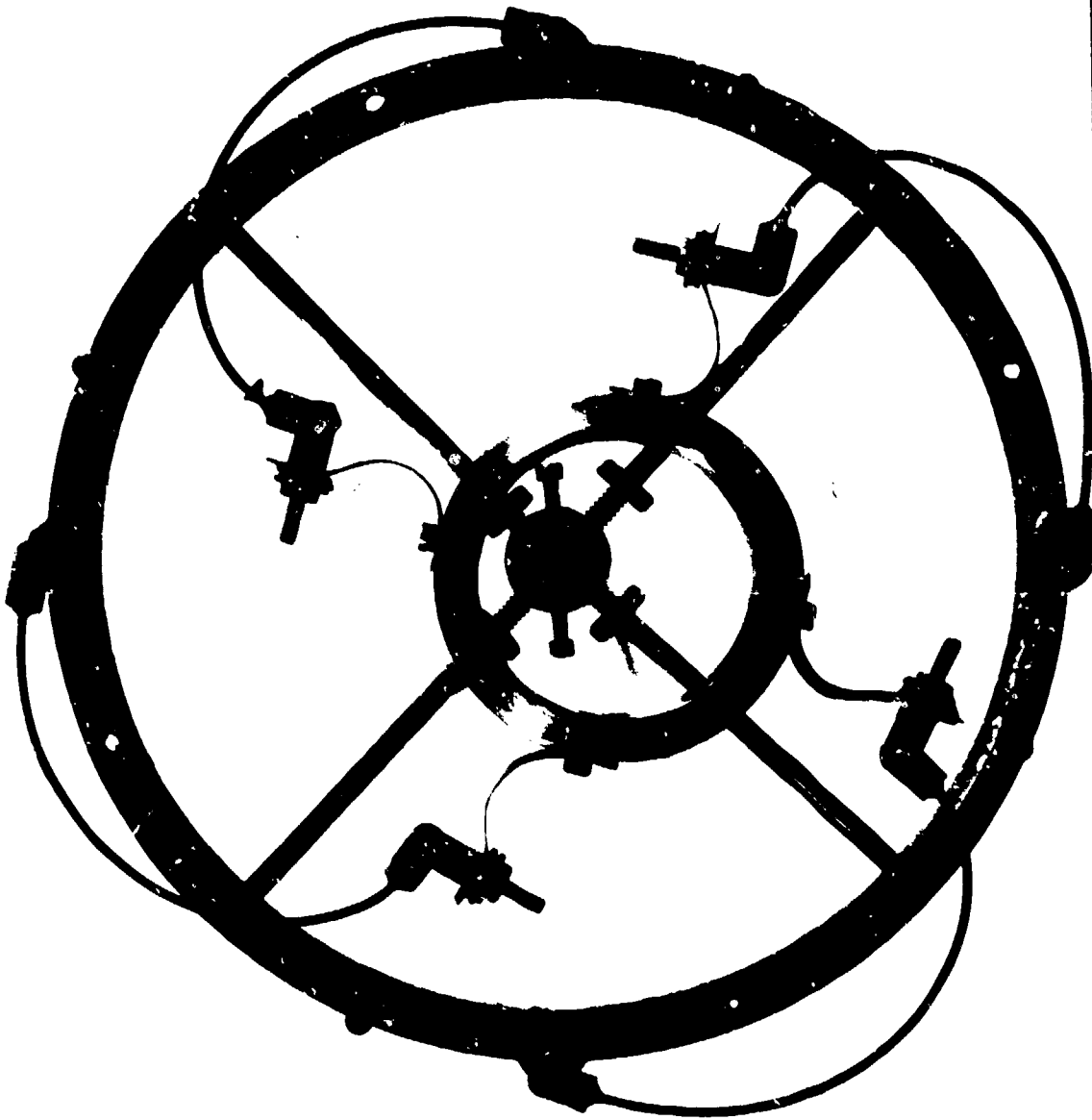
FIGURE 1(b) A UNIT OF THE CRANKING SOLID-STATE ENGINE MADE WITH WITH 1-mm-dia NITINOL WIRE ELEMENTS
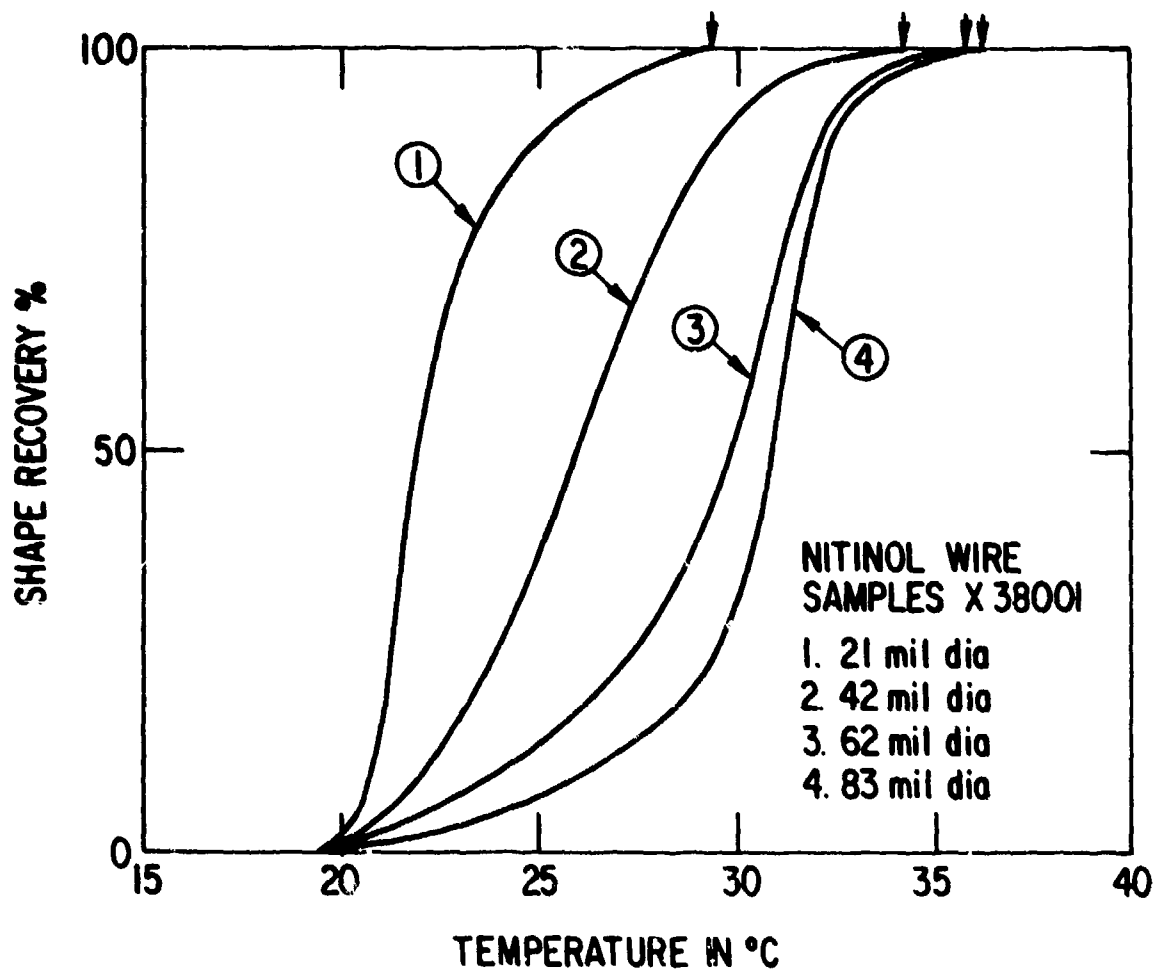
FIGURE 2   FRACTIONAL SHAPE-RECOVERY OBTAINED ISOTHERMALLY AT DIFFERENT TEMPERATURES. THE X-INTERCEPTS OF THE CURVES INDICATE T_C^+ AND T_C^-, THE UPPER AND LOWER LIMITS OF THE SR CRITICAL TEMPERATURE T_C, FOR WIRE SPECIMENS WITH DIFFERENT DIAMETERS.
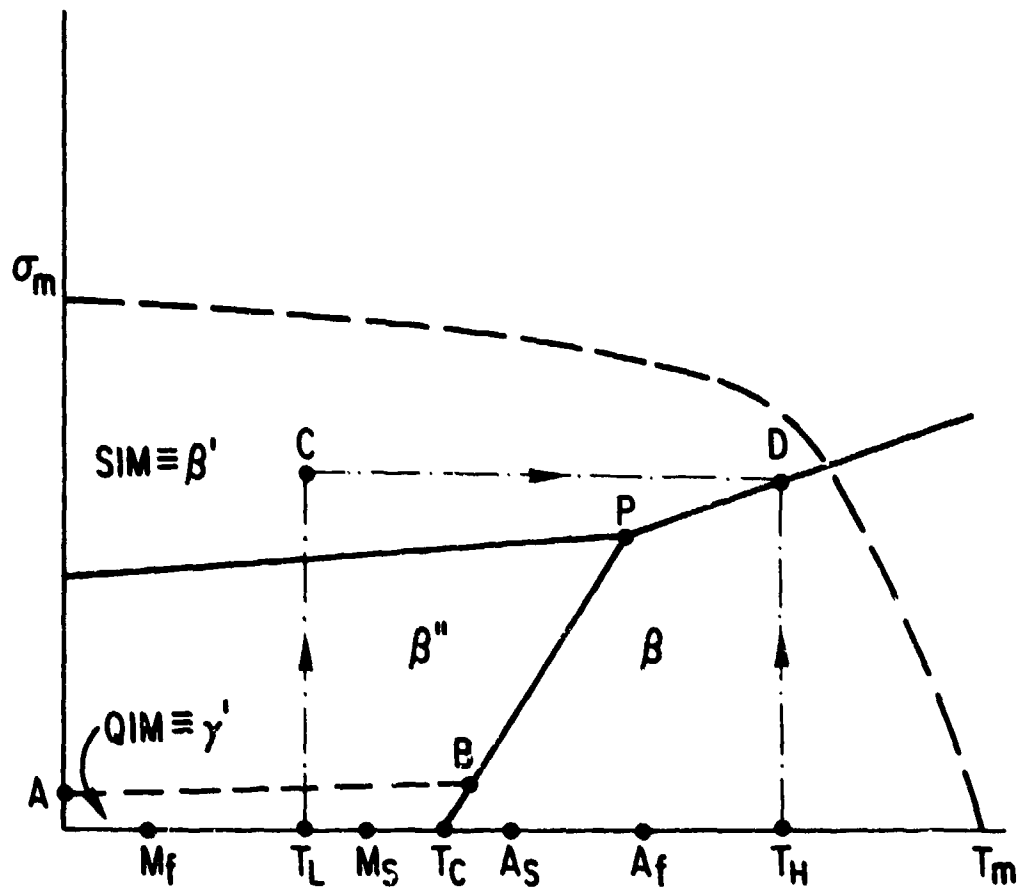
FIGURE 3 THE SCHEMATIC STRESS-TEMPERATURE PHASE DIAGRAM FOR A BINARY NITINOL SM ALLOY. THE DASHED CURVE DEFINES THE LIMIT BEYOND WHICH THE SRP MAY NOT OCCUR.

ELEMENT E ENTERS THE HR.

COLD RESERVOIR, T_L HOT RESERVOIR, T_H

γ' γ' γ' β

β' β' β'

(1)   (2)   (3)   (4)

ELEMENT E WITH THE β STRUCTURE ENTERS THE CR.
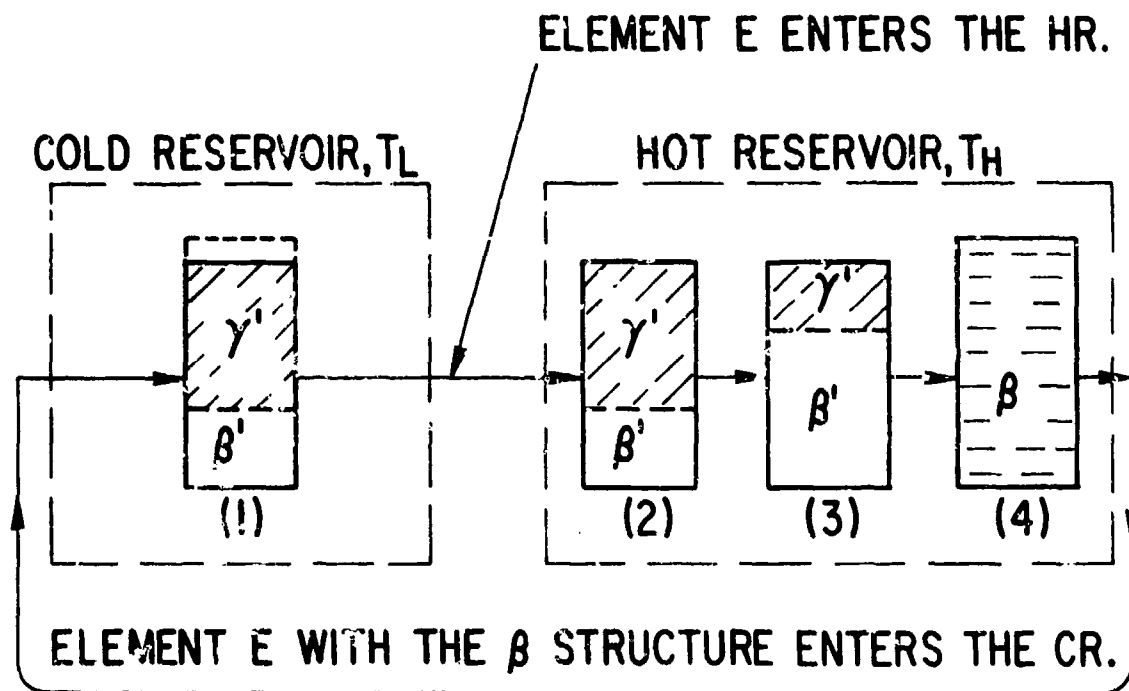
FIGURE 4   SCHEMATIC REPRESENTATION OF THE M→P TRANSFORMATION UNDER AN APPLIED STRESS, ACCORDING TO REACTIONS (3a) TO (3c) OF THE TEXT. (1) ELEMENT IS COMPRESSED BY A STRESS σ_i AT T_L; (2) AND (3), REACTION (3c) OCCURS AT T_H, PRIOR TO THE SR; (4) THE TRANSFORMATION AND SR UNDER A RESISTANCE STRESS σ_r HAVE BEEN COMPLETED.
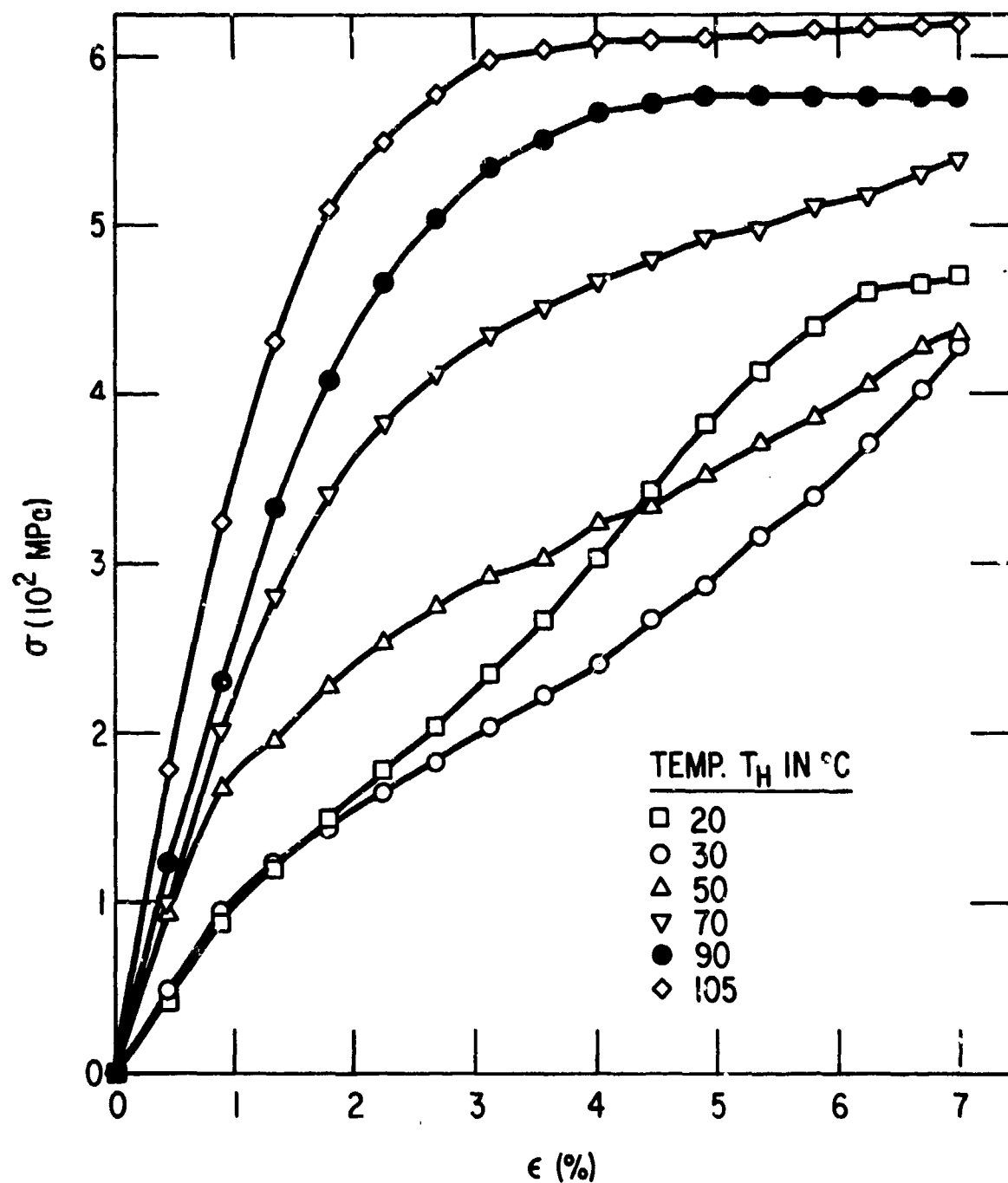
FIGURE 5   ISOTHERMALLY OBSERVED STRESS-STRAIN ($\sigma - \varepsilon$) CURVES FOR NITINOL
WIRE SPECIMEN (1 mm dia x 56 mm) WITH $T_C \simeq 33 \pm 7^O C$.
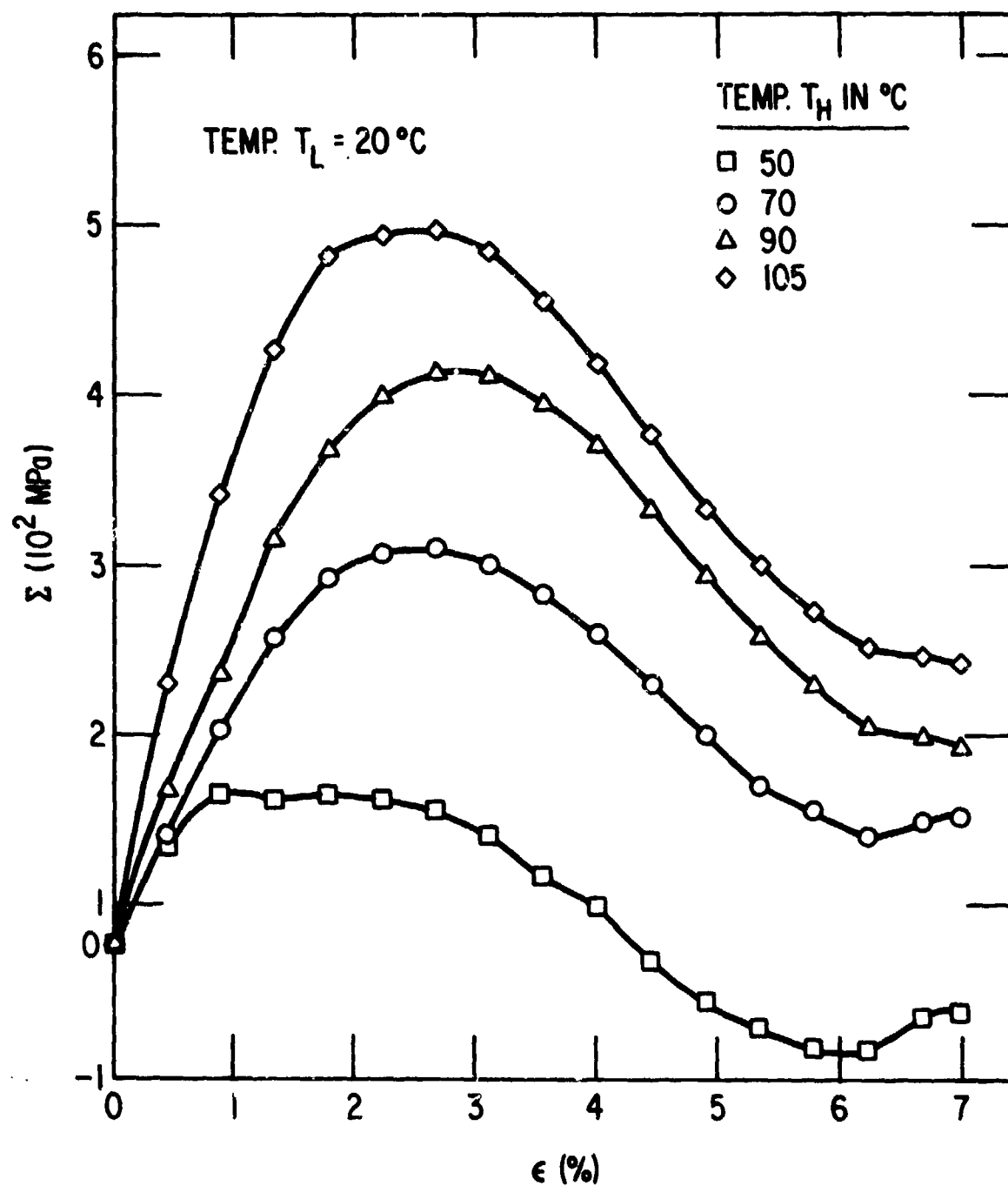
FIGURE 6   PLOTS OF Σ VS ε, EQ. (10), OBTAINED FROM ISOTHERMAL STRESS-STRAIN
DATA ON A NITINOL WIRE SPECIMEN (1 mm dia x 56 mm) WITH $T_C \simeq 33 \pm 7^{\circ}C$.
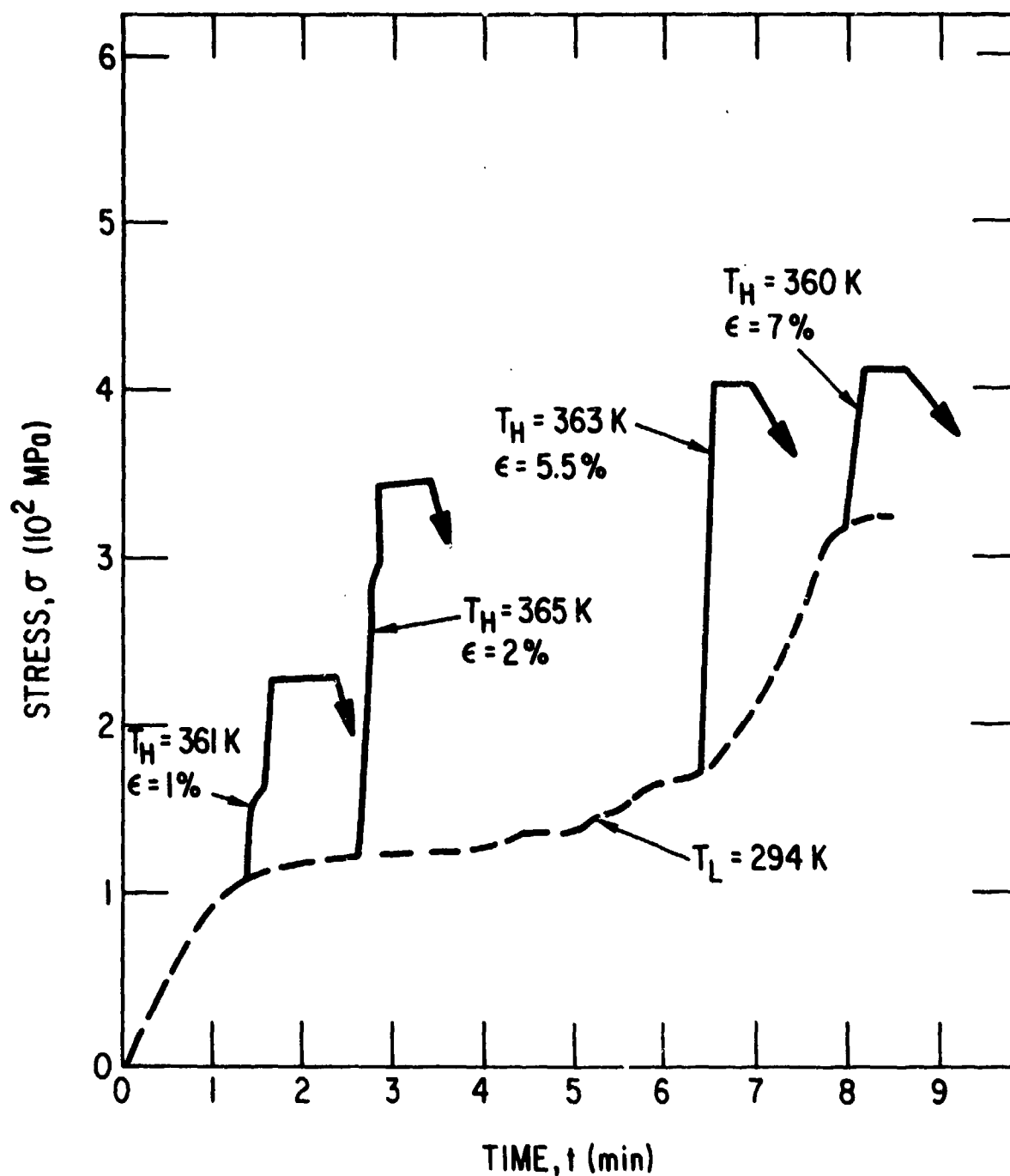
FIGURE 7   TRANSIENT STRESS RESPONSE OF A STRAIGHT NITINOL WIRE SPECIMEN
(1 mm dia x 56 mm) UNDER A CONSTANT STRAIN, SUBJECTED TO A
SUDDEN INCREASE IN TEMPERATURE.
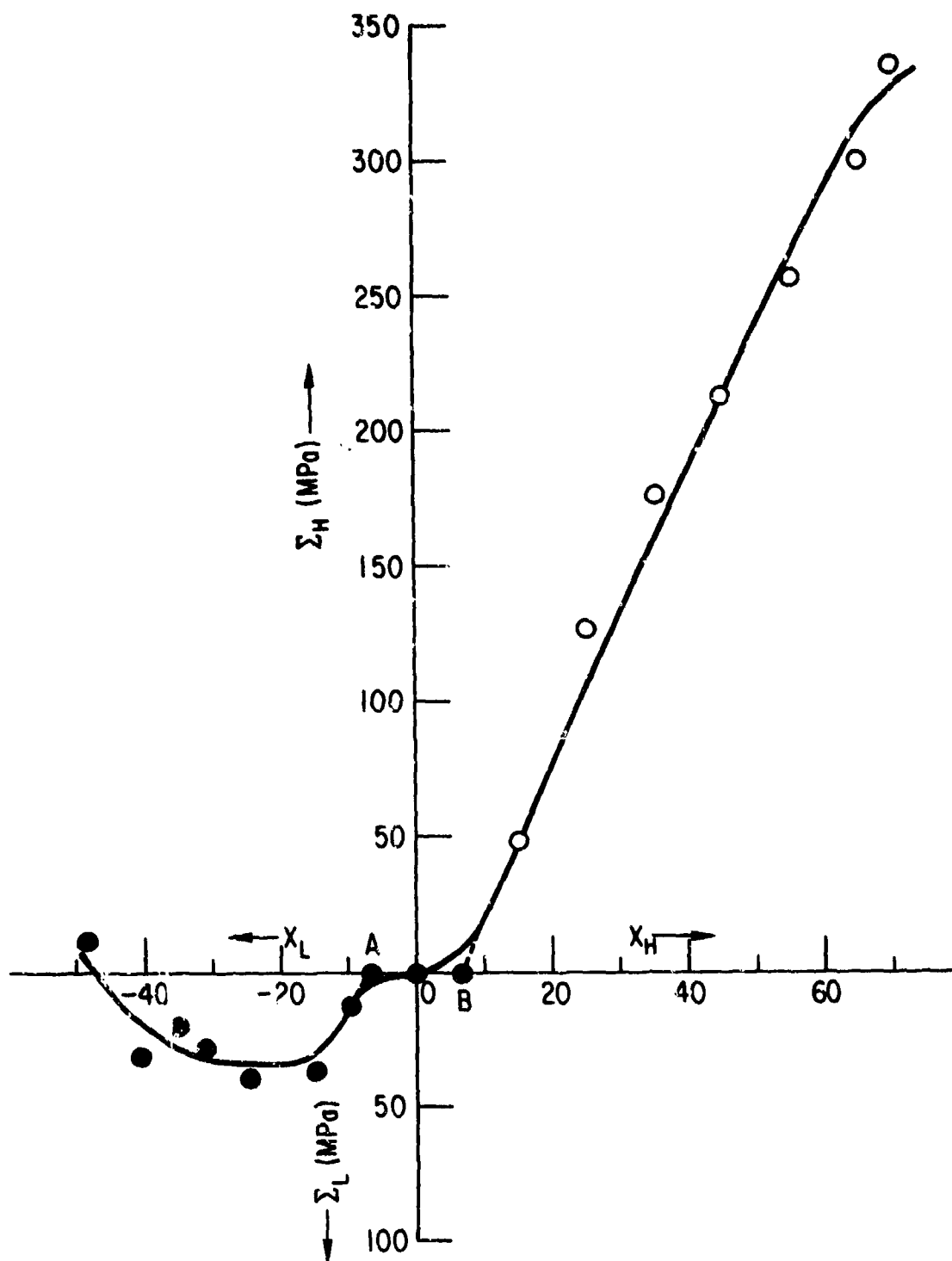
FIGURE 8   VARIATION OF Σ, EQ. (10), WITH ISOTHERMAL TEST TEMPERATURE FOR
FIXED $\varepsilon_i = 2.5\%$, $X_L = T_L - T_C$ AND $X_H = T_H - T_C$.
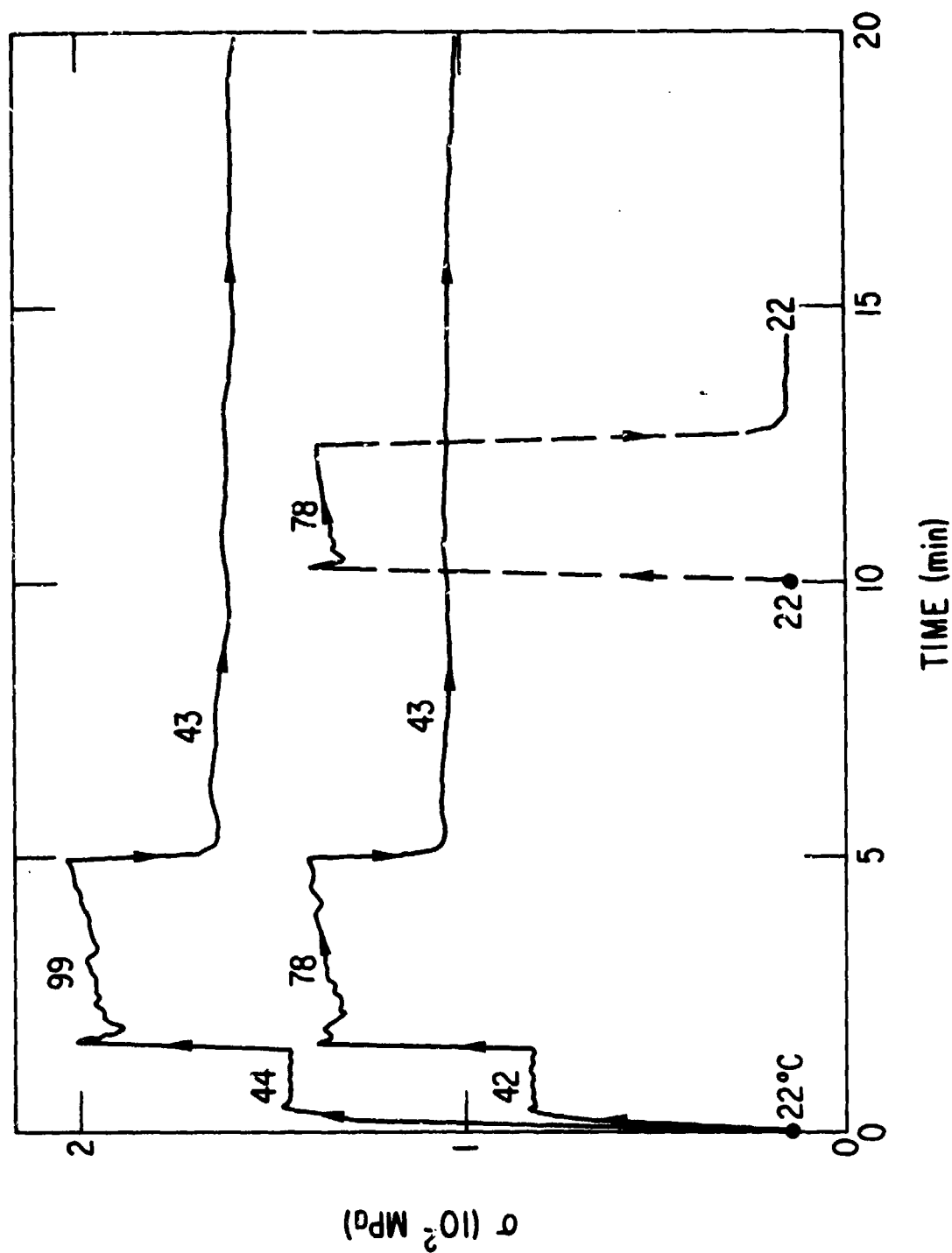
FIGURE 9   TRANSIENT STRESS RESPONSES OF NITINOL WIRE SPECIMEN (1 mm dia x 56 mm)
TRAINED IN CURVED SHAPE WITH SPAN 65 mm AND HEIGHT 13 mm. FIGURES
ON EACH CURVE ARE TEMPERATURES T_H AND T_L AT WHICH THE SR STRESS WAS
MEASURED.

REFERENCES

1. Many authors have studied various aspects of the shape-memory alloys. See, for instance, Shape Memory Effects in Alloys, edited by J. Perkins (Plenum Press, New York, 1975), and New Aspects of Martensitic Transformation, edited by Kobe, supplement to Trans. Jpn. Inst. Met., Vol. 17 (1976).

2. See, for instance, R. Banks and M. Wahlig, Technical Report LBL-5293, Lawrence Berkeley Laboratory (1976); and A. D. Johnson, IECEC 75 Record No. 759082, p. 530 (1974).

3. M. Ahler, Scripta Met. 9, 71 (1975).

4. H. C. Tong and C. M. Wayman, Met. Trans. 6A, 29 (1975). See also C. M. Wayman and H. C. Tong, Scripta Met. 9, 737 (1975) and 10, 1129 (1976).

5. B. Cunningham and K. H. B. Ashbee, Acta Met. 25, 1315 (1977).

6. A. A. Golestaneh, J. Appl. Phys. 49 (3), 1241 (1978). A somewhat different treatment was used in this paper, as we will explain in more detail in the present paper.

7. P. Wollants, M. DeBonte, L. Delaey, and J. R. Roos, Z. Metallkde, Part I, p. 147, Bd 70 (1979) H.3 and Part II, p. 298, Bd 70 (1979) H.5.

8. A. A. Golestaneh, "Martensitic Phase Transformation in Shape Memory Alloys," Proceedings of International Conference on Martensitic Transformation (ICOMAT - 79) at Massachusetts Institute of Technology, Boston, MA, June 24, 1979, pp. 679-692.

    See also A. A. Golestaneh, "Energetic Shape Recovery Associated with Martensitic Transformation in Shape Memory Alloy," Acta Metallurgica in press.

9. H. A. Mohamed Tawancy, J. Mater. Sci. 14, 1339 (1979).

10. The engine described here operates at ⌢40 r/min and generates 5 mW of power. Engines with different geometries have also been constructed; for instance, see Reference 5, and the article by R. Banks in Shape Memory Effects in Alloys (Reference 1).

11. The process of "training" the SM element into a given shape essentially consists of annealing the element (kept constrained in the desired shape) at a temperature T for a time t. Both T and t depend on the SM alloy composition and geometry.

12. A detailed description of the latent heat $\Delta H_{\gamma'\beta}$ and $\Delta H_{\beta'\beta}$ is in Reference 8.

13. In the present work we exclude the effects of element geometry and other material parameters which affect the heat exchange rate and kinetics of the SRP.

14. The kinematics of the SRP will be presented in a separate article.

15. A. A. Golestaneh, The Shape-recovery Phenomenon in Shape-memory Alloys, with Particular Reference to the NITINOL System—Review and Recommendations, Argonne National Laboratory Special Report (August 1978).

16. The transient stress data are obtained as follows: (a) Strain the specimen, surrounded by a water bath at temperature T_L, to a fixed value; (b) change the water temperature rapidly from T_L to T_L while keeping the specimen constrained under constant strain; and (c) measure the stress change due to the change $T_H - T_L$.

17. A more detailed comment on the work of Reference 9 is given by A. A. Golestaneh, "Comments on the Thermal Efficiency of an Ideal Shape-Recovery Cycle," Scripta Met., V. 14, August, 1980, pp. 845-848.

THERMODYNAMICS OF SME-ENGINES

P. Wollants, M. De Bonte, L. Delaey and J. R. Roos
(Department Metaalkunde, Katholieke Universiteit Leuven, Belgium)

ABSTRACT

Recently a number of papers discussed the possibility of using the shape memory effect and two-way shape memory effect for direct conversion of heat into mechanical energy through a work performing transformation cycle.[1,2,3,4,5,6,7] Some authors tried to calculate the efficiency of this work performing cycle. However, the results published were very divergent and even contradictory and consequently caused some serious misunderstandings. The literature highly overestimated many efficiency values due to the selection of wrong thermodynamic data and to the violation of some basic thermodynamic principles. A rigourous thermodynamical treatment of the stress-induced martensitic transformation in a single crystal has been published by P. Wollants, et al.[8] The results of this analysis are extremely important for any calculation concerning efficiency or power capacity of a solid state engine. Therefore, this paper summarizes the most important conclusions of this analysis. Next a work performing cycle of a CuZnAl single crystal is described, and finally efficiency values reported in the literature are discussed and corrected.

[1] Tong, H. C., and Wayman, C. M., Met. Trans. 6A (1975) 29.

[2] Ahlers, M., Scripta Met. 9 (1975) 71.

[3] Wayman, C. M., and Tong, H. C., Scripta Met. 9 (1975) 757.

[4] Delaey, L., and Delepeleire, G., Scripta Met. 10 (1976) 959.

[5] Tong, H. C., and Wayman, C. M., Scripta Met. 10 (1976) 1129.

[6] Johnson, A. D., IECEC '75 Record, 759082.

[7] Cunningham, B., and Ashbee, K. H. G., Acta Met. 25 (1977) 1315.

[8] Wollants, P.; De Bonte, M.; and Roos, J. R., accepted for publication in Zeitschr. Metallk.

1. A THERMODYANIC ANALYSIS OF THE STRESS-INDUCED MARTENSITIC TRANSFORMATION IN A SINGLE CRYSTAL[8]

For describing the thermodynamic behavior of the stress-free crystal and the crystal under stress, the following important thermodynamic state functions are defined:

Stress-free crystal		Crystal under stress	
$H = U + PV$	(1)	$H^* = U + PV - FL$	(1)'
$G = H - TS$	(2)	$G^* = H^* - TS$	(2)'

From thermodynamic standpoint both the stress-free and the stressed crystal may be considered at closed systems, for which the fundamental equations are expressed as the total derivatives of their independent thermodynamic variables P and T, and P, F, and T, respectively.

$dG = VdP - SdT$	(3)	$dG^* = VdP - LdF - SdT$	(3)'

It follows that the important partial derivatives of the characteristic functions G and G* with respect to their independent variables are:

$$\left(\frac{\partial G}{\partial T}\right)_P = -S \qquad (4) \qquad \left(\frac{\partial G^*}{\partial T}\right)_{P,F} = -S \qquad (4)'$$

$$\left(\frac{\partial G}{\partial P}\right)_T = V \qquad (5) \qquad \left(\frac{\partial G^*}{\partial F}\right)_{P,T} = -L \qquad (5)'$$

Fig. 1 represents these relations.

From the fundamental equations (3) and (3)' we obtain immediately the conditions for thermodynamic equilibrium:

$$dG_{T,P} = 0 \qquad (6) \qquad dG^*_{T,P,F} = 0 \qquad (6)'$$

For an isobaric change of state of the stress-free crystal, the heat exchange ΔQ (o) equals the enthalpy change ΔH; and in the same way for an isoforce-isobaric change of state of the crystal under stress the heat exchange ΔQ (F) equals ΔH^*, the change of the state function H*

$$\Delta H = \Delta Q (o) \qquad (7) \qquad \Delta H^* = \Delta Q (F) \qquad (7)'$$

Between ΔH and ΔH^* there exists thus the important relation

$$\Delta H^* = \Delta H - F \Delta L \qquad (8)$$

---

[8]See footnote 8 on page 6-1.

which explains the work performing capacity associated with the martensitic transformation in a crystal under stressed conditions. The variation of ΔH^* with thermodynamic equilibrium (this means changing F and T to maintain thermodynamic equilibrium, P being kept constant) is given by the equation:

$$\frac{d(\Delta H^*)}{dT} = \Delta C_F + \frac{\Delta H^*}{T} \tag{9}$$

If the value of $\frac{\Delta H^*}{T}$ is much larger than the value of ΔC_F it follows from equation (9) that

$$\frac{\Delta H^*}{T_0\,(F)} = \text{constant} \tag{10}$$

From the equilibrium criteria (6) and (6)' the most important Clausius-Clapeyron and Clausius-Clapeyron-like relations are deduced:

$$\frac{dP}{dT} = \frac{\Delta H}{T_0\,(0).\Delta V} \tag{11} \qquad \Big| \qquad \frac{dF}{dT} = - \frac{\Delta H^*}{T_0\,(F).\Delta L} \tag{11'}$$

$$\text{or} \qquad \frac{\Delta H - F.\Delta L}{T_0\,(F).\Delta L}$$

which relate the values of P and T and F and T at thermodynamic equilibrium.

If (10) remains valid over a wider range of temperatures and forces, integration of equation (11)' becomes very simple:

$$F = \text{const. } \Delta T \tag{12}$$

It must be emphasized that in equation (11)' "F" is written instead of "P" and "Δl" instead of "ΔV", and that the minus sign appears. The reason is that the partial derivative of the characteristic function "G" of the unstretched crystal $\frac{\partial G}{\partial P}\Big|_T = V$, has the opposite sign of the analogous derivative of the characteristic function "G*" of the stretched crystal: $\frac{\partial G^*}{\partial P}\Big|_T = -L$. Also, "$\Delta V$" for thermo-elastic martensites is much smaller than the transformation elongation "ΔL" due to the formation of stress-induced thermo-elastic martensite. Therefore the influence of hydrostatic pressure on the shift in equilibrium temperature will be much smaller than the influence of an uniaxially applied force.

Fig. 2 illustrates schematically, the Clapeyron-like relation, approaching the G* - T curves by straight lines. This implies that the transformation entropy remains constant in the interval of temperature under consideration. Further, if equation (10) is correct, it follows that G* - T and the G - T lines are parallel to each other. Equation (11)' suggests ΔH^* P→M can be calculated if the F-T relationship and the transformation elongation ΔL are known (e.g. from tensile experiments). It also follows that a linear F-T relation--which is usually reported--implies a linear ΔH^* - T_0 (F) relation, since ΔL is constant at first approximation. But since in that case $\Delta H^*/T_0$ (F) is constant, ΔS also must be constant.

2. A THERMODYNAMIC ANALYSIS OF A WORK PERFORMING CYCLE ASSOCIATED WITH THE MARTENSITIC TRANSFORMATION

Based on the results of the thermodynamic analysis of the stress-induced martensitic transformation in a single crystal[8], a work performing cycle of this single crystal has been analysed thermodynamically.[9] A correct formula for the theoretical attainable efficiency "η" of this energy conversion system is deduced. The cycle is represented in a TS-diagram. Assuming some justified approximations, both the efficiency formula and the TS-diagram are converted into a convenient form.

Let us assume we have at our disposal a rod shaped single crystal showing the shape memory effects, and trained under compression and tension, such that the shorter shape can be associated with the martensitic phase and the longer one with the parent phase. We will describe now the work performing cycle of this crystal between the lower transformation temperatures $M_f(o)$ and $M_s(o)$ and the transformation temperatures at high stress level $A_s(\sigma)$ and $A_f(\sigma)$.

In "state 1" the crystal is stress-free at a temperature $M_f(o)$, which is the temperature at which the P$\rightarrow$M transformation of the unstressed crystal is completed. At this temperature the crystal is reversibly stressed until a compressive stress level σ is reached. This is "state 2" of the crystal. From the temperature $M_f(o)$ the crystal is now reversibly heated at constant external stress until at the temperature $A_s(\sigma)$ "state 3" is reached.

$A_s(\sigma)$ is the temperature at which the M$\rightarrow$P transformation starts when the crystal is under stress σ. The transformation is completed at $A_f(\sigma)$, reaching "state 4." Next the crystal is reversibly unloaded at constant temperature, so "state 5" is realised. The stress-free crystal is then cooled reversibly from $A_f(\sigma)$ to $M_s(o)$ ("state 6"), and finally at the temperature $M_s(o)$ the stress-free P$\rightarrow$M transformation starts, and is completed at $M_f(o)$. The crystal is now back in its initial "state 1." The cycle is closed and may be repeated.

The results of a rigourous thermodynamic analysis of this work-performing cyclic process are presented in Table 1, where, for the successive changes of state of the crystal (1$\rightarrow$2; 2$\rightarrow$3; 3$\rightarrow$4; 4$\rightarrow$5; 6$\rightarrow$1), the respective changes in T, σ, and L of the crystal are given, as well as the work exchanges, heat exchanges, and changes in entropy involved.

By means of the information in Table 1, various diagrams such as a σ-T diagram, a σ-L diagram, a L-T diagram, a σ-T-L diagram and a T-S diagram are easily constructed. As an example, in Fig. 3 a T-S diagram is drawn in a qualitative way.

Concerning Table 1 the work performing cycle can be simplified substantially by introducing some justified approximations.

(1) First of all, the elastic deformation work during isothermal loading is approximately identical to the work performed during reversible isothermal unloading:

---

[8] See footnote 8 on page 6-1.

[9] Wollants, P.; De Bonte, M.; Delaey, L.; and Roos, J. R., accepted for publication in <u>Zeitschr. Metallkde.</u>

$$\frac{\sigma \, \epsilon_e^M}{2} \simeq \frac{\sigma \, \epsilon_e^\beta}{2} \; ; \; \text{if } \epsilon_e^M \simeq \epsilon_e^\beta.$$

Therefore, concerning the closed cycle, there is no net to work performance due to the elastic loading and unloading of the crystal. Even when $\epsilon_e^M \neq \epsilon_e^\beta$ then still $\epsilon_e^M - \epsilon_e^\beta$ is much smaller than ϵ_{tr} so that no significant error is introduced by neglecting these work terms.

(2)   It can be shown that the entropy effects due to isothermal elastic loading and unloading of the crystal are negligibly small.[9]

(3)   For a single crystal in which one martensitic varient is stress-induced, M_f (o) and M_s (o) are nearly identical. The same holds for A_s (o) and A_f (o). This is confirmed by experiments of Salzbrenner and Cohen[10] on a CuAlNi single crystal and by tensile tests of Van Humbeeck[11] on a Cu-25,33 at % Zn - 9,11 at % Al single crystal (Fig. 4). Especially in the last case, the hysteresis between M_s (σ) and M_f (σ) was remarkably small. If, however, no hysteresis effects are considered, then M_f (o), M_s (o), A_s (o) should coincide. In this case the martensitic transformation is completely described by the chemical equilibrium temperatures To (o) and To (σ).

(4)   Concerning the heat capacity C_σ (or C_F), it can be shown that it is almost identical to C_p (heat capacity of constant pressure) and that its value is extremely insensitive to even large variations in F.[9] So we can replace "C_σ" by "C_p". Further we suppose C_p^M to be nearly identical to C_p^P, which is--in view of the usually reported linear σ-T relationship--a good approximation.[1]

As a good approximation, C_p can be regarded to be independent of temperature in the T-interval under consideration, if T_o (o) is $\gg$ T-Debye. If this is not so, C_p can be replaced by $\bar{C}_p$, the mean specific heat for the T-interval.

Taking into account all these approximations, the thermodynamic analysis of the cyclic process leads to much simpler results (Table 2).

Defining the efficiency of this cyclic process as the ratio of work output to heat added from the hot reservoir, Table 2 immediately leads us to the following expressions:

$$\eta = \frac{W}{Q} = \frac{- F \, \Delta L}{\bar{C}_p \cdot \Delta To = \Delta H_{To \, (\sigma)}^*} \times 100\% \tag{13}$$

---

[9] See footnote 9 on page 6-4.

[10] Salzbrenner, R. J., and Cohen, M. submitted to Acta Met.

[11] Van Humbeeck, J.; Delaey, L.; and Deruyttere, A., Z. Metallkde 69 (1978) 575.

[1] See footnote 1 on page 6-1.

which is identical to:

$$\eta = \frac{\Delta H_{To(\sigma)} \times \Delta To}{To(o)\left[\bar{C}_p \cdot \Delta To + \Delta H^*_{To(\sigma)}\right]} \times 100\% \tag{14}$$

since

$$\Delta H^* = \Delta H - F\Delta L \quad \text{(see Eq. 8)}$$

and

$$\frac{\Delta H^*}{To(\sigma)} = \frac{\Delta H}{To(o)} \quad \text{(see Eq. 10).}$$

3. THE WORK PERFORMING CYCLE OF A CuZnAl SINGLE CRYSTAL[12]

We calculate a work performing cycle for a single crystal of a Cu-25, 33 Zn - 9,11 Al (at %) alloy. The necessary data are in Table 3 and Fig. 7.

For To (o) = 206 K, work, power, and efficiency have been calculated. Fig. 6 and 7 show the results as a function of ΔTo. Efficiencies are also calculated (Fig. 7) for To (o) values of 100 K, 300 K, and 400 K (for the lower temperatures, corrections for C_p have been made).

From Fig. 5 it follows that only for a cold reservoir at about $100^\circ K$ efficiencies of 10 to 11% may be realised. For To (o) temperatures in the vicinity of room temperature, maximum efficiencies of 3 to 4% are to be expected.

The TS-diagram is constructed, using the ΔS-expressions in Table 2. To (o) is 206 K and the $\bar{C}_p$ value used is 5.7 cal. mole^{-1} K$^{-1} \simeq 23.85$ J. mole^{-1} K^{-1}. Fig. 8 represents the result.

4. DISCUSSION

From the foregoing calculations it is obvious that the theoretical maximum efficiency of this work-performing cycle of this CuZnAl-single crystal with the low temperature reservoir at about room temperature is 3 to 4%. Other authors, however, have reported efficiency values up to 20% (and even higher). A thorough investigation of their published results revealed:

-- that $\Delta Q(o)$ has always been used instead of $\Delta Q(\sigma)$

-- that many times wrong thermodynamic data have been selected

-- and that some basic thermodynamic principles have been violated.

---

[12]Wollants, P.; De Bonte, M.; Delaey, L.; and Roos, J. R., accepted for publication in Zeitschr. Metallkde.

Let us first consider the formula arrived at by Tong and Wayman:[1]

$$\eta = \frac{\Delta Q \left(\frac{\Delta To}{To\,(o)}\right) \left(\frac{\ln(1+\epsilon)}{\epsilon}\right)}{\Delta Q + C_p \,\Delta To}$$ (15)

The same ΔQ has been used both in the numerator and the denominator. In a reply to the remark of Delaey and Delepeleire[4] that $\Delta Q\,(o)$ and $\Delta Q\,(\sigma)$ should be different in order to obtain any work at all, Tong and Wayman[5] nevertheless affirmed that $\Delta Q\,(o)$ and $\Delta Q\,(\sigma)$ should be equal, except for a correction factor which could be neglected. The statement, however, is based on a wrong interpretation of Kirchoff's equation:

$$\Delta Q\,(\sigma) = \Delta Q\,(o) + \int_{To\,(o)}^{To\,(\sigma)} \Delta C_p \cdot dT$$ (16)

This equation should be used only for constant pressure processes in the absence of any external load. If ΔC_p is much smaller than $\frac{\Delta H^*}{To\,(\sigma)} = \Delta S_{tr}$, then the relation $\Delta Q\,(\sigma) = \Delta Q\,(o)\frac{To\,(\sigma)}{To\,(o)}$ is valid. Since $\Delta Q\,(\sigma) - \Delta Q\,(o) = -F \cdot \Delta L$ it is evident that there would be no work performance at all if $\Delta Q\,(o)$ and $\Delta Q\,(\sigma)$ were equal.

For a AgCd alloy Tong and Wayman[1] further estimate C_p to be 4 cal mole^{-1} K^{-1}. This value is far too low. A reasonable value for C_p can be obtained from the Neumann-Kopp rule which states that $C_{p\,(alloy)} \simeq \Sigma_i N_i C_{pi}$. Using this rule we calculated for $\bar{C}_{p\,(alloy)}$ in the T-interval $|100\,K - 200\,K|$ a value of about 5.46 cal. mole^{-1} K^{-1}, selecting C_p - values for Ag and Cd from Hultgren.[13]

If Tong and Wayman had used $C_p = 5.46$ cal. mole^{-1} K^{-1} and $\Delta Q\,(\sigma) = \Delta Q\,(o)\frac{To\,(\sigma)}{To\,(o)} = 200$ cal. mole^{-1} instead of $\Delta Q\,(o) = 100$ cal. mole^{-1}, they would have found an efficiency value of about 12.8%. This value is still high, but the reason herefore is their extremely low To (o) value. One can see from Fig. 7 that for To (o) = 100 K we found approximately the same efficiency value.

---

[1]See footnote 1 on page 6-1.

[4]See footnote 4 on page 6-1.

[5]See footnote 5 on page 6-1.

[13]Hultgren, R.; Desai, P. D.; Hawkins, D. T.; Gleiser, M.; Kelley, K. K.; and Wacman, P. D., Selected Values of the Thermodynamic Properties of the Elements, American Society for Metals (1973).

Ahlers[2] calculated the efficiency of a work delivering cycle performed by a Cu-36 at % Zn - 1.75 at % Al single crystal using the equation:

$$\eta = \frac{\gamma_M \left(\frac{d\tau}{dT}(T_2 - T_1) - \Delta\tau\right)}{C(T_2 - T_1) + \Delta H} \times 100 \qquad (17)$$

and found a value of 4.1% with $\gamma_M = 0.17$; $d\tau/dT = 0.096$ kg mm^{-2} K^{-1}, $\Delta\tau = 0.5$ kg mm^{-2}, C = 6 cal mole^{-1} K^{-1}; $\Delta H = 4.45$ kg mm^{-2}, M_s (o) = 273 K and ΔT_o = 100 K. Taking into account the F-T dependence of ΔH, Ahlers would have arrived at 3.95%. Ahlers' result agrees well with our calculations. Wayman and Tong[3] however claim that this low value is only due to the use of unfavourable thermodynamic data. Consequently they recalculated η with another set of—according to them—more accurate values. First of all they "select" for M_s (o) 193 K and put $\bar{C}$ = 4 cal mole^{-1} K^{-1}, arguing as follows: "... Since the M_s temperature is probably 100 K below the Debye temperature for the CuZnAl alloy it is reasonable to take: $C = \bar{C}_p = 2/3 \times 6$ cal mole^{-1} K^{-1} ...." We prefer to estimate $\bar{C}_p$ with the Neumann-Kopp rule mentioned above. Taking C_p values for Cu, Zn, and Al from Hultgren[13], we arrive at a $\bar{C}_p$ value for T | 193 K 293 K| of 5.72 cal mole^{-1} K^{-1}.

Furthermore, Ahlers uses the product of shear stress and shear strain to calculate the work performed during the transformation. As a matter of fact the contribution of the normal to the habit plane is much less and can generally be neglected. Wayman and Tong[3] claim that the value of $d\tau/dT$ used by Ahlers is far too small. They derive a value for $d\tau/dT$ from a figure published by Pops and Ridley.[14]

This figure, however, shows a σ-T relationship and not a τ-T relationship. In so doing, Wayman and Tong combine a shear strain with a uniaxial tensile stress, which is, of course, much higher than the resolved shear stress in the habit plane. Therefore, the efficiency value as calculated by Wayman and Tong (21.3%) is wrong, a better estimate being the one by Ahlers. The same remarks apply to their calculations made for a CuAlNi alloy.[3]

The "Carnot Efficiency of the Marmem Engine" as introduced by Cunningham and Ashbee:[7]

$$\eta = 1 - \frac{M_f(\sigma \to o)}{A_f(\sigma = o) + \sigma_{max} \frac{dA_f}{d\sigma}} \qquad (18)$$

---

[2]See footnote 2 on page 6-1.

[3]See footnote 3 on page 6-1.

[13]See footnote 13 on page 6-7.

[14]Pops, H., and Ridley, M., Met. Trans. 1 (1970) 2653.

[7]See footnote 7 on page 6-1.

is not a good indication for the true maximum attainable efficiency of the Marmem Engine, since it does not take into account the heat capacity of the system. The high "$\sigma_{max}\frac{dA_f}{d\sigma}$" - values of β-brass and NiTi alloys may indicate the fact that the work-output will be large. Anyhow, the conclusion of the authors that efficiencies higher than 10% (i.e. at least half of the Carnot efficiency is realised as useful work) are obtained is not justified by their arguments.

The work performing cycle as proposed by Johnson is shown in a σ-ε diagram (Fig. 9a) and in a T-S diagram (Fig. 9b). From state A to state B, the material undergoes a sudden adiabatic contraction followed by an approach to thermal equilibrium at temperature T_H. According to Johnson[6] the entropy effect involved is positive and larger than the entropy effect due to cooling and transformation. We showed that the entropy change due to isobaric isothermal stretching of the wire is given by

$$\Delta S = \alpha L_o F + \frac{\alpha L_o F^2}{2E\,A} \tag{19}$$

So, if the wire snaps back isothermally, the entropy change is the negative of this value. Therefore point B on Fig. 9b should be on the left side of point A. The absolute value of the entropy change involved, according to formula (19) is of the order of magnitude of 0.1 J. mole^{-1}. K^{-1}. From B to C the wire cools down and simultaneously transforms to the martensitic phase. Both the entropy effects involved--first a decrease in entropy due to the isostress cooling of the wire, and second a decrease in entropy due to the parent to martensite transformation--are a few orders of magnitude larger than the entropy change involved in step A→B.[9] Steps C→D, and D→A must be treated in an analogous way as steps A→B and C→D, respectively. It is now evident that the T-S diagram proposed by Johnson is not correct. Fig. 9c presents a correct T-S diagram. Points A and B are very close to one another. At B the wire starts cooling and at B^l the parent to martensite transformation is initiated. At C the transformation stops and from C to D the material is loaded again isothermally. From D to D^l the wire is heated. At D^l the martensite to parent transformation starts and is completed at A. Johnson's[6] efficiency formula

$$\varepsilon = \frac{(\Delta Q_{AB} - \Delta Q_{BB'} - \Delta Q_{CD} - \Delta Q_{DD'})}{\Delta Q_{AB} - \Delta O_{BB'}} \tag{20}$$

apart from being based on a faulty T-S diagram is also wrong. The heat effects $\Delta Q_{AB'}$.... are associated with the adiabatic (un)loading of the wire. So this formula does not take into account the latent heat of transformation. It has been shown[8,9] that precisely the difference between the latent heat of the stress-free transformation and the latent heat of the

_____

[6]See footnote 6 on page 6-1.

[9]See footnote 9 on page 6-4.

[8]See footnote 8 on page 6-1.

transformation under stressed conditions is mainly responsible for the work performance. Further the heat capacity of the system is also neglected.

Cory and Mc Nichols[15] claim that the efficiency of heat engines for low-grade thermal energy conversion is critically dependent on thermodynamic cycle selection. They select three cycles for discussion: a "TA-cycle," consisting of two isotherms and two adiabats; a "T^1-cycle," consisting of two isotherms and two paths of constant length; and a "F^1-cycle," consisting of two paths of constant force and two paths of constant length. For each of these cycles, the efficiency is calculated for various temperature differences, and compared to the Carnot efficiency. For the TA-cycle they calculate a η/η_C value of 80%. However, since ΔT in this case is limited to 25 K (with the lower temperature at $\sim$ 300 K), true efficiency is restricted to $\frac{325 - 300}{325}$ x 80 $\simeq$ 6.2%. For the "T1-cycle" and the "F1-cycle," lower η/η_C ratios are found, but since in these cases ΔT can be made larger, true efficiencies still range from 5..to..3%. The authors' remark that "... With a 150 degree temperature difference between the heat source and sink, and an engine efficiency of 80 percent of Carnot, the net efficiency of 25 percent is comparable ...." is in straight contradiction to their own calculations, since 80 percent of Carnot is only realised for the "TA-cycle," and for this cycle ΔT is restricted to about 25 K (if such a cycle can be realised at all, considering the two adiabats involved).

Golestaneh[16] discusses the efficiency of a solid state engine made from NITINOL memory material. He defines the thermal energy per cycle which can be converted to mechanical energy as

$$W = \alpha m \Delta H - W_D \tag{21}$$

where W_D is the energy required for producing m mass of the martensitic structure by a deformation process at To; α is the fraction M$\to$P transformation; and ΔH is the latent heat of transformation. This expression assumes the latent heat of transformation may be entirely converted to mechanical energy if $\alpha = 1$ (M$\to$P transformation complete) and $W_D = 0$ (low stress-level at zero stress). We have shown this is not true at all.[8] Golestaneh further defines $W_D = \alpha' \alpha m \Delta H$ and $(1-\alpha') = \beta$. It follows that $W = \alpha \beta m \Delta H$. This expression is substituted in $\eta = \frac{W}{Q_a}$, where $Q_a = m \int_{To} C_M \, dT + \alpha \, m \, \Delta H +$ $m \int_{T\sigma} |\alpha C_p + (1-\alpha) C_M| \, dT$. Taking $C_p = C_M = C$; $h = C^{-1} \Delta H$ and $x = T\sigma - To$ Golestaneh arrives at

$$\eta = \beta \alpha h \ |x + \alpha h|^{-1} \tag{22}$$

---

[15]Cory, J. S., and Mc Nichols, J. L., IECEC '78 Record.

[16]Golestaneh, A.A., J. Appl. Phys. 49 (3), 1978.

[8]See footnote 8 on page 6-1.

for the efficiency of the solid state engine. However, since the definition of W is wrong, this formula cannot be correct, and all further arguing of Golestaneh about relations and restrictions between the parameters α, β. X...is rather irrelevant. Due to the use of an incorrect formula for η, the estimated efficiencies of 12 to 20% are again largely exaggerated.

Based on measurements on a Ni 55 Ti 45 wire, Baumgart[17] has calculated a maximum efficiency of about 1.5% if only the latent heat of transformation is added. This value seems very low, but the author says it only roughly estimates a realistic order of magnitude.

From the foregoing discussion it appears that very high efficiencies ($\sim$ 20%) for the work delivering cycle of an SME-engine are to be excluded. Maximum energy conversion efficiencies for completely transforming single crystals, with the low temperature reservoir at about room temperature, of 4 to 5% are to be expected.

If a heat source is available at a very low cost, this low efficiency may not be objectionable if the generated power per unit mass of working substance is high enough. Table 4 collects both calculated and experimentally determined power-values. Experimentally determined values are at least an order of magnitude lower than the theoretically calculated values.

CONCLUSIONS

1. Based on a rigourous thermodynamical treatment of the stress-induced martensitic transformation in a single crystal, it has been shown that

— the condition for thermodynamic equilibrium at constant T, P, and F of the stretched crystal is the minimization of the characteristic function $G^* = U + PV - FL - TS$;

— the Clausius-Clapeyron-like equation which describes the influence of F (or σ) and T on the transition temperature To (F) is:

$$\frac{dF}{dT} = \frac{-\Delta H}{To(F) . \Delta L}$$

— and the difference between ΔH^* (σ) ($\equiv \Delta Q(\sigma)$) and $\Delta H(o)$ ($\equiv \Delta Q(o)$) equals the work performance during the reverse transformation.

2. A work performing cycle for a CuZnAl single crystal has been analysed thermodynamically. A correct efficiency formula has been derived and a convenient TS-diagram constructed.

3. With the temperature of the cold reservoir at about 300 K, maximum theoretical efficiencies (η) of 3 to 4% are to be expected. Increasing Δ To above 30 or 40°K does not influence η markedly, but the power generated increases almost linearly as a function of T.

4. The available literature concerning TS-diagrams, η and power of the solid state engine is very confusing, contradictory, and often erroneous. The construction of faulty TS-diagrams and the selection of incorrect thermodynamic data have been responsible for the appearance in the literature of too many highly overestimated efficiency values.

---

[17] Baumgart, F., Jorde, J; and Reiss, H. G., Techn. Mitt. Krupp 34 (1976) 1.

5. Concerning power generation of the solid state engine, theoretical maximum values of the order of magnitude of 10^3 Watt kg^{-1} are found. Reported values of true existing machines are much lower: 130 Watt kg^{-1}, 9 Watt kg^{-1}, 2.85 Watt kg^{-1} and 0.5 Watt kg^{-1}. If one wants to use the solid state engine for conversion of low grade thermal energy to mechanical energy, values of at least 10^3 Watt kg^{-1} should be realised.

6. Direct applications can rather be found where power generation is not the principal aim. One might think of special devices such as regulation systems, tube fittings ... where a small but controllable work output is needed or generation of T-controlled stresses is required.

ACKNOWLEDGEMENTS
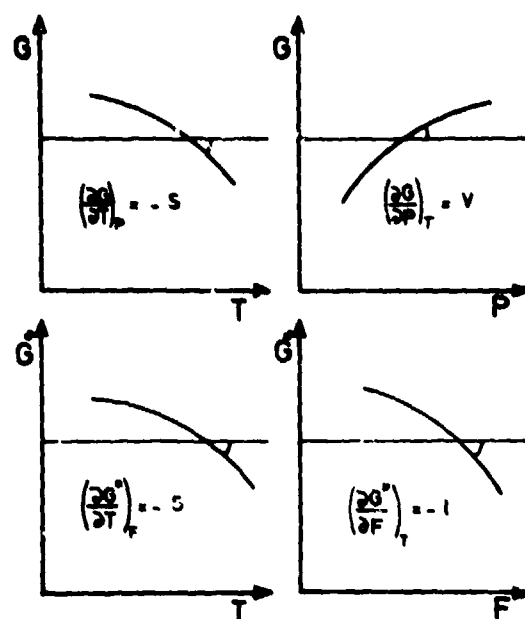
FIGURE 1   SCHEMATIC REPRESENTATION OF THE PARTIAL DERIVATIVES OF THE
CHARACTERISTIC FUNCTIONS G AND G*.
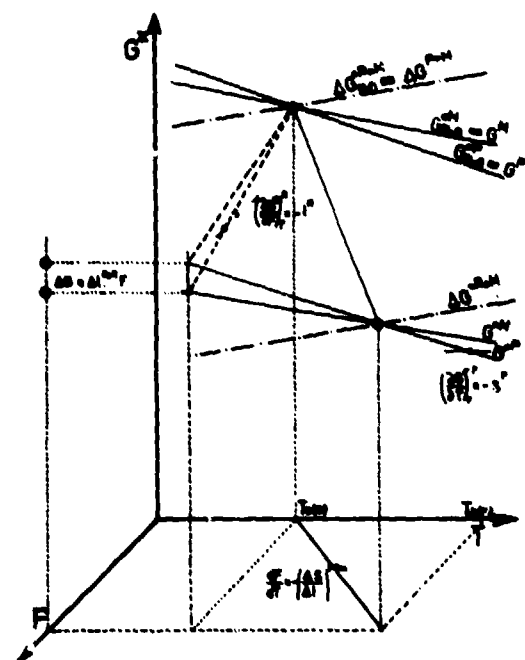
FIGURE 2   THREE-DIMENSIONAL SCHEMATIC REPRESENTATION OF THE CLAPEYRON-
LIKE RELATION: dF/dT = −(ΔS/ΔL)$^{P=M}$.
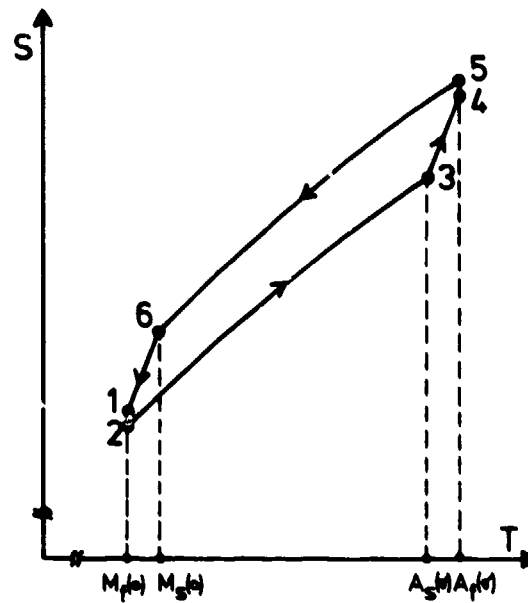
FIGURE 3 SCHEMATIC REPRESENTATION IN A TS-DIAGRAM OF THE WORK PERFORMING
CYCLE OF A SINGLE CRYSTAL.
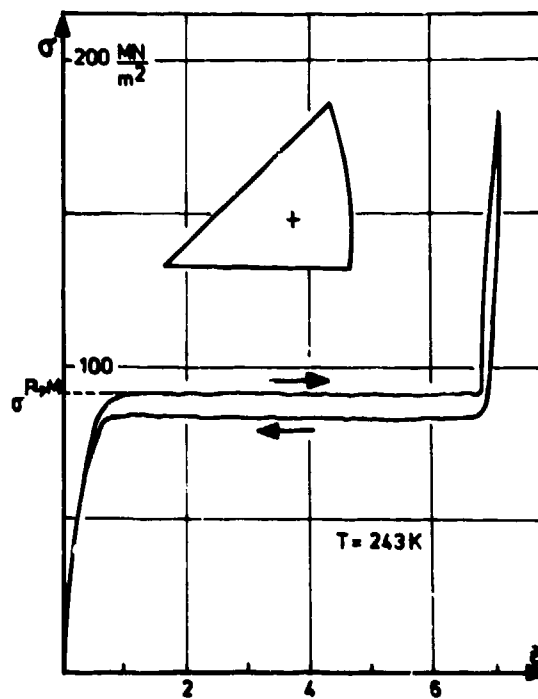
FIGURE 4 TYPICAL TENSILE CURVE FOR A Cu - 25, 33 AT % Zn - 9, 11 AT % Al SINGLE
CRYSTAL AS DETERMINED BY VAN HUMBEECK[14].
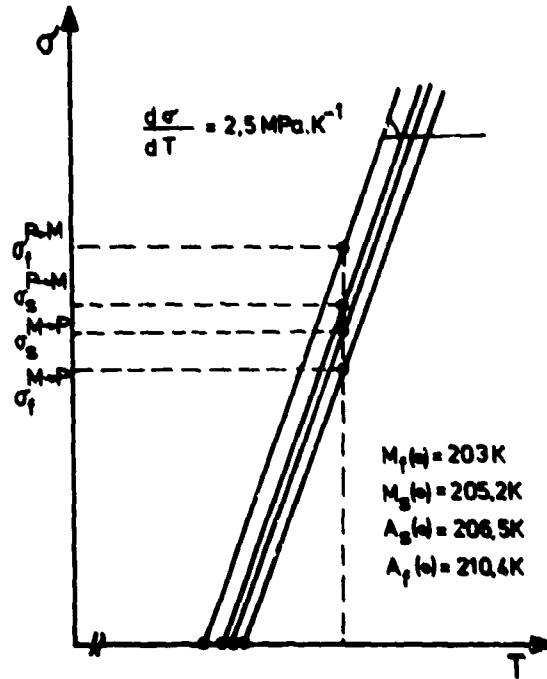
FIGURE 5   SCHEMATIC REPRESENTATION OF THE σ-T RELATIONSHIPS AS DERIVED
FROM A NUMBER OF TENSILE TESTS AT DIFFERENT TEST TEMPERATURES.
AT THE ZERO STRESS AXIS, THE EXTRAPOLATED $M_f(o)$, $M_s(o)$, $A_s(o)$ AND
$A_f(o)$ VALUES ARE FOUND.
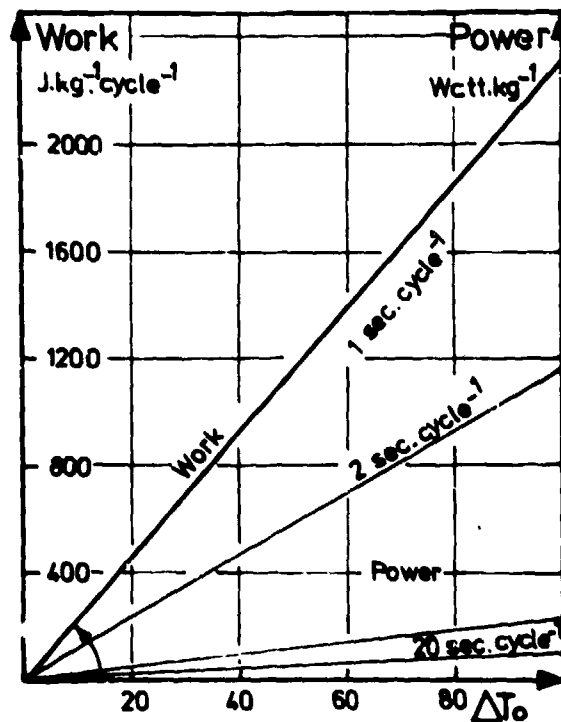
FIGURE 6   WORK PER CYCLE AND POWER (FOR VARIOUS CYCLE SPEEDS) OF THE
CuZnAl SINGLE CRYSTAL AS A FUNCTION OF ΔT_o ($T_o(o)$ = 206 K).
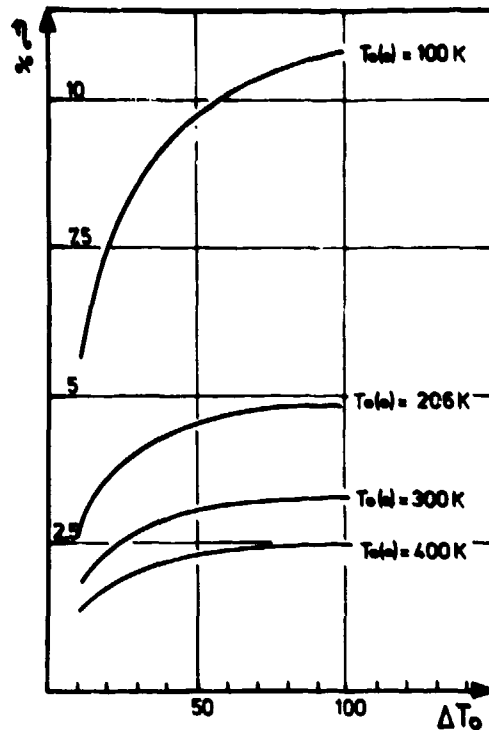
FIGURE 7 EFFICIENCY VS. ΔTo DIAGRAM FOR To(o) TEMPERATURES OF 100 K, 200 K, 300 K AND 400 K.
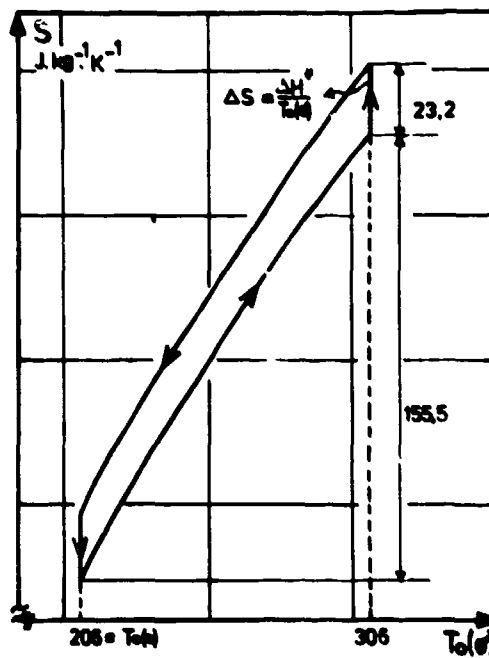
FIGURE 8 SIMPLIFIED QUANTITATIVE TS-DIAGRAM FOR THE WORK PERFORMING CYCLE AS DESCRIBED IN THIS PAPER.
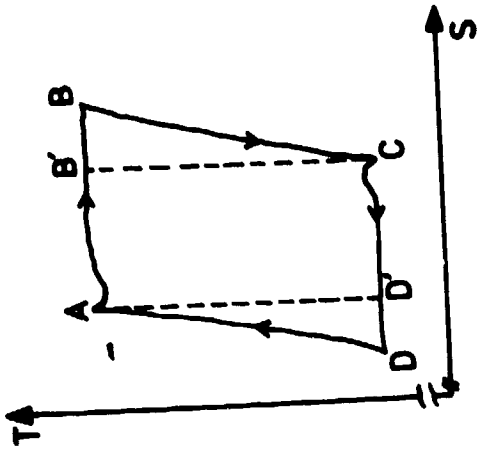
FIGURE 9b TS-DIAGRAM AS PROPOSED BY JOHNSON.
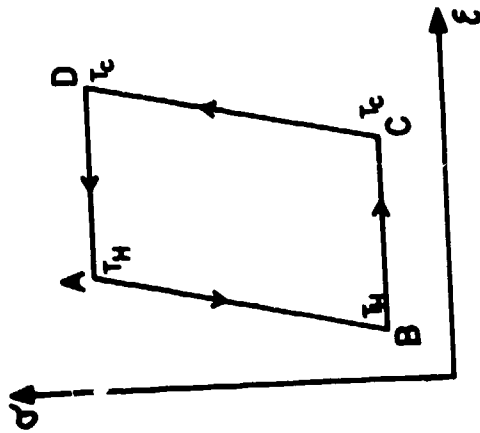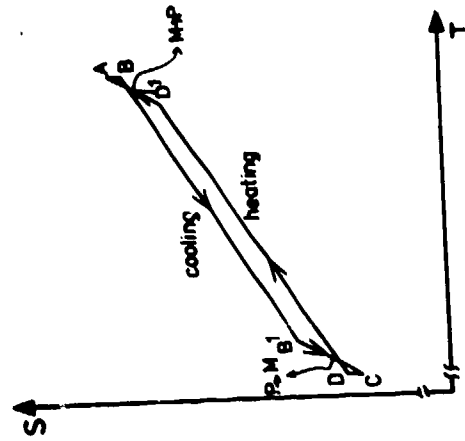
FIGURE 9c TS-DIAGRAM OF THE WORK PERFORMING CYCLE PROPOSED BY
JOHNSON; CORRECTED BY THE PRESENT AUTHORS.

FIGURE 9a σ-ε-DIAGRAM AS PROPOSED BY JOHNSON[6].

Table 1: Results of a thermodynamic analysis of the work performing cycle as described in the text.

change of state	work exchange	heat exchange	entropy change	T	σ	L
1 → 2	$\dfrac{\sigma \epsilon_e}{2}$	$q_{rev.} = T \Delta S$	$\alpha LF + \dfrac{\alpha LF^2}{2EA}$	$M_f(o)$	$0 \to \sigma$	$L_n \to L_o(1-\epsilon_e)$
2 → 3	-	$\displaystyle\int_{M_f(o)}^{A_s(\sigma)} C_\sigma^M \, dT$	$\displaystyle\int_{M_f(o)}^{A_s(\sigma)} C_\sigma^M \frac{dT}{T}$	$M_f(o) \to A_s(\sigma)$	σ	$L_o(1-\epsilon_e)$
3 → 4	$-F \cdot \Delta L$	$\displaystyle\int_{A_s(\sigma)}^{A_f(\sigma)} fC_\sigma^\beta+(1-f)C_\sigma^M \, dT$ $+ \Delta H_{tr}(\sigma)$	$\displaystyle\int_{A_s(\sigma)}^{A_t(\sigma)} \frac{fC_\sigma^\beta+(1-f)C_\sigma^M}{T}\, dT$ $+ \dfrac{\Delta H^*}{T_o}\; (= \Delta S_{tr}^{M\to\beta})$	$A_s(\sigma) \to A_f(\sigma)$	σ	$L_o(1-\epsilon_e)\to L_o(1-\epsilon_e+\epsilon_{tr})$
4 → 5	$\dfrac{\sigma \epsilon_e}{2}$	$-q_{rev} = T\Delta S$	$-\left(\alpha LF + \dfrac{\alpha LF^2}{2EA}\right)$	$A_f(\sigma)$	$\sigma \to 0$	$L_o(1-\epsilon_e+\epsilon_{tr})\to L_o(1+\epsilon_{tr})$
5 → 6	-	$\displaystyle\int_{A_f(\sigma)}^{M_s(o)} C_\sigma^\beta \, dT$	$\displaystyle\int_{A_f(\sigma)}^{M_s(o)} C_\sigma^\beta \frac{dT}{T}$	$A_f(\sigma) \to M_s(o)$	0	$L_o(1+\epsilon_{tr})$
6 → 1	-	$\displaystyle\int_{M_s(o)}^{M_f(o)} f'C_\sigma^M+(1-f')C_\sigma^\beta \, dT$ $+ \Delta H_{T_o}(o)$	$\displaystyle\int_{M_s(o)}^{M_f(o)} \frac{f'C_\sigma^M+(1-f')C_\sigma^\beta}{T}\, dT$ $+ \dfrac{\Delta H}{T_o(o)}\; (= \Delta S_{tr}^{\beta\to M})$	$M_s(o) \to M_f(o)$	0	$L_o(1+\epsilon_{tr})\to L_o$

Table 2: Results of a simplified thermodynamic analysis of the work performing cycle.

change of state	T	σ	L	work exchange	heat exchange	ΔS
1 → 2	$T_o(o)$	$0 \to \sigma$	L_o	-	-	-
2 → 3	$T_o(o) \to T_o(\sigma)$	σ	L_o	-	$\bar{c}_p \cdot \Delta T_o$	$\bar{c}_p \ln \dfrac{T_o(\sigma)}{T_o(o)}$
3 → 4	$T_o(\sigma)$	σ	$L_o \to L_o(1+\epsilon_{tr})$	$-F \cdot \Delta L$	$\Delta H^{*\,M \to B}_{T_o(\sigma)}$	$\dfrac{\Delta H^*}{T_o(\sigma)} = \Delta S^{M \to B}_{tr}$
4 → 5	$T_o(\sigma)$	$\sigma \to 0$	$L_o(1+\epsilon_{tr})$	-	-	-
5 → 6	$T_o(\sigma) \to T_o(o)$	0	$L_o(1+\epsilon_{tr})$	-	$-\bar{c}_p\,\Delta T_o$	$\bar{c}_p \ln \dfrac{T_o(o)}{T_o(\sigma)}$
6 → 1	$T_o(o)$	0	$L_o(1+\epsilon_{tr})\,L_o$	-	$\Delta H^{\,M \to \beta}$	$\dfrac{\Delta H}{T_o(o)} = \Delta S^{\beta \to M}_{tr}$

Table 3: Data for the calculation of the work performing
cycle of a CuZuAl single crystal.

Alloy composition	Cu-25,33 Zn - 9,11 Al (at %)
calculated molecular weight	$60,67$ mole^{-1} (1 kg $=$ 16,48 mole)
calculated density	$7,007$ kg . dm^{-3}
$\sigma_S^{P\to M}$-T relation (Fig. 4 and 5)	$\sigma_S^{P\to M} = 2,5\ T - 513$ MPa
	$\dfrac{d\sigma_S^{P\to M}}{dT} = 2,5$ MPa . K^{-1}
extrapolated stress-free transformation temperatures (Fig. 5)	M_f (o) $= 203$ K; M_s (o) $= 205,2$K
	A_s (o) $= 206,5$ K; A_f (o) $= 210,4$ K
thermodynamic equilibrium temperature	T_o (o) $= \dfrac{A_s\ (o) + M_s\ (o)}{2} = 206$ K
transformation elongation	$\varepsilon_{tr} = 0,065$ %
ΔH_{T_o} (o) as calculated from Eq. (11)'	$289,83$ J. mole^{-1}
work per cycle	$W = \dfrac{\Delta H_{T_o}\ (o)}{T_o\ (o)}\ .\ \Delta T_o$
power	$P = W \times n$ \qquad (n $=$ cycles . sec^{-1})
efficiency	$\eta = \dfrac{\Delta H_{T_o}\ (o) \times \Delta T_o}{T_o\ (o)\quad \overline{C}_p.\Delta T_o + \Delta H_{T_o}^*\ (\sigma)} \times 10$

Table 4: Measured and estimated values of the power generated by SME engines.

P. kg^{-1}	cycles sec^{-1}	material		ref.	
2,85	0,05	CuZnAl	measured	Neys	(20)
0,5	?	NITINOL	measured	Cunningham	(7)
9	1 ... 1,3	NITINOL	measured	Banks	(19)
130	?	NITINOL	measured	Johnson	(6)
1000	1	NITINOL	estimates	Johnson	(6)
2000	?	NITINOL	of the ma-	Cory	(10)
1000	0,5	CuZnAl	ximal ob-	this work	
			tainable		
			work		

BIBLIOGRAPHY

Ahlers, M., Scripta Met. 9 (1975) 71.

Banks, R., "Shape Memory Effects in Alloys," ed. J. Perkins, Plenum Press, 1975, p. 542.

Baumgart, F.; Jorde, J.; and Reiss, H. G.; Techn. Mitt. Krupp 34 (1976) 1.

Cory, J. S., and Mc Nichols, J. L., IECEC '78 Record.

Cunningham, B., and Ashbee, K. H. G., Acta Met. 25 (1977) 1315.

Delaey, L., and Delepeleire, G., Scripta Met. 10 (1976) 959.

Golestaneh, A. A., J. Appl. Phys. 49 (3), 1978.

Hultgren, R.; Desai, P. D.; Hawkins, D. T.; Gleiser, M.; Kelley, K. K.; and Wacman, P. D., Selected Values of the Thermodynamic Properties of the Elements, American Society for Metals (1973).

Johnson, A. D., IECEC '75 Record, 759082.

Kopa, R. D., Presented at the American Section of the International Solar Energy Society, Inc., Aug. 28-29, 1978, Denver, Co.

Neys, J., Energiekonversie steunend op het vormgeheugeneffekt, Eindwerk K. U. Leuven, 1976.

Pops, H., and Ridley, M., Met. Trans. 1 (1970) 2653.

Salzbrenner, R. J., and Cohen, M., submitted to Acta Met.

Tong, H. C., and Wayman, C. M., Met Trans. 6A (1975) 29.

Tong, H. C., and Wayman, C. M., Scripta Met. 10 (1976) 1129.

Van Humbeeck, J., Delaey, L., and Deruyttere, A., Z. Metalikde 69 (1978) 575.

Wayman, C. M., and Tong, H. C., Scripta Met. 9 (1975) 757.

Wollants, P.; De Bonte, M.; Delaey, L.; and Roos, J. R., accepted for publication in Zeitschr. Metallkde.

Wollants, P.; De Bonte, M.; and J. R. Roos, accepted for publication in Zeitschr. Metallk.

THERMOMECHANICAL BEHAVIOR OF NITINOL

Dr. J. S. Cory
Cory Laboratories
Escondido, CA

Two hundred fifty years experience with heat engines has taught engineers the importance of a state equation or state relation for the thermodynamic working material. The state relation is used in engine design, for example, to predict the design forces on an automobile piston and bearings, and the number and size of cylinders required for a given horsepower. A thermodynamic state relation, like $PV = nRT$, is also used to optimize and invent new and better heat engines, such as the diesel, the jet engine, and turbines. The entire engineering history of heat engines has been solidly based on a quantitative understanding of the relationship between the temperature of the working fluid, and the force and volume of that fluid.

The importance of a state equation was widely recognized in the 60's by the early workers in NITINOL. Many measurements were made of stress versus strain as a function of temperature. State equations were proposed which were analogous to conventional, multiphase thermodynamic working fluids, such as water. These measurements and equations were very useful for initial surveys of the potential of NITINOL Heat Engines (NHEs) but broke down completely when applied to operating engines. Also, the experimental results were not repeatable. At a given temperature and length, for example, at one time a force of one newton would be measured and then later, with the same wire, a force of ten newtons would be measured. These measurements and state equations were completely inadequate for engine design. A wide gap opened between the analytical and hardware engineers.

To close this gap, an exhaustive set of experimental measurements was initiated to find an empirical state relation between the temperature, length, and force on a NITINOL element. This empirical state relation was to accurately describe all possible NITINOL behavior, including stress-strain measurements, engine behavior reported in the literature, and the results of the ad hoc experiments.

In this experimental program, the first breakthrough occurred when it was realized that (Fig. 1) all observed thermodynamic states and all observed thermodynamic paths occupied a bounded volume in state space. This behavior is in sharp contrast with conventional thermodynamics, where all possible states occupy a surface, not a volume in Force-Length-Temperature (FLT) space. This fundamental difference accounts for the confusion and inaccuracies of the early measurements and state equations: at a single value of temperature and length, for example, the force on a conventional material would be uniquely determined, but the force on a NITINOL element could range from 0 to 50 newtons, depending on its location within the bounded volume.

As usual, the reason for this phenomenon later became obvious: NITINOL is a lossy material in contrast with even the most complex, multiphase, multicomponent gas or liquid, where phase and concentration changes are almost exactly reversible. Non-equilibrium

thermodynamics shows a one-to-one correspondence between internal losses and hysteresis in the force-length plane. So NITINOL should, as it does, occupy a volume in state space. This phenomenon explains the inadequacy of the early reversible state equations, and is presently fairly widely recognized.

The second breakthrough in the experimental program occurred when it was realized that the location of the boundary surfaces changed as the NITINOL was stressed, strained, or heated. Thus many of the reported phenomena, such as second memory and creep, could be described in terms of the migration of the boundary surfaces with cold working. This cold working effect complicated the problem of determining the empirical relation locating the state of a NITINOL element within the bounded volume since the location of the bounded volume changed. Fortunately, the boundary surfaces migration could be eliminated by two procedures.

First, limiting the cyclic stress, strain, and temperature excursions to small values kept the boundaries for a large number of cycles. Reproducible measurements could be made. Second, preconditioning the NITINOL element for about 20,000 cycles could stabilize even large FLT excursions. Either procedure was adequate to experimentally isolate boundary surface migration from the problem of predicting the precise location of the FLT state within the bounded volume, and also incidentally, to stabilize engine performance.

The final breakthrough occurred with the observation of two phenomena:

First was the observation that reversible paths existed (Fig. 2). In constant force, or constant length, or constant temperature measurements as shown in Figure 2, specific conditions existed where reversing the sense of the path would result in an exact retracing of the path. For example, the lines labled A were formed in the stretching isotherms of Figure 2 by reversing from stretching to contraction, for a small excursion, and then reversing again back to stretching. This behavior strongly constrasts with the normal hysteresis. All these reversible paths, everywhere within the bounded volume, have nearly the same slope and can be used to define a set of reversible planes. These planes can be conveniently described by the new state function, Z(FLT). The utility of these planes is that whenever a change in the direction of phase conversion occurs, for example the change from creating martensite to creating parent phase material, the thermodynamic path leaving this starting point is <u>always</u> initially parallel to the local reversible plane. Thus the initial slope of all paths is determined.

The second phenomenon (Fig. 3) was the observation that all thermodynamic paths approached one or the other boundary surfaces asymptotically. This was ascertained by plotting the element length against the force separation between the observed path and the boundary surface (distance X in the figure) on semi log paper. For all measured paths, this plot always produced a straight line with the slope independent of the starting point. This behavior was also observed in constant temperature, constant length, and constant force experiments.

These observations allowed <u>all</u> the published data on NITINOL wire and helices and engine behavior, and also the ad hoc experiments, to be correlated by a fourfold infinite set of state surfaces. The state surfaces of each kind--those describing the martensitic and those describing the austenitic transformation--completely fill the volume between the boundary surfaces, and allow prediction of the FLT behavior of NITINOL. Examples of predicted constant force, constant length, and constant temperature thermodynamic paths are shown in Figure 4. The projections of these paths onto the corresponding two-dimensional planes are also illustrated.

These state surfaces can be approximated by the equations in Figure 5. In these equations the reversible surfaces, Z=const and the boundary surfaces, N=const, are flat planes

when the coefficients a through h are constants. The values of these coefficients determine the location and slope of the planes. The state equations then say that the force differences between the thermodynamic path and the boundary (F_B-F for the martensitic transformation, and F minus the lower boundary force for the austenitic transformation) are exponentially dependent on the temperature and length excursion from the starting point, which is defined by the state (F_1, L_1, and T_1; or F_2, L_2, T_2).

These state surfaces are an empirical correlation of data, with no theoretical basis, and are claimed to include all possible thermodynamic behavior. So a single, measured, experimental path that does not lie on one of the surfaces, a single counter example, is sufficient to weaken the correlation. This is a strong (and useful) claim. The immediate response to such a claim by any self-respecting experimentalists is to try to find a counter example. Figures 6, 7, and 8 illustrate the efforts so far to find a counter example by comparing the predictions of the correlation with experimental observations.

The correlation predicts a uniqueness on a single state surface: that is, that the subsequent behavior or thermodynamic path is uniquely determined by its location on the surface, regardless of the path used to arrive at that point. Figure 6 illustrates the experiments to check this prediction. A single point on a specific state surface was approached by constant length, constant force, and constant temperature paths. In each case, the subsequent constant force path leaving the point was the same, within the accuracy of the experiment. Note that this uniqueness is equivalent to the statement that stress-induced martensite is energetically (and probably entropically) equivalent to thermally induced martensite.

A second prediction is the non-uniqueness of a point in state space if that point was arrived at by paths on two different state surfaces. The experimental verification of this prediction is illustrated in the isothermal paths in Figure 7. In the top example, the two isothermal paths lie on two intersecting state surfaces because the starting points for the two paths are different (points labled A and B in the figure). As predicted, the subsequent isothermal paths leaving the common point B in state space are different. This experimental behavior confirms Wang's conjecture that a single unique energy equation does not exist for NITINOL. Therefore, the observed thermodynamic paths cannot be simply described as the minimum of a conventional free energy function, and the phase transformation must involve a change in the Gibbs free energy. The consequence of this non-uniqueness for closed thermodynamic cycles is illustrated in the lower set of isotherms of Figure 7. Cycles do not necessarily retrace themselves, but may drift in length, force, or temperature.

The important consequence of this property of the state surfaces for heat engine design is illustrated in Figure 8. Any stable, non-drifting closed cycle must lie on a unique pair of state surfaces, characterized by being symmetrically located between the two boundary surfaces. Any other cycle will be unstable and will drift (within the constraints of the experiment or device). This property is used in heat engine design to identify the particular pair of state surfaces that will contain the operating (stable) thermodynamic cycle.

This state surface correlation is much more complex than a simple PV=nRT, in that it involves a fourfold infinite set of state surfaces, rather than a single state surface. But, because of the regularities in the data, this complexity merely means that one additional step must be added to conventional thermodynamic calculations. This additional step is just locating the starting point (or extremum of the state function Z) and then using the stability condition to specify the two particular state functions which must contain all thermodynamic paths. From this point, NITINOL thermodynamic calculations follow the familiar, non-equilibrium thermodynamic procedures.

The remainder of this paper describes examples of the use of the state surface correlation. For instance, the first step in NITINOL heat engine design is to measure the coefficients (Fig. 5) a, b, f, g, N, h, and c for the specific NITINOL element to be used in the heat engine. Then, a lower limit of the Z state function is selected, $Z_1(F_1, L_1, T_1)$ and the cycle stability criteria used to specify $Z_2(F_2, L_2, T_2)$. These conditions define the applicable pair of state surfaces. The next step is to locate, on this pair of surfaces, the thermodynamic paths followed by the heat engines (Fig. 9). The example illustrates a cycle consisting of the popular constant length and constant temperature legs. Note that the paths must be constructed so that the extreme values of Z_1 and Z_2 are achieved at the corners of the cycle. This first step is sufficient to specify several critical dimensions of the heat engine, for example the throw of the crank and the initial length of the NITINOL element for an off-set crank type machine.

The next step is to evaluate the specific work and thermodynamic efficiency. The specific work can be easily found (Fig. 10) using the state equations and the integration limits found in the previous step to evaluate the cyclic intergral of FdL. This specific work is the amount of heat energy this particular cycle will convert into mechanical work, per unit of mass of NITINOL cycled. Therefore, when multiplied by the element mass, it is also the torque contribution of a single element and, when also multiplied by the cycle rate, gives the output power from a single element. This quantity, easily obtained from the state equations, therefore indicated the number of elements required to achieve, say, a one kilowatt output. This calculational procedure has been verified experimentally.

To calculate the thermodynamic efficiency, it is necessary to find the functions dS and d_iS, representing the entropy and entropy generation. The entropy as a function of the FLT state variables can be derived using a procedure similar to the Clausius-Clapeyron derivation, and the entropy generation evaluated using the equivelance of hysteresis and energy dissipation. Because NITINOL is dissipative, non-equilibrium thermodynamics shows the heat flow to the system must be modified as shown in Figure 10 (for many cycles $d_iS << dS$ and can be neglected). Then, from the state relations, the known thermodynamic paths and the derived entropy and entropy generation, the heat flow for the particular cycle can be calculated and the efficiency evaluated. This evaluation procedure has not been experimentally verified.

Thus the state equations provide the necessary and sufficient basis for NITINOL device engineering: designing machines to meet performance requirements.

A second important use of the state surfaces correlation is in parametric studies. Since, by using the state equations, one can predict the performance of a NITINOL heat engine, the effect on various performance criteria of new designs, new alloys, new thermodynamic cycles, and new NITINOL element designs can be evaluated without building the hardware. And, as engineering experience has shown, analytical parametric studies are much cheaper and more efficient (but less accurate) than hardware parametric studies. Some of the results of such a preliminary parametric study of the effect of different types of thermodynamic cycles are illustrated in Figure 11.

In this study, the two major performance criteria--specific work (which is closely related to capital costs) and efficiency (which is closely related to operating costs)--are used to evaluate various thermodynamic cycles. For the cycles studied, it is apparent there is a trade-off between efficiency and work. Very high efficiencies can be achieved by a cycle with constant temperature and adiabatic legs, but at the cost of low specific work. Similarly, low capital costs can be achieved by a cycle with constant temperature and length legs, but such a cycle has relatively low efficiency. What is desired, and is probably possible, is a cycle in the upper right hand corner of the graph.

Figure 11, in isolation, can be misleading, since there are other important performance criteria besides specific work and efficiency. And there are other possibilities for improving performance besides selecting the "best" thermodynamic cycle. For example, the element characteristics can have a large effect on performance as illustrated by the two curves marked "TL cycle" in Figure 11. These two curves illustrate the change in performance that can be achieved by decreasing the hysteresis losses of a helical element. A complete parametric study would evaluate the effect of all available "improvements" on all significant performance criteria.

The state surface correlation applies to all alloy compositions and element configurations, so a third important use is in connection with element development. Figure 12 lists the items required to completely characterize a NITINOL element.

The first seven items are the coefficients of the state equations and could be used, for example, by the NITINOL producers to characterize their product. The engine designer could then use this information to select a particular alloy that best matches his/her particular mix of performance requirements. This procedure is already being followed to some extent in requesting a specific transition temperature material. But by using the state surface correlation, one could specify not only item 7, the transition temperature, but also the other six items that ultimately determine engine performance.

Another use of the first seven items is in selecting whether to use helices, plates in the bending mode, wires in tension, or newly invented element configurations. The numerical values of the first seven items, for different configurations, can be related for a given alloy by mechanics of materials calculations. So this list provides an interface among element designers, engine designers, and alloy producers.

The last five items are quantities outside the present state-of-the-art of the state surfaces correlation. Item 8, cold working or training, is well known to modify the thermodynamic properties of an element. The first seven items, however, implicitly provide the outline of an experimental program to evaluate just how training affects performance.

Items 9, 10, and 11 in Figure 12 are concerned with optimization. Obviously the state surface correlation here applies only over a limited range in FLT space: Actual behavior is not described by infinite, exactly parallel planes. Beyond that range the two-boundary surfaces coalesce and the shape memory effect disappears. Maximum specific work is achieved by using maximum force, length, and temperature excursions possible, so identifying and extending the limits is important in device optimization.

This final use of the state surfaces correlation is, perhaps, of the most immediate importance. Using this list as an interface, alloy producers, crystallographers, element designers, inventors, and hardware engineers are provided with a common language for intercommunication.

The state surface correlation is much more complex than I would have preferred. It requires considerable study to learn and a willingness to discount much of the equilibrium, reversible thermodynamics we learned in school. In addition, in its present form (flat infinite surfaces) it is obviously only an approximation. Nevertheless, it is sufficiently simple and accurate to provide a powerful tool for engineering NITINOL thermodynamics. It allows the engineer to design, shows the inventor what to invent, quantifies tradeoffs for the system analyst, provides the program manager with priorities, and in short is the powerful engineering tool that 250 years of heat engine experience had predicted.
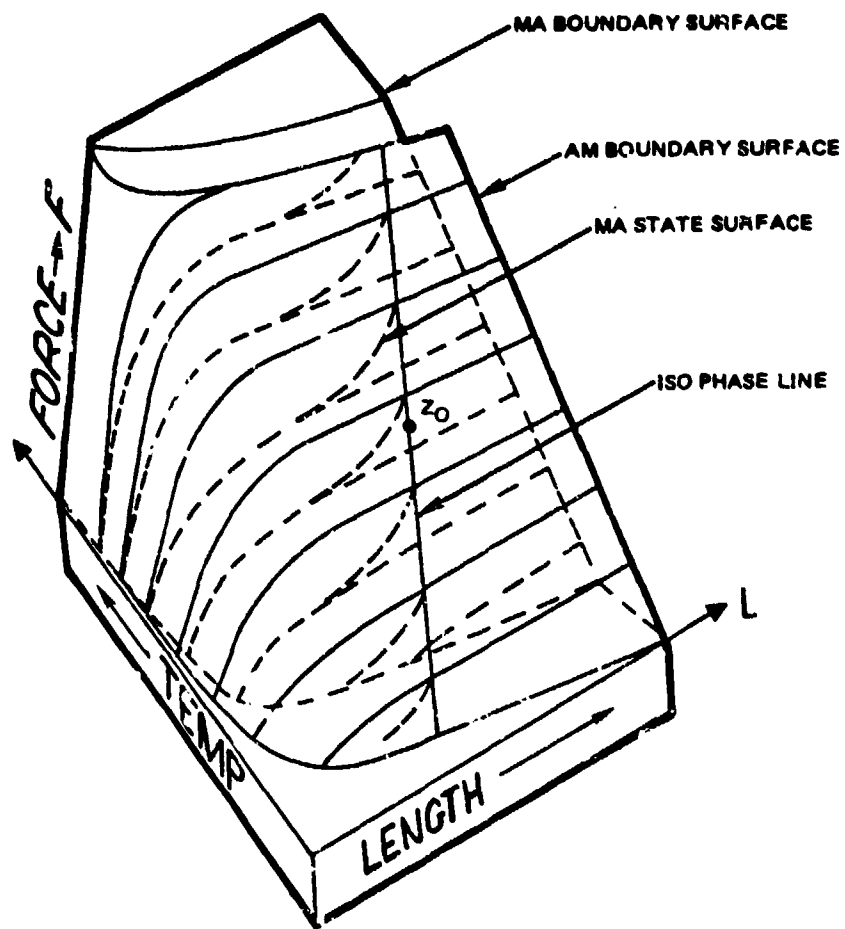
FIGURE 1   POSSIBLE THERMODYNAMIC STATES AND PATHS OF NITINOL
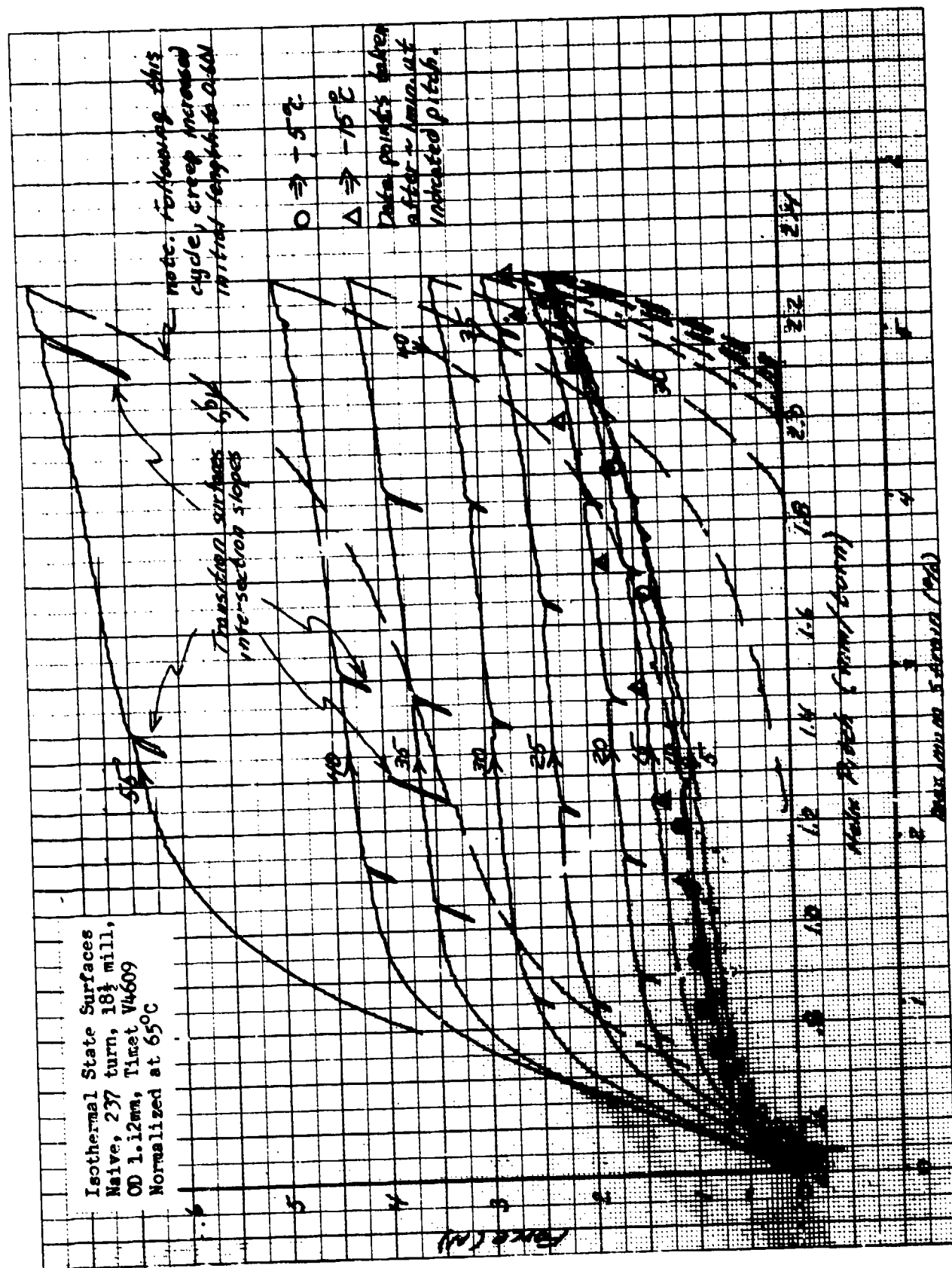
FIGURE 2   ISOTHERMS AND TRANSITION SURFACE INITIAL SLOPES
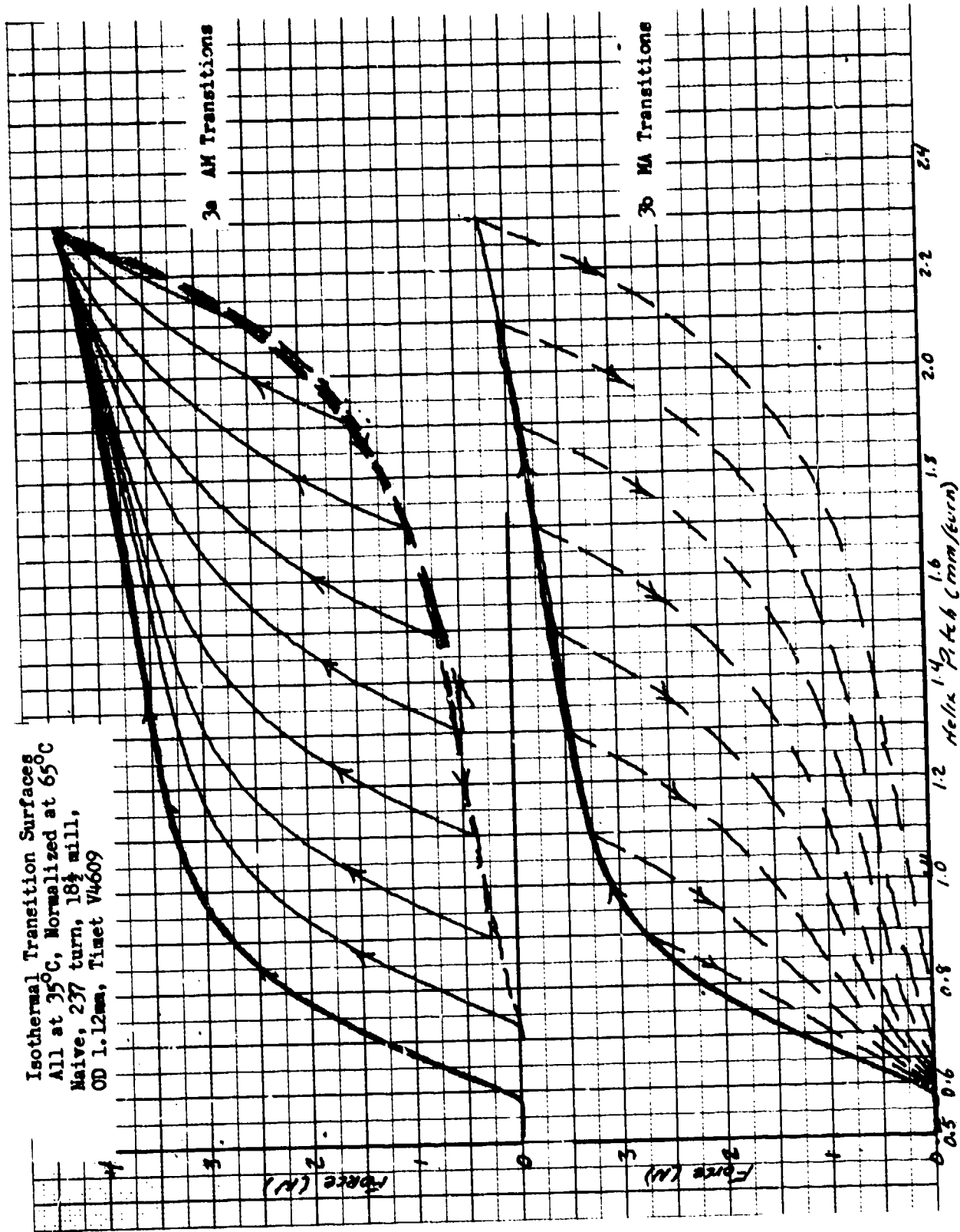
FIGURE 3   ISOTHERMS OF TRANSITION SURFACES
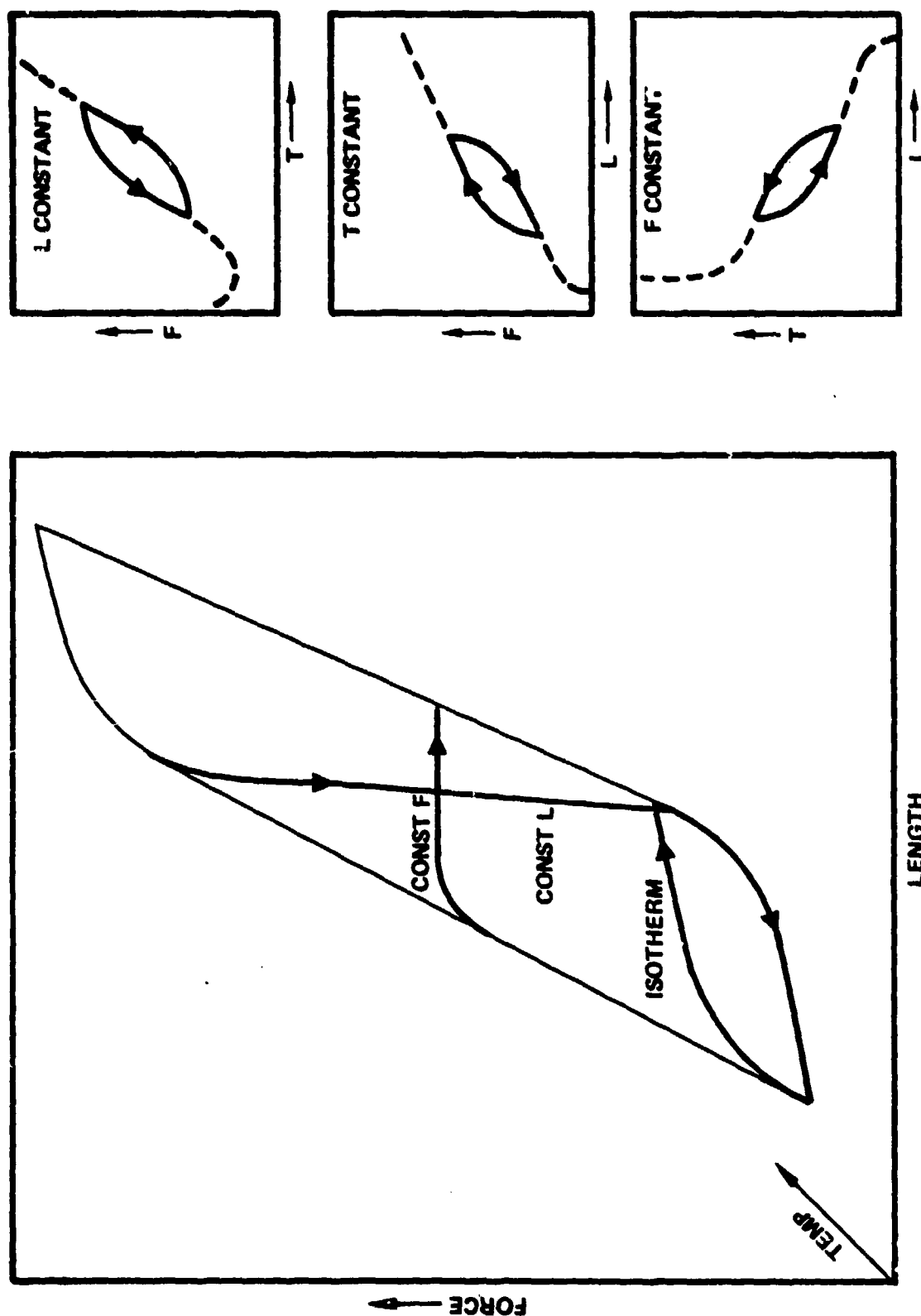
FIGURE 4   POSSIBLE CONSTANT F, L, AND T THERMODYNAMIC PATHS ON A SINGLE STATE SURFACE

$$\frac{F_B - F}{F_{B1} - F_1} = EXP \left[\frac{g(T - T_1) - f(L - L_1)}{F_{B1} - F_1}\right]$$

$$\frac{F - (F_B - h)}{F_2 - (F_{B2} - h)} = EXP \left[\frac{g(T_2 - T) - f(L_2 - L)}{F_2 - (F_{B2} - h)}\right]$$

WHERE: L (M/KG), F (N), T (^{O}K)

$$F_B(L,T) = (a - f) L + (g + b) T - N$$

$$z(F, L, T) = aL + bT - F$$

$$h = F_B(T_i, L_i)_{AM} - F_B(T_i, L_i)_{MA}$$

$$c = c_{LR} = dq/dT)_{z,L}$$

FIGURE 5   NITINOL STATE EQUATIONS
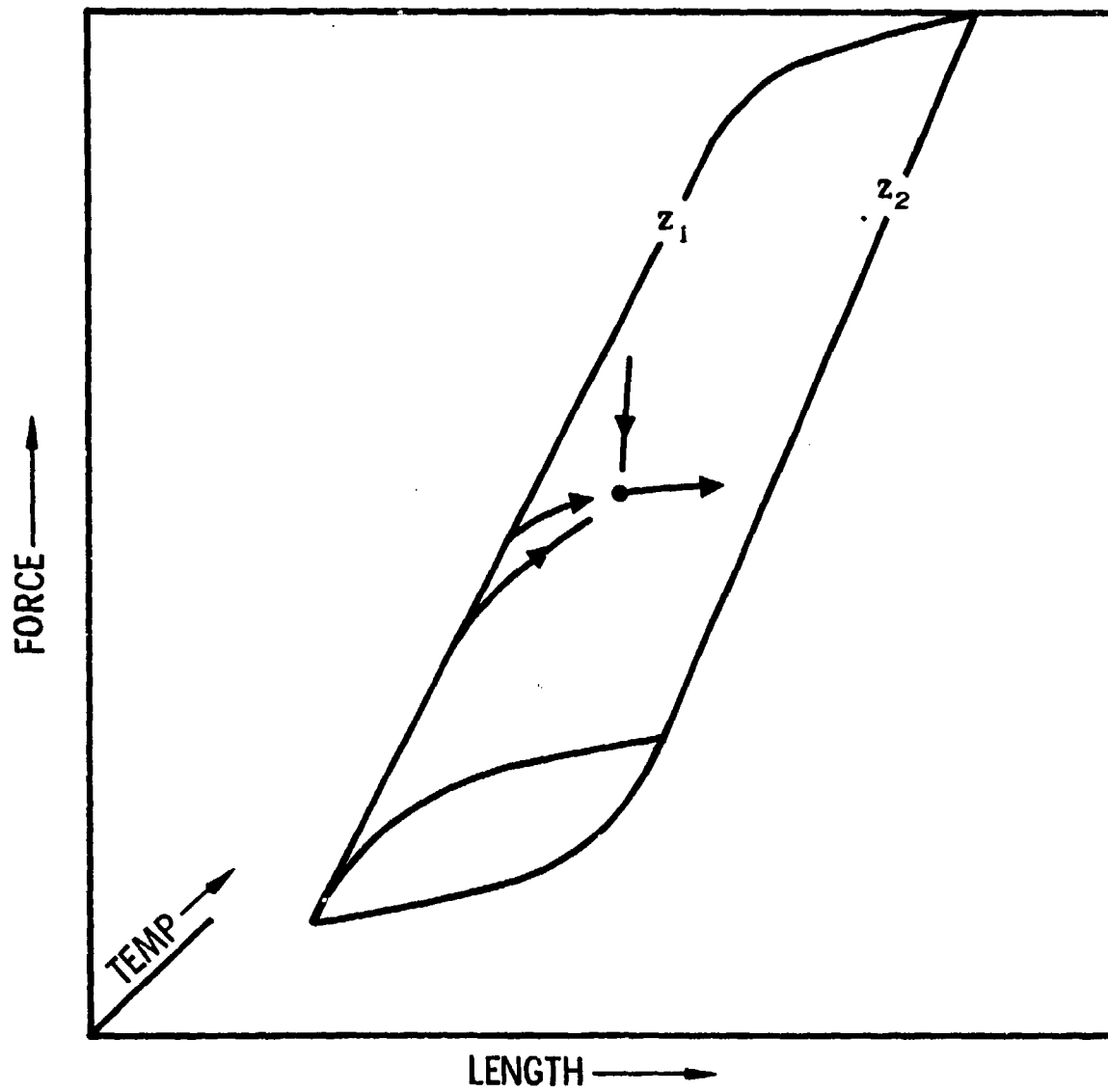
FIGURE 6 UNIQUENESS OF STATE SURFACES
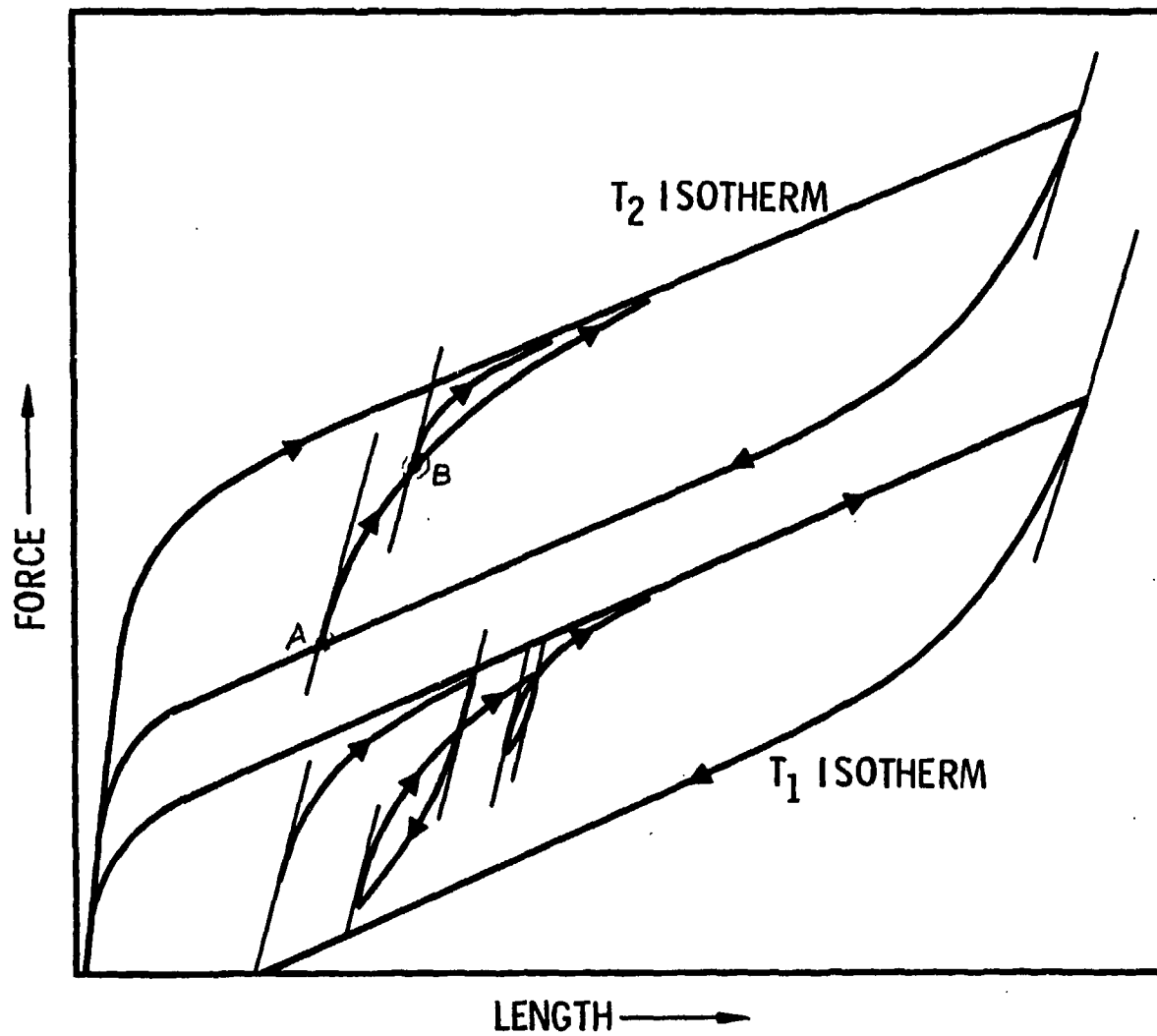
FIGURE 7   NON-STABLE, ISOTHERMAL THERMODYNAMIC PATHS
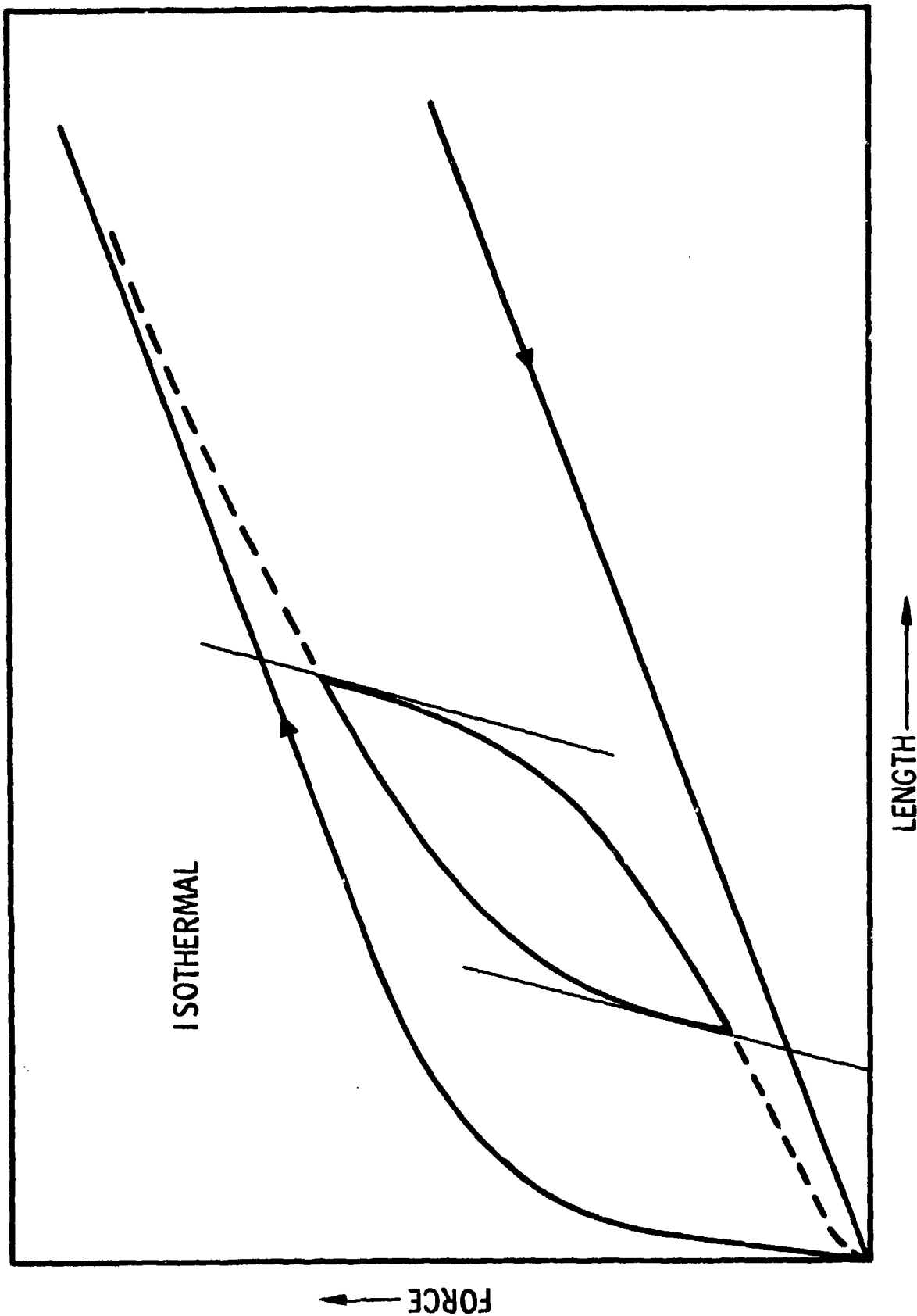
FIGURE 8   STABLE, CYCLIC, ISOTHERMAL THERMODYNAMIC PATHS
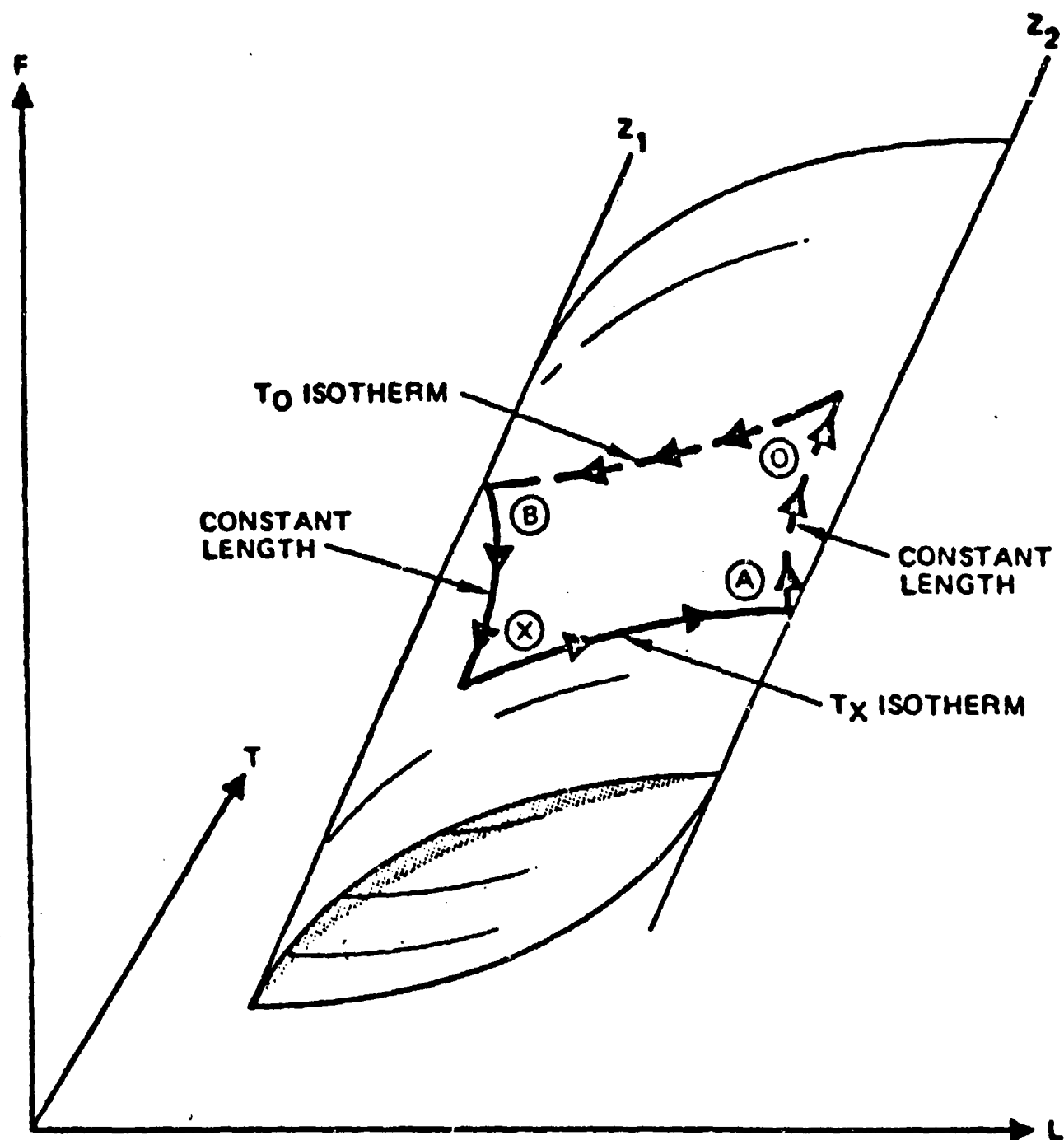
FIGURE 9 THERMODYNAMIC PATHS OF A CONSTANT TEMPERATURE — CONSTANT LENGTH (TL) NITINOL ENGINE CYCLE, SOLID LINES ARE DRAWN ON UPPER SURFACE — DASHED LINES ON LOWER SURFACE
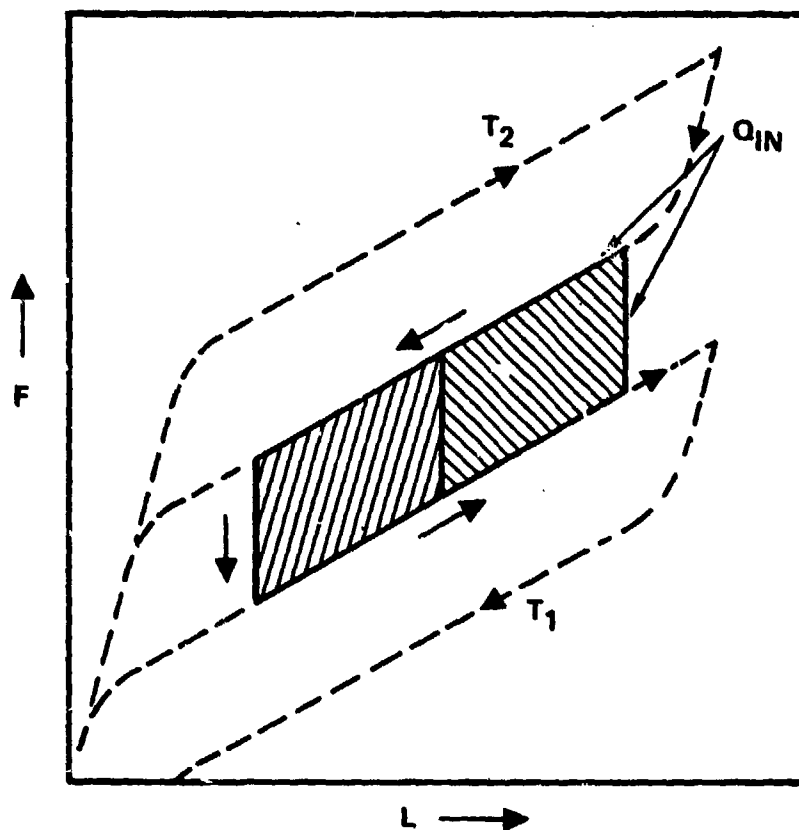
$$W \text{ (J/KG)} = \oint F \, dL = \text{AREA}$$

$$\eta = W/Q_{IN}, \quad \eta_c = \frac{T_2 - T_1}{T_2}$$

$$Q_{IN} = \int dq = \int (T \, ds - T \, d_i S)$$

$$\oint T \, d_i S = \text{HYSTERESIS LOSSES}$$

FIGURE 10   PERFORMANCE CALCULATIONS USING THERMODYNAMIC PATHS
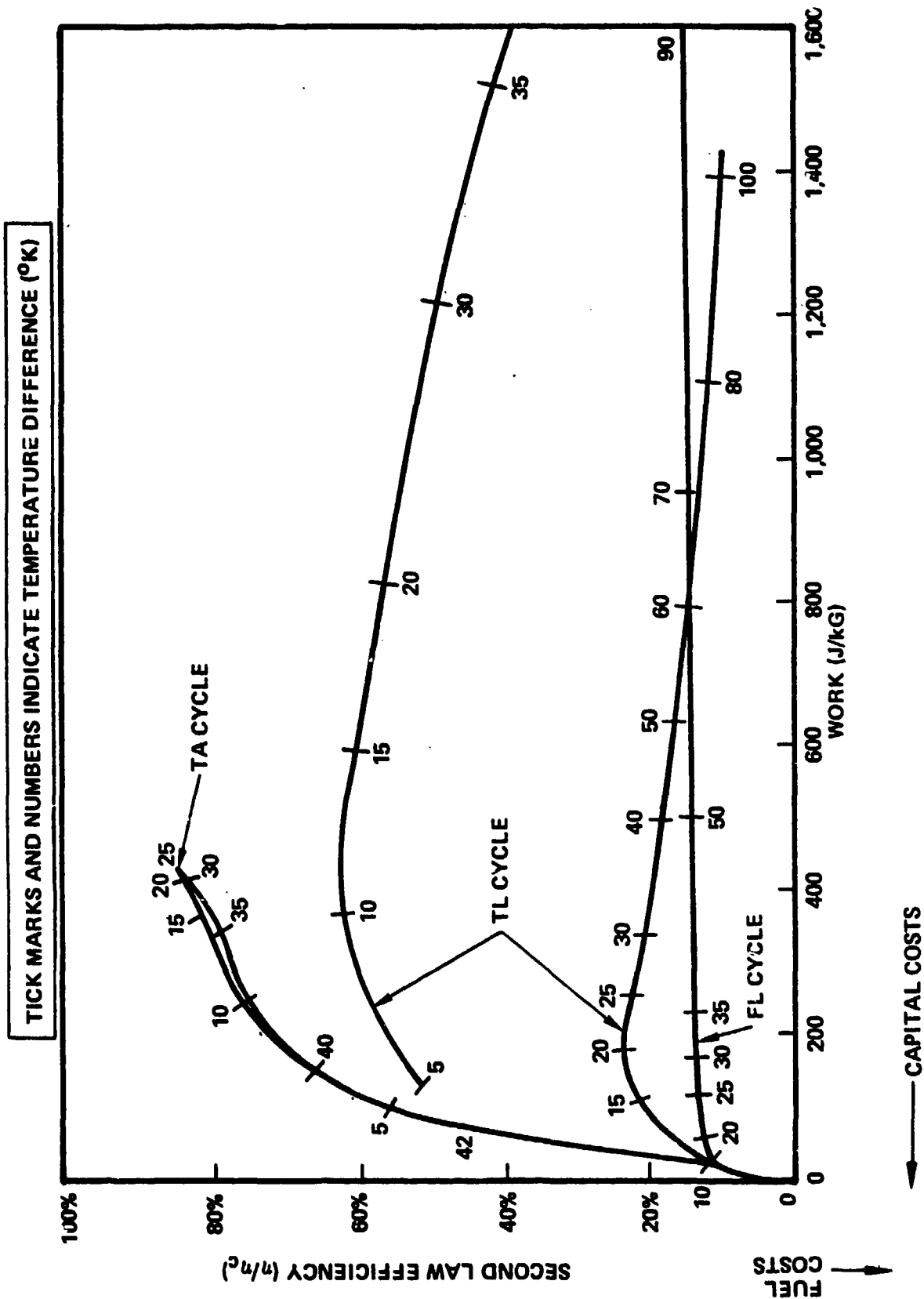
FIGURE 11   RELATIVE PERFORMANCE OF DIFFERENT CYCLE TYPES

(1)   a $\equiv$ $\partial Z/\partial L)_{F,T}$

(2)   b $\equiv$ $\partial Z/\partial T)_{L,T}$

(3)   f $\equiv$ $a - \partial F_B/\partial L)_T$

(4)   g $\equiv$ $\boxed{\partial F_B/\partial T)_L} - b$

(5)   c $\equiv$ $dq/dT)_{Z,L}$

(6)   h $\equiv$ **HYSTERESIS WIDTH**

(7) F_B (L = 0, T = 0) $\equiv$ **RELATED TO TRANSITION TEMPERATURE**

(8)   **RESPONSE TO "TRAINING"**

(9)   **MAXIMUM USABLE LENGTH CHANGE (RELATED TO A_f, M_f)**

(10)   **MAXIMUM USABLE TEMPERATURE DIFFERENCE (RELATED TO A_f, M_f)**

(11)   **MAXIMUM USABLE FORCE (RELATED TO A_f, M_f)**

(12)   **DEVIATIONS FROM FLAT PLANES APPROXIMATIONS**

FIGURE 12   ELEMENT SHAPE AND ALLOY CHARACTERIZATION

EXPERIMENTAL RESULTS ON A CONTINUOUS-BAND NITINOL ENGINE

Dr. A. D. Johnson
Energy Research Associates
Oakland, CA

ABSTRACT

This report summarizes work done by Energy Research Associates during calendar years .)75-76. It covers our efforts to obtain ballpark answers to two separate but closely related questions asked by everyone first seeing these engines. How much power can you get out of them, and what is the efficiency?

EFFICIENCY STUDIES

The development of solid-state heat engines precipitated several theoretical discussions of th achievable thermodynamic efficiency of such engines. The problem was misunderstood by some physicists who considered only the delta-T associated with the phase transition at zero stress, and who therefore predicted maximal efficiencies of ten percent or less. Recent works t n o agree that the ultimate limit in efficiency is nearly the same for these engines as for oι heat engines, namely $(T_1-T_2)/T_1$. For liquid water heat source and sink this sets a the tical limit of about 25 percent. Actual experimental efficiencies may be expected to be muc maller than this.

The prototype continuous-band NITINOL engine[1] is a suitable vehicle for first attempts at mea ring efficiencies, because the heat source and sink may be thermally isolated and power output from the working element may be measured directly. For this purpose, a varia on previous linear-tension engines was constructed and instrumented (Fig. 1). The methoo for measurement of efficiency was suggested to me by Dr. Jack Cory of Cory Laboratories, Escondido, California, in August 1975.

Speed was measured with an Elinco Midget dc generator coupled to an Esterline-Angus strip-chart recorder. Force F_H, the force on the hot pulley, was measured by a Hamilton-Baldwin load cell energized by a Luchter transducer power supply and read by a Leeds and Northrup Speedomax recorder. Force F_T, the sum of the forces on hot and cold pulleys, was effected by weights attached to a cable running above the engine. Temperatures in hot and cold tanks were registered by copper-constantan thermocouples whose emf was recorded by a Leeds and Northrup Speedomax recorder. A glass mercury-bulb thermometer made an auxiliary measurement of the temperature in the hot tank. Weston thermometers monitored temperatures elsewhere in the system.

---

[1] J. S. Cory, et al. "NITINOL Heat Engines for Economical Conversion of Low Grade Thermal Energy," Proceedings of the 13th Intersociety Energy Conversion Engineering Conference, Vol. III, San Diego, CA, August 20-25, 1978, Paper #789031, pp. 1998-2004.

Heat input was by a measured volume of water in the insulated hot tank. For heat sink, cold water was circulated by a pump into the cold tank, and into a vertical water jacket surrounding the wire as it traveled from the cold tank to the cold drive pulley.

Energy input to the system was inferred from the time rate of change of temperature of the known volume of water in the hot bath. The heat capacity of the container and the enclosed idler pulley was negligible compared to that of the water. Heat was rejected into a cold bath maintained at nearly constant temperature by contact with ice.

Power output of the NITINOL wire, which was the active element (or "working solid") in this engine, was calculated as the product of torque times angular velocity of the pulley set. The drive pulleys, which had a 1.03:1.00 diameter ratio, were nominally 10 cm in diameter.

Typical running speed for a 3-gram NITINOL wire 2.2 meters long pulling the generator was 1000 RPM, corresponding to a linear velocity of the wire of 5.2 m/sec. At this rate the wire made about 2.5 complete engine cycles/sec. and generated approximately 7 watts with a weight 133N and F_H= 93N. However, at this speed there was considerable loss of water which spattered from the rapidly-moving parts. It was therefore decided to limit the speed by coupling the engine to a synchronous electric motor. Subsequent tests, which form the basis of this report, were taken with the engine running in this captive mode at a nominal pulley speed of 300 RPM.

The thermodynamic efficiency of a solid-state engine will vary with speed, temperature, elongation ratio (or pulley diameter ratio), and force w. Not all these variables have been ranged in this preliminary study. Rather, a set of conditions was arrived at by trial and error which gives reasonable power output at a measurable rate of temperature change. Then an attempt was made to deduce the "energy budget" for the engine in this condition. Obviously families of curves could be generated by ranging each of the above variables: the values we have established should be taken as typical rather than definitive. On the other hand, our engine cycle simulations show that the work output per unit mass per cycle at maximum output is not more than a factor of two greater than that achieved in the test engine. This engine is designed by intuitive judgment rather than engineering equations: we feel certain that sizable improvement is possible.

The "heat budget" for this engine should consist mainly of these contributions:

1) + Heat input, from cooling of water in hot reservoir.

2) - Heat required to cause the phase transition.

3) - Sensible heat to change temperature of the wire.

4) - Heat discarded by the water carried around the circuit by the wire (mixing of hot and cold fluids)

5) - Static heat losses, by conduction and evaporation.

6) - Power output by the wire.

It is important to note that we measure power output by the wire, before friction losses, etc. This is grossly different from the engine shaft output power, and is a reasonable way to measure power on a prototype scale model.

Item 1), the caloric input, is determined from the rate of temperature decrease in a known volume of water. Items 2) and 3), the heat required for causing the phase transformation and for sensibly heating, can be estimated from data available in NASA 5110[2], although it must be recognized that latent heat is a function of thermodynamic path. Our method allows a consistency check by measuring these quantities as will be shown below. Item 4) can be estimated by replacing the NITINOL wire with a nearly equal diameter steel wire (with a 1.0:1.0 drive pulley ratio) and measuring the rate of heat loss. Item 5) is measured by the rate of temperature decrease for a known volume of water when the engine is standing still. Item 6) is measured as torque times angular velocity as discussed previously.

Table I gives the numbers obtained, with sizable systematic errors but with overall consistency of about 10%.

Replacement of the NITINOL wire by a steel wire of approximately the same dimensions allows measurement of the latent heat required to drive the phase transformation, since all other parameters of the experiment are approximately the same. Table II shows results of doing this.

We conclude that at a delta-T of 75 degrees C, losses for the simple NITINOL engine are almost equally divided into three parts: latent heat; sensible heat; and losses which include mixing, conduction, and evaporation. Conductive loss itself is only about 10 percent of the heat budget.

With this engine, and with presently attainable power output levels, the maximum achievable efficiency will be about 2.5% after the obvious losses have been minimized. The present engine operates at 1.2 percent efficiency, which is less than 10 percent of the theoretical maximum efficiency. This is due to the large amount of entropy generated by heating and cooling the wire by direct immersion in hot and cold baths, which is far from an equilibrium process.

Several approaches might improve efficiencies. Adiabatic heating and cooling may be used, but only at relatively low delta-T because adiabatic heating of NITINOL wire by stretching will pull the wire apart before a temperature difference of 30 degrees C is achieved.

Increase of the specific power density will increase efficiency directly. There is a good probability that the present work output of one joule per gram cycle may be increased to 2 or even 3 joules, with a corresponding increase in efficiency.

Another approach is through the use of a regenerator. An engine incorporating a regenerator has been built and tested[3], but was not instrumented for calorimetry. We present here the result of an experiment using a regenerator which was not operated as an engine. Conclusions about regenerative engine efficiency should be interpreted with this caveat.

---

[2]C. M. Jackson et al., "55-NITINOL—the alloy with a memory: Its Physical Metallurgy, Properties, and Applications," NASA-SP 5110, National Aeronautics and Space Administration, Washington, DC, 1972.

[3]A. D. Johnson, "NITINOL Heat Engines," Record of the Tenth Intersociety Energy Conversion Engineering Conference, Newark, DE, August 18-22, 1975, Paper #759082, pp. 530-534.

EFFICIENCY MEASUREMENTS ON A REGENERATOR

In May 1976, preliminary measurements estimated the efficiency improvement in a regenerator (Fig. 2). This consisted of two sets of pulleys (P1P2) and (P3P4) each reeved about by a NITINOL wire, all contained in an insulated enclosure. Pulleys P1 and P3 were immersed in hot water, P2 and P4 in cold. If (P1P2) rotate clockwise while (P3P4) rotate counterclockwise, as shown by the arrows in Fig. 2, then, in each of the long narrow passages which connect the hot and cold baths, heat rejected by the wire leaving P1 (or P3) is absorbed by the cold wire leaving P4 (or P2). Thus a temperature gradient was established and maintained along each of these narrow passages. If the wires pass slowly through a passage, a state of quasi-equilibrium minimizes entropy generation. Wipers may be placed in each regenerative passage to reduce water transport through the tubes.

This configuration of NITINOL loops and pulleys could be run as an engine by coupling (P1P2) and (P3P4) and making P4 and P2 a few percent smaller than P3 and P1, respectively. For this study, the machine was not operated as an engine. Instead, losses when the pulleys were counter-rotated as shown, i.e. in a regenerative mode, were compared with losses when the pulleys were corotated, i.e. with two wires traveling in the same direction through each regenerative passage. Table III summarizes the results. The power consumed with counter-rotating pulleys (regenerative mode) was approximately 3.6 times less than in a non-regenerative mode. These data were taken at a relatively low speed, so that the calculated power density is reduced to about .2 watts/gm.

This experiment clearly requires much more work to determine whether this efficiency can be obtained at higher speeds, and to check on the assumption that latent heat is constant under load, which is surely only approximately true. However, we feel these results indicate the regenerator has potential use in situations in which the increased efficiency justifies the expense of lowered power density.

POWER OUTPUT STUDIES

Power output per unit mass from a continuous-band NITINOL engine is determined by the cycle rate multiplied by the work output per unit mass per cycle. Maximum cycle rate is governed by heat transfer rates which depend upon the surface area to volume ratio. Work output per cycle is a function of temperatures and tensions in the hot and cold segments of the band. For this study, power output measured in a simulated engine cycle is compared with the result of running an actual engine, the same engine used for the above efficiency measurements (Fig. 1).

Engine cycle simulation data (Fig. 3) were taken using the stress-strain fixture employed for training studies reported at this Conference.

Engine cycle simulation consisted of four phases, indicated by lines on Fig. 3. At point A the temperature was that of the hot bath T_H, and tension S_1 was at a minimum. The wire was contracted. Hot water was valved out and replaced with cold water at temperature T_C from the cold reservoir. The wire relaxed and elongated to length B, still at minimum tension but now at cold temperature T_C. Next, weights were added, increasing the tension and stretching the wire isothermally to point C, where the temperature remained T_C and the tension was at maximum, S_2. The cold water was then removed and replaced with water at temperature T_H from the hot reservoir. The NITINOL wire contracted, raising the weight and shortening the wire to elongation D. Here the temperature was T_H and tension was maximum. The cycle was completed by reducing the tension to S_1, during which the wire again contracted to elongation A. The Figure shows three successive cycles at three increasing values of tension S_2.

The work done in this cycle is the area ABCD enclosed in the figure. Segments AB and CD are straight lines, while BC and DA are curves which depend upon the stress-strain characteristics of the material. The area within the curve is estimated to be 1.75 joules for a wire whose mass is 1.75 grams, for a density of one joule/gm cycle.

This result may be compared with data taken with the non-regenerative continuous-band engine. Table IV shows a typical set of run parameters. The results agree well with the simulation. It seems reasonable to conclude that power densities approaching one joule/gram cycle have been achieved in continuous-band engines, and that these bands may be cycled more than once per second, yielding in excess of a watt per gram of NITINOL.

Power density may be further enhanced at the same stress level by impovements in design. In the above example (Fig. 1), at least half of the NITINOL wire length is wasted in traveling from bath to pulley and return. In terms of optimal power density, the most desirable engine is very long, with pulleys small in relation to the length, and an element having a large surface to volume ratio such as a flat ribbon or multiple fine wires. Such a device might cycle 10 or more times per second, with a corresponding power density of 10 or more watts per gram. Such high speed would, of course, be accompanied by larger viscous losses.

CONCLUSIONS

A non-regenerative continuous-band NITINOL engine operating at liquid water temperatures has been shown to have an overall efficiency greater than one percent. The upper limit for this design, due to entropy generation during heating and cooling, is not much more than 2 or 3 percent. Power density in this design is of order 1 watt per gram of NITINOL. Input power is divided among latent heat (approximately 25 watts/gm), sensible heat (approximately 25 watts/gm), and heat losses (about 25 watts/gm). A regenerator can increase efficiency by at least a factor of three. Further experimentation is required to determine what fraction of Carnot efficiency is possible with this configuration.
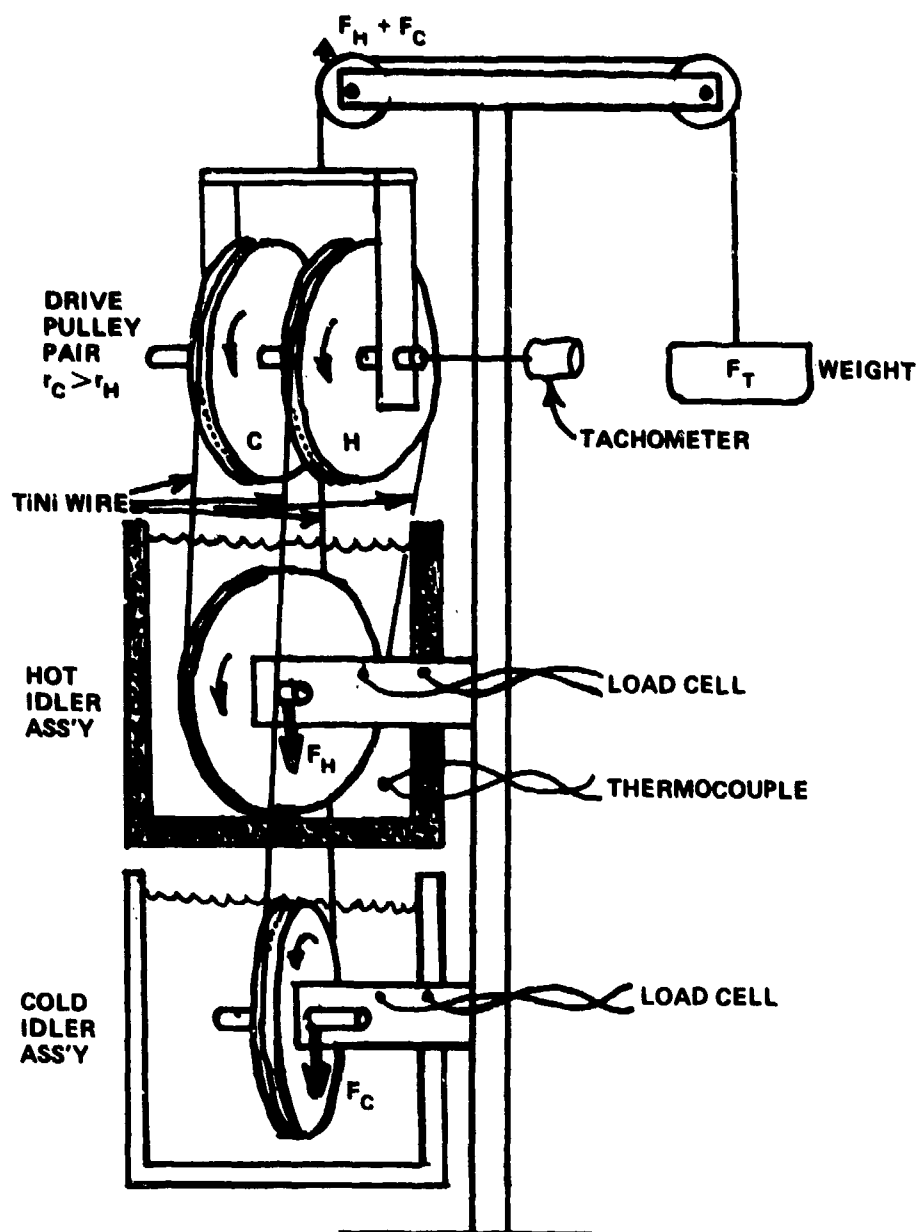
CONTINUOUS-BAND
NITINOL HEAT ENGINE
INSTRUMENTED FOR
EFFICIENCY MEASUREMENTS

TORQUE $= 1/2\,(F_H - F_C)(r_C - r_H) = (F_H - w/2)(r_C - r_H)$
WHERE F_H = FORCE ON HOT IDLER
$\quad\quad F_C$ = FORCE ON COLD IDLER
$\quad\quad w = F_H + F_C$ = FORCE ON DRIVE PAIR

r_H, r_C ARE DRIVE PULLEY RADII
POWER = TORQUE x ANGULAR VELOCITY
$\quad\quad = (F_H - w/2)(r_C - r_H) \times$ RPM x $2\pi/60$
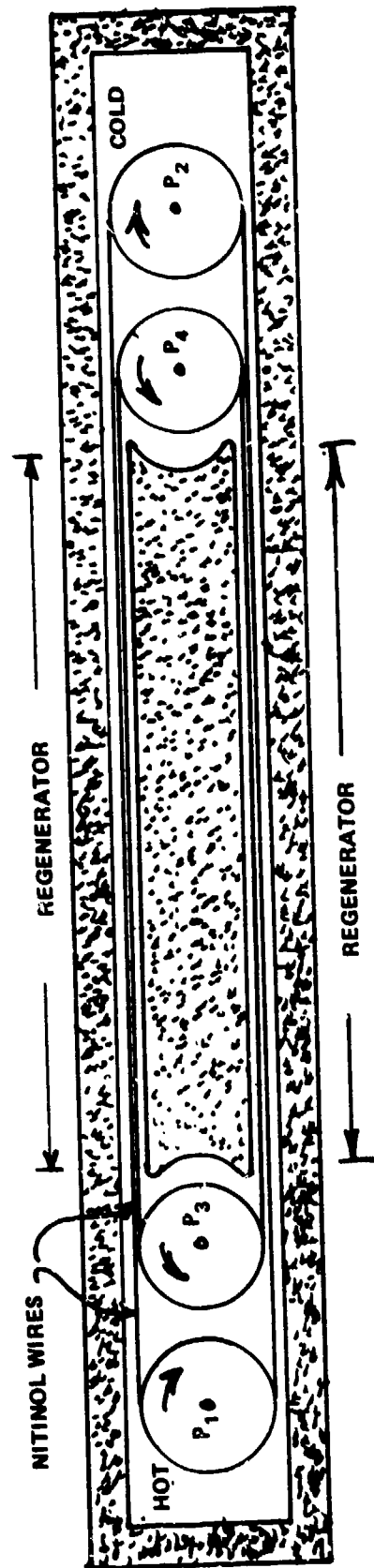
FIGURE 1

FIGURE 2

DOUBLE REGENERATOR
AS USED IN EFFICIENCY MEASUREMENTS

FIGURE 3

NO. 2 TIMET 0.030″ WIRE, TRAINED ON ENGINES NO. 10-14 (1974-75)
(SEVERAL HOURS ACCUMULATED RUN TIME)
3% ELONGATION RATIO (1.75 gm)
3 CONSTANT FORCE CYCLES, $T_C < 4°C$ $T_H > 95°$
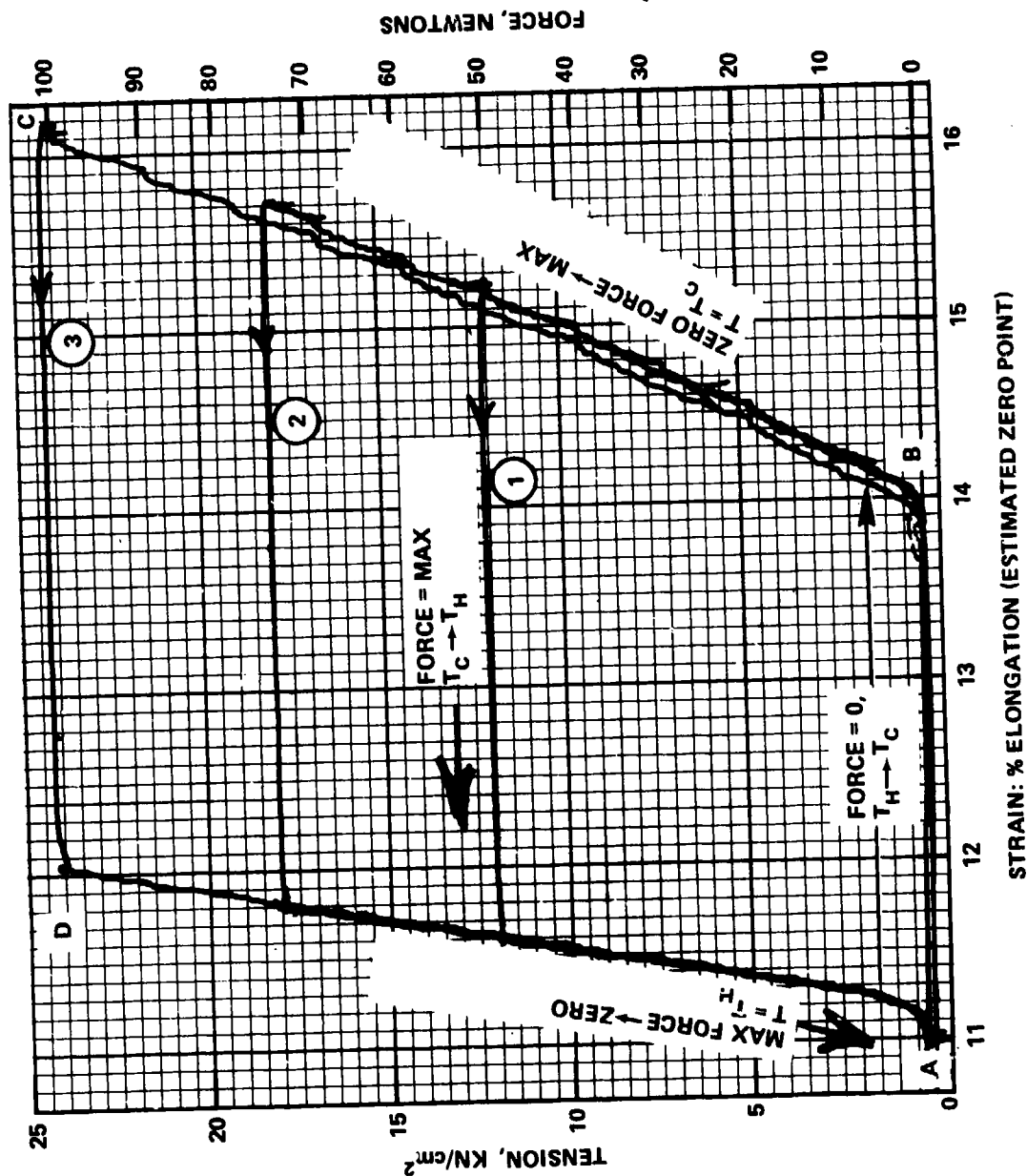
A — D, B — C
1) NOTE: EXCESS SLOPE DUE, IN PART,
TO FLEXIBLE CABLE USED TO
SUPPORT WEIGHTS
2) AREA $\cong 0.0175 \times 100 = 1.75$ JOULE
METER   NEWTON

STRAIN: % ELONGATION (ESTIMATED ZERO POINT)

FORCE, NEWTONS

TENSION, KN/cm²

TABLE 1 RESULT OF EFFICIENCY TEST: NON-REGENERATIVE NITINOL ENGINE

Specific heat of NITINOL	C_p	.08 cal/gm^{o}C
Latent heat of NITINOL (assumed constant)	C_t	5.8 cal/gm
Temperature in Hot tank	T_1	85 to 65°C
Temperature in Cold tank	T_2	∿ 5°C
Mass of NITINOL wire	m	3.3 gm
Length of NITINOL wire	l	2.13 m
Pulley diameter	d	.1 m
Speed 300 RPM		3 gm/sec
Volume of Hot water	V	800 ml
Rate of temperature change	dT/dt	2.80/min
Power input		+ 164 watts
Power dissipated as Latent Heat		- 58 watts
Power dissipated as Sensible Heat		- 54 watts
Power lost due to mixing and other losses		- 55 watts
Power output, calculated from speed and torque		- 2

Balance   -   5 watts

Efficiency = power out/power in = 1.2%

TABLE 2 RESULT OF EFFICIENCY TEST: NONREGENERATIVE ENGINE WITH STEEL WIRE

Specific Heat of Steel	C_p	. 077 cal/gm^{o}C
Latent Heat		0.
Temperature in Hot Tank	T_1	85 to 65°C
Temperature in Cold Tank	T_2	5°C
Mass of Steel wire	m	4.8 gm
Length of Steel wire	l	2.33 m
Pulley diameter	d	.1 m
Speed 300 RPM		3.2 gm/sec
Volume of Hot water	V	790 ml
Rate of Temperature change	dT/dt	2.0 ^{o}/min
Power input		÷ 110 watts
Power dissipated as Sensible heat		- 67 watts
Power lost due to mixing etc (same as TiNi)		- 54 watts
Power output		0

Balance — 1 watt

TABLE 3   RESULT OF EFFICIENCY TEST: REGENERATOR

		Co-Rotation	Counter-Rotation
Volume Hot Water	V	650 ml	600 ml
Rate of Temp Change	dT/dt	1.6^{o}C/min	$.7^{o}$C/min @70°C
Power Input	P	+ 72 watts	29 watts
Static Losses		- 12 watts	12 watts
Power into Wires		- 60 watts	17 watts
Pulley Diameter		.1 m	.1 m
Linear Speed		.38 m	.38 m/sec
Mass rate (two wires)		1.1 gm/sec	1.1 gm/sec
(Calculated power output assuming 1 joule/gm cycle)		1.1 watts	1.1 watts
(Calculated efficiency assuming constant latent heat)		1.8%	6.5%

TABLE 4 TYPICAL RUN PARAMETERS FOR POWER OUTPUT STUDY ON A CONTINUOUS-BAND NITINOL ENGINE

Radius of Hot drive Pulley	r_h	.0475 meter
Radius of Cold drive Pulley	r_c	.0492 meter
Wire length	1	2.13 meter
Wire mass	m	3.3 gm
Mass velocity	v	4.8 gm/sec
Weight = $f_c + f_h$	W	136 newton
Force on Hot Pulley	f_h	102 newton
Rotation rate 600 RPM	w	62.8 radians/sec

Power output by NITINOL wire = $(f_h - W/2)(r_h - r_c)_w$ = 3.3 watts

Power density - 1 watt/gm TiNi

Work output/gm cycle = 3.3/4.8 - .69 joule/gm cycle

BIBLIOGRAPHY

A. D. Johnson, "NITINOL Heat Engines," Record of the Tenth Intersociety Energy Conversion Engineering Conference, Newark, DE, August 18-22, 1975, Paper #759082, pp. 530-534.

C. M. Jackson et al., "55-NITINOL--the alloy with a memory: Its Physical Metallurgy, Properties, and Applications," NASA-SP 5110, National Aeronautics and Space Administration, Washington, DC, 1972.

J. S. Cory, et al. "NITINOL Heat Engines for Economical Conversion of Low Grade Thermal Energy," Proceedings of the 13th Intersociety Energy Conversion Engineering Conference, Vol. III, San Diego, CA, August 20-25, 1978, Paper #789031, pp. 1998-2004.

EFFICIENCY OF ENERGY CONVERSION IN NITINOL

Richard D. Kopa

Lawrence Berkeley Laboratory
University of California, Berkeley

ACKNOWLEDGMENT

ABSTRACT

NITINOL--one of several Shape Memory Effect (SME) alloys--is known to be a suitable medium for converting heat to usable mechanical work in a "solid state" heat engine. The present study experimentally investigates the efficiency of the energy conversion in NITINOL.

An electronically controlled Cycle Simulator subjects a single NITINOL wire element to the stress-strain-temperature cycles corresponding to a specific thermodynamic cycle (constant-strain isothermal, stress-limited isothermal, constant-stress isothermal, semi-adiabatic, etc.), as selected during the investigation. The test parameters, which are varied singly or in combination, include various stress levels, stress rates, percent of elongation of the wire, temperature levels, heating and cooling rates, cycling speeds, etc. Efficiency values as a function of these variables are plotted in graphs, and the factors affecting efficiency are discussed. The highest thermodynamic efficiency thus far determined is 1.2 percent (approximately 6 percent of Carnot efficiency), with a concomitant NITINOL wire life expectancy on the order of 10^4 cycles. However, these values are not regarded as the highest attainable. It is anticipated that higher efficiency as well as life expectancy would be realized with NITINOL alloys perfected through basic materials research and development. Nevertheless, the fundamental limitation of the energy conversion efficiency is set by the inefficient type of thermodynamic cycle--namely, the isothermal cycle--to which the "solid state" heat engine operation (with presently available SME materials, such as NITINOL) is restricted. The reasons for this restriction are discussed in pp. 9-12 through 9-22.

The simple contant-strain isothermal cycle is analyzed and described in stress-strain coordinates and in a T-S diagram. An analytic expression for the calculation of the energy conversion efficiency is presented, along with experimental investigation of the proposed postulates. A few preliminary investigations of various approaches to efficiency improvement are reported, and one promising research area is suggested.

Further basic and materials research is needed for better understanding of the energy conversion process in NITINOL, for the clarification of the extent of validity of the proposed postulates, and for the determination of a rigorous expression for the efficiency of the constant-stress isothermal cycle.

1. INTRODUCTION

Devices and heat engines which employ Shape Memory Effect (SME) alloys (e.g., NITINOL) as the energy conversion media have been described in the literature.[1] Since these engines can work at nearly ambient temperatures and at a relatively small temperature difference between the hot and cold reservoir, they appear particularly suitable to applications involving solar flat plate collectors and geothermal and industrial waste heat sources, or for bottoming cycles of conventional power plants. Suggested commercial applications include solar cooling of buildings, agricultural pumping, and decentralized solar power generation. However, thus far only information on the theoretically estimated efficiencies, and some fragmentary information on experimentally determined efficiencies of these devices, have been published.

This paper describes an experimental parametric study of a NITINOL alloy subjected to a number of simulated thermodynamic engine cycles, in which the test parameters are systematically varied so that efficiency values as a function of these parameters are obtained, and the most efficient type of thermodynamic cycle is identified.

The information derived can serve as a basis for designing a "solid state" heat engine with the highest attainable efficiency and/or power density, for comparing theoretical and experimental efficiencies, as well as for providing reference data for further research and development of thermoelastic materials.

Another objective of the study is the determination of an engine cycle which offers the lowest progressive degradation, irreversible damage and creep, and therefore the longest life of the investigated thermoelastic material, which in this study is used in the form of wire elements subjected to cyclic tension stress.

2. BACKGROUND

The Shape Memory Effect in alloys has been extensively treated in the literature and therefore will not be discussed here. For familiarization with the subject, Reference 2, and

_____

[1] W. S. Ginell, J. L. McNichols and J. S. Cory, "Low-Grade Thermal Energy-Conversion Joule Effect Heat Engines," American Society of Mechanical Engineers, Paper 78-ENAs-7, July 1978.

[2] C. M. Jackson, H. J. Wagner and R. J. Wasilewski, "55 NITINOL - the Alloy with a Memory," Report NASA-SP 5110, 1972.

for more in-depth study, References 3, 4, 5, and 6 are suggested. Among the alloys exhibiting SME, NITINOL has been most widely studied and used in various technical applications. Reference 2 presents a comprehensive overview and an extensive literature survey of research activity on NITINOL.

More recently, the efficiency of the energy conversion in SME alloys underwent theoretical study by several investigators. Reference 7 predicted thermodynamic efficiency of 4.9 percent; References 8-11 calculated efficiencies in the range of 10 percent to over 20 percent. Moreover, some limited information on experimentally determined energy conversion

[3] J. Perkins, "Shape Memory Effects in Alloys," Proc. of the Inter. Symp. on Shape Memory Effects and Applications, Toronto, Ontario, Canada, May 1975; Plenum Press, New York.

[4] H. F. Mohamed, "Martensite Transformation and Shape Memory Effect in Ni-Ti Alloy," Report LBL-5112, Lawrence Berkeley Laboratory, University of California, Berkeley, May 1976.

[5] D. S. Lieberman, "Crystal Geometry and Mechanisms of Phase Transformations in Crystalline Solids," Paper presented at Seminar of Am. Soc. for Met., October 1968.

[6] Z. Nishiyama, Martensitic Transformations, Academic Press, New York, 1978.

[7] M. Ahlers, "On the Usefulness of Martensitic Transformations for Energy Conversion," Scripta Metallurgica, Vol 9 (1975), p. 71.

[8] H. C. Tong and C. M. Wayman, "Thermodynamic Considerations of 'Solid-State Engines' Based on Thermoelastic Martensitic Transformations and the Shape Memory Effect," Metallurgical Transactions A, Vol. 6A, January 1975.

[9] C. M. Wayman and H. C. Tong, "The Efficiency of the Shape Memory Effect for Energy Conversion," Scripta Metallurgica, Vol. 9 (1975), p. 757.

[10] B. Cunningham and K. H. G. Ashbee, "Marmem Engines," Acta Metallurgica, Vol. 25 (1977), p. 1315.

[11] A. A. Golestaneh, "Efficiency of the Solid-State Engine Made with NITINOL Memory Material," J. Appl. Phys., 49 (3), March 1978.

efficiencies in NITINOL has been reported in Reference 2, ranging from 10 percent to 16 percent, and in Reference 12, amounting to 2.7 percent. These studies were based on considerably differing assumptions and/or experimental conditions as well as on SME alloys of substantially different properties.

The previous study at this Laboratory[12] investigated the thermodynamic efficiency of the energy conversion process in NITINOL, with particular interest in determining the repeatability of the results over a large number of work cycles. It was estimated that for economically feasible technological applications, the life of the SME alloy, before failure due to fatigue, should extend to over 10^6 cycles.

3.   EXPERIMENTAL SYSTEM AND METHOD

Briefly, the conversion process of heat to mechanical work during the NITINOL engine cycle is:

1)   The NITINOL wire is cooled by submerging it into the cold bath to a temperature well below its transformation temperature. Consequently its crystalline structure stabilizes in a martensitic phase.

2)   While in the cold bath, it is easily stretched (NITINOL in the martensitic phase is highly ductile) by applying a moderate external force and elongated to a predetermined length (typically 1.0 percent to 5.0 percent strain).

3)   Thereupon the wire--while still elongated--is heated by submerging it into the hot bath, where it developes high stress (as the result of the reversed martensitic phase transformation process).

4)   Overcoming applied external load, the NITINOL wire contracts with a great force until it attains its original length. During the contraction, the wire produces useful mechanical work $\underline{W}$ equivalent to the product of the force $\underline{F}$ times the linear change $\underline{\Delta L}$ of the wire length during the contraction ($W = F \Delta L$).

At the completion of the wire contraction, a stabilized crystalline structure of the high temperature phase (austenitic) is again attained. The NITINOL is now ready for the next cycle, which starts with the cooling of the wire element.

To facilitate an accurate and repeatable execution of the above cycle, at various parametric conditions, an electronically controlled Cycle Simulator was designed.

Figure 1 schematically presents the major components of the test apparatus. A test sample of NITINOL wire $\underline{N}$ is stretched between arm $\underline{A_1}$, axially sliding on a rotating shaft, and arm A_2, solidly attached to the same shaft. Arm $\underline{A_2}$ carries a flexible beam on which is

---

[2] See footnote 2 on page 9-3.

[12] R. Banks, P. Hernandez and D. Norgren, "NITINOL Engine Project - Test Bed," Final Report, UCID-3739, Lawrence Berkeley Laboratory, University of California, Berkeley, July 31, 1975.

cemented strain gage $\underline{S}$, measuring the force exerted by the NITINOL wire $\underline{N}$. The axial motion of arm $\underline{A}_1$ is effected by a lead screw L driven by servomotor $\underline{M}_1$. The position of the arm $\underline{A}_1$ in respect to arm $\underline{A}_2$ is transmitted by means of a potentiometer readout $\underline{R}$ to the oscilloscope $\underline{OS}$ as a horizontal deflection of the electron beam. The vertical deflection of the beam is effected by an amplified signal from the strain gage $\underline{S}$. The stress-strain diagram displayed on the oscilloscope screen is recorded by means by a video camera and stored on a video tape.

The NITINOL wire $\underline{N}$ is transferred back and forth from the hot reservoir H and cold reservoir C by a 300° rotation of the shaft driven by the servomotor $\underline{M}_2$. Two linear servoamplifiers in the electronic control system $\underline{EC}$ electronically control the clockwise and counterclockwise rotation of the shaft as well as of the lead screw $\underline{L}$. The sequence of events, of positions, and of the speed of motion is programable to permit simulation of a desired type of the thermodynamic engine cycle.

Figure 2 shows the actual design drawing of the mechanical part of the apparatus; Figure 3 shows the complete experimental setup.

Since all known NITINOL engines operate on the (constant-strain, stress-limited, or constant-stress) isothermal cycle, this type of thermodynamic cycle was selected for the first series of experiments. The isothermal cycle consists of stretching an SME wire element in a cold bath under constant low temperature (isothermally), and thereupon transferring the stretched wire into a hot bath where it contracts, while developing strong force, under constant elevated temperature (isothermally). Typical isothermal work cycles (Figures 4-7) are discussed below:

Figure 4 is a sample of a video record of a constant-strain isothermal cycle with the pertinent parametric information (e.g., cycle No. 1554, NITINOL wire No. 1, length of wire 21.8 in, diameter of wire 0.019 in, temperature of cold reservoir +2.3°C and of hot reservoir +56.3°C, elongation $\Delta L = 0.29$ in, and type of cycle ISOTHERMAL).

The horizontal line at the bottom represents stretching of the wire (from left to right), under constant temperature; the vertical line represents the rise in stress after transfer of the wire into the hot bath; and the sloping line from right to left represents the contraction of the wire in the hot bath (at constant temperature). The area enclosed by these lines represents the effective work or mechanical energy produced by the wire element during one cycle.

In the following series of tests, the NITINOL wire was heated by an electric pulse, instead of submerged in a hot bath. Figure 5 shows the resulting record taken by a Polaroid camera from the oscilloscope screen.

The intensity and duration of the electric pulse (24V, 9A, 350 ms) in Figure 5 were adjusted to produce the same peak stress as in Figure 4. This procedure can correlate the temperature of the hot bath and the heat input to the wire during the phase transformation which generates the peak stress (see Appendix). The peak stresses in this series of tests ranged from 30Kpsi to 50Kpsi. The elongation (strain) of the wire ranged from 1.3 percent to 1.8 percent.

A noticeable difference exists between the horizontal lines of the records in both Figures. In Figure 4, the perfectly horizontal line signifies complete absence of stress during the stretching of the wire. This was attained by subjecting the virgin wire to 1000 training cycles of heating and cooling with a progressive change of the strain. Johnson[13] extensively investigate training of NITINOL wires. By this treatment, a "second memory" effect developed in the wire which consequently caused an elongation of the wire automatically upon submerging it into the cold bath. In Figure 5, the training did not produce so perfect a result and only a part of the elongation is stress-free.

Another series of tests investigated a "stress-limited" cycle. Figure 6 presents a typical result. The NITINOL wire, in this case, was suspended on a preloaded compression spring attached to the sliding arm A_1 (Figure 1). As the record indicates, a lower peak stress at higher elongation (2.7 percent) resulted. The durability of the wire element subjected to this type of cycle is presently under investigation. This cycle is an intermediate type between the constant-strain isothermal and the constant-stress isothermal cycle.

Figure 7 shows a typical record of a constant-stress isothermal cycle. The lower horizontal line and its extension sloping upwards (from left to right) represent the isothermal stretching of the NITINOL wire at constant temperature in the cold bath. The following short vertical line results when the strained wire is transferred into the hot bath. The upper horizontal line represents the contraction of the NITINOL wire (power stroke) at constant temperature and constant stress (in the hot bath). The following steeply downward sloping line represents the drop of stress at the end of the wire contraction (end of power stroke).

To execute this cycle, it was necessary to slightly modify the Cycle Simulator apparatus by attaching one end of the NITINOL wire to a cable (guided over three pulleys) which transmits a constant force exerted by suspended calibrated weights.

In these tests, the NITINOL wire was initially stretched in the cold bath (2°C) to 8 percent strain, then transferred into the hot bath (80°C) where the wire contracted under constant stress of 37Kpsi (26.0Kg/mm^2), lifting a weight of 4.78Kg. After several cycles, the load was reduced to produce 29Kpsi and the cycle was repeated about 200 times. A stabilized work diagram similar to that in Figure 7 was then recorded in all successive cycles. The permanent (irreversible) wire elongation amounted to approximately 3 percent of the original strain (portion of the lower horizontal line extending to the left and outside the area enclosed by stress-strain lines), and the remaining 5 percent constituted the effective periodic strain of the "stabilized" cycles.

---

[13]D. A. Johnson, "Training Phenomena in NITINOL," presented at the NITINOL Heat Engine Conference, September 1978, Naval Surface Weapons Center, Silver Spring, Maryland (printed elsewhere in the present volume).

4.   EXPERIMENTAL RESULTS

The efficiency η of the conversion of heat to mechanical work is defined as the ratio of the useful work $\underline{W}$, produced by the NITINOL wire, and of the heat input $\underline{Q}$ to the wire element during every engine cycle.

$$\eta = \frac{W}{Q} \qquad (1)$$

The mechanical work is determined by the planimetry of the work diagram (area on the oscilloscope screen enclosed by the stress-strain lines). The heat input was calculated from experimental data in Reference 2, or directly measured when an electric pulse (see Appendix) supplied heat to the wire.

Equation (1) can be written as follows:

$$\eta = \frac{F E \alpha L_{[g]}/L \; 0.981}{Q_{[g]}} \qquad (2)$$

where F is the force in $\underline{Kg}$ exerted by the wire at the peak stress, $\underline{E}$ is elongation of the wire in $\underline{mm}$, $Q_{[g]}$ is the total heat input per cycle in Joules per gram of wire element, α is the work diagram area factor, $L_{[g]}/L$ is the ratio of the length of wire weighing 1.0 gram to the length of the test wire (for NITINOL wire of $\underline{D}$ = 0.019 in = 0.483 mm, the length $L_{[g]}$ = 846 mm).

For a constant-strain isothermal cycle $\underline{\alpha} \approx 0.5$, and for the theoretically ideal cycle $\underline{\alpha}$ would approach unity.

Equation (2) can further be written as follows:

$$\eta = \frac{\sigma_3 \; \epsilon \alpha/\gamma \; 0.249}{Q_{[g]}} \qquad (3)$$

where σ_3 is the maximum peak stress in $\underline{Kpsi}$, $\underline{\epsilon}$ is strain in percent of elongation, $\underline{\gamma}$ = 0.234 lb/in^3 is the density of NITINOL, and 0.249 is a conversion factor.

Figure 8a graphically represents equation (3) for a typical value of the heat input to the wire element Q = 50 Joule/g (for full martensitic transformation) and α = 0.5, corresponding to a typical constant-strain isothermal cycle. Similarly, Figure 8b presents the plot of Equation (3) for $\underline{\alpha}$ = 1.0, which would apply to an ideal engine cycle.

---

[2]See footnote 2 on page 9-3.

Figure 8 indicates the theoretically predicted efficiencies in References 8 to 11 of 10 percent and above are not attainable in any type of thermodynamic cycle involving heat input of the order of 50 Joules (or more) per gram of the SME material. For example, to obtain efficiency of 10 percent with an ideal engine cycle (α = 1.0), the NITINOL wire would have to develop a recovery stress over 80Kpsi at 6 percent of elongation. However, no presently known SME alloy would sustain cyclic (heat-stress-strain) loads at this stress level for more than a few cycles. Even at considerably lower stress and elongation levels, the NITINOL wire element would fail after a few cycles because of cumulative permanent deformation and irreversible damage due to progressive creep.

The following figures present the typical test results obtained in this study. The SME material used in all tests was NITINOL wire of diameter D = 0.019 in., 50.4 percent atomic Ni, produced by TIMET. The individual types of engine cycle investigated are:

A   Symbol O represents isothermal constant-stress cycle (ϵ = 5.0 percent) at constant T_3 = 75°C, with variation of σ_3 from 17.7 to 37.1Kpsi.

B   Symbol ∇ represents isothermal constant-strain cycle (ϵ = 1.3 percent) with variation of T_3 from 45°C to 70.4°C.

C   Symbol $\diamondsuit$ represents isothermal constant-strain cycle (ϵ = 0.5 percent) with variation of T_3 from 34°C to 84°C.

D   Symbol $\lozenge$ represents isothermal stress-limited cycle (ϵ = 0.5 percent) with variation of T_3 from 37°C to 70°C.

E   Symbol $\square$ represents isothermal constant-strain cycle, strain varied in steps: ϵ = 0.5 percent, ϵ = 1.1 percent, and ϵ = 1.6 percent, at constant T_3 = 51°C.

F   Symbol $\lozenge$ represents isothermal constant-strain cycle, strain varied in steps: ϵ = 0.5 percent, ϵ = 1.1 percent, and ϵ = 1.6 percent, at constant T_3 = 71°C.

G   Symbol Δ represents isothermal constant-stress cycle (ϵ = 5.0 percent) and constant peak stress σ_3 = 37.1Kpsi, with variation of T_3 in steps: 53°C, 61°C, and 77°C.

Every data point in Figures 9 through 15 represents, on 1 average, several hundreds--and every curve several thousands--of repeated test cycles. Every series of tests has been started with a new trained and stabilized wire after at least 500 repeated cycles.

---

[8] See footnote 8 on page 9-4.

[9] See footnote 9 on page 9-4.

[10] See footnote 10 on page 9-4.

[11] See footnote 11 on page 9-4.

Figure 9 represents the recovery peak stress, resulting during various types of the isothermal engine cycle, as the function of the hot reservoir temperature T_3. The temperature of the cold reservoir T_1, was maintained for all tests between +1°C and +2°C, except for the stress-limited cycles (curve Ⓓ), for which it was +25°C.

Figure 9 reveals the following:

a)   Generally, the peak recovery stresses appear substantially higher than the recovery stresses reported in the literature (e.g. Reference 14). However, the peak recovery stresses of the test series Ⓑ , Ⓒ , Ⓔ , and Ⓕ for the same ϵ are noticeably different. This could be due to the nonidentical thermal and mechanical history (resulting during manufacture,"training" period, and the test period) of the individual NITINOL wire elements. For example, in test series Ⓑ the strain ϵ = 1.3 percent was kept constant, but in Ⓔ and Ⓕ it was varied from ϵ = 0.5 percent to ϵ = 1.6 percent.

b)   The peak recovery stresses of the stress-limited cycles (curve Ⓓ) are substantially higher than the recovery stresses of the constant-strain cycles (curve Ⓒ), although the strain ϵ = 0.5 percent was maintained the same for both test series. This effect resulted when the temperature T_1 of the cold reservoir for the stress-limited cycles was raised to +25°C. In such case the phase transformation process is incomplete. Only part of the austenitic phase is transformed during the cooling of the NITINOL wire to thermal martensite, while another part is contributed by the stress-induced martensite during the wire straining. Because of the substantial stress σ_2 at the end of straining, a correspondingly higher peak recovery stress σ_3 results. Therefore, for T_1 = +25°C, the stress-limited operation was necessary to prevent excessively high peak recovery stresses, which otherwise would rapidly degrade the wire element.

Figure 10 presents the useful work W produced by the various types of engine cycles as the function of the peak recovery stress σ_3. Generally, the useful work increases linearly with the peak recovery stress. The yield is highest for the constant-stress cycle (curve Ⓐ), and is more than three times as high as the constant-strain cycle (curve Ⓑ) at the same peak stress level.

In contrast to this, the stress-limited cycle Ⓓ produces lower useful work W than the constant-strain cycle Ⓒ when both cycles are performed at the same strain (e.g., ϵ = 0.5 percent). This may be explained by the fact that a substantial amount of work has to be expended for straining of the wire in the cold reservoir at T_1 = 25°C, because at this temperature, the NITINOL has been only partially transformed to the martensitic phase.

Figure 11 presents the thermodynamic efficiency η of the conversion of heat to mechanical work in NITINOL as the function of the hot reservoir temperature T_3. For the determination of η, the heat input to the wire element must be known (see Equation (1)). For the test series Ⓖ and Ⓑ (broken lines), the heat input Q_H was calculated as follows: to the value of the latent heat of transformation ΔH = 5.78 cal/g was added the sensible heat $C_p(T_3 - T_1)$, where C_p = 0.11 cal/g deg (data taken from Reference 2). This represents only a first order, rough approximation to the actual heat input, as will be shown later. For the test series Ⓒ , Ⓓ , Ⓔ , and Ⓕ -- Ⓔ and Ⓕ are plotted in Figure 13--the heat input was

---

[14]W. B. Cross, A. H. Kariotis and F. J. Stimler, "NITINOL Characterization Study," NASA CR-1433, September 1969.

[2]See footnote 2 on page 9-3.

measured by the electric pulse method (see Appendix). Thus far no reliable method has been developed to measure the heat input Q_H to the wire element during the constant-stress isothermal cycle. The electric pulse method cannot be applied, because at high strains (as employed in contant-stress cycles, e.g., ε = 5.0 percent) the wire element cannot be contracted fast enough during the shape recovery, and therefore the heat losses from the wire element to the surroundings would introduce a significant error. For the test series G , the heat input Q_H was estimated, assuming for the constant-stress cycles the same relative difference between the calculated and measured values of Q_H as was experimentally determined for the constant-strain cycles.

The highest efficiency was obtained for most of the test-cycles at hot reservoir temperature T_3 = 60°C, and for the series D at about T_3 = 55°C. Figure 12 illustrates the effect of this shift (of the efficiency maximum toward the lower temperature T_3) on the ratio of the engine cycle efficiency η to the Carnot efficiency η_c. Particularly pronounced effect is evident for the stress-limited cycle series D , where it is the consequence of the smallest temperature difference $\Delta T = T_3 - T_1$ between the hot and cold reservoir. From Figure 12 it can be inferred that by a proper selection of the temperature T_1, T_3 and of the maximum stress level σ_3, a stress-limited or a constant-stress isothermal cycle can be found with a substantially higher η/η_c ratio than shown. Such a cycle would make the NITINOL heat engine more competitive with other energy conversion devices where heat sources with small temperature difference between the hot and cold reservoir (e.g., $\Delta T \leq 20$°C) are available.

Figure 13 shows the thermodynamic efficiency as the function of heat input Q_H to the wire element for various types of engine cycles. The superiority of the constant-stress cycle A and G is apparent.

Figure 14 presents the thermodynamic efficiency as the function of the peak recovery stress and points out the advantage of the constant-stress cycle A over the constant-strain cycle C . If, for example, the requirement of the wire durability should dictate the peak recovery stress limit at 25Kpsi, the efficiency of the constant-stress cycle would be almost three times higher than that of the constant-strain cycle.

Indeed, the experimental results obtained to date indicate that, for continuous cycling without noticeable progressive elongation of the NITINOL wire element, the maximum permissible recovery stress should not exceed 25Kpsi (17.6 Kg/mm^2). This limits the strain (for the tested material) to about 1.0 percent for the constant-strain isothermal cycle, and to about 5.0 precent for the constant-stress isothermal cycle. At this writing, all tests were repeated for fewer than 10^4 cycles, and the durability as well as the cumulative permanent elongation of the wire element due to creep have not been determined beyond that limit.

Nevertheless, in the case where a perfect "second memory" was established in the trained wire element (Figure 4), no detectable cumulative permanent elongation was observed even after several thousand cycles.

Only a small part of the planned research program has been completed thus far. Therefore the measure efficiency values reported should not be regarded as the highest attainable. Some improvement of energy conversion efficiency may be possible by thermal and mechanical pretreatment and by alloying of NITINOL with another metal.

However, results to date clearly indicate the energy conversion efficiency could be substantially improved only if the required heat input Q_H to the NITINOL wire during the engine cycle could be substantially reduced.

5. ANALYSIS OF THE ISOTHERMAL CYCLE

The isothermal NITINOL heat engine cycle can be described in a stress-strain diagram, and the flowpath of energy through the cycle can be defined in the corresponding temperature-entropy diagram. Figure 15a presents a simple constant-strain isothermal cycle in the stress-strain coordinates. The cycle starts at point 1 with straining of the NITINOL wire in the cold bath (along the isotherm T_1) until point 2. Then the wire is transferred into the hot bath and heated (under constant strain ε_2) until it attains the temperature T_3 (while developing high recovery stress) at point 3. Thereupon it is allowed to contract at constant temperature T_3, performing useful work and returning to the inital strain ε_1 at point 4. Point 4 does not lie on the isotherm T_3 (as theoretically would be expected for an ideal SME material), but on or near the isotherm T_1. This drop in stress is due to non-ideal thermodynamic behaviour of NITINOL, and the resulting magnitude of irreversible losses depends on the type of cycle used. It is well known that the change of the thermodynamic state of NITINOL (and other SME materials) from one point to another in the stress-strain-temperature space continuum depends on the path by which the new state has been reached. This means that the new state depends on the previous thermal and mechanical history, and consequently the initial state may not necessarily be attained by a reversed change of the state parameters. Therefore, the thermodynamic state parameters (σ, ε, T, U, H, S) are not uniquely definable in terms of specific thermodynamic functions.

Figure 15b schematically shows a hypothetical "entropy diagram." The cycle is defined again by the isotherms T_1 and T_3 and by the lines of constant strain ε_1 and ε_2. If we start the cycle at point 1 by straining the wire, the exothermic heat of elastic deformation Q_D generated in the NITINOL wire during the straining (because the coefficient of linear thermal expansion of NITINOL in the transition region is negative[15]) is rejected to the cold reservoir (point 1 to point 2). Therefore, the entropy of the NITINOL wire during isothermal straining decreases; this means that in the entropy diagram, point 2 must lie to the left of point 1. Conversely, during the wire contraction (point 3 to point 4), the endothermic heat of elastic recovery Q_R is absorbed by the wire from the surroundings (i.e., isothermic contraction in the hot bath), and the entropy increases (point 4 lies to the right of point 3 Figure 15b).

For isothermal elastic deformation[16,17] (of completely martensitic NITINOL) the heat Q_D can be expressed as:

[15] R. J. Wasilewski, S. R. Butler, and J. E. Hanlon, "On the Martensitic Transformation in TiNi," Metal. Sci J., Vol. 1 (1967), p. 104.

[16] M. B. Bever, D. L. Holt and A. L. Titchener, "The Stored Energy of Cold Work," Progress in Material Science, Vol. 17, Pergamon Press, Oxford, 1973.

[17] F. W. Sears, An Introduction to Thermodynamics, the Kinetic Theory of Gases and Statistical Mechanics, Addison-Wesley Press Inc., Cambridge, Mass., 1950 (p. 154).

$$Q_D = (\sigma_2 - \sigma_1) T_1 \frac{\alpha_T}{\gamma J} \tag{4}$$

In this equation, α_T is the negative coefficient of linear thermal expansion $[(^{\circ}C)^{-1}]$ in transition region, T_1 is the absolute temperature of the cold reservoir, $(\sigma_2 - \sigma_1)$ is the isothermal change in stress during straining $[kg/m^2]$, γ is the density of NITINOL $[kg/m^3]$, and J is the mechanical equivalent of heat $[427.8 \ mkg/kcal]$.

During the heating of the wire in the hot bath (from point 2 to point 3), the heat Q_H is absorbed by the NITINOL wire:

$$Q_H = C_p(T_3 - T_1) + \Delta H^{M \rightarrow A}_{(\sigma)} \tag{5}$$

where C_p is specific heat of NITINOL 0.11 kcal/kg (nearly constant in the range considered),

and $\Delta H^{M \rightarrow A}_{(\sigma)}$ is the latent heat of phase transformation (martensite $\rightarrow$ austenite) in the prestrained wire while the recovery stress rises from σ_2 to σ_3 ($\Delta H^{M \rightarrow A}_{(\sigma)}$ to be determined experimentally).

In Figure 15b, this change is schematically represented by a straight line connecting points 2 and 3. In reality, this would be an integral curve indicating the progressive entropy increase of the NITINOL during the reverse phase transformation, as the wire element is heated from T_1 to T_3. Moreover, during the cooling of the wire in the cold bath (point 4 to point 1), the progressive decrease in entropy would in reality be indicated by a similar curve of a reverse trend.

During the wire contraction (point 3 to point 4), the endothemic heat of shape recovery Q_R is absorbed by the NITINOL (assuming no phase transformation occurs during the contraction):

$$Q_R = (\sigma_3 - \sigma_4) T_3 \frac{\alpha_T}{\gamma J} \tag{6}$$

where $\sigma_3 - \sigma_4$ is the isothermal change in stress during the shape recovery (point 3 to point 4).

Finally, during cooling of the wire in the cold bath (point 4 to point 1), the heat Q_C is rejected

$$Q_C = C_p(T_3 - T_1) + \Delta H^{A \rightarrow M}_{(o)} \tag{7}$$

where $\Delta H^{A \rightarrow M}_{(o)}$ (to be determined experimentally) is the latent heat of transformation of austenite to martensite in relaxed NITINOL wire (zero external force).

Note that $\Delta H^{M \to A}_{(\sigma)}$ and $\Delta H^{A \to M}_{(o)}$ are not equal; the Lechatelier principle demands that $\Delta H^{M \to A}_{(\sigma)} > \Delta H^{A \to M}_{(o)}$. Their difference is:

$$\Delta h = \Delta H^{M \to A}_{(\sigma)} - \Delta H^{A \to M}_{(o)} = Q_H - Q_C \tag{8}$$

Similarly, Q_R and Q_D are not equal and their difference is:

$$\Delta r = Q_R - Q_D \tag{9}$$

The sum

$$\Delta q = \Delta h + \Delta r = W \tag{10}$$

represents the total amount of heat which theoretically could be converted into mechanical work during the isothermal cycle. The major part of the total heat, namely the sensible heat $C_p(T_3 - T_1)$ and the latent heat of phase transformation at zero external force $\Delta H^{A \to M}_{(o)}$ (and the heat of elastic deformation Q_D), is wasted--i.e., is transferred from the hot to the cold reservoir.

The theoretical energy conversion efficiency of any type of thermodynamic cycle can be expressed as:

$$\eta = \frac{W}{Q} = \frac{Q_{in} - Q_{out}}{Q_{in}} = 1 - \frac{Q_{out}}{Q_{in}} \tag{11}$$

where Q_{in} is the total heat absorbed by the SME wire element in the hot reservoir, and Q_{out} is the heat rejected from the wire to the cold reservoir. For the constant-strain isothermal cycle employing SME material, this becomes:

$$\eta = 1 - \frac{Q_C + Q_D}{Q_H + Q_R} \tag{12}$$

Substituting Eqs. (4), (5), (6), and (7) in (12) yields for the efficiency of the constant-strain isothermal cycle:

$$\eta = 1 - \frac{C_p(T_3 - T_1) + \Delta H^{A \to M}_{(o)} + (\sigma_2 - \sigma_1)T_1 \frac{\alpha_T}{\gamma J}}{C_p(T_3 - T_1) + \Delta H^{M \to A}_{(\sigma)} + (\sigma_3 - \sigma_4)T_3 \frac{\alpha_T}{\gamma J}} \tag{13}$$

or substituting Eqs. (8) and (9) in (12) gives:

$$\eta = \frac{\Delta h + \Delta r}{Q_H + Q_R} = \frac{\Delta q}{Q_H + Q_R} \tag{14}$$

Equation (14) proposes the theoretical limit of the efficiency of energy conversion in NITINOL subjected to a constant-strain isothermal cycle.

From equation (13) it is evident that the efficiency $\underline{\eta}$ will increase with increasing peak recovery stress $\underline{\sigma}_3$, since both terms $\Delta H_{(\sigma)}^{M \rightarrow A}$ and $(\sigma_3 - \sigma_4)$ increase with $\underline{\sigma}_3$. Peak recovery stress $\underline{\sigma}_3$, however, is the function of $\underline{\sigma}_2$ (and of $\Delta T = T_3 - T_1$), and furthermore, $\underline{\sigma}_2$ is the function of the effective strain $\underline{\varepsilon} = \varepsilon_2 - \varepsilon_1$.

The size of the area 1-2-3-4 in Figure 15b (which indicates the cycle efficiency) increases with $\underline{\varepsilon} = \varepsilon_2 - \varepsilon_1$ (i.e., increases with the distance between point 3 and 4). Conversely, if the strain $\underline{\varepsilon}$ is reduced (in the limiting case) to zero, the efficiency $\underline{\eta}$ becomes zero, because $\Delta r = 0$, $\Delta \bar{h} = 0$. Consequently by definition:

$$\Delta H_{(\sigma)}^{M \rightarrow A} + \Delta H_{\substack{(o) \\ (\sigma=0)}}^{M \rightarrow A} \equiv \Delta H_{(o)}^{A \rightarrow M} \tag{15}$$

For this case, the area 1-2-3-4 in Figure 15b reduces to a single curve between points $\underline{1}$ and $\underline{4}$, which then represents a simple strain-free thermal cycling of the (free, unrestrained) NITINOL wire between the temperatures T_1 and T_3.

The present analysis assumes the NITINOL absorbs the latent heat of transformation $\Delta H_{(\sigma)}^{M \rightarrow A}$ before the contraction of the wire begins (before point 3 in Figure 15b is reached). Although this assumption conflicts with the theorems of other investigators[8,18], it is nevertheless supported by the experimental evidence presented by Melton and Mercier[19] and by the following observation. Figure 16 shows a dual-beam oscilloscope record of the constant-strain isothermal cycle taken from the test series F. The electrical resistivity (higher beam) of the NITINOL wire during the engine cycle is recorded above the stress-strain diagram (lower beam). As indicated, the maximum change in resistivity occurs upon submerging the wire in the hot bath (from point 2 to point 3), and the resistivity subsequently remains nearly constant during the contraction of the wire element

---

[8]See footnote 8 on page 9-4.

[18]L. Delaey and G. de Lepeliere, "The Temperature-Entropy Diagram of Solid State Engines and Solid State Heat Pumping Systems with Shape Memory Alloys," Scripta Metallurgica, Vol. 10 (1976), p. 959.

[19]K. N. Melton and O. Mercier, "The Effect of Opposing Stress on Shape Memory and Martensitic Reversion," Scripta Metallurgica, Vol. 12 (1978), p. 5.

(point 3 to point 4). It has been well established[20] that the resistivity of NITINOL is distinctly different for the austenitic and for the martensitic phase. Moreover, the diagram in Figure 16 can be nearly duplicated when the heat input Q_H is effected by an electric pulse (Figure 20 in the Appendix). The pulse can be timed to be completed before the wire element begins to contract. Consequently, positively no external heat is supplied to the wire element during the shape recovery process.

On the basis of the above experimental evidence, it is proposed that, during the constant-strain isothermal cycle, the constrained NITINOL wire absorbs the latent heat of phase transformation before the beginning of the contraction, which implies that the phase transformation (martensite $\rightarrow$ austenite) may occur before the shape recovery event.

In the case of the constant-stress isothermal cycle, the experimental results to date are inconclusive. Further investigation is planned to identify the way $\Delta H_{(\sigma)}^{M \rightarrow A}$ is absorbed during this type of cycle.

Returning now to Equations (12) and (13), we may first calculate Q_D, Q_R, and Q_C. For a trained NITINOL wire with fully developed "second memory," no stress rise results during stretching of the wire in the cold reservoir, i.e., $\sigma_2 - \sigma_1 = 0$ and $Q_D = 0$. Taking the value of the coefficient of thermal expansion from Reference 15 gives us:

$$\alpha_T = 33 \times 10^{-6}/^\circ C$$

and the other material properties from Reference 2:

$$\gamma = 6.45 \times 10^3 \ kg/m^3 \ , \ \Delta H = 5.78 \ cal/g$$

and setting $(\sigma_3 - \sigma_4) = 30Kpsi$, and $T_3 = 343^\circ K$ in Equation (6) gives:

$$Q_R = 86.54 \times 10^{-3} \ cal/g = 0.363 \ Joule/g$$

Furthermore, assuming $\Delta H_{(\sigma)}^{A \rightarrow M} = \Delta H$ in Equation (7) yields for Q_C as the first approximation:

$$Q_C = 0.11 \times 70 + 5.78 = 13.48 \ cal/g = 55.4 \ Joule/g$$

---

[20] F. E. Wang, B. F. DeSavage, and W. J. Buehler, "The Irreversible Critical Range in the TiNi Transition," Jour. of Appl. Phys., Vol. 39 (1968), P. 2166.

[15] See footnote 15 on page 9-12.

In comparison to Q_C, the value of Q_R is relatively small and significantly contributes to the efficiency of the constant-strain isothermal cycle only if Q_R is comparable to the difference between Q_H and Q_C (Equation 12).

For the calculation of Q_H, the value of $\Delta H^{M \to A}_{(\sigma)}$ has to be determined. Tong and Wayman[21] concluded there will be only a small correction factor when calculating the difference between $\Delta H^{M \to A}_{(\sigma)}$ and $\Delta H^{M \to A}_{(o)}$. Several investigators derived expressions for $\Delta H^{M \to A}_{(\sigma)}$ based on the Clausius-Clapeyron relation.[22-25] Furthermore, Salzbrenner and Cohen[26] pointed out the difference between the chemical and elastic component of $\Delta H^{A \to M}_{(o)}$. Thus far, however, no calculated or measured values of $\Delta H^{M \to A}_{(\sigma)}$ as the function of recovery stress have been published for NITINOL. Therefore, this study attempted to determine experimentally the effect of stress on the latent heat of phase transformation.

In the test series Ⓔ and Ⓕ, the total heat input Q_H was determined as follows: the constant-strain isothermal cycle was repeated (at least one hundred times for every data point) at ε = 0.5 percent, 1.1 percent, and 1.6 percent elongation with $T_1 = +1°C$ and $T_3 = 51°C$ held constant (test series Ⓔ); the cycles for each ε setting were duplicated when the heat Q_H was supplied by an electric pulse instead of the hot bath (see Appendix); the

[21]H. C. Tong and C. M. Wayman, "On Carnot Cycles, Transformation Temperatures, and Latent Heats Under an Applied Stress, as Related to the Shape Memory Effect," Scripta Metallurgica, Vol. 10 (1976), p. 1129.

[22]K. Otsuka, C. M. Wayman, K. Nakai, H. Sakamoto and K. Shimizu, "Superelasticity Effects and Stress-Induced Martensitic Transformations in Cu-Al-Ni Alloys," Acta Metallurgica, Vol. 24 (1976), p. 207.

[23]C. Rodriguez and L. C. Brown, "The Thermodynamics of Stress-Induced Martensites in Cu-Al-Ni Alloys," Metallurgical Transactions A, Vol. 7A (1976), p. 1459.

[24]R. Smoluchowski, "Phase Transformation in Solids," in Phase Transition and Critical Phenomena, edited by H. Stanley (Chapter 8), Oxford University Press, New York, 1971.

[25]J. W. Allen, "Stress Dependence and the Latent Heat of the Morin Transition in Fe_2O_3," Physical Review B, Vol. 8, No. 7 (1973), p. 3224.

[26]R. J. Salzbrenner and M. Cohen, "On the Thermodynamics of Thermoelastic Martensitic Transformations," Acta Metallurgica, Vol. 27 (1979), p. 739.

voltage level of the pulse was adjusted so that the same peak recovery stress σ_3 was obtained as when the wire was heated in the hot bath; the product of voltage, current, and time interval of the pulse expressed in Joules/g is plotted in Figure 17a; also plotted are the data from the second test series Ⓕ run at the same parameter settings, except for the hot bath temperature which was maintained at 71°C. When the sensible heat ($C_p \Delta T$) was subtracted, the data points from both test series fell on one curve (Figure 17b). For comparison, the value $\Delta H = 5.78$ cal/g $= 24.2$ Joule/g, from Reference 2, is indicated by a cross (near the vertical scale). On the basis of these tests, the latent heat of transformation $\Delta H_{(\sigma)}^{M \to A}$ appears strongly influenced by the magnitude of the peak recovery stress.

The curve Ⓔ and Ⓕ is replotted again on a larger scale in Figure 18 and extrapolated to $\sigma_3 = 0$ which should theoretically yield:

$$\Delta H_{(o)}^{A \to M} \equiv \Delta H_{(\sigma=0)}^{M \to A}$$

If this value could be taken as the true $\Delta H_{(o)}^{A \to M}$, then the energy conversion efficiency as calculated by Equation (13) should indeed be high, approaching the Carnot efficiency in isothermal cycles with peak recovery stress of about 32 Kpsi. The real value of $\Delta H_{(o)}^{A \to M}$ is, however, quite different if defined in accordance with the law of conservation of energy: No energy can be lost during the entire cycle, and therefore the latent heat of transformation $\Delta H_{(o)}^{A \to M}$ (austenite $\to$ martensite) during the cooling period must include all the "unused" heat energy which, by definition, is the difference between the energy absorbed by the NITINOL (as the latent heat of transformation: martensite $\to$ austenite) during the heating period and the amount of heat that was converted to the useful mechanical work (neglecting Δr).

Based on the above definition, the latent heat $\Delta H_{(o)}^{A \to M}$ can be calculated from Equations (8) and (10), substituting for $\underline{\Delta h}$ the mechanical work $\underline{W}$, which has been determined by the planimetry of the stress-strain diagram (for each data point). Figure 18 shows the plotted results as the curve $\Delta H_{(o)}^{A \to M}$. (Note that $\Delta H_{(o)}^{A \to M}$ as derived by the calculation appears not as a constant value, but as a function of σ_3). Similar curves of the latent heat of transformation ($\Delta H_{(\sigma)}^{M \to A}$ and $\Delta H_{(o)}^{A \to M}$) can be experimentally derived for other types of engine cycles, such as the constant-stress isothermal and the semi-adiabatic cycle.

At present, an attempt is being made to define the fundamental causes of energy degradation during the SME energy conversion process and to determine whether a correlation exists between these causes and the characteristic trend of the latent heat of transformation ($\Delta H_{(\sigma)}^{M \to A}$ and $\Delta H_{(o)}^{A \to M}$) as the function of the peak recovery stress. Among the causes of the energy degradation, the following are being considered:

---

[2] See footnote 2 on page 9-3.

1) Internal friction in the lattice which causes dissipation of the elastic strain energy. This occurs particularly when stress and strain changes are not in phase.[26]

2) The irreversibility of spontaneous thermodynamic processes, such as spontaneous martensitic transformation. (The reversible processes are never spontaneous and require careful guidance from outside their boundaries.[27]

3) The residual internal stress fields in the lattice which contribute to hysteresis and the loss of the pseudo-elasticity.[28]

6. PRELIMINARY INVESTIGATIONS OF VARIOUS APPROACHES TO EFFICIENCY IMPROVEMENT

Besides the studies discussed above, a few preliminary investigations have aimed to improve the energy conversion efficiency in NITINOL. These investigations deal with: a) Favorable orientation of martensite variants. b) Adiabatic engine cycles. c) Engine cycles with heat recuperation.

a) FAVORABLE ORIENTATION OF MARTENSITE VARIANTS

During the martensitic phase tranformation in a stress-free NITINOL wire, theoretically 24 random oriented martensite variants develop in the parent (austenitic) lattice structure. Upon subsequent heating of the wire above the transition temperature, the martensite variants transform to the parent phase (austenite). However, when the martensitic (forward) transformation takes place under the action of stress (e.g., resulting from external force acting on the wire element in the direction of the wire centerline), only some preferentially oriented variants of martensite are likely to form, while the formation of others will be suppressed.[29] If it can be assumed that upon heating (reversed transformation) these preferentially oriented variants are those which most effectively contribute to the magnitude of the resulting recovery stress, then a way should be sought to assure such preferential orientation of the martensite variants also under the conditions of the actual engine cycle operation.

---

[26]See footnote 26 on page 9-17.

[27]F. H. Crawford and W. D. VanVorst, Thermodyamics for Engineers, Harcourt, Brace and World, Inc., New York, 1968, p. 225.

[28]S. Mendelson, "Mechanisms for Martensite Formation and the Shape Memory Effect," in Shape Memory Effect in Alloys, edited by J. Perkins, Plenum Press, New York, 1975 p. 487.

[29]R. J. Wasilewski, "The Shape Memory Effect in TiNi: One Aspect of Stress-Assisted Martensitic Transformation," in Shape Memory Effect in Alloys, edited by J. Perkins, Plenum Press, New York, 1975, p. 266.

Unfortunately, in the practical case of relatively rapid cooling of NITINOL during the engine cycle (after contraction and relaxation of the wire element has been completed), the orientation of the variants may rather follow the direction of the resulting internal (thermal) stresses which are generally oriented perpendicularly to the centerline of the wire element. Thus far, it has not been ascertained whether or not all these variants reorient themselves in the more favorable direction during the subsequent straining of the NITINOL wire. Perhaps it can be argued that a complete reorientation of all martensitic variants would generate additional lattice dislocations, resulting in increased hysteresis and decreased life of the wire element[28,30] and also decreased engine cycle efficiency. On the other hand, if a method could be devised to orient the martensitic variants in the more favorable direction during the rapid cooling of the NITINOL wire, perhaps a larger recovery force could be produced upon heating of the wire element, resulting in a larger amount of mechanical work during the engine cycle.

Preliminary test results of isothermal constant-strain cycles with very slow cooling rate of the wire element indicate the cycle efficiency improves by a factor of 2.0. This is interpreted as the consequence of more favorable orientation of the martensite variants due to the absence of thermal stresses during very slow cooling of the wire element in air (as compared to the fast cooling by submerging the wire in a liquid bath).

The most favorable orientation of the martensite could be expected if the isothermal engine cycle is performed entirely in the austenitic region (at a cold reservoir temperature above 50°C). Reference 31 suggested this. In such a case, only the stress-induced martensite would be generated during the straining of the wire, with the favorable orientation of the variants. However, the disadvantage of such a cycle is the inherently high recovery stress level and consequently short life of the NITINOL wire element.

b) ADIABATIC ENGINE CYCLES

For the highest possible thermodynamic efficiency, the NITINOL engine cycle should ideally closely approximate the Carnot cycle. The Carnot cycle consists of two adiabatic and two isothermal changes of the thermodynamic state. The heat from the hot reservoir must be supplied during the engine cycle only at the highest cycle temperature T_3 (isothermally), and the rejected heat must be transferred to the cold reservoir only at the lowest cycle temperature T_1 (isothermally). In contrast to the previously discussed isothermal engine cycle (Figure 15), no heat is exchanged with the surroundings at any temperature intermediate between T_3 and T_1 (Reference 32). The necessary heating of the NITINOL wire from T_1 to T_3 must be accomplished by the adiabatic heating resulting from rapid straining of the wire

---

[28] See footnote 28 on page 9-19.

[30] M. Ahlers, R. Rapacioli, and W. Arneodo, "The Martensitic Transformation in β-Brass and the Shape Memory Effect," in Shape Memory Effect in Alloys, edited by J. Perkins, Plenum Press, New York, 1975, p. 379.

[31] O. Weres, "On the Thermodynamics of the Shape Memory Alloys," Report LBL-3297, Lawrence Berkeley Laboratory, University of California, Berkeley, November 1975.

[32] E. A. Guggenheim, Thermodynamics, North-Holland Publishing Company, Amsterdam, Third Edition, 1957, p. 94.

element. Similarly, the adiabatic cooling of the wire element should be attained by rapid contraction of the wire. Unfortunately, this type of cycle does not appear realizable with SME polycrystalline materials, because the phase transformation process can be accomplished (i.e., the latent heat of transformation can be absorbed) over only a definite span of the temperature range (e.g., 50°C). This means that, in the strict sense of the definition, the condition of a total heat input at the highest cycle temperature cannot be satisfied.

A part-way approach to the Carnot cycle can be attained by a semi-adiabatic cycle. Such a cycle is schematically shown in Figure 19a in the stress-strain coordinates and in Figure 19b in the T-S coordinates. The cycle starts with the removal of the NITINOL wire from the cold bath and adiabatic rapid straining of the wire in air (point $\underline{1}$ to point $\underline{2}$), while the stress rises from σ_1 to σ_2, and the temperature from $\underline{T}_1$ to $\underline{T}_2$. Thereafter, the wire is instantly submerged in the hot bath (hot reservoir) which is maintained at the temperature T_3. Here the wire absorbs the latent heat of transformation and the sensible heat $C_p(T_3 - T_2)$, while the stress rises to σ_3. At this point, the wire is removed from the hot bath and allowed to rapidly contract (point 3 to point 4), while the stress drops to σ_4 and the temperature to $\underline{T}_4$. At the end of this interval, the original length of the wire is recovered and the power-stroke completed. Finally the wire is transferred back into the cold bath (point 1), where it is cooled to temperature $\underline{T}_1$ while rejecting the latent heat of transformation and the sensible heat $C_p(T_1 - T_4)$.

Experience shows that the temperature $\underline{T}_1$ must be adjusted so that only a partial martensitic transformation takes place in the cold bath. If a complete transformation is allowed, the NITINOL wire becomes too ductile and the temperature will not rise during the subsequent rapid straining (point 1 to point 2).

The major difficulty in realization of the semi-adiabatic cycles, aside from the necessity of accurate timing of all cycle events, is the requirement for rapid straining of the NITINOL wire. If the straining time is more than one-half second, much of the heat (which was generated by straining the wire) is lost by convection to the surrounding air, and the adiabatic temperature rise (point 1 to point 2) is reduced. Rapid straining, however, may cause nonuniform stress and temperature distribution in the wire. This in turn may increase internal friction in the lattice, leading to a decrease of the efficiency and life of the wire element.

The adiabatic temperature rise that can be accomplished by rapid straining of the presently available NITINOL wire is quite limited. This is because the strain-temperature coefficient of adiabatic heating (resulting in the heat of elastic deformation) is small. As the first approximation, ΔT_D can be calculated from Equation (4) dividing the heat of elastic deformation Q_D by the specific heat of NITINOL:

$$\Delta T_D = \frac{(\sigma_2 - \sigma_1)\alpha_T T_1}{C_p \gamma J} \tag{16}$$

Simultaneously, an additional temperature rise ΔT_M is effected by the exothermic latent heat of transformation, originating from the stress-induced martensite which grows during the stressing of the wire element. ΔT_M can be calculated only if the amount of the stress-induced martensite $(\%)_M$ is known:

$$\Delta T_M = \frac{(\%)_M \, \Delta H^{A \rightarrow M}_{(\sigma)}}{C_p} \tag{17}$$

9-21

(where $\underline{C}_p$ is taken as the average value). The total temperature rise is then:

$$(T_2 - T_1) = \Delta T_D + \Delta T_M \tag{18}$$

Preliminary tests were conducted to determine the total temperature rise $(T_2 - T_1)$ experimentally. For 1.0 percent strain effected in 65 ms (starting at $T_1 = 24^{o}C$), the total temperature rise was about $4^{o}C$. The method employed in these tests will be published later. The present result is tentative, and additional tests employing other measurement methods are in preparation.

The efficiency of the semi-adiabatic cycle can be written as:

$$\eta = 1 - \frac{Q_C}{Q_H} = 1 - \frac{C_p(T_4 - T_1) + \Delta H^{A \to M}_{(o)}}{C_p(T_3 - T_2) + \Delta H^{M \to A}_{(o)}} \tag{19}$$

Comparing Equation (19) to (13), and assuming all other factors the same, we see that an efficiency improvement over the isothermal cycle can be expected only if the reduction of the sensible heat $C_p(T_3 - T_2)$ and $C_p(T_4 - T_1)$ relative to $C_p(T_3 - T_1)$ is substantial. This, of course, depends on the magnitude of the adiabatic temperature rise $(T_2 - T_1)$ and the temperature drop $(T_4 - T_3)$, respectively.

Preliminary tests of the semi-adiabatic cycle have been conducted; however, no data indicating a substantial efficiency improvement were obtained to date.

c) ENGINE CYCLES WITH HEAT RECUPERATION

One evident approach to efficiency improvement is based on the principle of heat recuperation during the engine cycle. The objective is to transfer the heat available from a NITINOL wire element which has just completed the engine cycle (end of power stroke) to another wire element which has been strained and is ready to be heated and to start the power stroke. However, because of the relatively low heat conductivity of NITINOL and the small temperature gradient between the wires in a (counterflow) heat exchanging relationship, the heat transfer rate is low, limiting the potential efficiency improvement. Depending on the sophistication and type of the engine design concept, an efficiency improvement by a factor of 1.5 to 2.5 appears feasible.

7. DISCUSSION AND CONCLUSION

The studies here experimentally investigated the efficiency of converting heat to useful mechanical work in a "solid state" NITINOL heat engine. Various thermodynamic engine cycles were performed on a specially designed cycle-simulator apparatus. Each test series covered a specific range of test parameters, and repeated each specific setting of the test parameters over several hundreds of cycles.

The highest thermodynamic efficiency on the order of 1.2 percent (approximately 6 percent of Carnot efficiency) has been demonstrated, with NITINOL wire life expectancy of about 10^4 cycles. At more conservative stress and strain levels, lower thermodynamic efficiency resulted (about 0.5 percent); however, the wire life expectancy could be estimated to exceed 10^6 cycles.

These experimentally determined efficiencies do not agree with the theoretical calculations in References 8-11. The reason for this discrepancy might be as follows: The referenced calculations presume that the chemical free energy difference between the martensitic and the austenitic phase represents the maximum energy theoretically available for conversion to useful mechanical work. Although the chemical free energy difference constitutes the "driving force" for the phase transformation, it does not present a sufficient basis for the analytical determination of the energy conversion efficiency.

Determining the efficiency of any thermodynamic cyclic process requires adequately defining the sequence of events and the mode of energy transaction during each event of the specific type of thermodynamic cycle under consideration. This study's analysis of the constant-strain isothermal cycle is an example of such a procedure. To define the mode of energy transaction during the individual events of the isothermal cycle, several models have been considered and subjected to experimental verification. As a result, the following postulates were proposed:

1) The effective useful work obtainable during the (constant-strain) isothermal cycle equals the difference between the latent heat of reverse transformation $\Delta H^{M \to A}_{(\sigma)}$ (during increasing stress) and the latent heat of forward transformation $\Delta H^{A \to M}_{(o)}$ (during "stress-free" state: $\sigma_4 = 0$). An additional small contribution comes from the difference between the heat of elastic deformation Q_D (during the straining of the SME element) and the heat of elastic recovery Q_R (during the contraction of the SME element).

2) During the constant-strain isothermal cycle (the simplest NITINOL engine cycle), the latent heat of reverse transformation $\Delta H^{M \to A}_{(\sigma)}$ (martensite → austenite) is absorbed by the SME material before the shape recovery (contraction of the wire element) takes place.

3) The magnitude of the latent heat of reverse transformation $\Delta H^{M \to A}_{(\sigma)}$ (martensite → austenite) is a strong funciton of the peak recovery stress.

---

[8] See footnote 8 on page 9-4.

[9] See footnote 9 on page 9-4.

[10] See footnote 10 on page 9-4.

[11] See footnote 11 on page 9-4.

4) The magnitude of the (apparent) latent heat of forward transformation $\Delta H_{(o)}^{A \to M}$ (austenite → martensite) under the zero external force condition (after the contraction of the wire element) is not constant, as would be expected for an ideal SME material. Becuase of the nonideal behavior of the SME material (NITINOL), the magnitude of the (apparent) latent heat of forward transformation increases with the increasing peak recovery stress. This increase is presently interpreted as the consequence of the energy degradation in the NITINOL lattice during the engine cycle.

In accordance with the above postulates, Equations (13) and (14) yield efficiency values consistent with the experimental results reported here. It is evident that extensive basic and materials research is needed for a better understanding of the energy conversion process in NITINOL. An important advancement in this direction is presented in Reference 26, which elucidates the effect of the grain boundaries in a polycrystalline (versus single crystal) Cu-Al-Ni alloy on the internal frictional resistance, on the stored elastic strain energy in the lattice, and on the temperature range of the martensitic phase transformation. Phase transformation stuides of a single crystal NITINOL alloy have been suggested and are in preparation.[33]

In summary, the following conclusions can be drawn:

a) Generally, only the heat engines operating on adiabatic thermodynamic cycles can theoretically approach the Carnot cycle efficiency.

b) Because of the very limited temperature rise during the wire straining and the relatively large temperature range of the NITINOL phase transformation, the NITINOL heat engine can't operate on an adiabatic cycle and therefore is restricted (for all practical purposes) to the isothermal cycle.

c) The isothermal cycle is inherently (thermodynamically) inefficient, no matter whether fluids or solid-state materials are employed as the working medium.

d) The magnitude of the latent heat of reverse transformation of NITINOL $\Delta H_{(\sigma)}^{M \to A}$ substantially increases with increasing peak recovery stress. As the consequence of this increase of heat which is absorbed during the engine cycle, the efficiency is further lowered.

e) The potential engine efficiency $\underline{\eta}$ is ultimately limited by the requirement of an acceptable life of the NITINOL wire element. The capacity of NITINOL to perform mechanical work cannot be utilized beyond the limits of the peak stress and strain set by this requirement.

---

[26]See footnote 26 on page 9-17.

[33]C. M. Gilmore, Private Communication. (This research was suggested and is in preparation by Professor Gilmore, George Washington University, School of Engineering and Applied Sciences, Washington, D.C.).

f)   Any improvement of the NITINOL material in respect to the strength and durability would extend the permissible peak stress and strain limits and therefore result in an improvement of the thermodynamic engine efficiency $\underline{\eta}$ (Figure 8).

g)   In planning future research, perhaps the most promising direction would be toward developing new NITINOL alloys with a very narrow temperature range of the phase transformation.   Such alloys would permit engine operation at a small temperature difference between the hot and cold reservoir, with the result of a higher η/η_C ratio. This would greatly enhance the potential usefulness of the NITINOL heat engine in application to heat sources with a very small temperature gradient.

APPENDIX

DETERMINATION OF THE HEAT INPUT Q_H

TO THE NITINOL WIRE DURING THE ENGINE CYCLE

The heat is supplied to the NITINOL wire element during the engine cycle at the instant when the wire is submerged in the liquid of the hot reservoir. It would be very difficult to attempt to measure directly (with any accuracy) the amount of heat which the wire absorbs. Therefore, this study employed the following two-step method of wire heating and heat input measurement:

1) First, the wire is subjected to the constant-strain isothermal cycles (in accordance with the chosen test parameters) on the Cycle Simulator, while it is heated in the standard way by submerging it in the hot bath. The stress-strain diagram (lower trace) and the wire ohmic resistance (upper trace) are recorded on the screen of a dual-beam oscilloscope (Figure 20).

2) Then (while the cycling is continued) the hot bath is removed and the wire is heated (while in air) by an electric pulse at the proper instant during each of the following cycles. All other test parameters are kept unchanged. The DC current of the electric pulse is timed and the voltage is adjusted so that the same peak recovery stress is obtained as when the wire has been heated in the hot bath. Now the stress-strain diagram is again recorded. The product of the current, voltage, and time interval of the electric pulse yields the total heat input Q_H in Watt-sec (= Joule) to the wire element. The electric pulse record is shown in Figure 21.

The final record (Figure 20) consists of the traces of a number of repeated cycles with heating of the wire by an electric pulse, which are superimposed over the traces of a number of repeated cycles when the wire has been heated in the hot bath. (Record in Figure 20 was obtained on Tektronix 7623A storage oscilloscope.)

Part of the stress-strain diagram—namely, the lines which slope downward from right to left—represents the contraction of the wire element after heating. The slightly convex line resulted when the wire was heated in the hot bath, and the slightly concave line (lower line) resulted when the wire was heated by the electric pulse. This difference is partially due to the fact that when the NITINOL wire element is heated in the hot bath, it is also allowed to contract in the hot bath. Consequently it absorbs an additional small amount of heat during the wire contraction. This additional heat—the heat of the elastic shape recovery Q_R (see text)—contributes a modest amount of energy to the engine cycle, which is also partially converted to useful mechanical work. As a result, the area of the stress-strain diagram under the convex line is slightly larger (about 10 percent).

Figure 20 also presents the following information: cold reservoir temperature T_1 = +2°C, hot reservoir temperature T_3 = +52°C, cyclic elongation ΔL = 6 mm of the wire element corresponding to 1.6 percent strain. The difference in the ohmic resistance of the NITINOL wire (upper trace) between the martensitic (lower line) and the austenitic (upper line) phase is 0.27 ohms. (The distance between the short horizontal calibration mark and the lower line indicates 0.1 ohms.) This corresponds to about 15 percent change in the absolute resistance of the NITINOL wire element.

The upper trace in Figure 21 represents the current pulse, the middle trace and the voltage pulse, and the lowest trace the time interval of the wire contraction. The duration of the heating pulse and of the wire contraction is about 350 ms each. Between the end of the heating pulse and the start of the wire contraction is a small time overlap—about 40 ms—which was determined experimentally for the optimal utilization of the pulse energy. The current was read across a calibrated shunt and the voltage across the terminals of the NITINOL wire element. The signal for the wire contraction was monitored directly from the electronic pulse control system of the Cycle Simulator.

The heat losses from the NITINOL wire element during the heating pulse and during the wire contraction period were determined as follows: During one test cycle the wire element was not allowed to contract, but was held constrained after the completion of the electric heating pulse. The peak recovery stress σ_3 was displayed on the oscilloscope screen with the horizontal sweep of the beam adjusted to 200 ms per cm. The rise of the recovery stress during the heating pulse and the subsequent decay of stress due to the heat losses to the surrounding air as the function of time are shown in Figure 22.

The heat losses were calculated from the slope of the asymptotic stress decay curve. For the total period of the electric pulse and the subsequent wire contraction period (700 ms), the heat losses amounted to approximately 5 percent of the pulse energy.
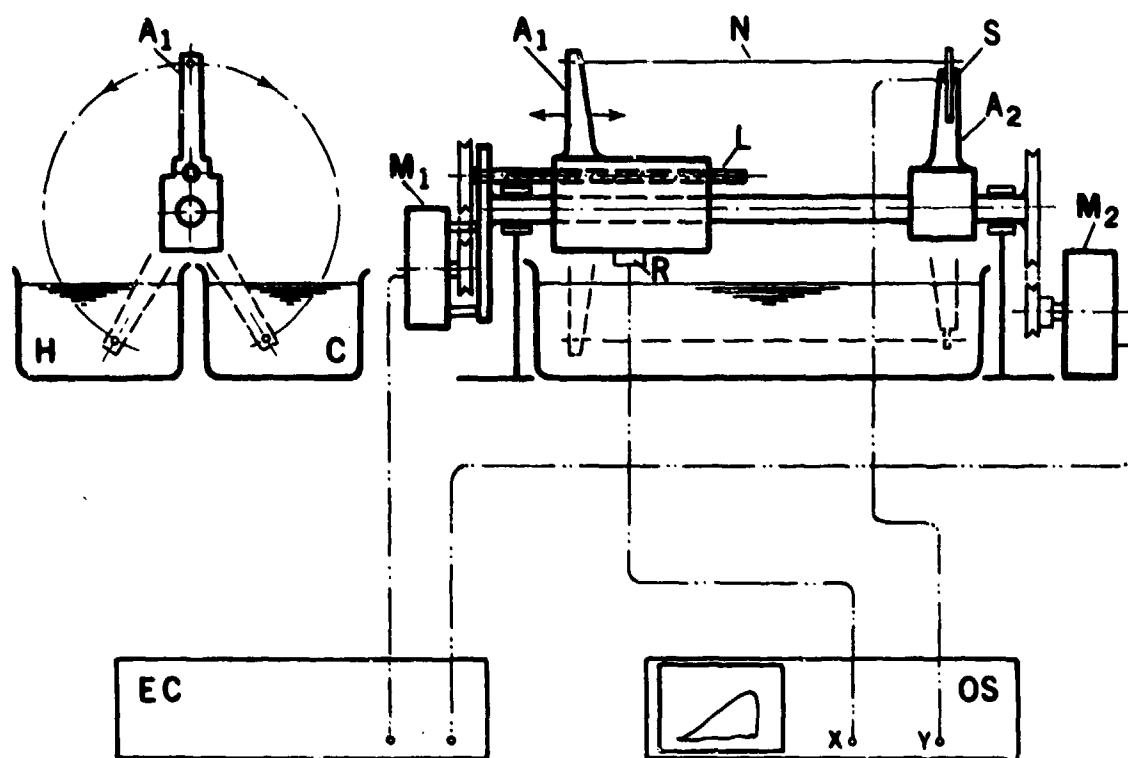
FIGURE 1   CYCLE SIMULATOR EXPERIMENTAL SYSTEM.

XBL 786-9411
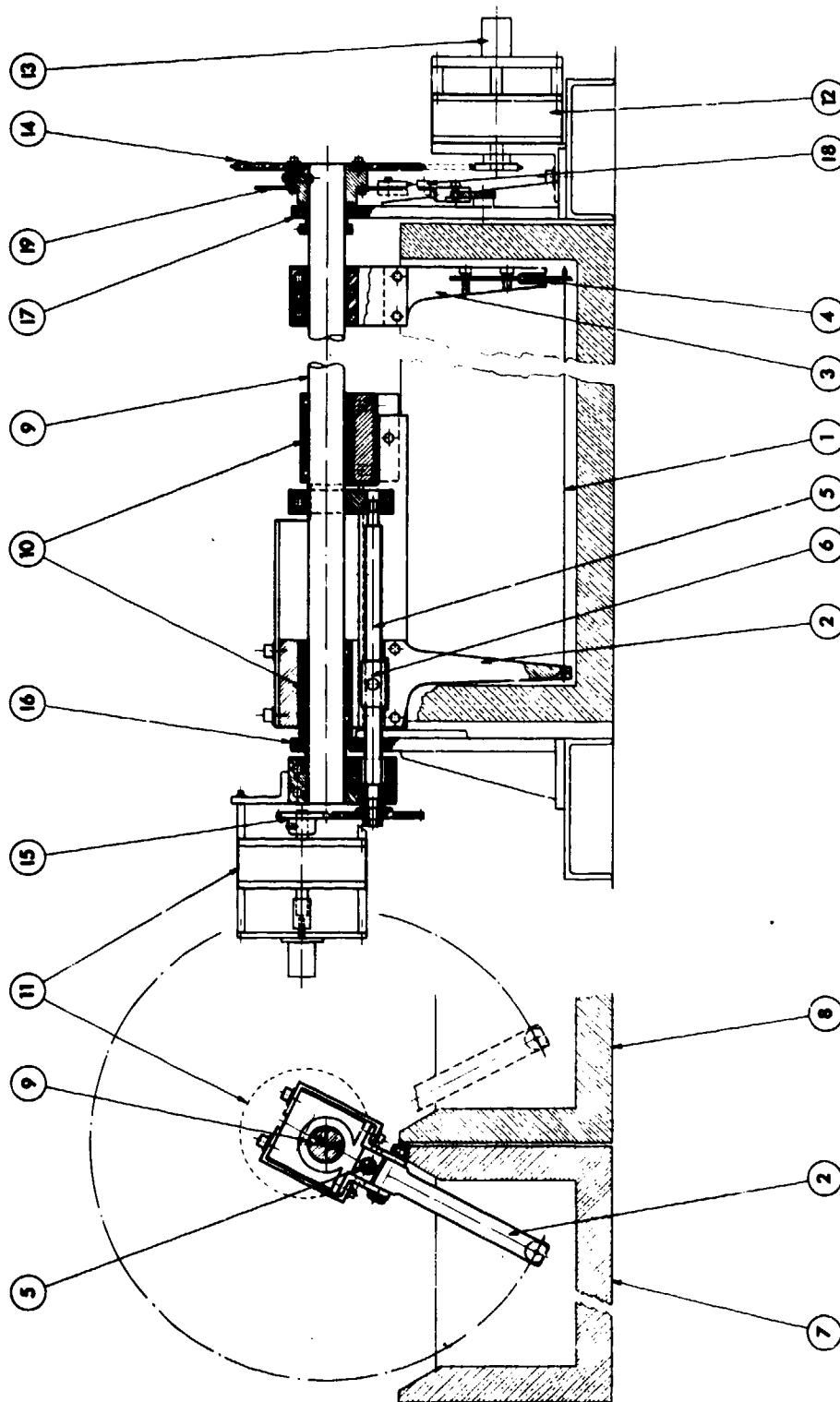
FIGURE 2   DESIGN DRAWING OF THE CYCLE SIMULATOR. LEGEND: 1 NITINOL WIRE, 2 SLIDING ARM, 3 FIXED ARM, 4 STRAIN GAGE, 5 LEAD SCREW, 6 DRIVING NUT, 7 HOT RESERVOIR, 8 COLD RESERVOIR, 9 SHAFT, 10 LINEAR BALL BEARINGS, 11 LEAD SCREW SERVOMOTOR, 12 SHAFT SERVOMOTOR, 13 TACHOMETER-GENERATOR, 14 SHAFT SPROCKET WHEEL, 15 LEAD SCREW DRIVE, 16 FRONT SUPPORT BEARING, 17 REAR SUPPORT BEARING, 18 POSITIONING MICROSWITCHES, 19 POSITIONING CAM.
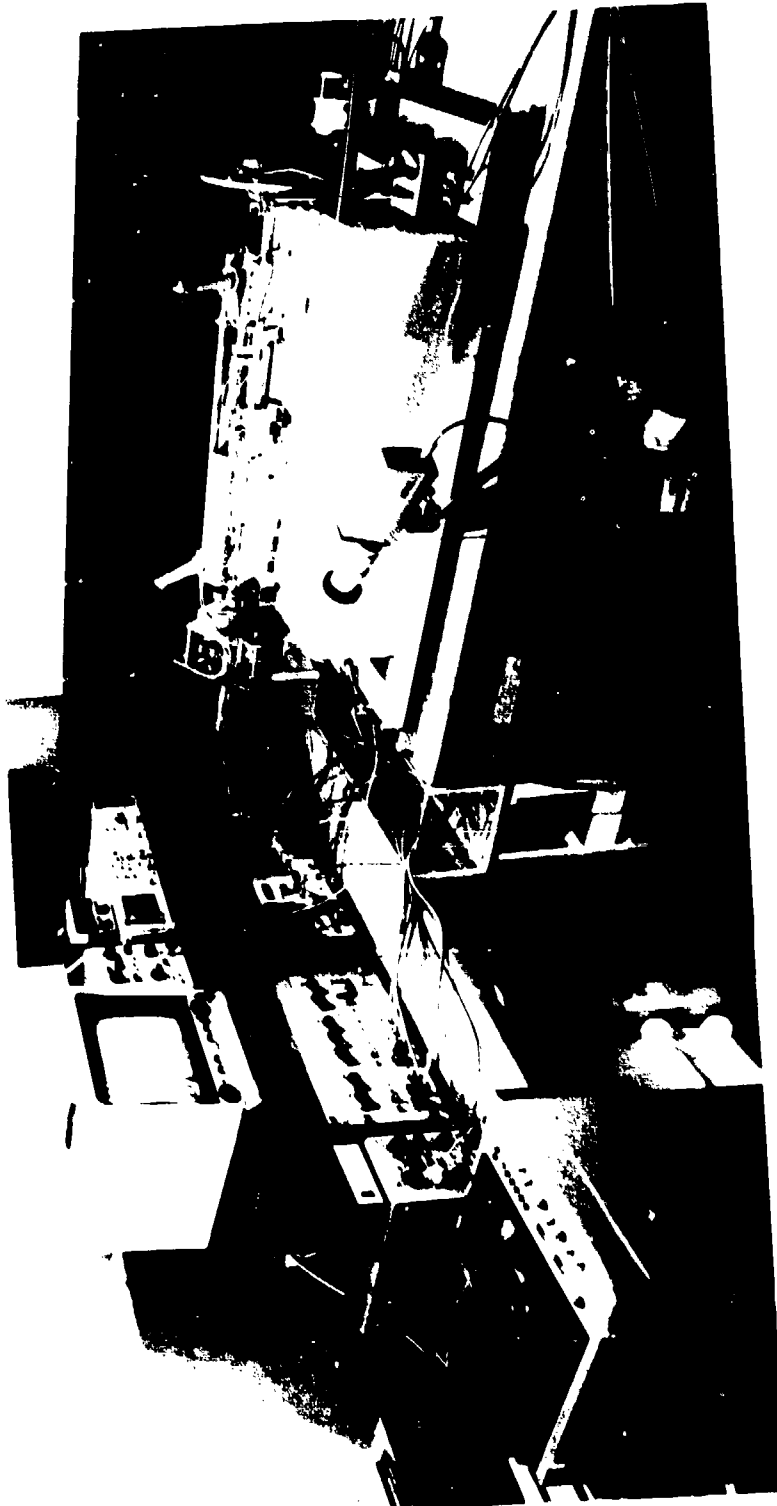
FIGURE 3   LABORATORY EXPERIMENTAL SET-UP, INCLUDING CYCLE SIMULATOR, ELECTRONICS
AND VIDEO DATA RECORDING SYSTEM.
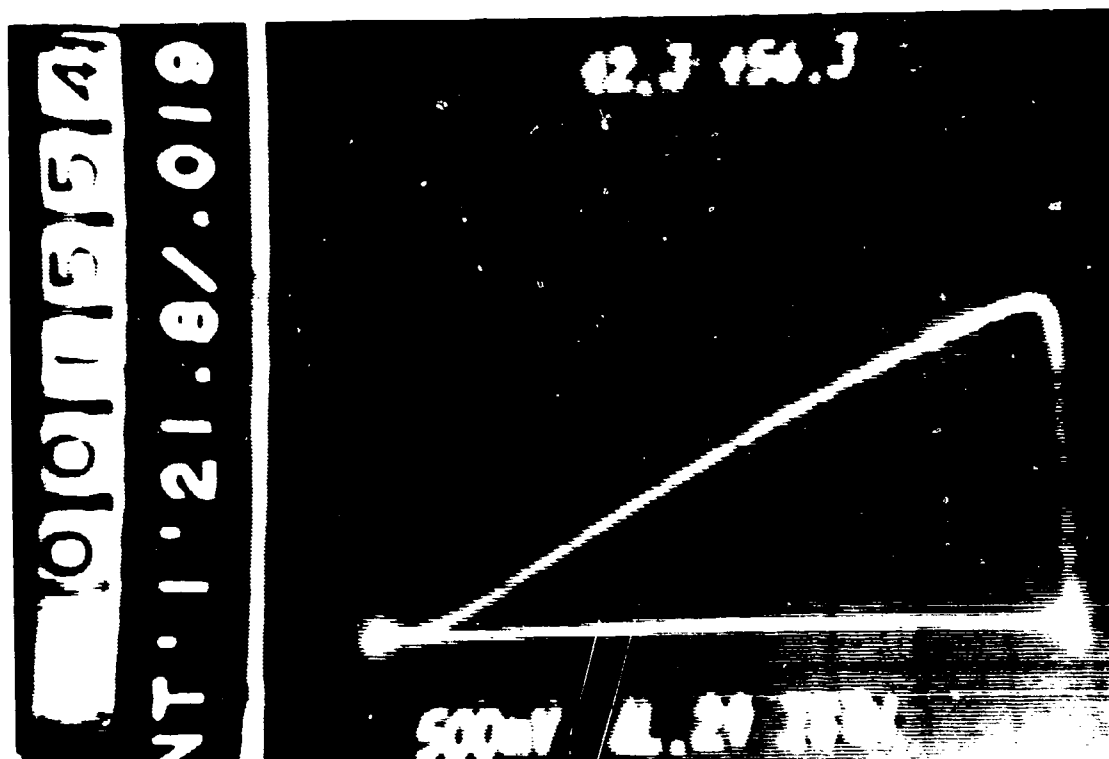
FIGURE 4   VIDEO RECORD OF A TYPICAL CONSTANT-STRAIN ISOTHERMAL CYCLE.
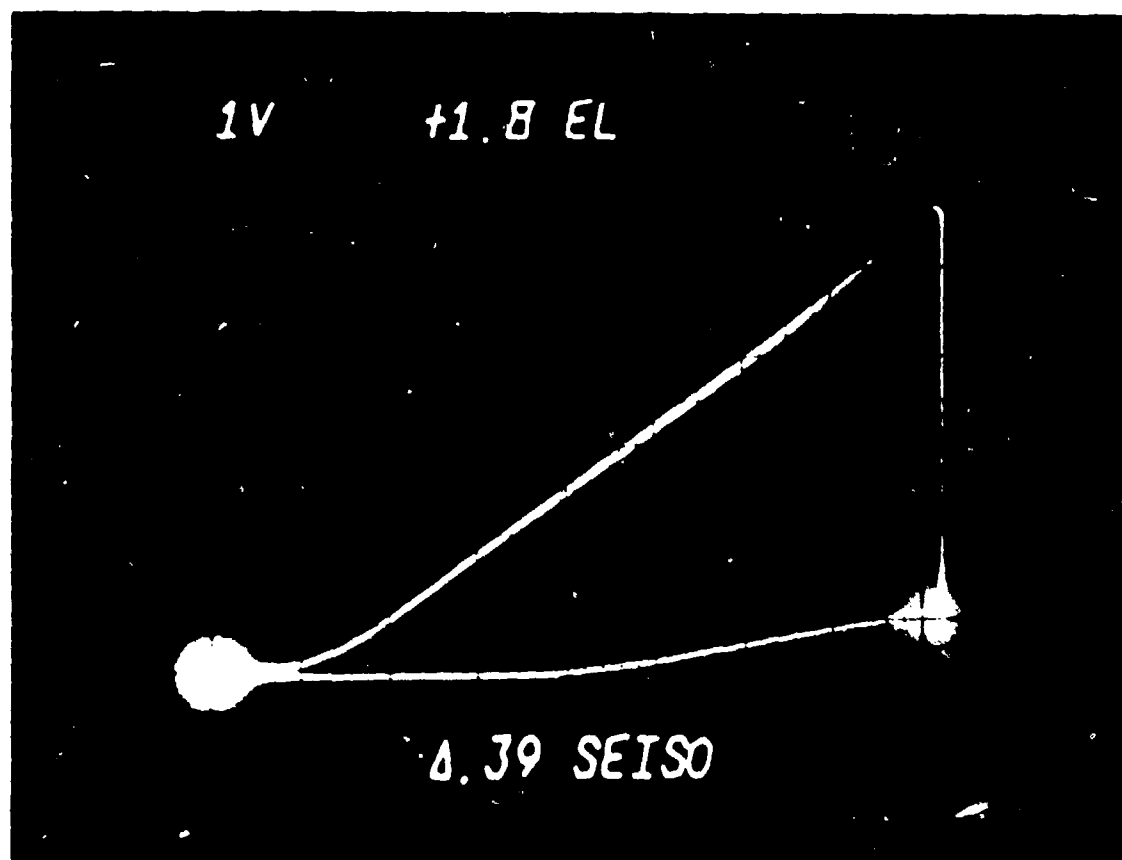
FIGURE 5   CONSTANT-STRAIN ISOTHERMAL CYCLE RESULTING WHEN HEAT IS SUPPLIED
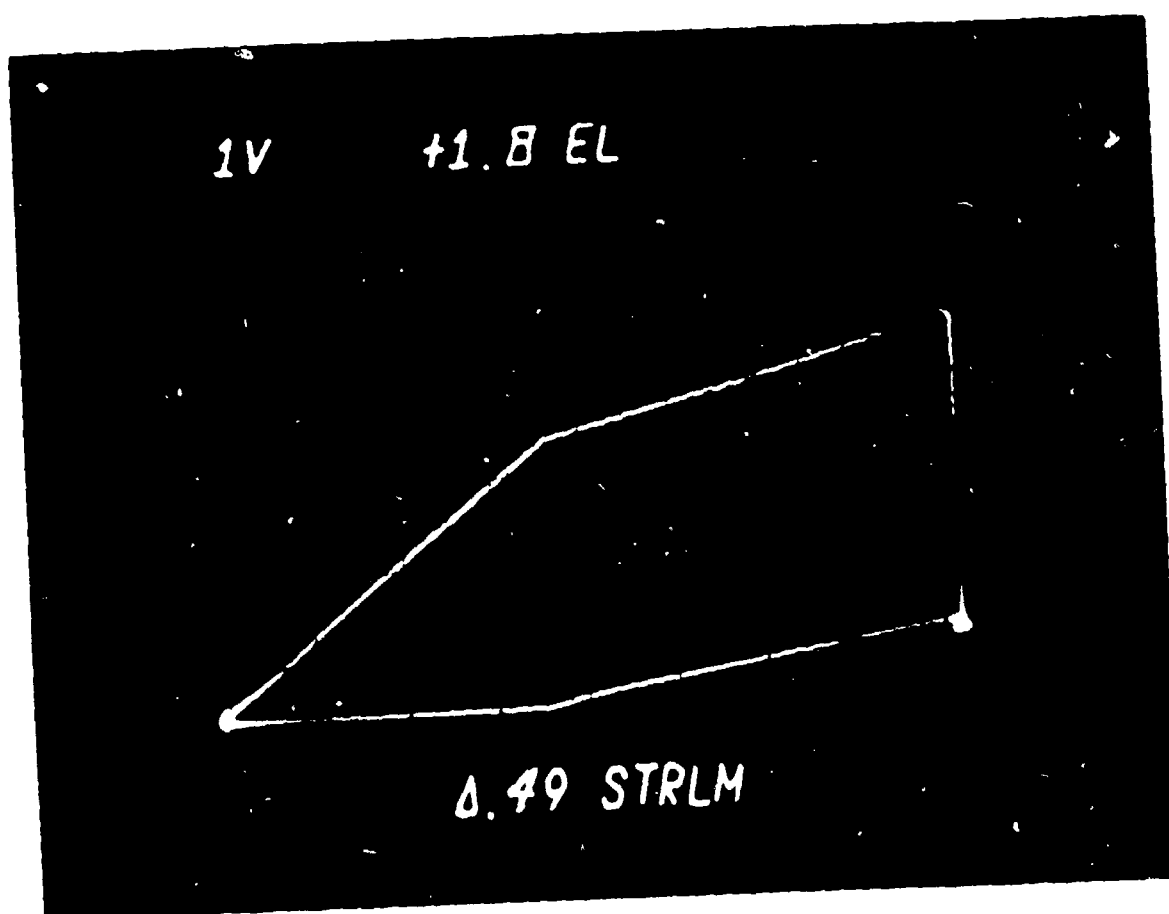BY ELECTRIC PULSE.

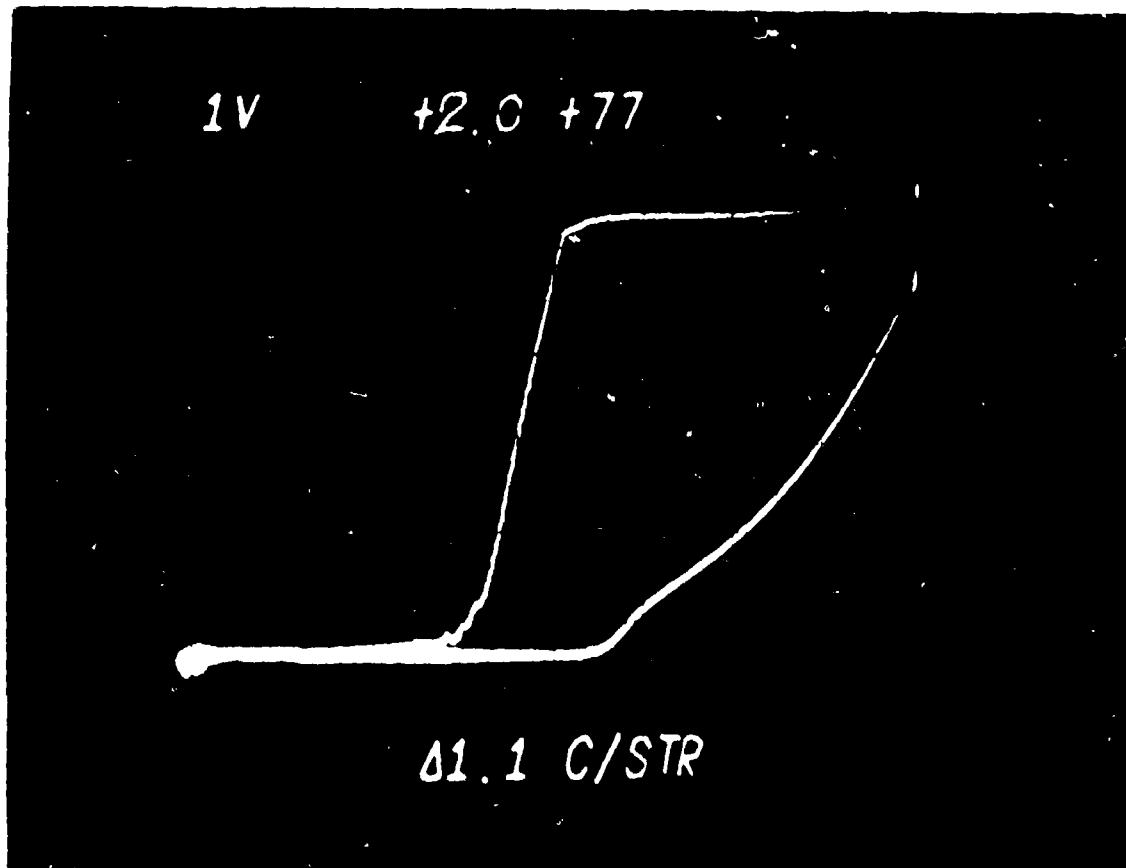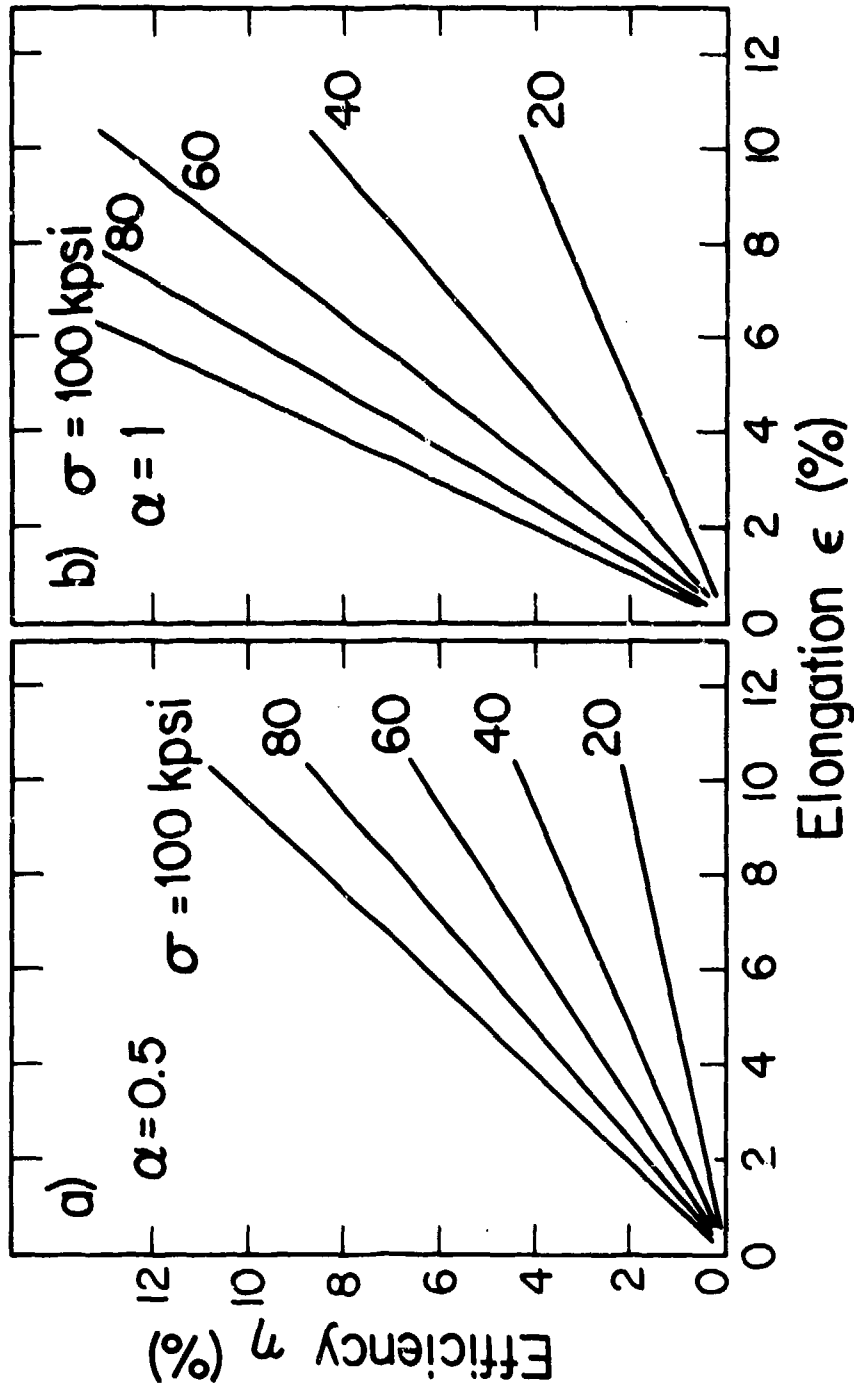FIGURE 6   STRESS-LIMITED ISOTHERMAL CYCLE. HEAT SUPPLIED BY ELECTRIC PULSE.

FIGURE 7   CONSTANT-STRESS ISOTHERMAL CYCLE.

XBL 798-2587

FIGURE 8   THERMODYNAMIC EFFICIENCY OF THE ENERGY CONVERSION IN NITINOL AS THE FUNCTION OF PEAK STRESS $\sigma(\sigma=\sigma_3)$, AND PERCENT ELONGATION ϵ OF THE WIRE ELEMENT
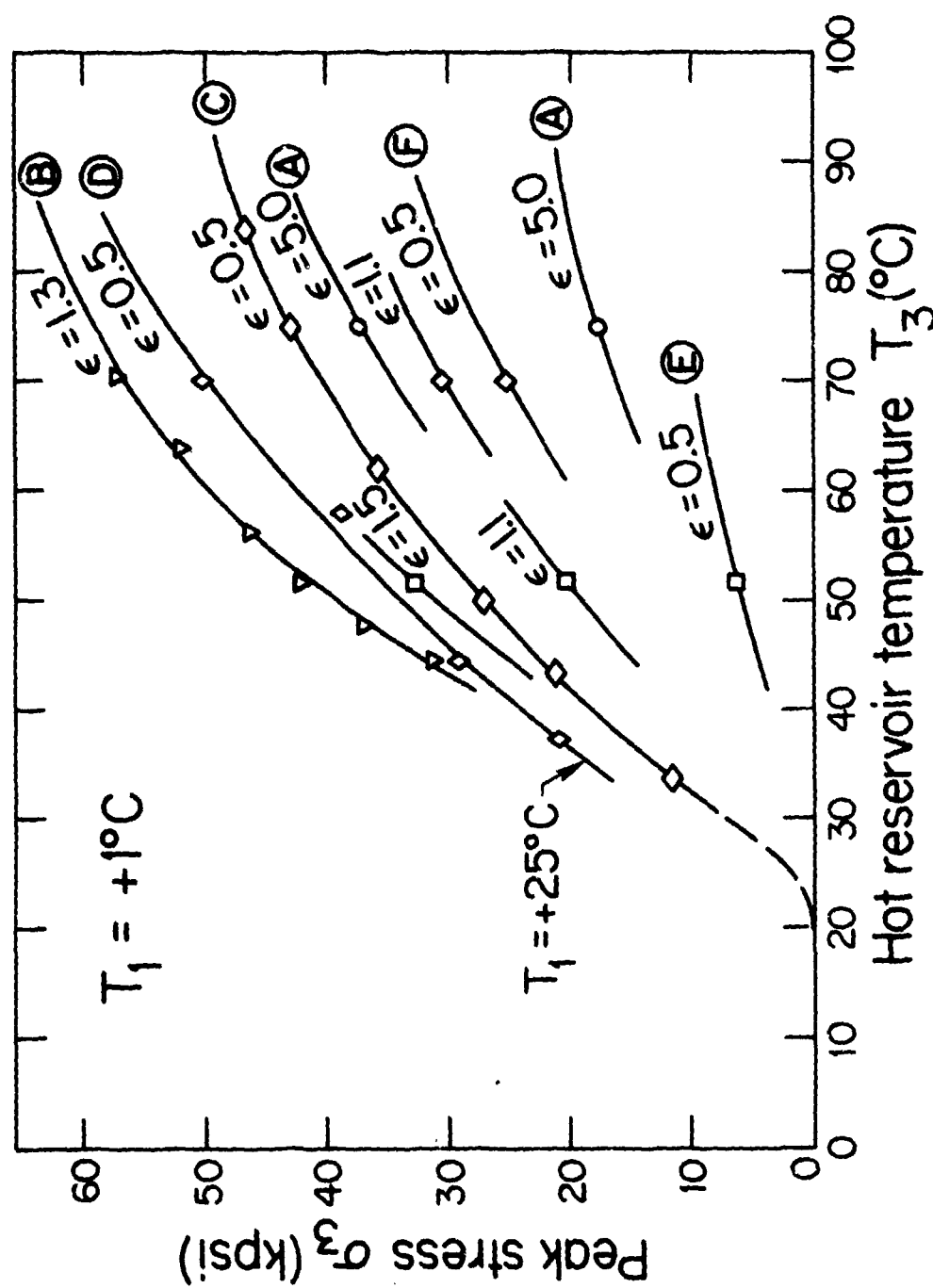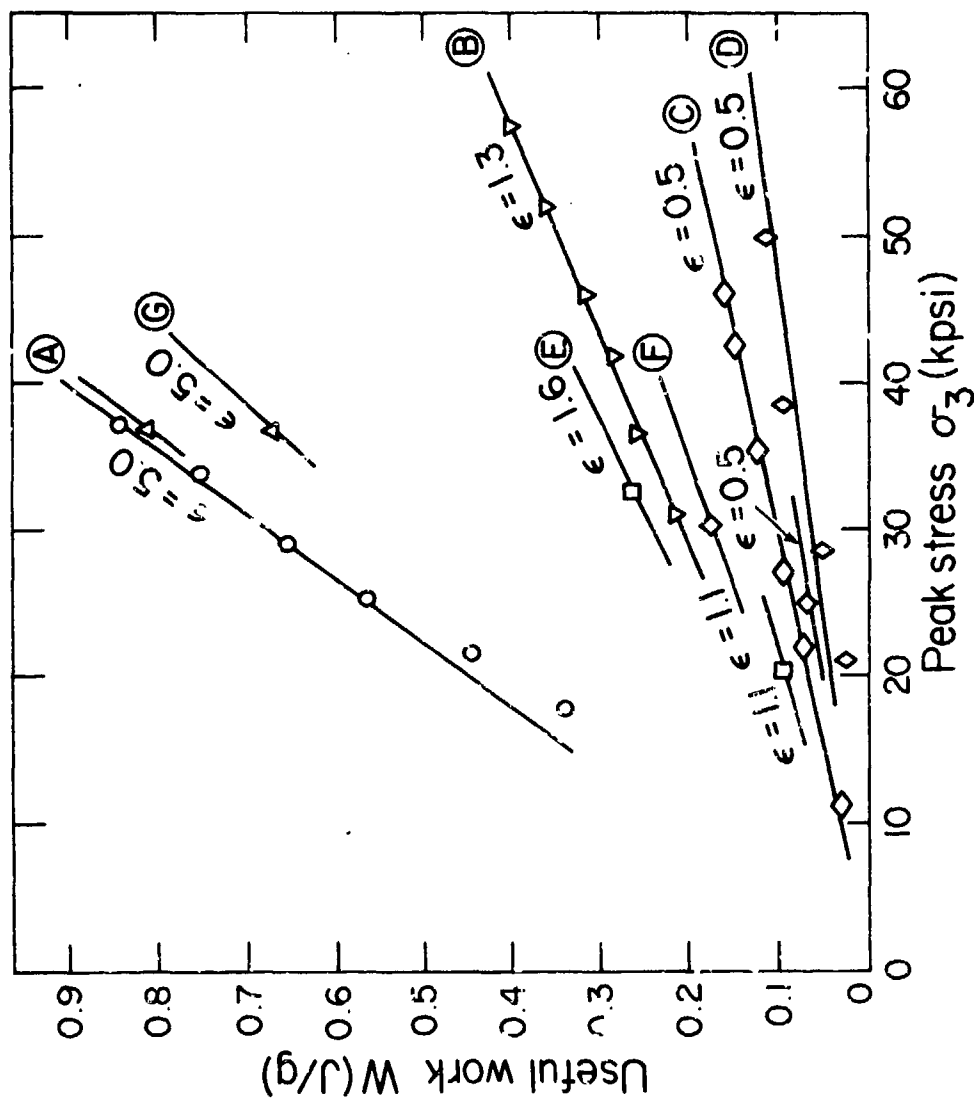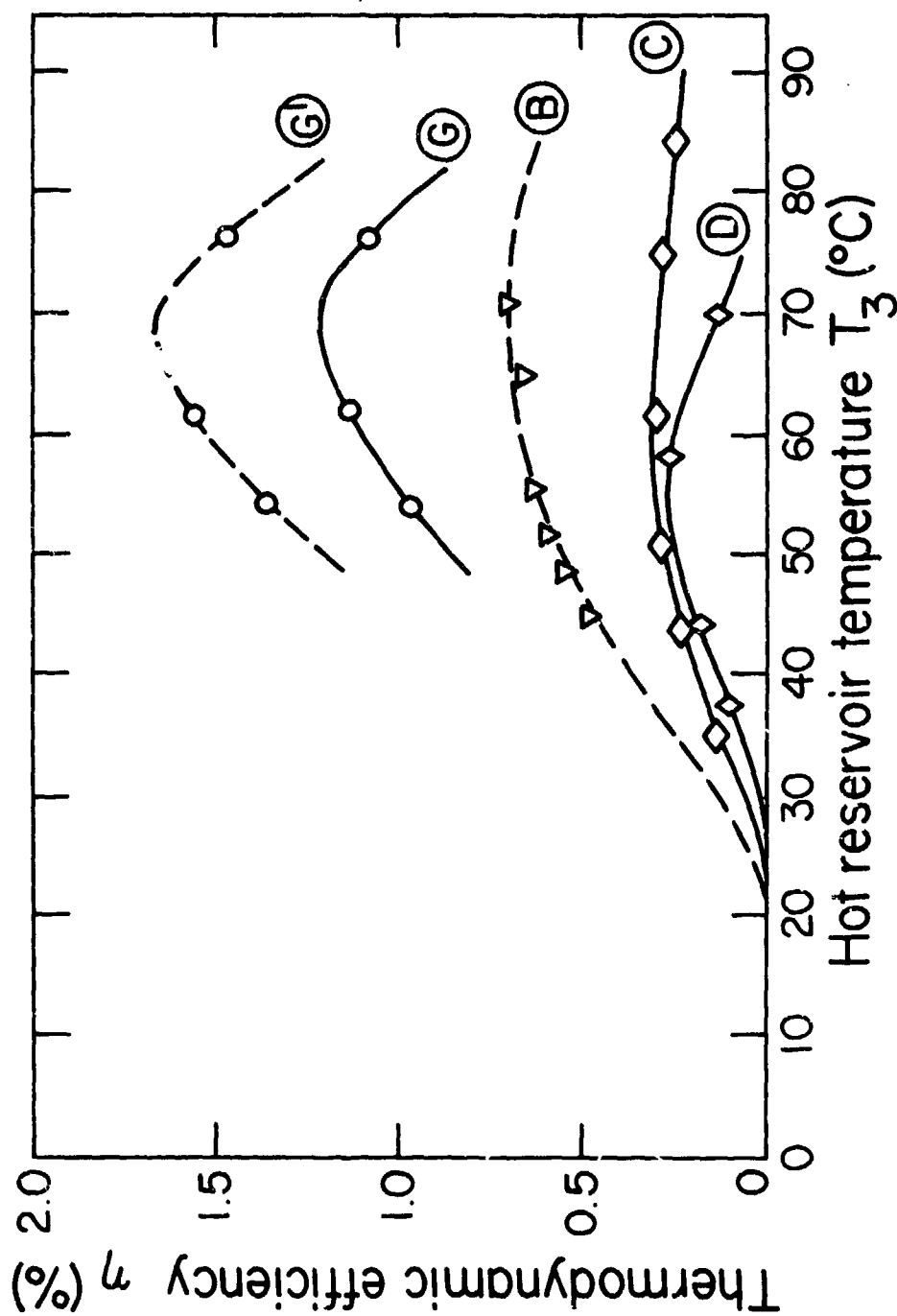
XBL 798-2588

FIGURE 9   PEAK RECOVERY STRESS DURING VARIOUS ENGINE CYCLES AS THE FUNCTION OF THE HOT RESERVOIR TEMPERATURE.

XBL 798 - 2589
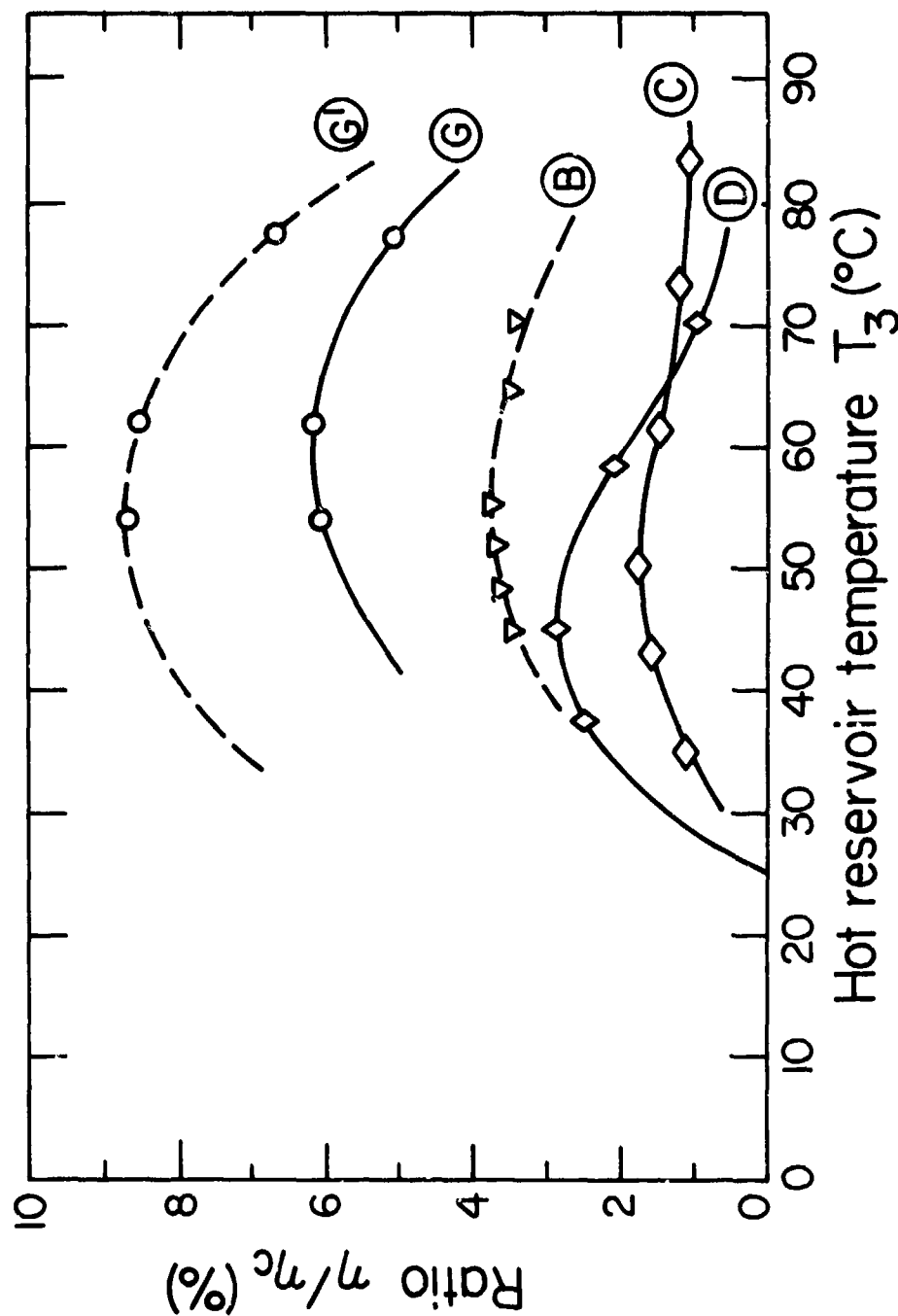
FIGURE 10   USEFUL MECHANICAL WORK PRODUCED BY VARIOUS CYCLES AS THE FUNCTION
OF PEAK RECOVERY STRESS.

FIGURE 11   THERMODYNAMIC ENGINE CYCLE EFFICIENCY AS THE FUNCTION OF
THE HOT RESERVOIR TEMPERATURE.

XBL 798-2591

FIGURE 12   RATIO OF THE THERMODYNAMIC ENGINE CYCLE EFFICIENCY TO THE
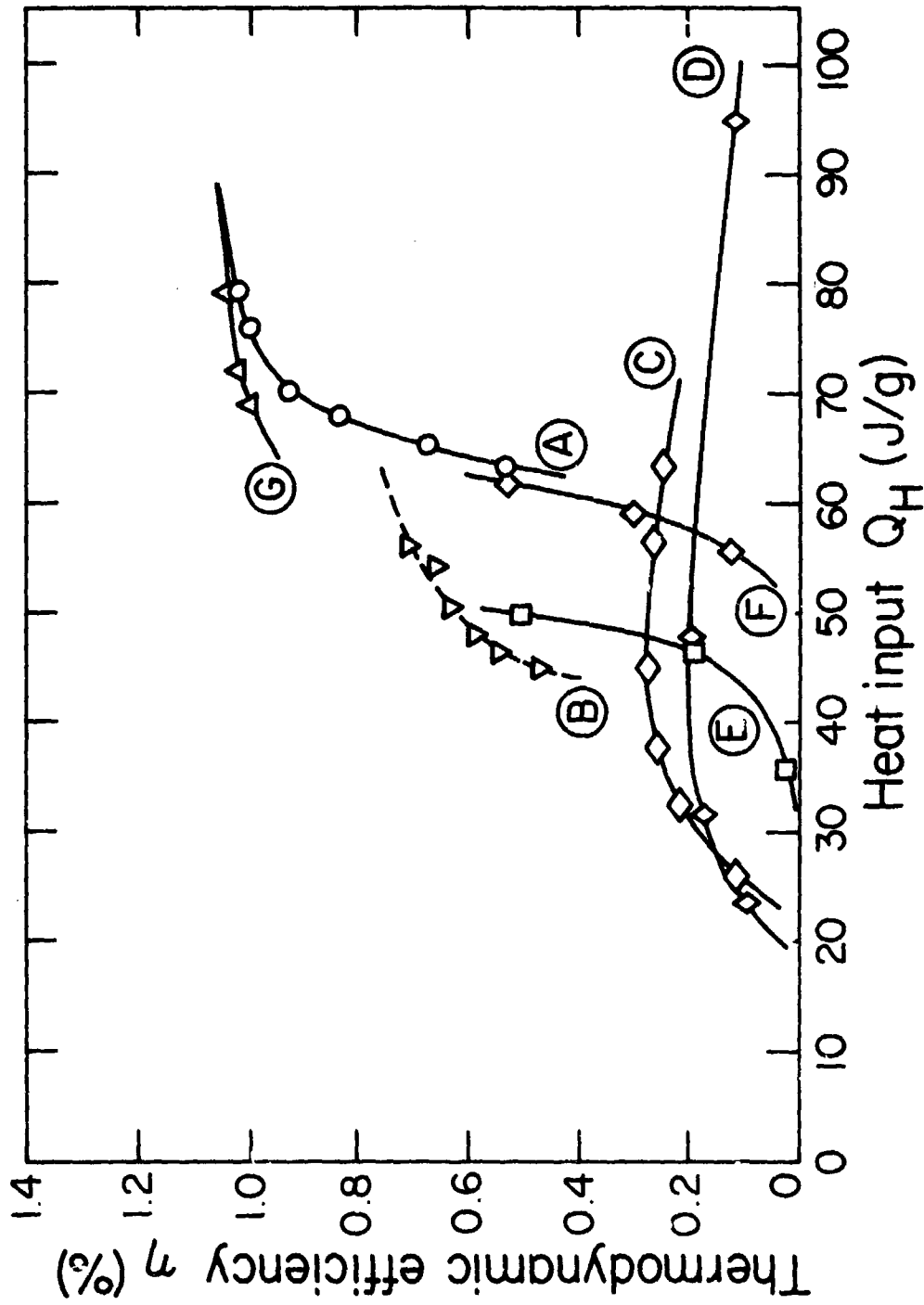CARNOT CYCLE EFFICIENCY AS THE FUNCTION OF THE HOT RESERVOIR
TEMPERATURE.

XBL 798-2592

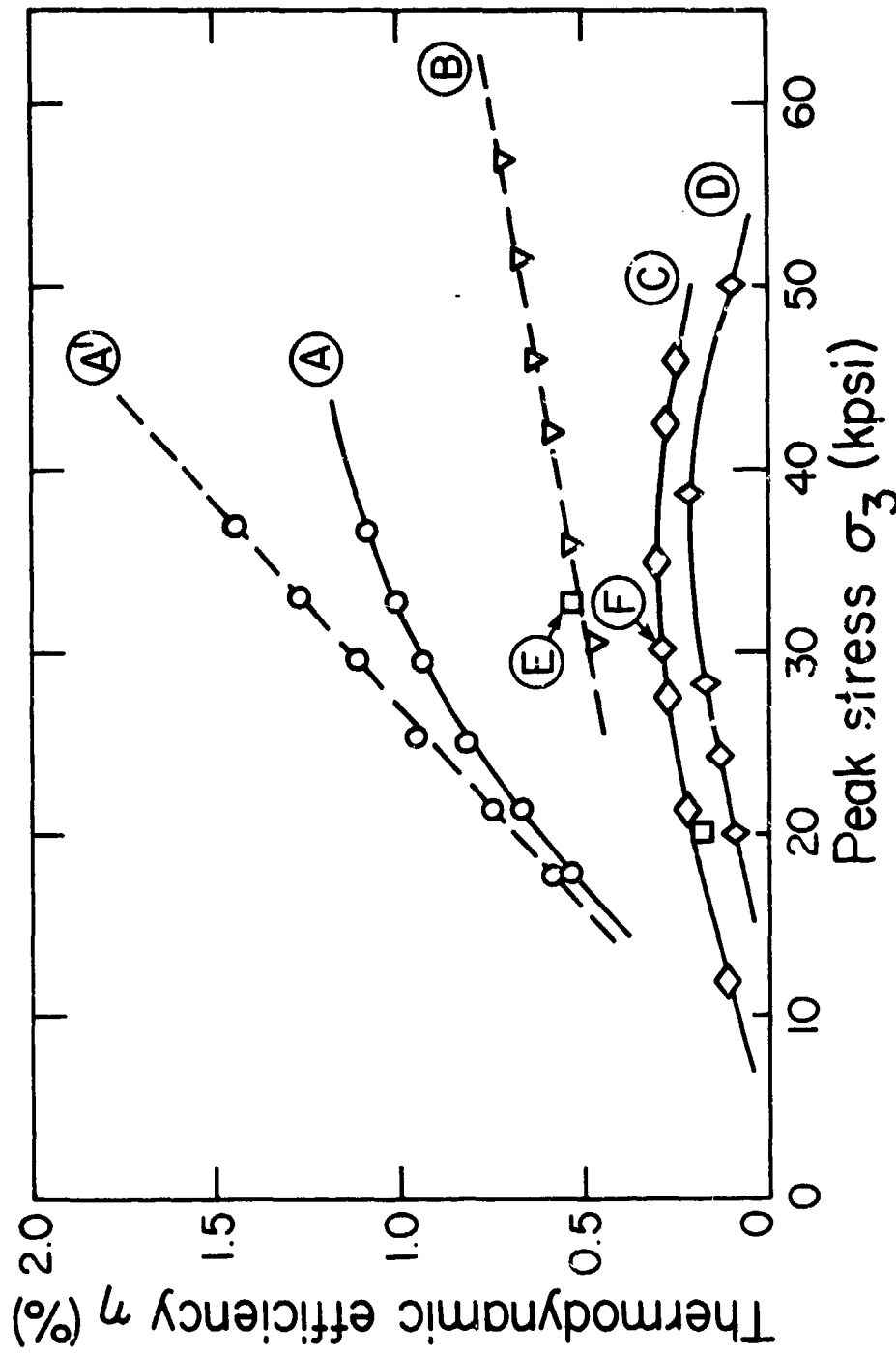FIGURE 13   THERMODYNAMIC ENGINE CYCLE EFFICIENCY AS THE FUNCTION OF
HEAT INPUT.

XBL 798-2593

FIGURE 14   THERMODYNAMIC ENGINE CYCLE EFFICIENCY AS THE FUNCTION OF
PEAK RECOVERY STRESS.

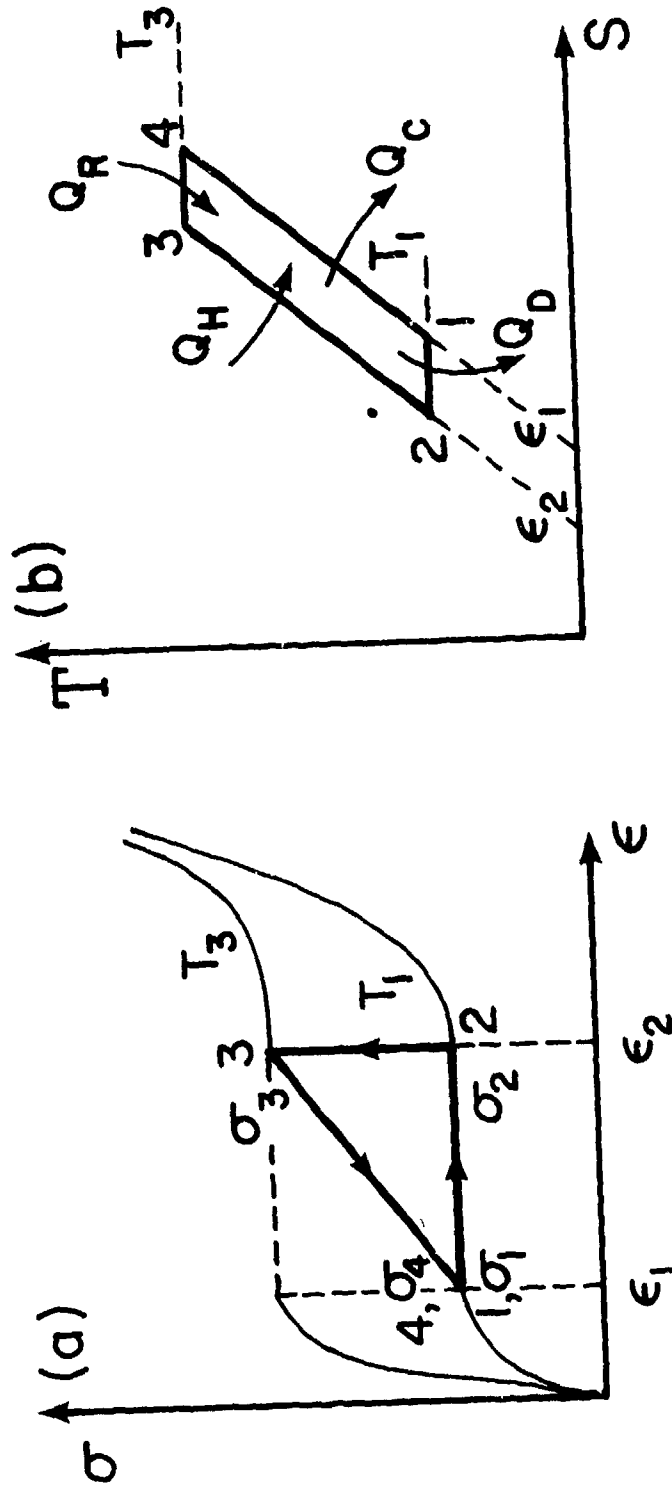FIGURE 15 SCHEMATIC DIAGRAM OF THE CONSTANT-STRAIN ISOTHERMAL CYCLE.

XBL 798-2595
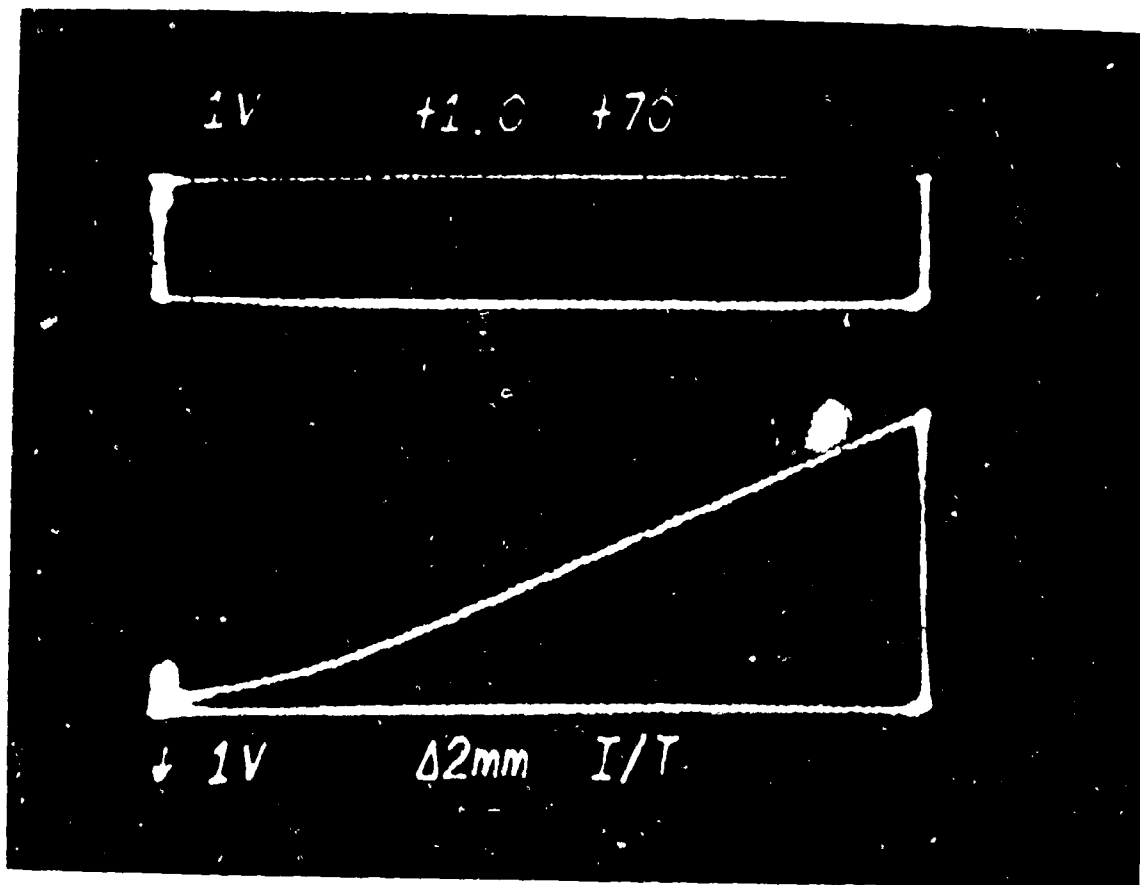
FIGURE 16   DUAL-BEAM OSCILLOSCOPE RECORD OF THE NITINOL RESISTIVITY (UPPER TRACE)
DURING THE CONSTANT-STRAIN ISOTHERMAL CYCLE (LOWER TRACE).
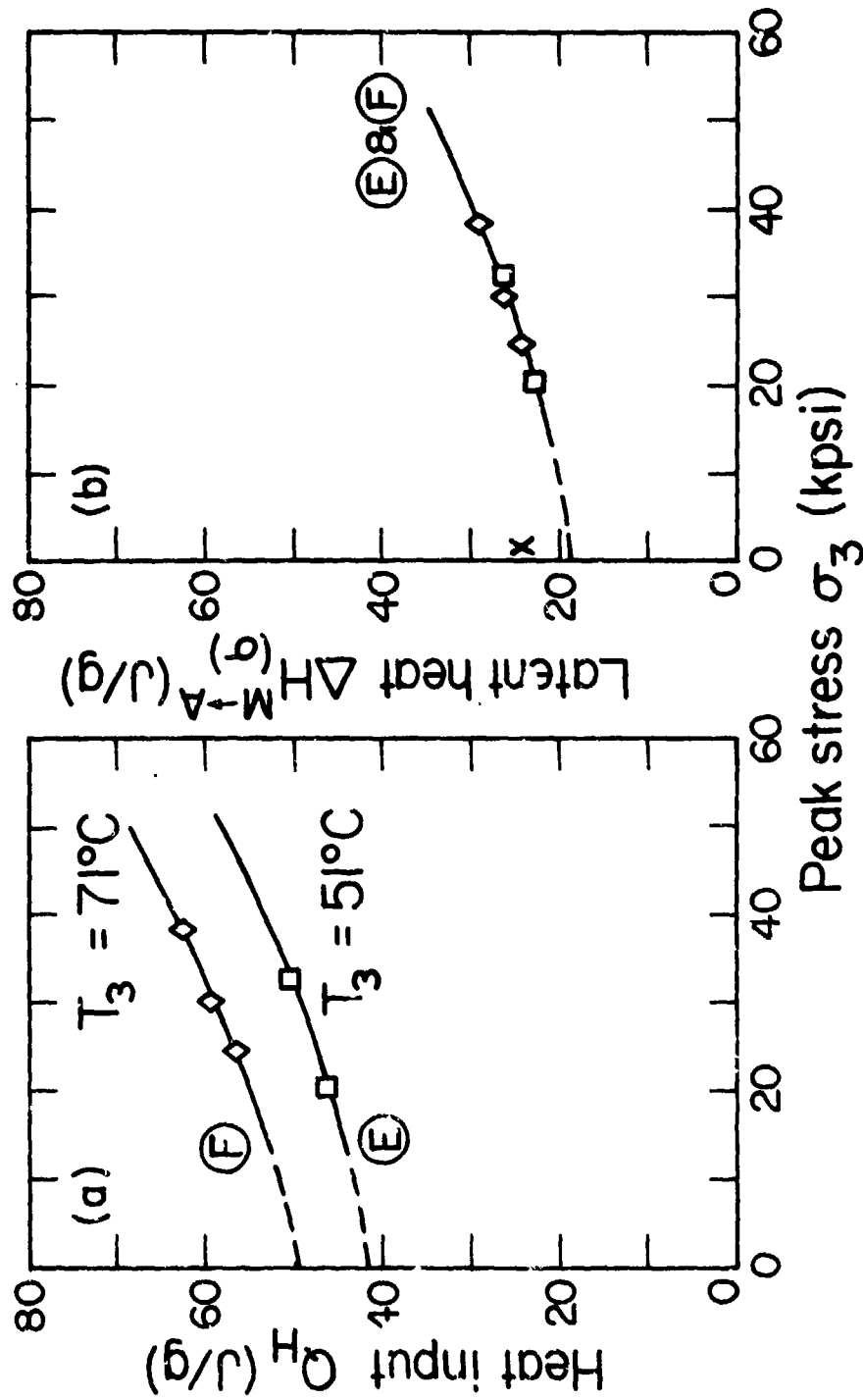
XBL 798-2597

FIGURE 17   TOTAL HEAT INPUT AND THE LATENT HEAT OF PHASE TRANSFORMATION AS THE FUNCTION OF THE PEAK RECOVERY STRESS DURING THE CONSTANT-STRAIN ISOTHERMAL CYCLE.
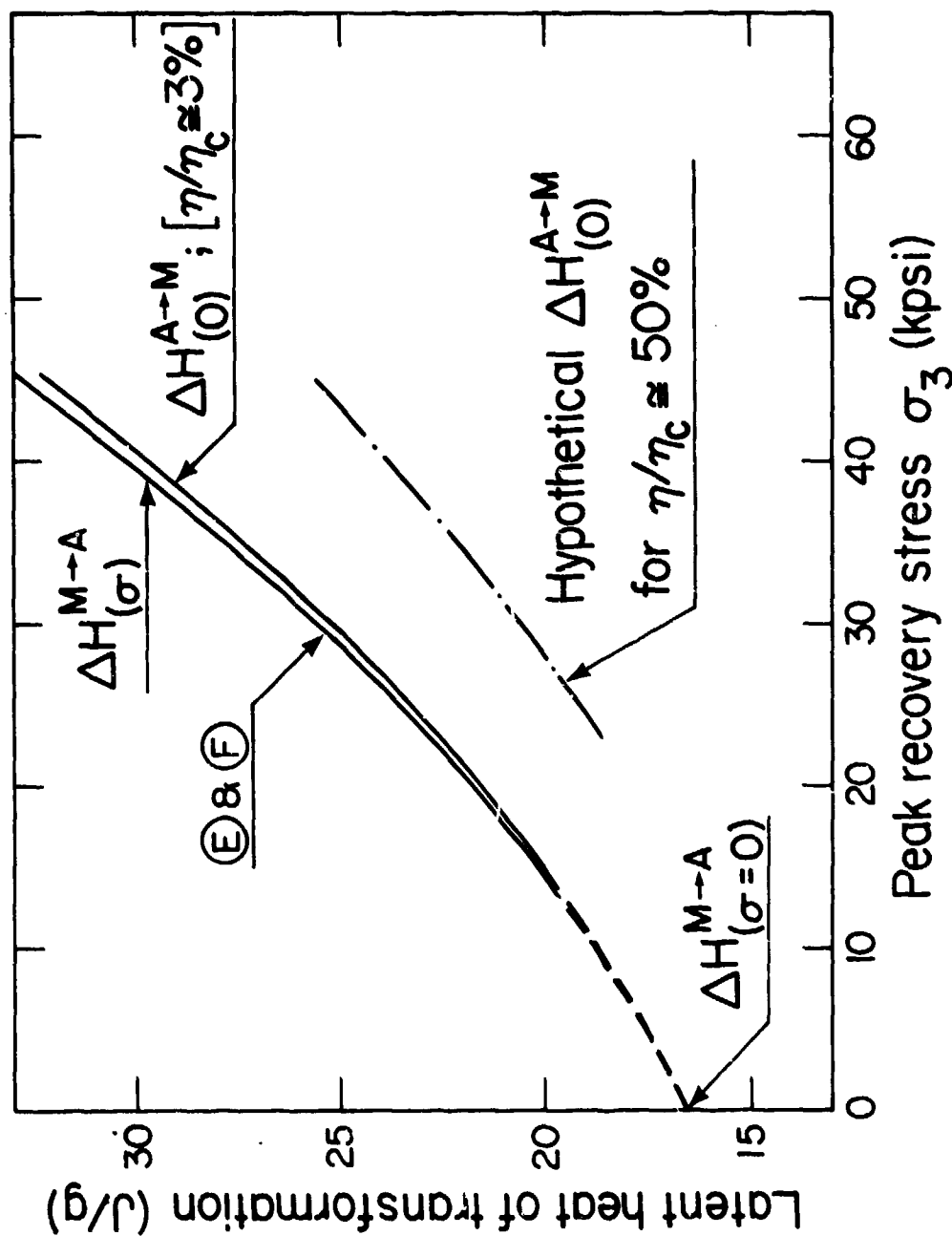
XBL 798-2594

FIGURE 18   LATENT HEAT OF REVERSE TRANSFORMATION (MARTENSITE → AUSTENITE)
AND THE "APPARENT" LATENT HEAT OF FORWARD TRANSFORMATION
(AUSTENITE → MARTENSITE) AS THE FUNCTION OF THE PEAK RECOVERY STRESS.
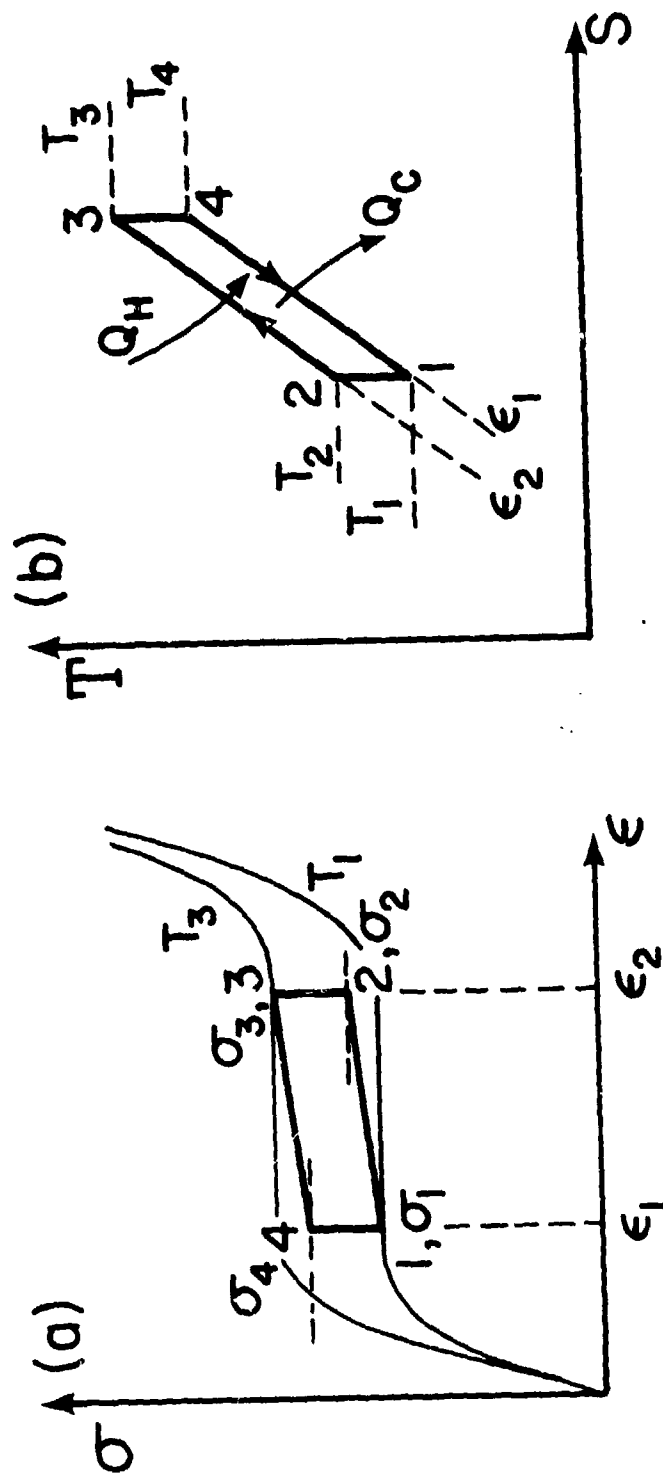
FIGURE 19 SCHEMATIC DIAGRAM OF THE SEMI-ADIABATIC CYCLE.

XBL 798-2596
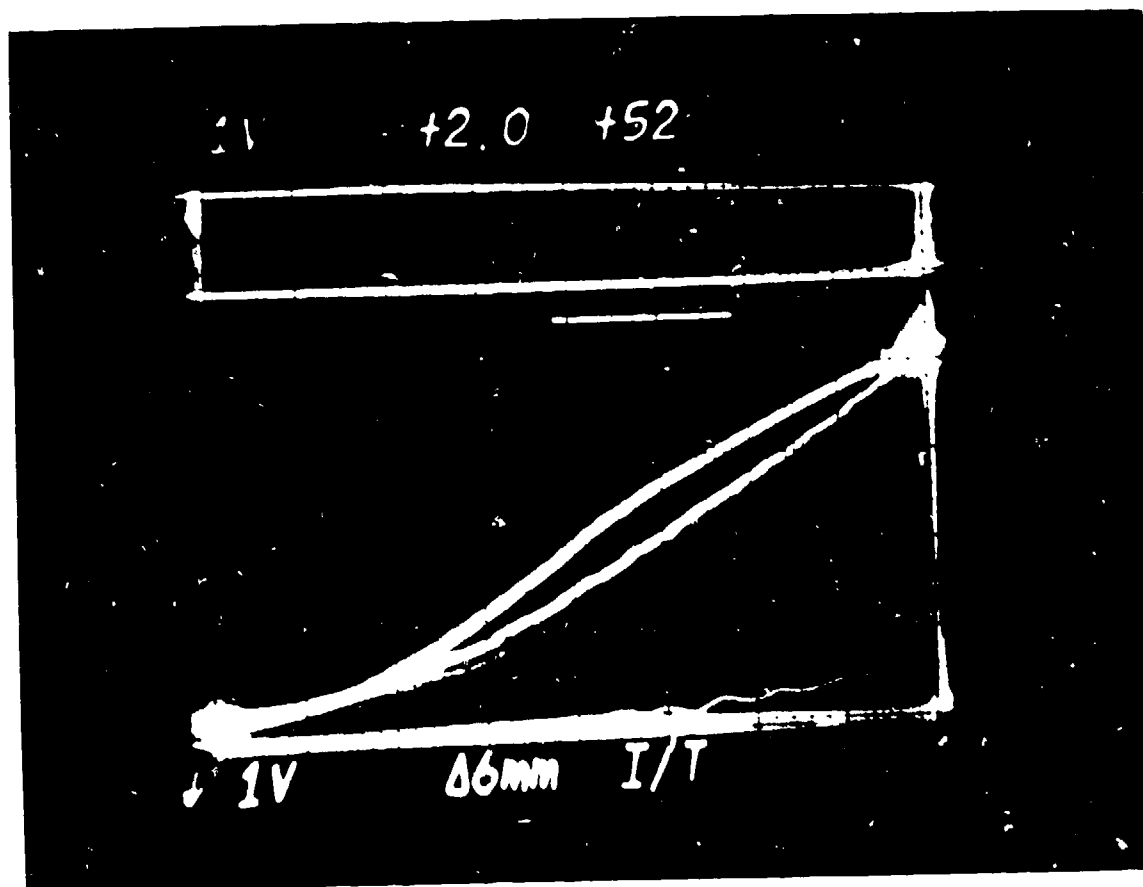
FIGURE 20   DETERMINATION OF THE HEAT INPUT TO THE NITINOL WIRE DURING THE CONSTANT-STRAIN ISOTHERMAL CYCLE.
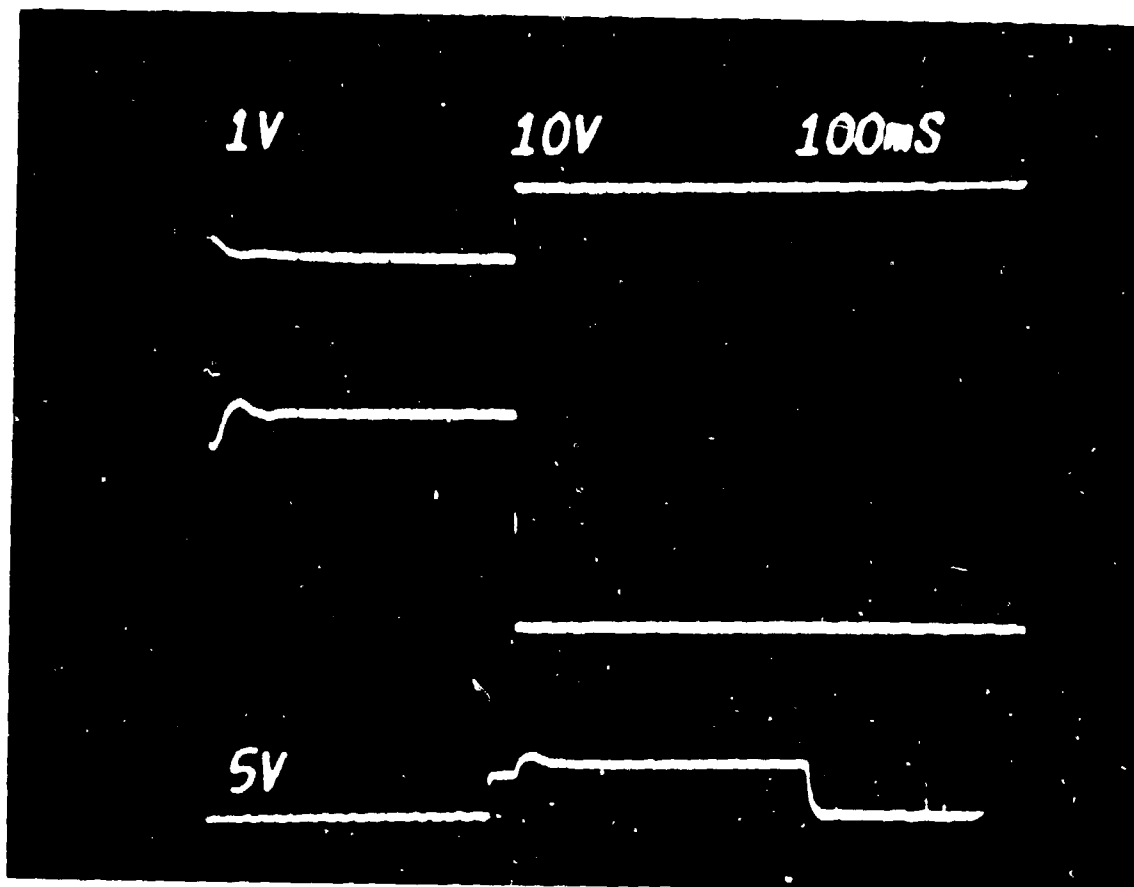
FIGURE 21   CURRENT AND VOLTAGE PULSES FOR HEATING OF THE NITINOL WIRE ELEMENT,
AND THE WIRE CONTRACTION TIMING TRACE.
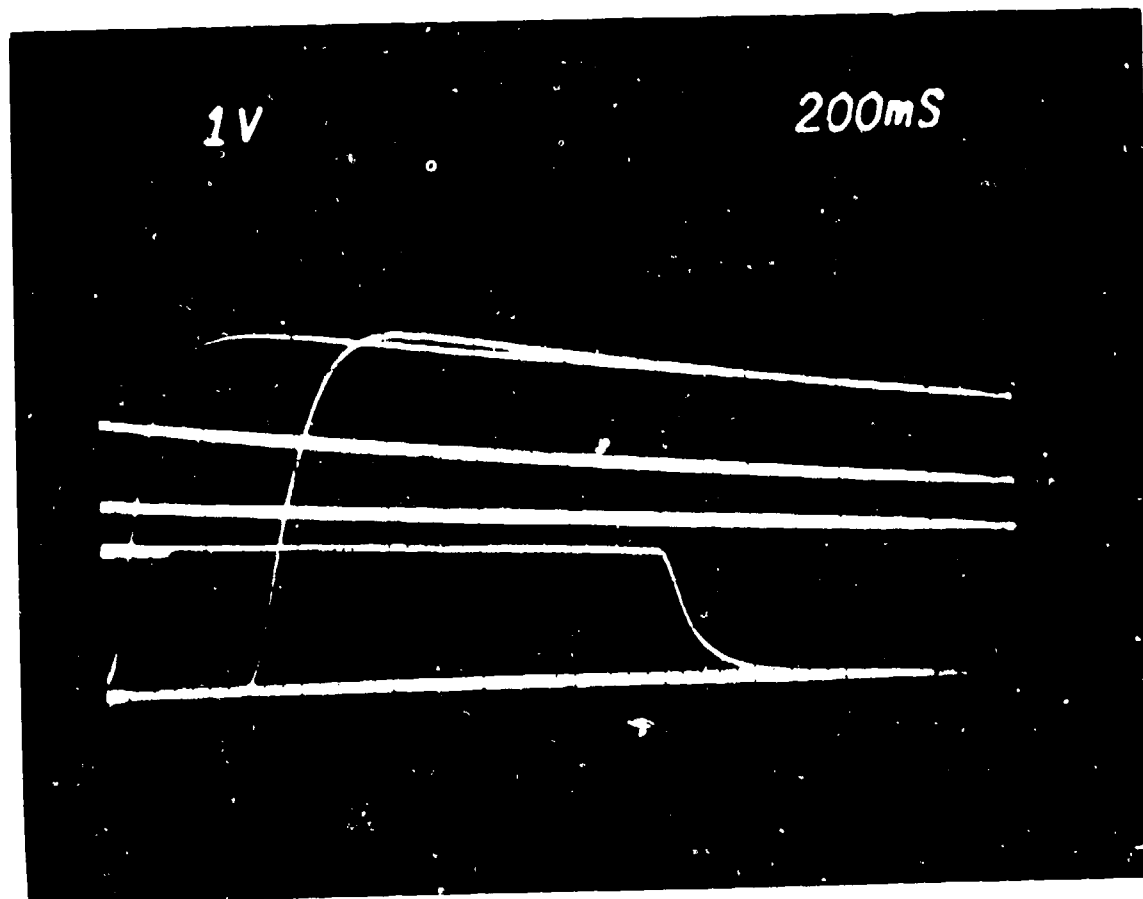
FIGURE 22 PEAK RECOVERY STRESS RISE DURING THE ELECTRIC HEATING PULSE AND THE SUBSEQUENT STRESS DECAY DUE TO THE HEAT LOSSES FROM THE NITINOL WIRE ELEMENT.

9. REFERENCES

1. W. S. Ginell, J. L. McNichols and J. S. Cory, "Low-Grade Thermal Energy-Conversion Joule Effect Heat Engines," American Socierty of Mechanical Engineers, Paper 78-ENAs-7, July 1978.

2. C. M. Jackson, H. J. Wagner and R. J. Wasilewski, "55 NITINOL - the Alloy with a Memory," Report NASA-SP 5110, 1972.

3. J. Perkins, "Shape Memory Effects in Alloys," Proc. of the Inter. Symp. on Shape Memory Effects and Applications, Toronto, Ontario, Canada, May 1975; Plenum Press, New York.

4. H. F. Mohamed, "Martensite Transformation and Shape Memory Effect in Ni-Ti Alloy," Report LBL-5112, Lawrence Berkeley Laboratory, Univiersity of California, Berkeley, May 1976.

5. D. S. Lieberman, "Crystal Geometry and Mechanisms of Phase Transformations in Crystalline Solids," Paper presented at Seminar of Am. Soc. for Met., October 1968.

6. Z. Nishiyama, Martensitic Transformations, Academic Press, New York, 1978.

7. M. Ahlers, "On the Usefulness of Martensitic Transformations for Energy Conversion," Scripta Metallurgica, Vol 9 (1975), p. 71.

8. H. C. Tong and C. M. Wayman, "Thermodynamic Considerations of 'Solid-State Engines' Based on Thermoelastic Martensitic Transformations and the Shape Memory Effect," Metallurgical Transactions A, Vol. 6A, January 1975.

9. C. M. Wayman and H. C. Tong, "The Efficiency of the Shape Memory Effect for Energy Conversion," Scripta Metallurgica, Vol. 9 (1975), p. 757.

10. B. Cunningham and K. H. G. Ashbee, "Marmem Engines," Acta Metallurgica, Vol. 25 (1977), p. 1315.

11. A. A. Golestaneh, "Efficiency of the Solid-State Engine Made with NITINOL Memory Material," J. Appl. Phys., 49 (3), March 1978.

12. R. Banks, P. Hernandez and D. Norgren, "NITINOL Engine Project - Test Bed," Final Report, UCID-3739, Lawrence Berkeley Laboratory, University of California, Berkeley, July 31, 1975.

13. D. A. Johnson, "Training Phenomena in NITINOL," presented at the NITINOL Heat Engine Conference, September 1978, Naval Surface Weapons Center, Silver Spring, Maryland (printed elsewhere in the present volume).

14. W. B. Cross, A. H. Kariotis and F. J. Stimler, "NITINOL Characterization Study," NASA CR-1433, September 1969.

15. R. J. Wasilewski, S. R. Butler, and J. E. Hanlon, "On the Martensitic Transformation in TiNi," Metal. Sci J., Vol, 1, (1967), p. 104.

16. M. B. Bever, D. L. Holt and A. L. Titchener, "The Stored Energy of Cold Work," Progress in Material Science, Vol. 17, Pergamon Press, Oxford, 1973.

17. F. W. Sears, An Introduction to Thermodynamics, the Kinetic Theory of Gases and Statistical Mechanics, Addison-Wesley Press Inc., Cambridge, Mass., 1950 (p. 154).

18. L. Delaey and G. de Lepeliere, "The Temperature-Entropy Diagram of Solid State Engines and Solid State Heat Pumping Systems with Shape Memory Alloys," Scripta Metallurgica, Vol. 10 (1976), p., 959.

19. K. N. Melton and O. Mercier, "The Effect of Opposing Stress on Shape Memory and Martensitic Reversion," Scripta Metallurgica, Vol. 12 (1978), p. 5.

20. F. E. Wang, B. F. DeSavage, and W. J. Buehler, "The Irreversible Critical Range in the TiNi Transition," Jour. of Appl. Phys., Vol. 39 (1968), P. 2166.

21. H. C. Tong and C. M. Wayman, "On Carnot Cycles, Transformation Temperatures, and Latent Heats Under an Applied Stress, as Related to the Shape Memory Effect," Scripta Metallurgica, Vol. 10 (1976), P. 1129.

22. K. Otsuka, C. M. Wayman, K. Nakai, H. Sakamoto and K. Shimizu, "Superelasticity Effects and Stress-Induced Martensitic Transformations in Cu-Al-Ni Alloys," Acta Metallurgica, Vol. 24 (1976), p. 207.

23. C. Rodriguez and L. C. Brown, "The Thermodynamcis of Stress-Induced Martensites in Cu-Al-Ni Alloys," Metallurgical Transactions A, Vol. 7A (1976), p. 1459.

24. R. Smoluchowski, "Phase Transformation in Solids," in Phase Transition and Critical Phenomena, edited by H. Stanley (Chapter 8), Oxford University Press, New York, 1971.

25. J. W. Allen, "Stress Dependence and the Latent Heat of the Morin Transition in Fe_2O_3," Physical Review B, Vol. 8, No. 7 (1973), p. 3224.

26. R. J. Salzbrenner and M. Cohen, "On the Thermodynamics of Thermoelastic Martensitic Transformations," Acta Metallurgica, Vol, 27 (1979), p. 739.

27. F. H. Crawford and W. D. VanVorst, Thermodyamics for Engineers, Harcourt, Brace and World, Inc., New York, 1968, p. 225.

28. S. Mendelson, "Mechanisms for Martensite Formation and the Shape Memory Effect," in Shape Memory Effet in Alloys, edited by J. Perkins, Plenum Press, New York, 1975 p. 487.

29. R. J. Wasilewski, "The Shape Memory Effect in TiNi: One Aspect of Stress-Assisted Maretensitic Transformation," in Shape Memory Effect in Alloys, edited by J. Perkins, Plenum Press, New York, 1975, p. 266.

30. M. Ahlers, R. Rapacioli, and W. Arneodo, "The Martensitic Transformation in β-Brass and the Shape Memory Effect," in Shape Memory Effect in Alloys, edited by J. Perkins, Plenum Press, New York, 1975, p. 379.

31. O. Weres, "On the Thermodynamics of the Shape Memory Alloys," Report LBL-3297, Lawrence Berkeley Laboratory, University of California, Berkeley, November 1975.

32. E. A. Guggenheim, *Thermodynamics*, North-Holland Publishing Company, Amsterdam, Third Edition, 1957, p. 94.

33. C. M. Gilmore, Private Communication. (This research was suggested and is in preparation by Professor Gilmore, George Washington University, School of Engineering and Applied Sciences, Washington, D.C.).

8. NOMENCLATURE

C_p specific heat of NITINOL $[0.11 \text{ cal/g}^{\circ}\text{C}]$

E   elongation of NITINOL wire after straining [mm]

F   force extracted by NITINOL wire at peak stress σ_3 kg

H   enthalpy

ΔH latent heat of phase transformation of undeformed (unstretched) and unrestrained NITINOL wire $[5.78 \text{ cal/g}]$

$\Delta H^{A \to M}_{(o)}$ latent heat of forward phase transformation (austenite $\to$ martensite) at zero external force, after contraction (shape recovery) of the NITINOL wire

$\Delta H^{M \to A}_{(\sigma)}$ latent heat of reversed phase transformation (martensite $\to$ austenite) of a prestrained NITINOL wire during the rise of a recovery stress σ_3

J   mechanical equivalent of heat $[427.8 \text{ mkg/kcal}]$

L   length of the NITINOL wire [mm]

L_g length of NITINOL wire per 1 gram weight

ΔL linear change of the wire length during the contraction ($\Delta L = E$)

Q   total heat input to the NITINOL wire during one engine cycle

Q_c heat rejected by the wire in the cold bath (cold reservoir)

Q_D exothermic heat of elastic deformation (stretching) of the NITINOL wire at constant temperature

$Q_{[g]}$ total heat input per 1 gram of NITINOL

Q_H heat absorbed by the NITINOL wire in the hot bath (hot reservoir)

Q_R endothermic heat of shape recovery, absorbed by the NITINOL wire during the elastic contraction at constant temperature

S   entropy

T_1 temperature of the cold bath

T_3 temperature of the hot bath

ΔT $= T_3 - T_1$

ΔT_D adiabatic temperature rise due to the heat of elastic deformation in rapidly strained NITINOL wire

ΔT_M adiabatic temperature rise due to the latent heat of phase transformation (austenite → martensite) in rapidly strained NITINOL wire

U internal energy

W useful mechanical work produced by NITINOL wire during the engine cycle [mkg]

ι work diagram factor (ratio of acutal diagram area to the ideal diagram area)

α_T coefficient of linear thermal expansion of NITINOL in the transition region $[^\circ C^{-1}]$

γ density of NITINOL 0.234 lb/in^3

ϵ $= \epsilon_2 - \epsilon_1$, effective strain of the NITINOL wire in percent

ϵ_1 initial strain

ϵ_2 final strain

η thermodynamic engine cycle efficiency

η_c Carnot cycle efficiency

σ_1 initial stress [kpsi]

σ_2 stress at the end of the straining period

σ_3 maximum peak recovery stress

σ_4 residual stress after the contraction (shape recovery) of the NITINOL wire

"TRAINING" PHENOMENA IN NITINOL

Dr. A. D. Johnson
Energy Research Associates
Oakland, CA

ABSTRACT

It is common experience that NITINOL will not generally repeat the same cycle if it is deformed very much in a stress-strain-temperature cycle. Clearly some of this conditioning is due to work-hardening. But NITINOL also can develop two-way shape memory under some conditions. The loss due to hysteresis may decrease with repeated cycling, contrary to what one would expect from ordinary work-hardening. These material changes affect engine function, either beneficially or harmfully, and it is important to understand these phenomena in order to engineer better engine elements.

This discussion attempts to distinguish between the various modes in which NITINOL has been observed to condition. Experimental data will be shown from naive and "trained" NITINOL wire. A tentative model for the "training" process will be outlined. An attempt will be made to outline the questions which remain to be answered, and some experiments suggested for a more general understanding of the phenomena involved.

OVERVIEW

This report is based on a set of experiments with NITINOL wire in linear tension. Figure 1 depicts the apparatus constructed for these experiments.

Figures 2, 3, 4, 5, and 6 show a sequence of operations on a NITINOL wire. Figure 2 is a set of isotherms taken when the wire was naive. Figures 3 and 4 show successive stress-strain-temperature cycles in which the tension in the wire is held constant during shape-memory recovery. Figure 5 demonstrates that the wire length is stable under reduced load. Figure 6 shows that the isotherms characterizing this wire have been drastically altered; the wire has been permanently deformed more than 5 percent and the horizontal plastic isotherms in Figure 2 have been rotated, resulting in a two-way shape memory.

Figures 7, 8, 9, and 10 are analogous, but with a significantly altered thermodynamic cycle. In figures 3, 4, and 5, the wire did external work during shape recovery, while in Figures 8 and 9 it does no external work. Comparison of Figures 6 and 10 shows that permanent deformation and rotation of isotherms do not result from this low-recovery-force cycle, while Figure 11 shows that the wire has not been stabilized.

Figures 12, 13, 14 show a different sequence. In Figure 13, the wire is held at constant length during heating so that the shape recovery takes place after heating. Figure 14 shows that this cycle does not result in rotation of the isotherms, but does induce some permanent deformation. I infer that these are independently modifiable characteristics of NITINOL.

Figure 15 shows a set of isotherms for a wire which was first trained by running on a continuous-band engine. There is a pronounced two-way shape memory, and the cold isotherms are very steeply rotated. The simulated engine cycle in Figure 16 yields a specific work output in excess of one joule per gram per cycle.

Figures 17, 18, 19, and 20 are traces of tension versus length at constant force as temperature is cycled. They demonstrate that the hysteresis of a NITINOL wire depends on the thermodynamic cycle history.

From these experiments I infer that the stress-strain-temperature characteristics of NITINOL wire in tension are critically dependent on the history of the wire sample. Three separate effects are observed: a permanent deformation, rotation of the isotherms, and reduction of hysteresis.

INTRODUCTION AND DISCUSSION

One of the most remarkable properties of NITINOL, and another reason for our keen interest in it as an engine element, is its behavior under "conditioning." By conditioning, I mean any repeated stress-strain-temperature cycling which changes the physical characteristics of the material. Most materials, when subjected to stress-strain cycling (such as bending) which plastically deforms them, undergo some work-hardening and embrittlement. Normally the hysteresis, that is the difference between the paths for increasing and decreasing stress and strain, increases due to piling up of dislocations in the crystal structure. This eventually leads to fatigue and failure. Repeated bending of a copper or soft iron wire exemplify this behavior.

NITINOL also undergoes work-hardening and embrittlement under conditioning, and in some stress-strain-temperature cycles this is the most conspicuous result. For example, in the wobble-plate test-bed built at Lawrence Berkeley Laboratory in 1975, the wires were observed to "creep" in length until they reached a maximum. This "creep" was followed by failure (breakage). In this case the work output per cycle diminished with each cycle.

However, NITINOL also exhibits a second behavior under certain conditions. If the maximum stress (tension) is held below some limit, and is constant during the heating phase of the stress-strain-temperature cycle, and if the temperature excursion goes well above and below the unstrained TTR, then the alloy develops a second memory and the hysteresis decreases significantly. By second memory we mean the alloy has two normal shapes: one to which it returns when heated; a second to which it goes when cooled. It will now do significant work when either heated or cooled, although the work done during cooling is only about 10 percent of that available during heating. The fact that the hysteresis decreases indicates that fatigue, in the ordinary sense, is eliminated. This means NITINOL subjected to an appropriate conditioning cycle will repeat that cycle indefinitely. Furthermore, the amount of work available per cycle may be significantly increased compared to that of the naive sample. These characteristics are of extreme importance in engine design.

This behavior was observed accidentally in early continuous-band engines and in the Banks engine. In these engines, performance improved as the NITINOL wire "learned" under repeated cycling; therefore we gave this the name "training." It appeared that the wire in these engines always adapted to the cycle given it, as if it were capable of modifying its own behavior. We now realize this adaptation takes place only under limited and not completely understood conditions. We now prefer to reserve the word "training" for a conditioning program which results in a) a pronounced second memory, b) stability, so that a given cycle may be repeated indefinitely, and c) reduced hysteresis, so that the work output per cycle is comparable to or greater than that for a naive wire. Thus a trained wire is suitable for designing a NITINOL engine, since it has known characteristics which may be expected to repeat, and which are desirable for optimization of design.

This definition specifically excludes processes which in sum lead to a non-repeatable cycle behavior and/or in which the ability of the NITINOL is seriously impaired.

This phenomenon has been made clearer by the research of Cory[1], who started in 1975 to make x-y plots of complete stress-strain cycles. He observed that the flat region of the stress-strain curve of naive (freshly-annealed) wire develops a slope as the material is cycled. He interpreted this as being due to development of internal stresses through work-hardening. Rotation of the stress-strain curves can result in negative external forces (stresses), which is a way of characterizing the second memory. At the same time the hysteresis—the distance between increasing and decreasing isotherms—is diminished. That contradicts the theory that these internal stresses are simply due to accumulation of dislocations in the crystal structure.

It now appears that at least two separate phenomena are at work in the training of NITINOL. The first is normal work-hardening, or creep, or fatigue. This second is more subtle, and probably closely associated with the memory property of NITINOL itself. We have tried to visualize a model for this process in terms of the martensite-austenite transition. This model seems to account for all the observed phenomena and makes some predictions which can be tested.

The behavior of a real sample of NITINOL is a complicated function of its cycle history. First, recovery, even of small deformations, is imperfect, at least in freshly annealed alloy. Second, the NITINOL in a wire helix which is repeatedly cooled, stretched, heated, and allowed to contract adapts to the cycle to some extent. After several thousand cycles, the helix elongates when cooled even in the absence of external force. Such a "trained" wire will not quite recover to its annealed length, but has now two natural or unconstrained lengths: one for each of its two phases, hot and cold.

The mechanism for this two-way shape memory is not well understood. I have speculated that . results from martensitic platelets which are trapped during the transition to the high-temperature phase, and release some of their trapped energy when most of the wire transforms to the martensitic form. This very tentative explanation requires introduction of the concept of stress-induced martensite.

We have referred to the phase transition as if it took place at a specific temperature. Actually, even when there are no external forces, the transition is gradual over a temperature range of as large as 30 degrees C. This is explainable as due to the inhomogeneous nature of the crystal structure. NITINOL does not exist as single large crystals. It is a mass of more or less randomly oriented crystal domains of a few micrometers in extent. For any particular deformation, only a small fraction of the martensite platelets are favorably oriented to accommodate the deformation by the migration of twinning boundaries. Those not so favorably oriented distort or move so as to minimize the total energy. A wire swaged and drawn from a billet will have large internal stresses not completely relieved by annealing. These stresses may exhibit themselves, when total energy is minimized, by creating domains which are not truly of the same phase as the majority of the sample. There may be islands of martensite in the high-temperature phase, and vice-versa. Another way to say this is that

---

[1]J. S. Cory, "NITINOL Thermodynamic State Surfaces," Journal of Energy, Vol. II, No. 5, September-October 1978, pp. 257-258. Full report is National Technical Information Service #N78-31206, "Engineering Data and Correlations," Springfield, VA.

NITINOL, between certain temperature limits, always exists as a mixture of the two phases. Furthermore, it is possible to generate or to enlarge these foreign domains through stress. When parent or high-temperature phase NITINOL is stressed, the islands of martensite created by the energy-minimization process are called stress-induced martensite. This is partially a misnomer, since there is no intrinsic difference between these platelets which appear as a result of stress and those which result from the phase transformation except for a preferred orientation. In fact, it is not possible to separate the external forces from the internal. The forces exerted upon a given domain in the interior of a sample of NITINOL are the sum of internal and, to a lesser extent, external forces. And these internal forces may be a function of temperature, as the phase change takes place.

It is necessary to consider all the thermodynamic variables, in this case stress, strain, and temperature, in describing the state of a sample of NITINOL. This was not appreciated by some early critics of the NITINOL engine effort, who argued that the transition takes place over a limited temperature range, that this is the only range which contributes to work output, and thus that the Carnot efficiency is extremly small. One may see the folly of this argument by applying it to the steam engine. Since the boiling point of water is exactly 100 degrees C, such an engine must have zero Carnot efficiency. The flaw in the argument is that there is no fixed transition temperature for water: The vaporization temperature is a function of pressure and temperature. The same is true for NITINOL, but the variables are stress and temperature, and the NITNIOL is also inhomogeneous so there is a spread in transition temperature (a mixture of high-temperature phase and martensite phase) at any given stress level.

The analogy to the steam engine is useful in describing the stress-strain-temperature cycle in the NITINOL engine. In a closed-cycle liquid-vapor heat engine, the working fluid is allowed to expand at constant pressure during which it takes in heat. Then it is cooled at constant volume so that the pressure is reduced. Next, it is further cooled so that it condenses, and the volume greatly reduces. Finally, it is heated at constant volume so that the pressure increases. As this cycle is repeated, the area traced out is the useful work done by the system. In the NITINOL engine, the role of the working fluid is assumed by the NITINOL, pressure is replaced by stress on the NITINOL, and volume of fluid becomes strain in the NITINOL. With these substitutions, the NITINOL cycle is: Heat the NITINOL wire so it contracts and does work externally; reduce the stress at this temperature; cool the wire under constant tension; stretch the wire under constant temperature and stress; increase the stress so the strain increases further. Then repeat the cycle. Both these cycles are, of course, highly idealized cases and could not be achieved precisely in practice. But they serve to illustrate the excursion in temperature and stress to which the NITINOL working material is subjected.

Figures 3-5 show examples of this cycle.

What happens internally as the NITINOL is subjected to this cycle? As it is cooled at constant stress, and consequently elongates, new martensite plates grow from the "seed" martensite which exists because the metal is a mixture. The growth is preferential in a direction which most easily accommodates the elongation. This is required by the minimization of energy. At the end of the constant-stress part of the cycle, the wire is mostly martensite, and the martensite platelets have a preferential orientation. When the plastic deformation is complete, the strain increases further as the stress increases further to the point in the cycle where there is maximum stress and maximum strain. As heat is applied, parent or high-temperature phase grows, again preferentially. Some of the more favorably oriented martensite platelets remain in the matrix of parent phase.

At the point in the cycle where contraction at constant stress ceases, some platelets thus remain, the ones oriented favorably to elongation of the wire. Next the stress is decreased. The matrix of parent phase tightens around these platelets, but some will remain because they cannot deform so as to become parent phase. These become distorted by forces exerted by the parent phase. One may visualize them as tiny bubbles which have become trapped and cannot escape, but are compressed, and hence have internal stored energy. They cannot relax because they are bound by the constraining matrix of parent phase. However, when the wire is cooled, martensite is allowed to form, and it forms again preferentially beginning with these trapped "seed" platelets, as the wire converts to mostly martensite. But the martensite no longer binds the compressed bubbles or compressed martensite platelets: Their energy now may be released by motion of twinning boundaries. These trapped platelets are oriented to be in their lowest energy state when the wire is elongated. Therefore they push out along the wire and cause it to elongate. This seems to explain how a "trained" wire may have a second memory, and how it reverts to the cold shape without application of external forces. The cold memory is a response to internal rather than external forces.

Next, I shall describe an experimental program to test some of these ideas, and to get quantitative information on the first few training cycles.

EXPERIMENTAL PROGRAM

Before one can design an optimal NITINOL engine, one clearly needs detailed knowledge of the characteristics of the material to be used. Data taken on naive wire are not satisfactory, for it has been the experience of everyone that NITINOL changes character as it is cycled. One should therefore measure the properties of NITINOL after it is trained so that a cycle is repeatable. But how can one best achieve a repeatable cycle? It is necessary to start at the beginning, with naive NITINOL, and develop some data as it is cycled.

For this study, I chose wire in tension, since in this form one should see the effects of training in purest form because all elements of the wire cross-section are deformed equally.

Three distinctly different cycles were selected for this exploratory work. First is a cycle which closely approximates that of the thermo-turbine or continuous-band engine (Fig. 16). In this cycle the wire contracts as it is heated at constant force. We designate this the constant-force cycle. Second, a cycle in which contraction is against very small force so that the wire does minimal work while being heated. This we call the low-hot-force cycle (Fig. 8). Third is a cycle in which the wire is constrained at a fixed length while it is heated. This we call a fixed-length cycle (Fig. 13).

The experimental stress-strain fixture (Fig. 1) was constructed to take the necessary measurements. A NITINOL wire is suspended inside an insulated tube through which water is circulated. Two pumps and two reservoirs permit switching from hot to cold baths by means of valves. Tension in the wire is measured by a load cell and used as input to the y-axis of a Mosely two-axis recorder. Length change is determined by a lead screw attached to a potentiometer, the variable voltage is used as x-axis input. Alternatively, the lead screw may be disengaged and wire elongation measured by a potentiometer coupled to a pulley over which a cable runs from the NITINOL wire to a weight. This arrangement is used for fixed-force measurements.

A sample of NITINOL wire may be characterized by a set of stress-strain isotherms which lie on state surfaces as defined by Cory.[1] Isothermal state surface measurements are shown in Figures 2, 6, 7, 10, 12, 14, 15. Differences between these measurements are due to the differences in conditioning. All except Fig. 15 were taken from a single piece of wire after annealing in an air oven for about one-half hour at 570-580 degrees C.

First consider freshly-annealed samples of wire measured in Figures 2, 7, and 12. These were taken from Timet heat V-4609 and obtained from Charles Raymond. Starting at zero force, with the wire pre-heated to 90-95 degrees C, each isotherm is drawn by increasing the elongation in stages of about one-quarter percent with pauses of a few seconds after each step. This results in vertical dips as the wire sags due to a slow component of the transformation. This phenomenon seems not to have been observed by other researchers who elongated at a constant rate. I believe it significant that the bottoms of these dips or sags lie on an almost perfectly horizontal line, indicating nearly perfect plastic deformation.

The first isotherm, at 6 degrees, is located at considerably greater stress than the second, at 10 degrees. This has been observed by other researchers.[1] It is of interest, however, that after stretching the wire in the first pull at 6 degrees, this cycle cannot be repeated (see pulls numbered ⑥ in Fig. 2, ② in Fig. 7). Even one pull on the naive wire has partially conditioned it.

Figures 3 and 4 record the first 14 constant-force cycles to which this naive wire was next subjected. After an initial stretching of more than 5 percent, which the wire retains as a permanent deformation, the cycle approaches a repeatable cycle asymptotically.

For the next set of data, the maximum force was reduced from 45 to 35 Newtons. Fig. 5 records cycles 15 through 21. The irregular variation along the right-hand side, where the force is applied in three steps by adding weights, results from very small variations in cold-reservoir temperatures. The remainder of the cycle is seen to be very nearly repeated, indicating this wire had been stabilized at this stress-strain-temperature cycle. This is an important result. It demonstrates that NITINOL may be pre-conditioned for use in a specified engine cycle.

Fig. 6 shows the isotherms measured on this wire after these 21 cycles. A two-way shape memory of about 3/4 percent has developed, and the isotherms have been rotated so that they are no longer horizontal. The alloy characteristics are dramatically modified.

Figures 7-10 show similar curves for a sample taken from the same annealed wire, but subjected to a low-hot-force cycling. Fig. 10 is particularly interesting compared to Fig. 6. They are clearly very different, and 10 is similar to that for the naive wire. I conclude that the two-way shape memory and rotation of isotherms, which I associate with training, do not occur unless the wire does work while it is being transformed. Fig. 11 shows this sample has not been stabilized.

The sequence of Figures 12-14 shows what happens to a wire under constant-length cycling. Fig. 13 demonstrates that this wire, initially stretched to 4 percent and then heated at constant length, does considerably less work on the twelfth cycle than on the first. This corroborates data taken by Hernandez et al.[2] Fig. 14 shows this wire has not been trained by this fixed-length cycle.

---

[1] See footnote 1 on page 10-4.

[2] H. P. Hernandez, R. M. Banks, D. Norgren, "NITINOL Test Bed Engine" Lawrence Berkeley Laboratory, Berkeley, CA (1975).

Finally, as an example of a more fully-trained wire, Figures 15 and 16 show the isothermal state surfaces measurement and constant-force cycle for a wire which was run on an engine for several thousand cycles during which it was elongated 3 percent each cycle. Temperatures and forces were not recorded, however. This wire shows a two-way shape memory of nearly 3 percent, and extremely rotated isotherms. In fact, the ascending curves at low temperatures (traces at 2, 6, and 10 degrees C) are nearly as steep as the high-temperature curves at 60 to 90 degrees. One might describe this sample as having two elastic regions, at high and low temperatures, and two corresponding unconstrained lengths.

Fig. 16 shows that this wire is stabilized up to a force of 100 Newtons (25 KN/cm^2), and at this stress level is capable of doing at least a joule per gram per cycle of work.

For us to look at the state surfaces in the temperature versus length projection, a thermocouple measured the temperature, recorded as displacement instead of force. Figures 17 through 20 measure temperature versus length at constant force. The first two plots are taken from the highly-trained wire whose isotherms are shown in Fig. 15. Figs. 19 and 20 are for the nearly-naive wire whose isotherms are in Fig. 12. The state-surface boundaries are separated by approximately 18 degrees C for the trained wire, and by more than 30 degrees for the untrained wire. From this I conclude that training decreases the hysteresis of NITINOL wire in tension.

CONCLUSIONS FROM THE EXPERIMENTAL RESULT

1. Anything done to NITINOL conditions it. It is virgin only once.

2. NITINOL can be trained, i.e. given a two-way shape memory, a stable and repeatable cycle, and reduced hysteresis, in a few cycles.

3. Rapid training does not occur under certain conditions, for example, in a cycle which does no external work.

4. A slow (several seconds) component of deformation, especially at low temperatures, diminishes with nearly all kinds of conditioning.

5. Work available from a naive cycle may be larger than for a trained cycle. But since no wire remains naive in an engine cycle, it is more relevant to study trained wires. These have been shown capable of doing a joule per gram per cycle of external work.

6. Although some questions regarding training of NITINOL wire in tension have been resolved, a number remain. Needed are studies which range over the variables: force, elongation, temperature, and number of cycles of a particular type. So far we have neglected consequences of differing metallurgy. This study has established only a few points in the continuum of each variable. It would be useful to measure stress versus strain at negative external force in order to better characterize the two-way memory.

7. The picture of training given by the concept of trapped martensites seems compatible with all the observations. This theory predicts other consequences which should be decided by experiments.

8. I differ with Cory's conclusion in that training is strictly a matter of maximum deformation. In particular, stress-strain isotherms for a highly-trained wire are not simply rotations of those for a naive wire. And the hysteresis for a trained wire is less than that for a naive wire, indicating that some process takes place besides simple work-hardening.
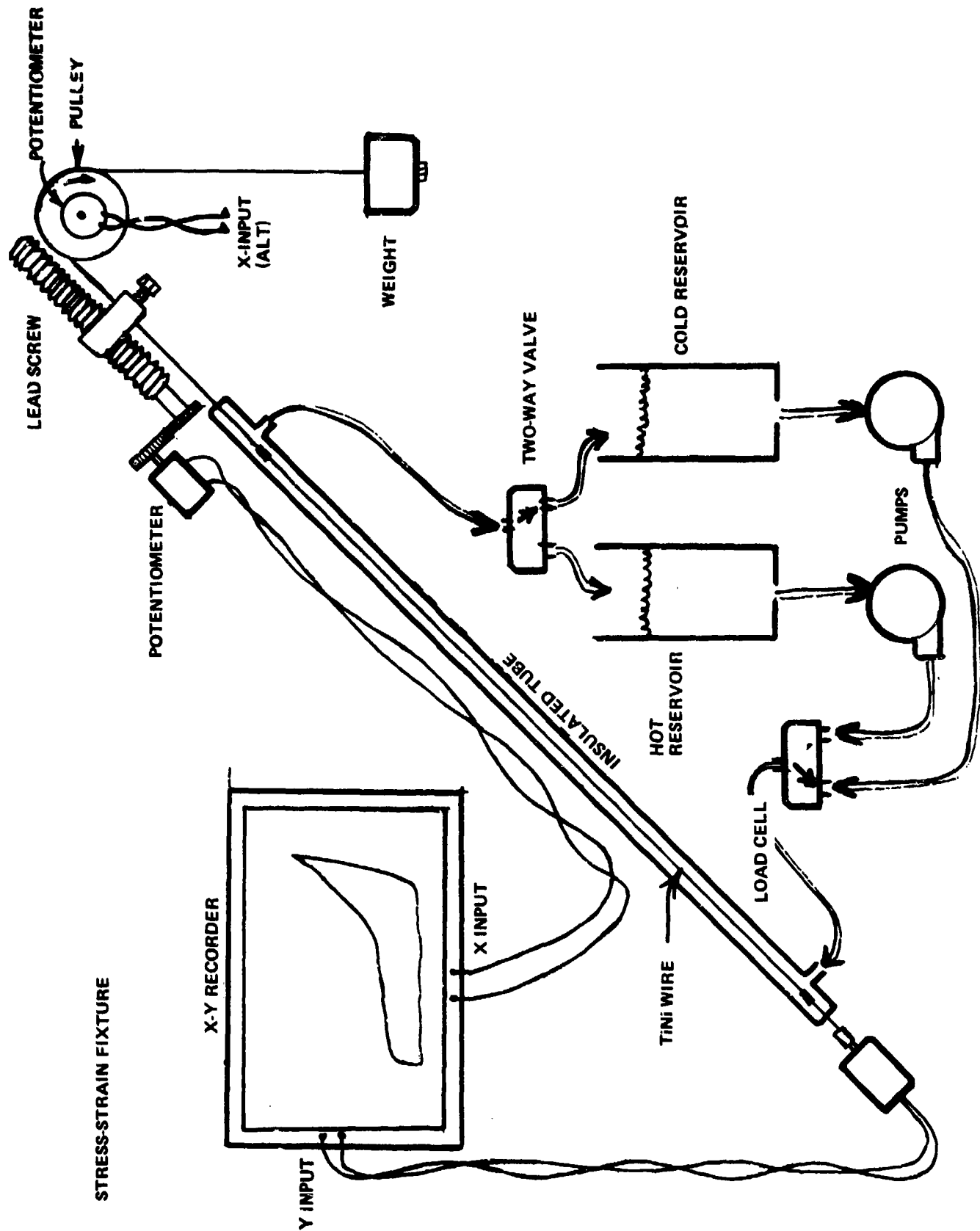
FIGURE 1

FORCE, NEWTONS

FRESHLY – ANNEALED RAYMOND – TIMET WIRE 0.018'' x 20'' LONG (0.7 gm)
ISOTHERMS: STATE SURFACES. RETURN TO ~ 90° AFTER EACH PULL

STRAIN, % ELONGATION

STRESS, KN/cm²

FIGURE 2

① 6° C
② 10
③ 15
④ 20
⑤ 25
⑥ 4°
⑦ 30→28
⑧ 35
⑨ 40
⑩ 50
⑪ 90° C

FORCE, NEWTONS
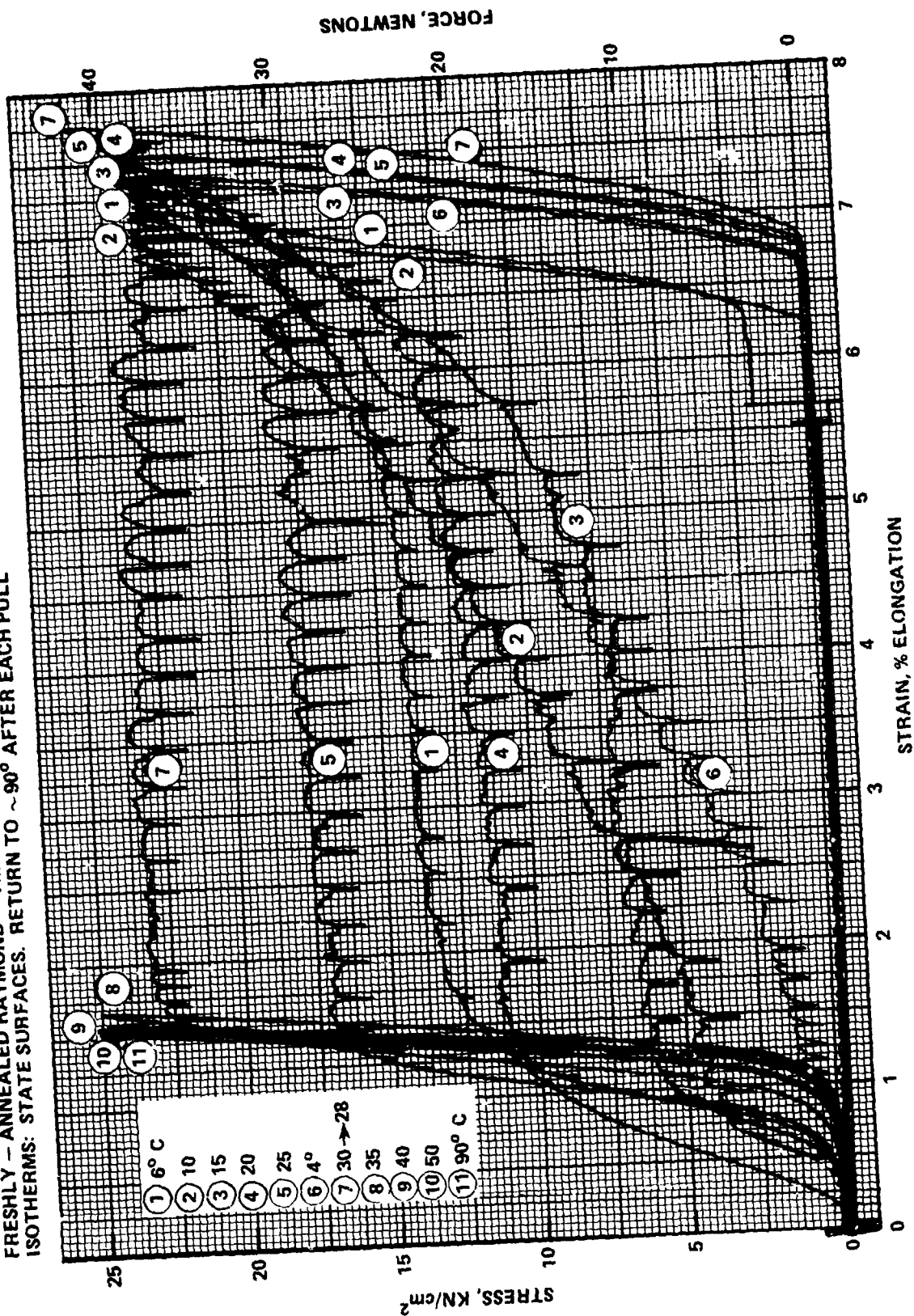
FRESHLY – ANNEALED RAYMOND – TIMET WIRE 0.018'' x 20'' LONG (0.7 gm)

CONSTANT FORCE CYCLE, FIRST 2 CYCLES ①/3

STRAIN, % ELONGATION

STRESS, KN/cm²
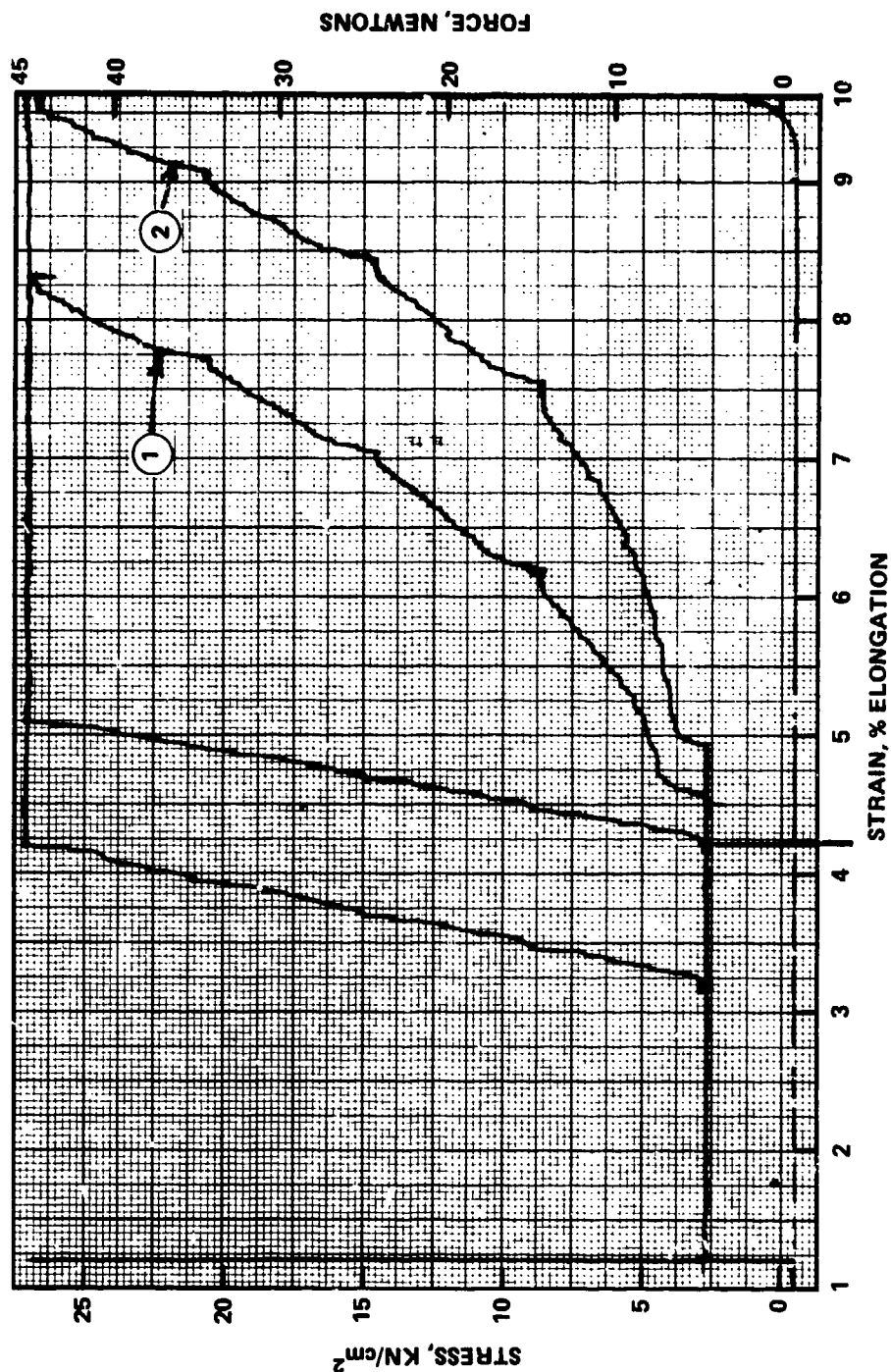
CONTINUE ON NEXT SHEET, LEFT 3''.

FIGURE 3

FRESHLY — ANNEALED RAYMOND — TIMET WIRE 0.018" x 20" LONG (0.7 gm)
CONSTANT FORCE CYCLE, CYCLES 3-14 (2/3)

FORCE, NEWTONS

STRESS, KN/cm²

STRAIN, % ELONGATION
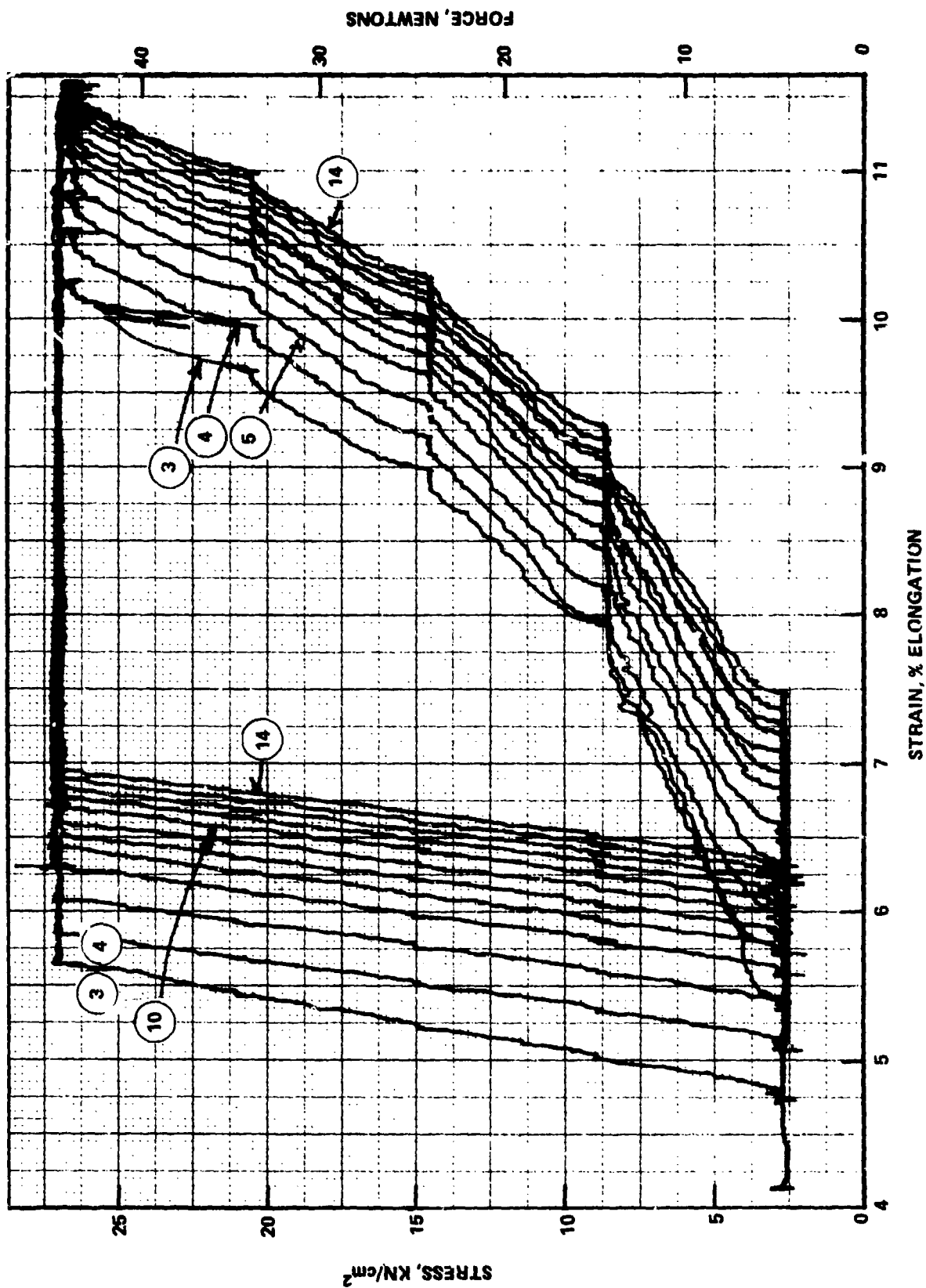
FIGURE 4

FRESHLY – ANNEALED RAYMOND – TIMET WIRE 0.018" x 20" LONG (0.7 gm)
CONSTANT – FORCE CYCLES: 15-21 ③/③
A →B CONST FORCE = 5N, DECREASING TEMP
B →C CONST TEMP ≅ 5°C, INCREASING FORCE
C →D CONST FORCE = 35N, INCREASING TEMP
D →A CONST T ≅ 95°C, DECREASING FORCE
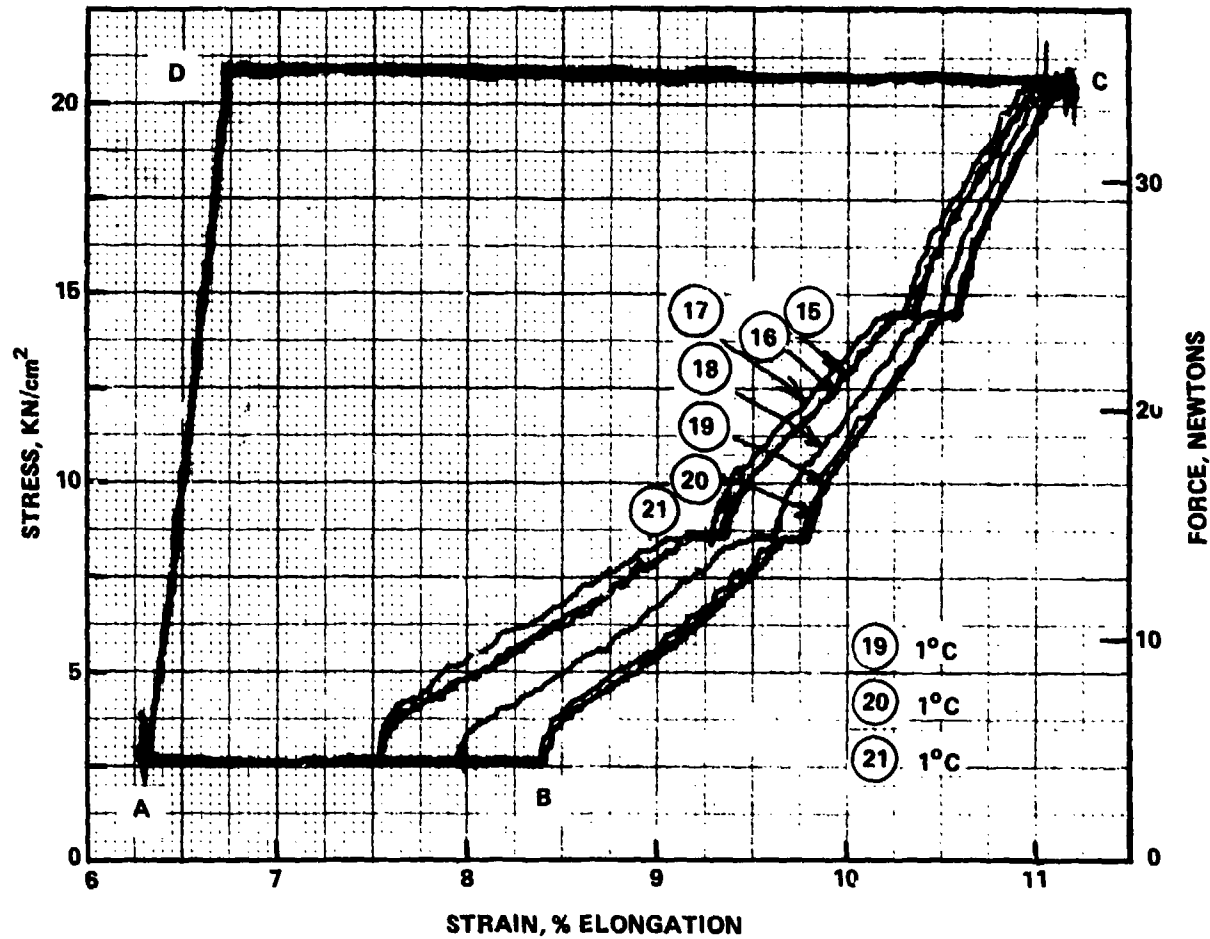
FIGURE 5

FRESHLY ANNEALED RAYMOND — TIMET WIRE 0.018" x 20" LONG (0.7 gm)
AFTER 21 CONSTANT — FORCE CYCLES, T ≥ 5° & 95°
F = 5N & 35 OR 45N

ISOTHERMS: STATE SURFACES
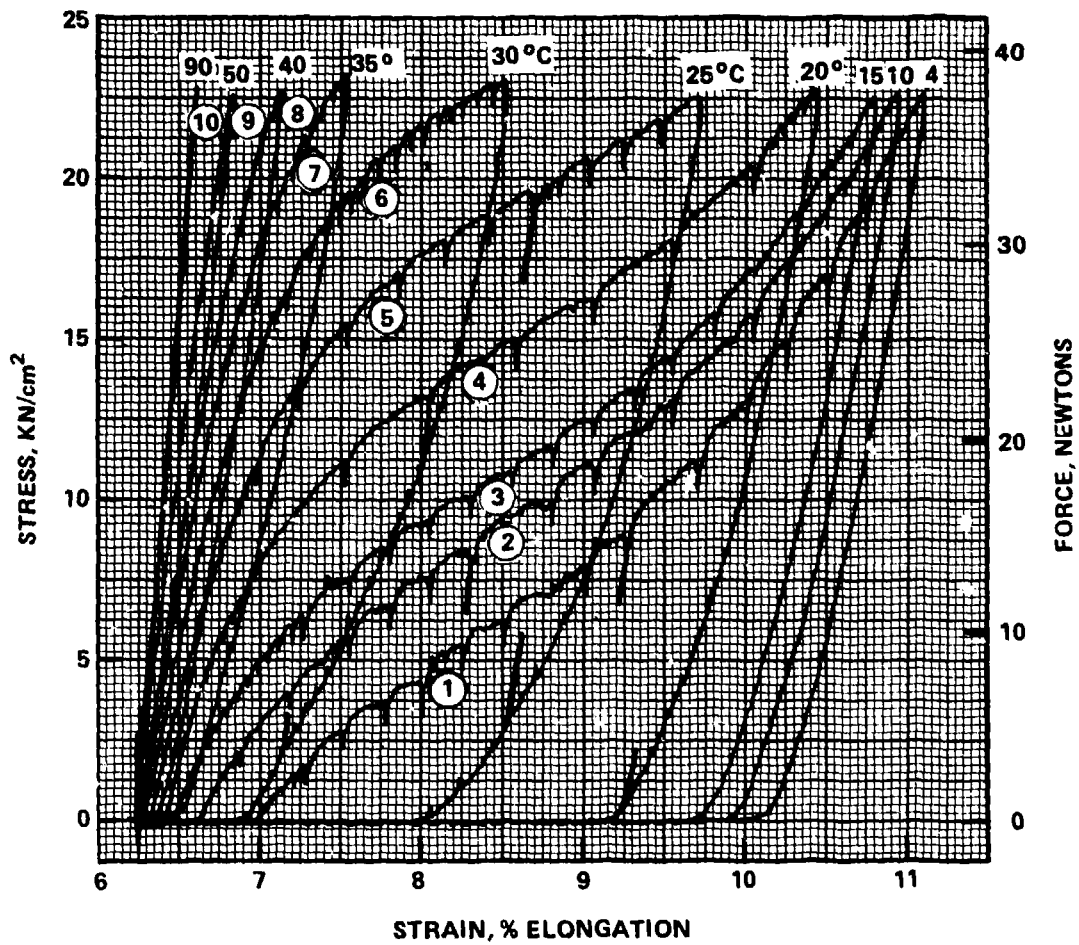
FIGURE 6
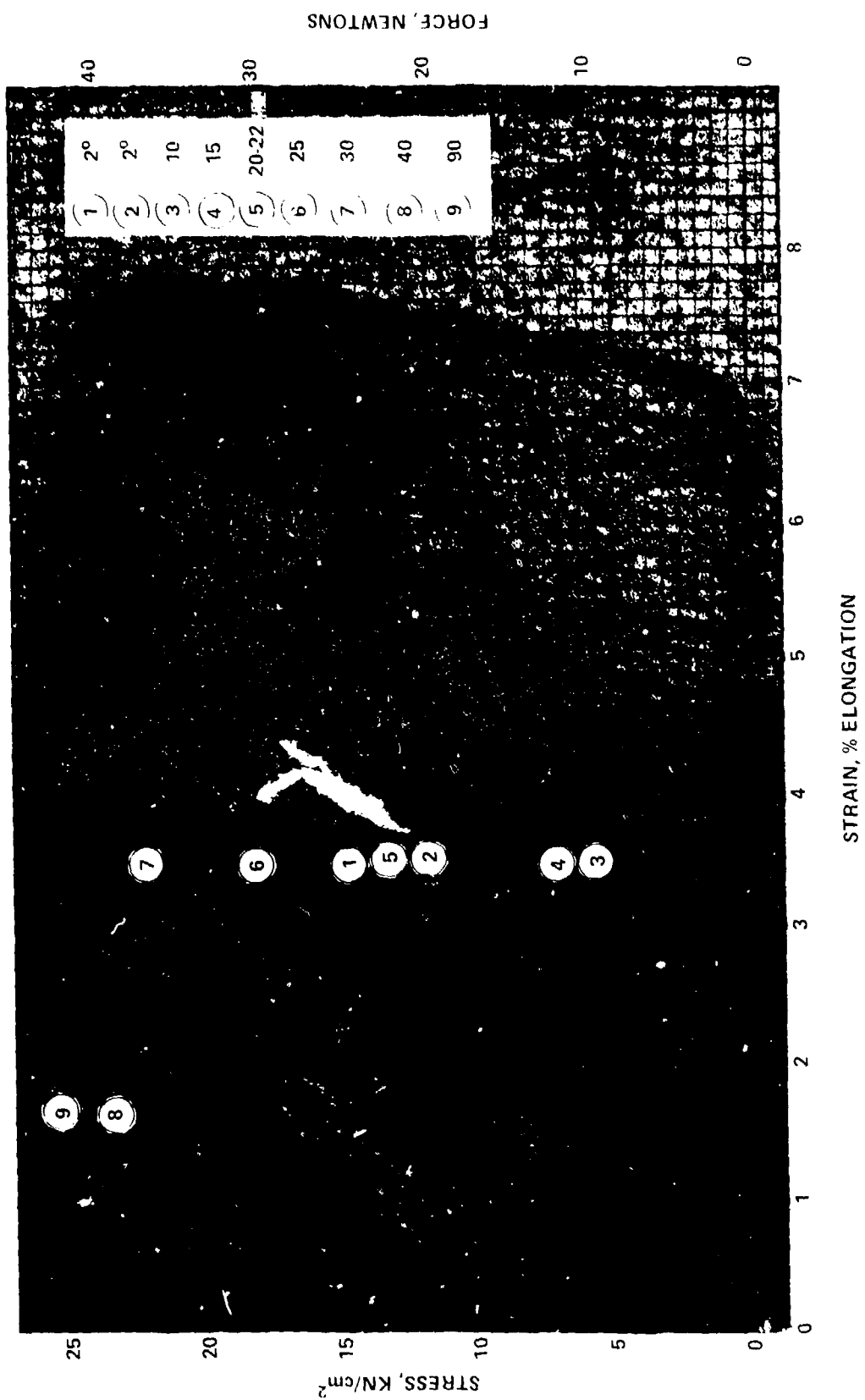
FIGURE 7

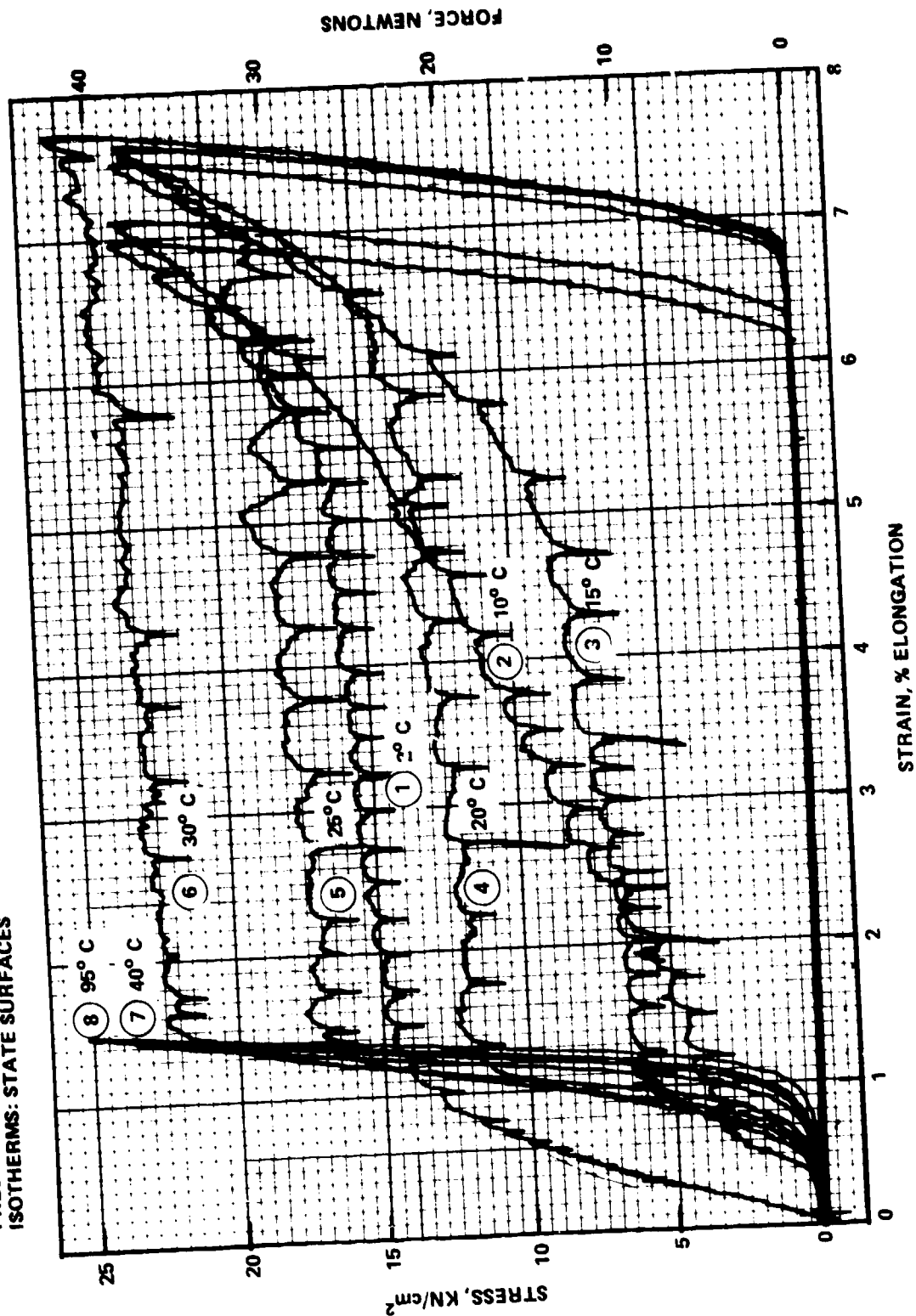FRESHLY – ANNEALED RAYMOND – TIMET WIRE 0.018" x 20" LONG (0.7 gm)
ISOTHERMS: STATE SURFACES
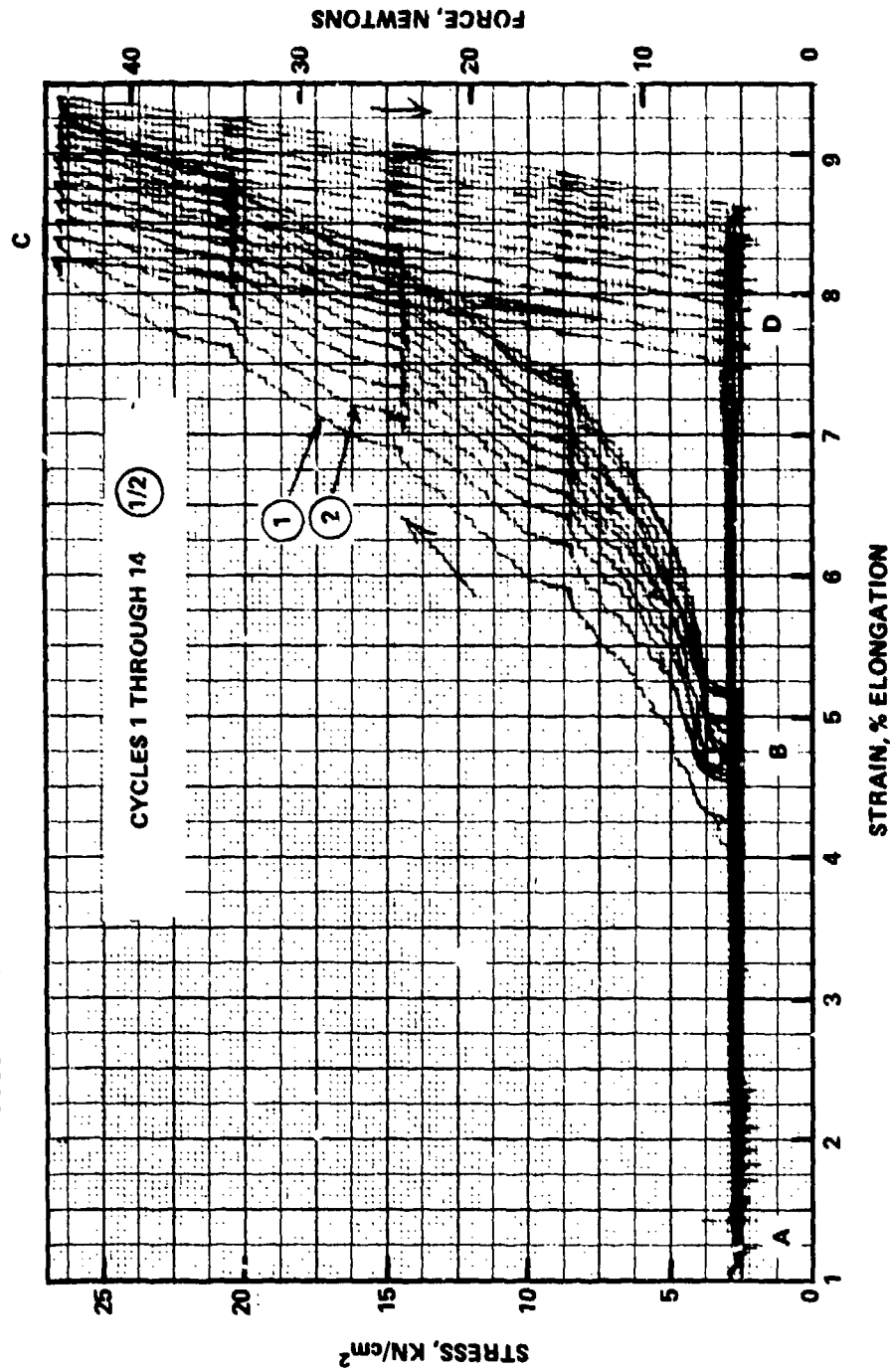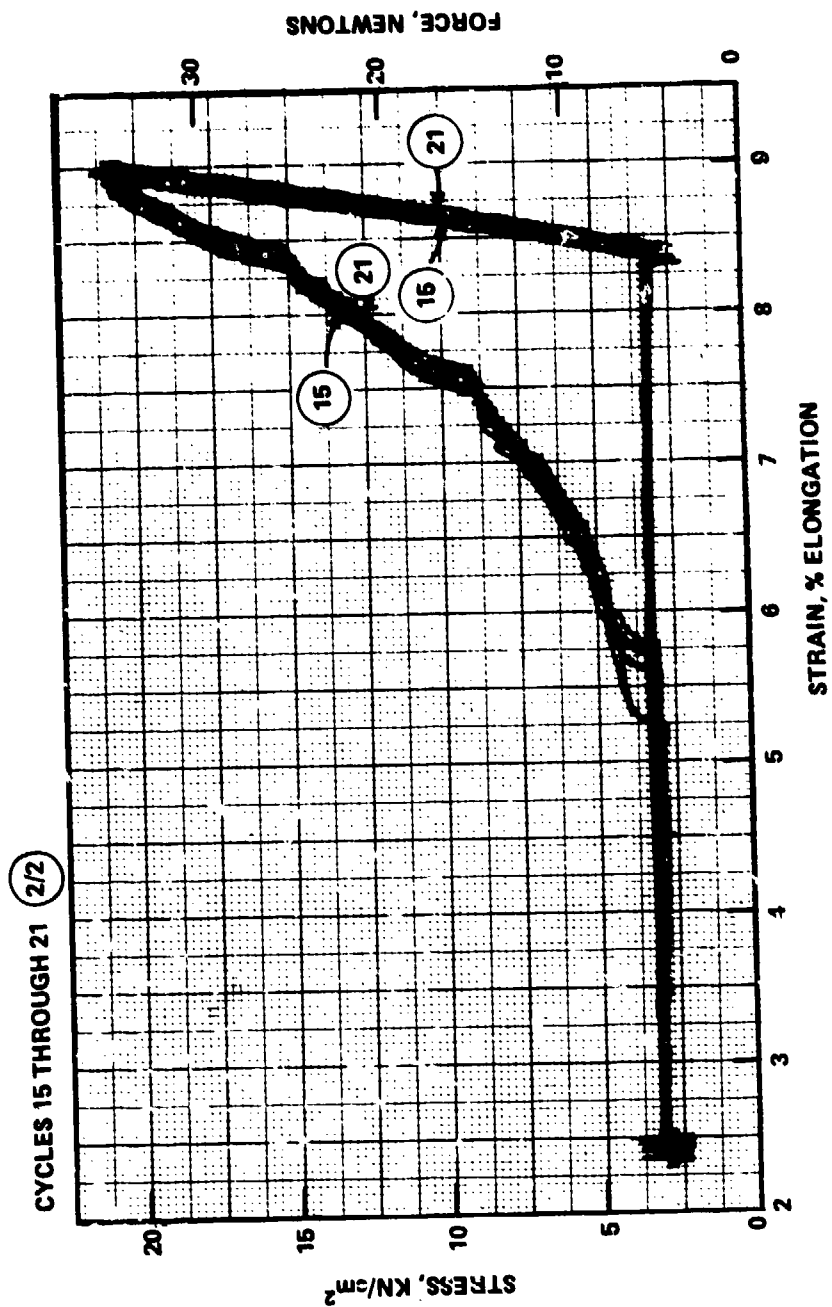
FIGURE 8

FIGURE 9

RAYMOND — TIMET WIRE 0.018" x 20" LONG (0.7 gm)
AFTER 21 LOW — HOT — FORCE CYCLES
ISOTHERMS: STATE SURFACES
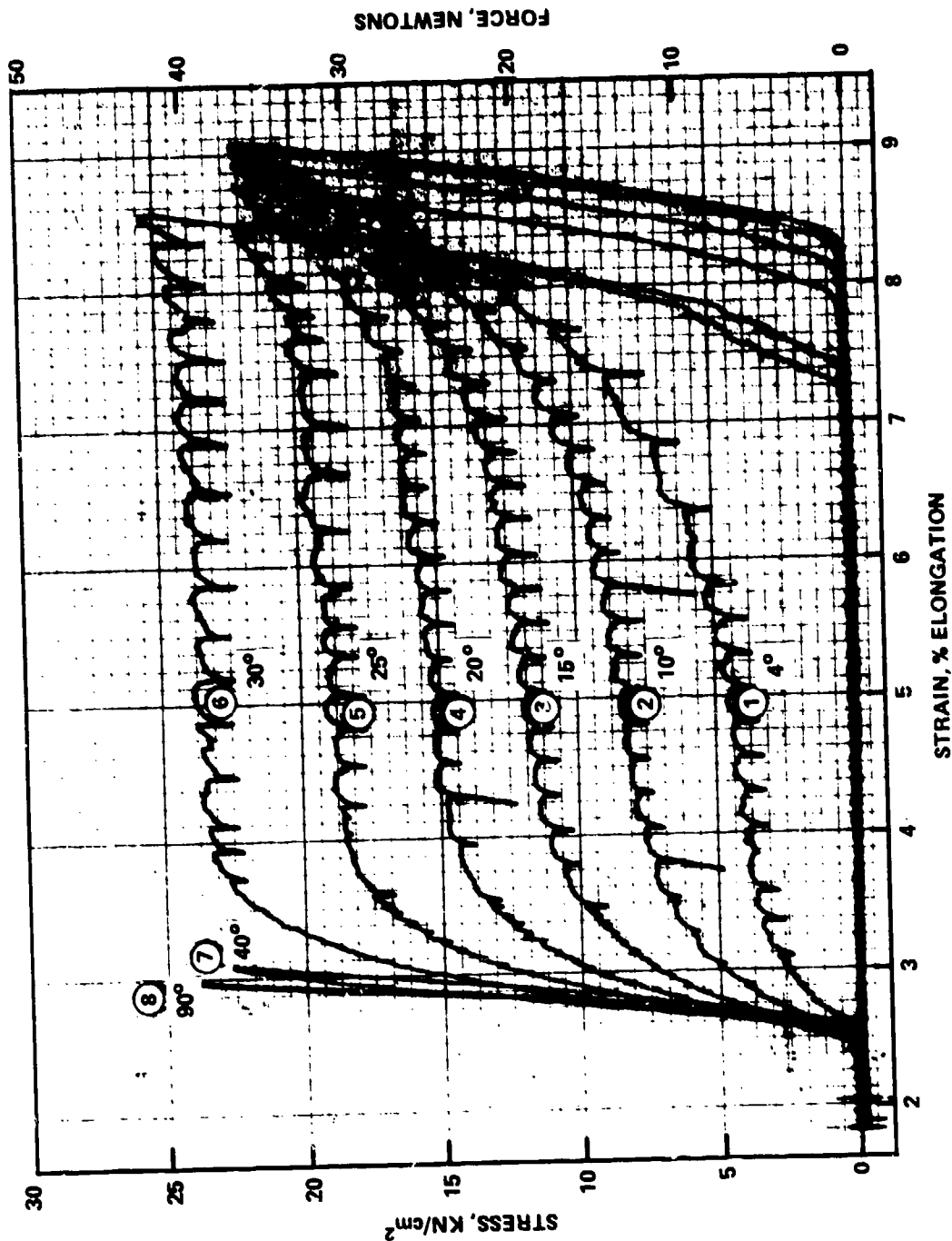
FIGURE 10
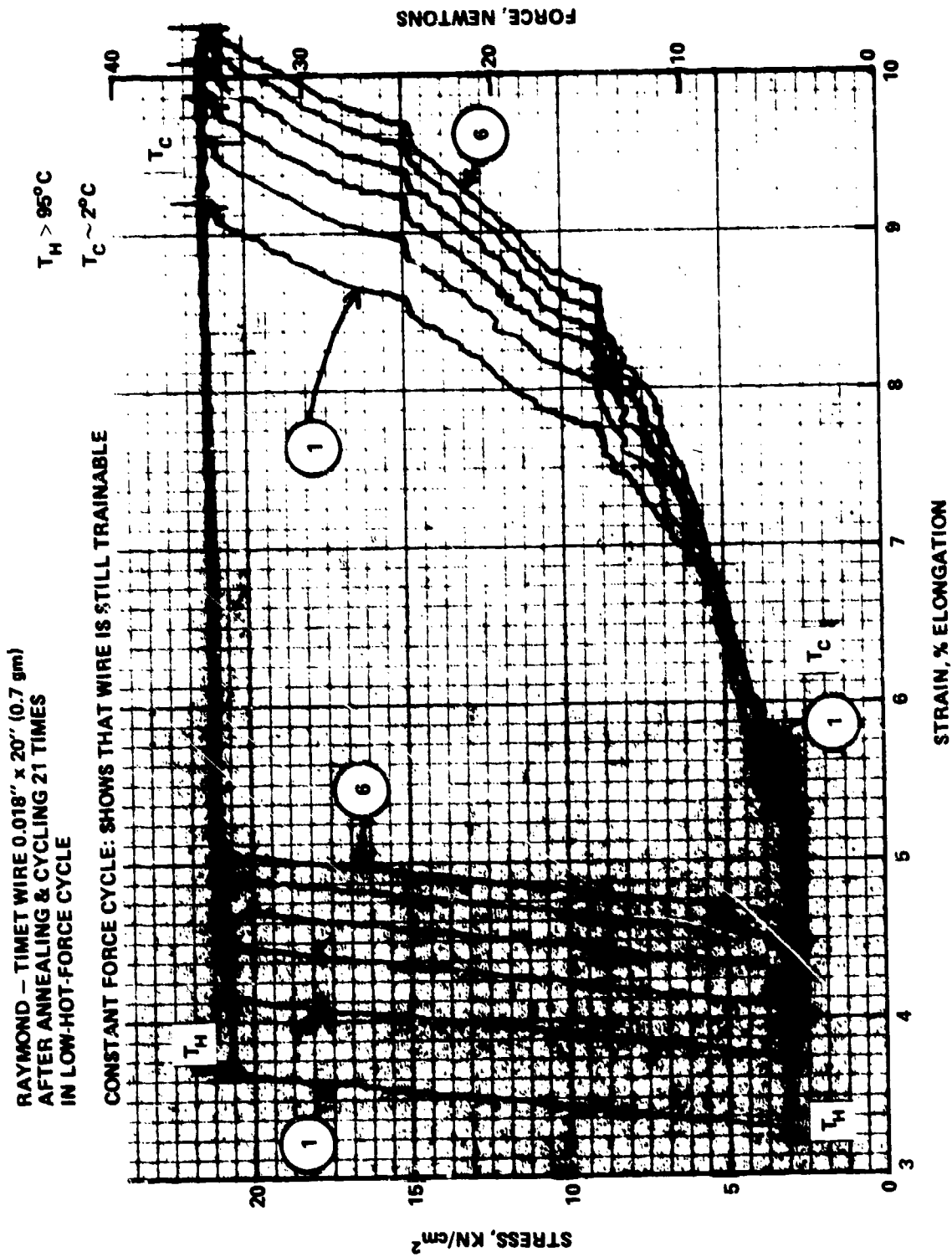
FIGURE 11

RAYMOND – TIMET WIRE 0.018" x 20" (0.7 gm)
AFTER ANNEALING & CYCLING 21 TIMES
IN LOW-HOT-FORCE CYCLE

CONSTANT FORCE CYCLE: SHOWS THAT WIRE IS STILL TRAINABLE

$T_H > 95°C$
$T_C \sim 2°C$

FIGURE 12

RAYMOND – TIMET WIRE 0.018″ x 20″ (0.7 gm)
FIXED – LENGTH CYCLES 1-12
$T_C \sim 2°C$
$T_H > 95°C$
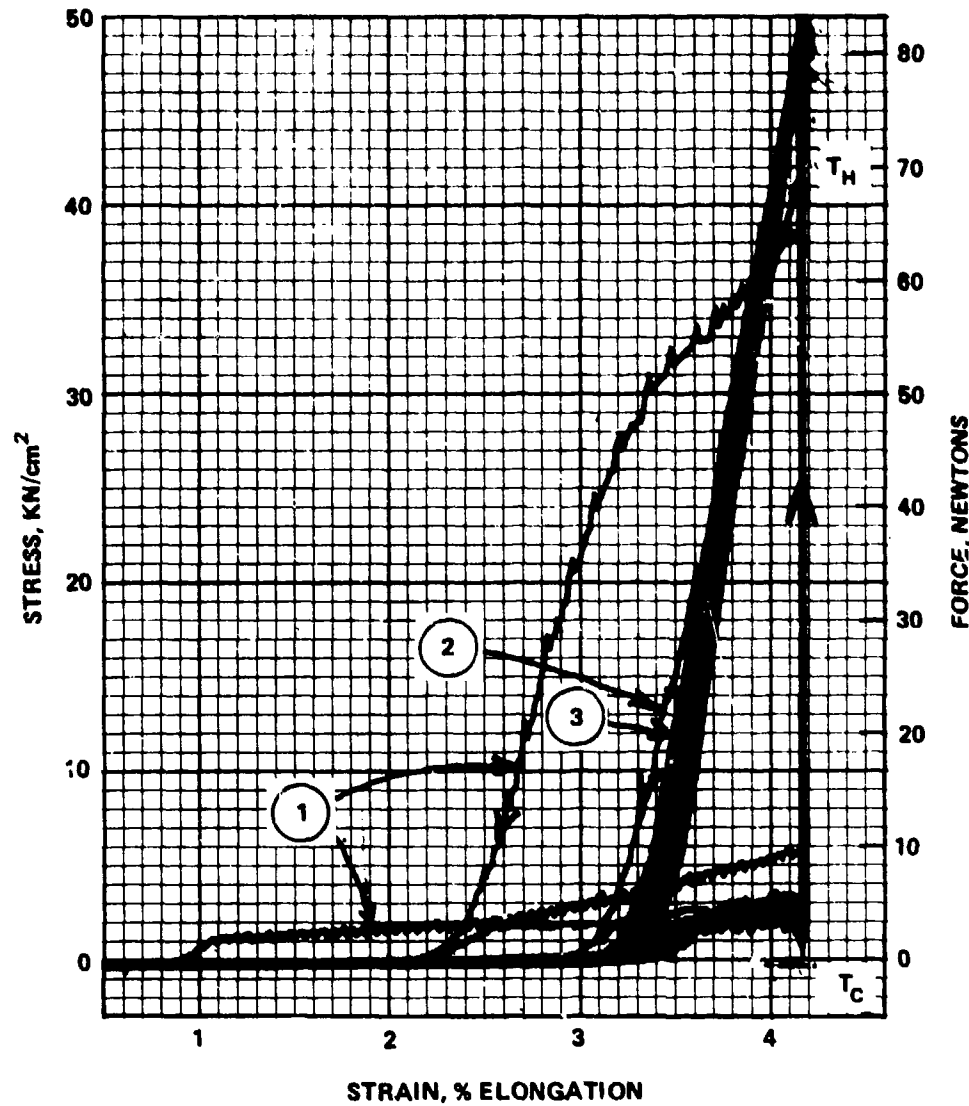
FIGURE 13

RAYMOND — TIMET WIRE 0.018" x 20" LONG (0.7 gm)
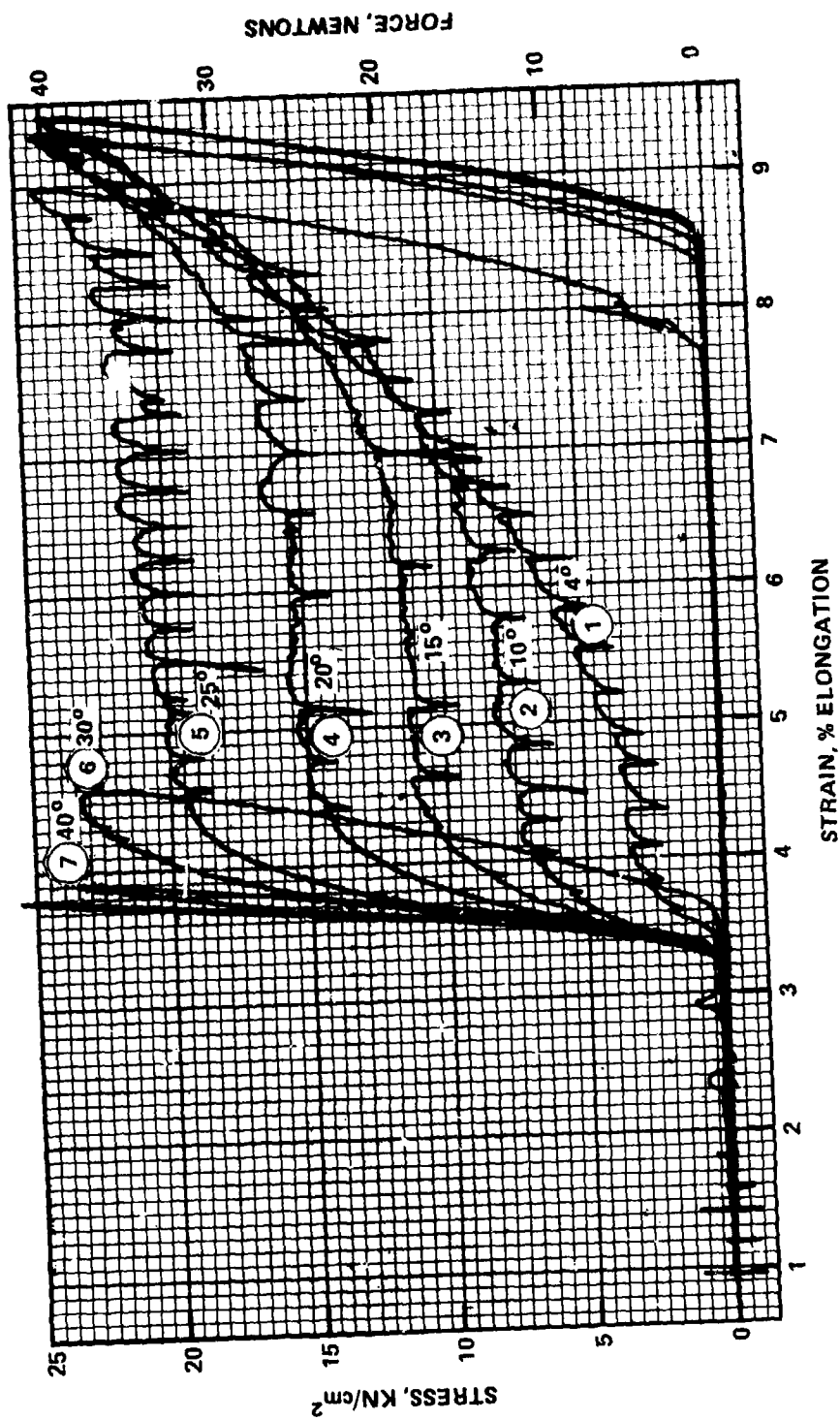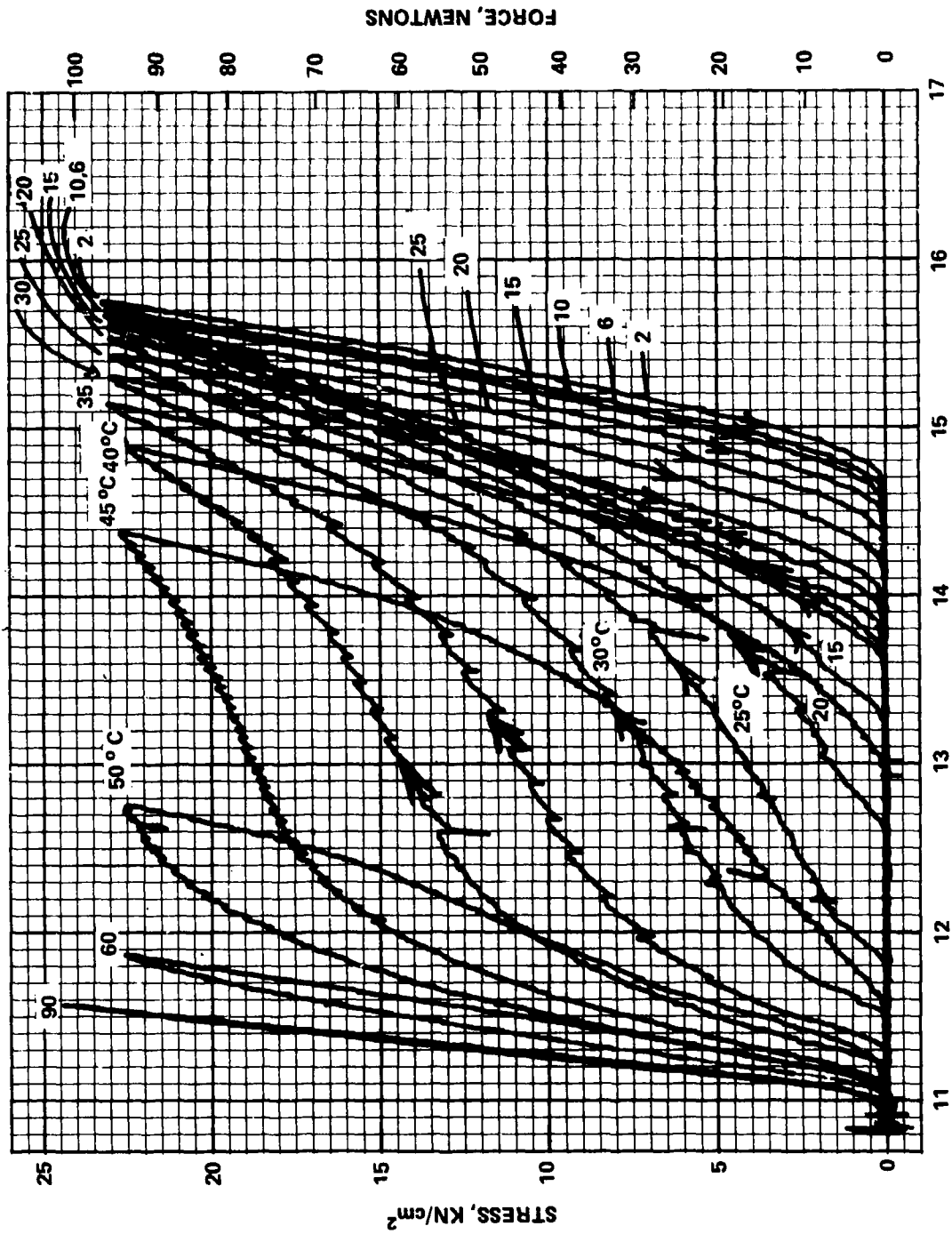AFTER 12 CONSTANT — LENGTH CYCLES
ISOTHERMS: STATE SURFACES

FIGURE 14

NO. 2 TIMET 0.030" WIRE, TRAINED ON ENGINES NO. 10-14 (1974-75)
(SEVERAL HOURS ACCUMULATED RUN TIME)
3% ELONGATION RATIO (1.75 gm)

ISOTHERMS: STATE SURFACES

FIGURE 15

NO. 2 TIMET 0.030" WIRE, TRAINED ON ENGINES NO. 10-14 (1974-75)
(SEVERAL HOURS ACCUMULATED RUN TIME)
3% ELONGATION RATIO (1.75 gm)
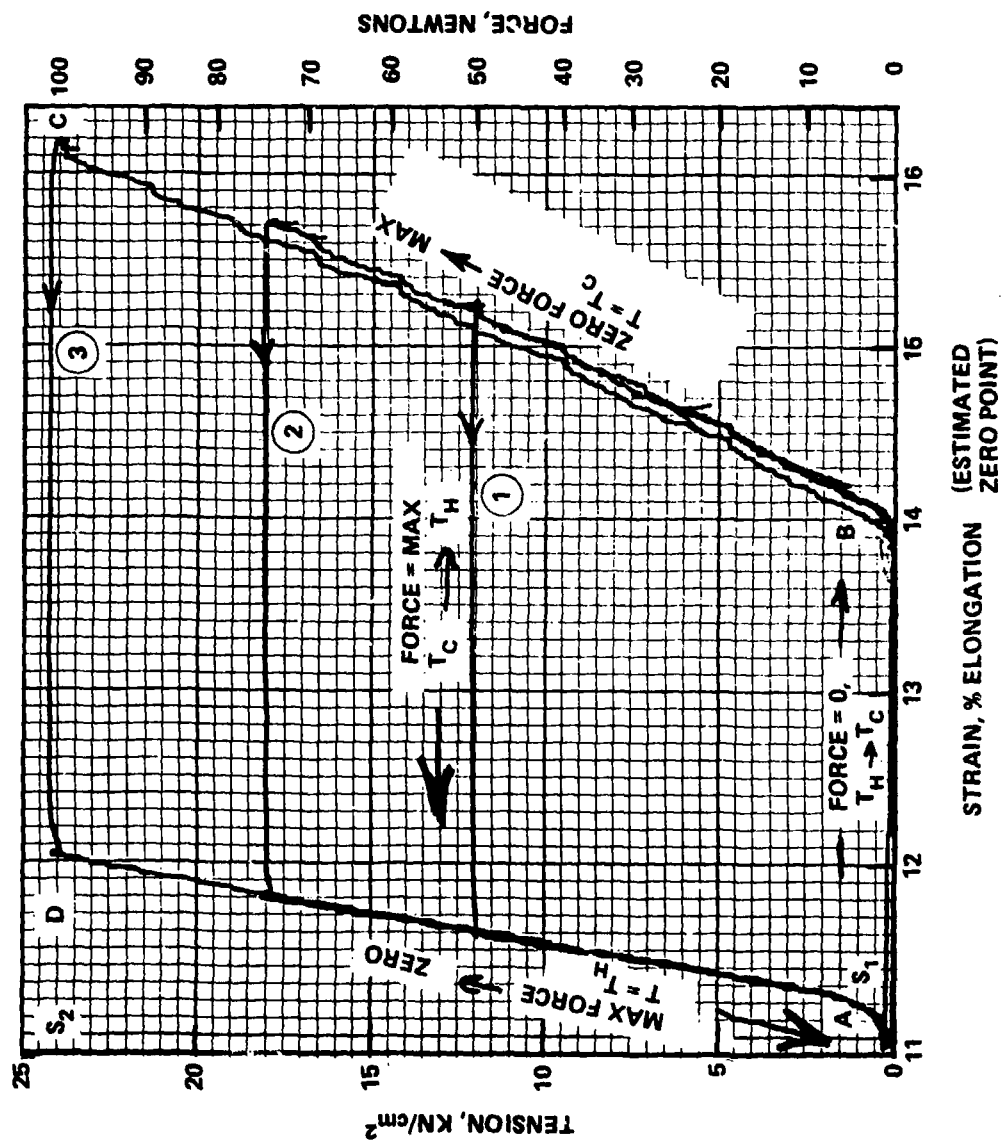3 CONSTANT FORCE CYCLES, T_C < 4° C T_H > 95° C

A – D, B – C
1) NOTE: EXCESS SLOPE DUE, IN
PART, TO FLEXIBLE CABLE
USED TO SUPPORT WEIGHTS
2) AREA ≅ 0.0175 x 100 = 1.75 JOULE
METER   NEWTON

FIGURE 16

NO. 2 TIMET 0.030" WIRE, TRAINED CN ENGINES 10-14 (1974-75)
(SEVERAL HOURS ACCUMULATED RUN TIME)
3% ELONGATION RATIO (1.75 gm)
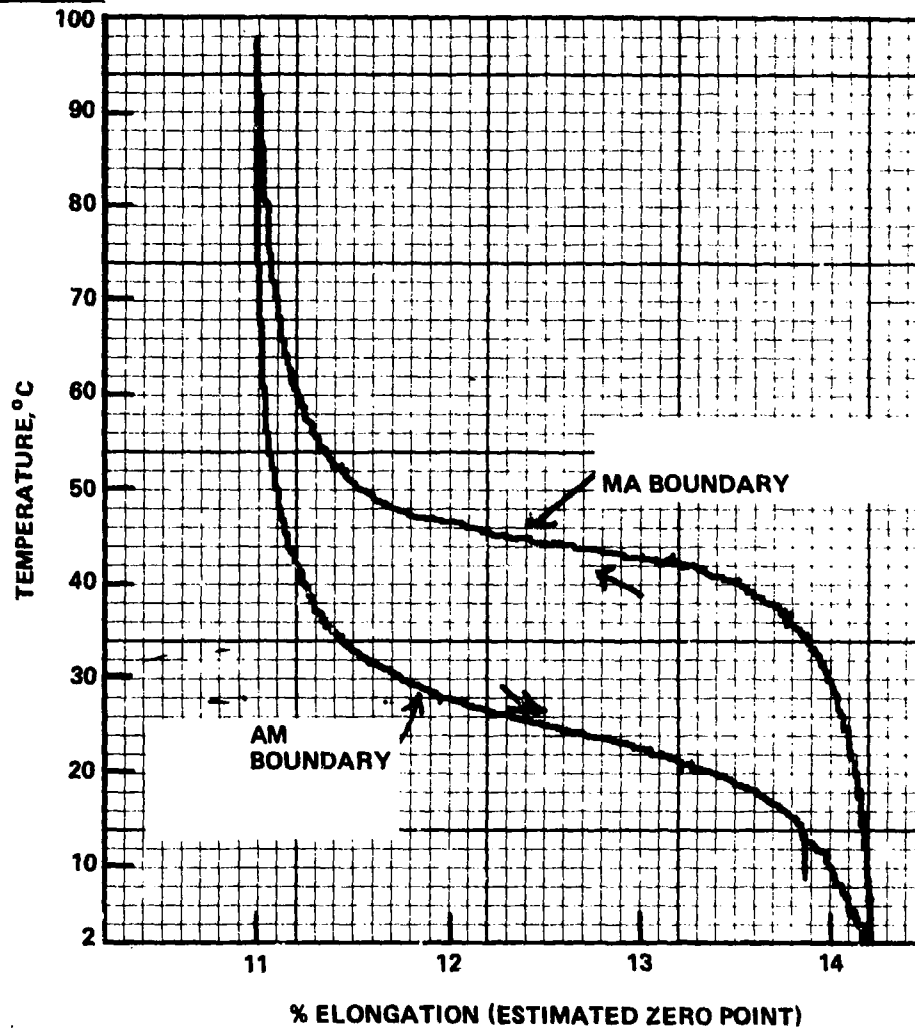LENGTH VS TEMP AT CONST FORCE

FORCE = 20N

FIGURE 17

NO. 2 TIMET 0.030" WIRE, TRAINED ON ENGINES NO. 10-14 (1974-75)
(SEVERAL HOURS ACCUMULATED RUN TIME)
3% ELONGATION RATIO (1.75 gm)
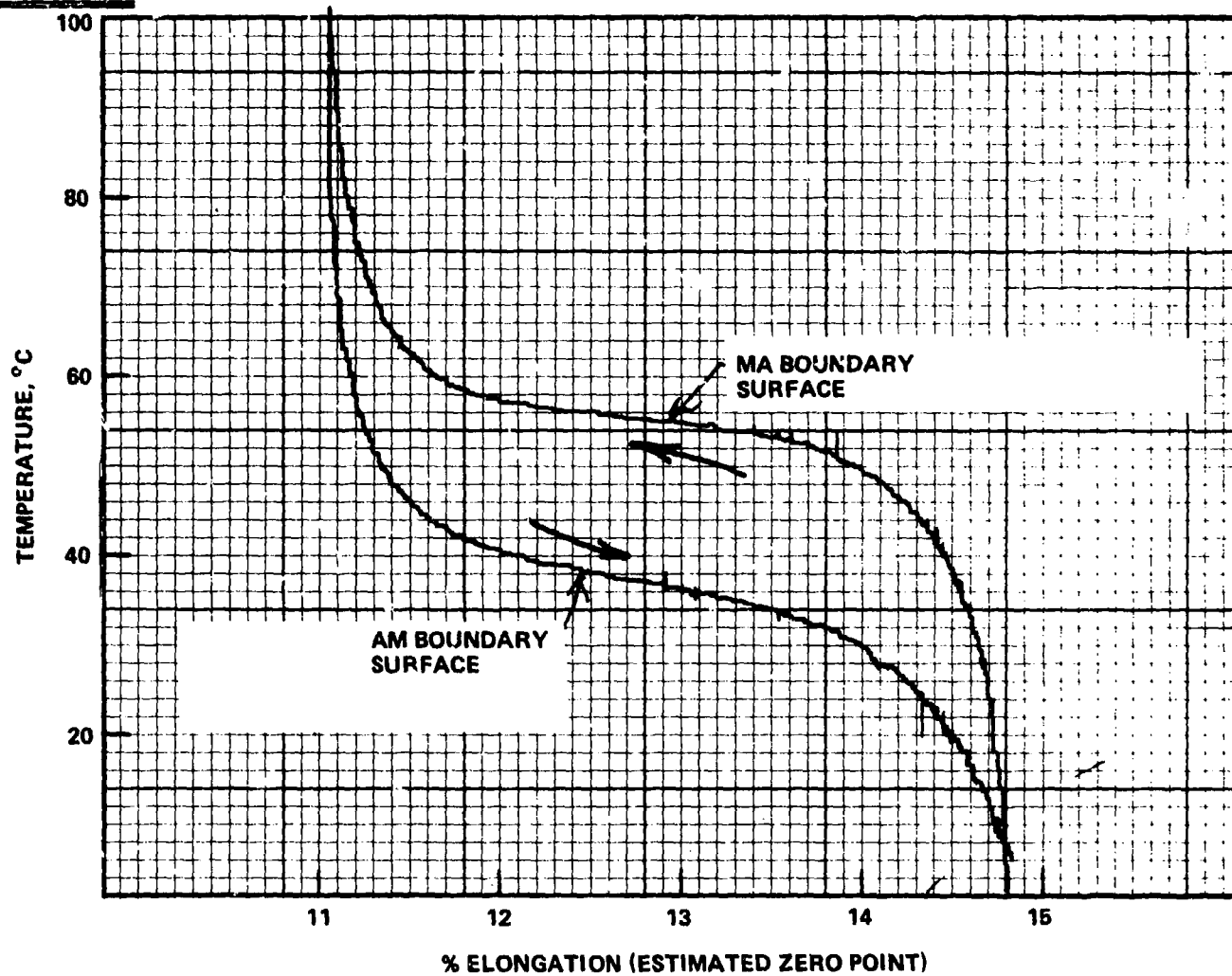LENGTH VS TEMPERATURE AT CONSTANT FORCE

FORCE = 60N

FIGURE 18

RAYMOND — TIMET WIRE 0.018" x 20"
AFTER CYCLING 21 TIMES IN LOW-
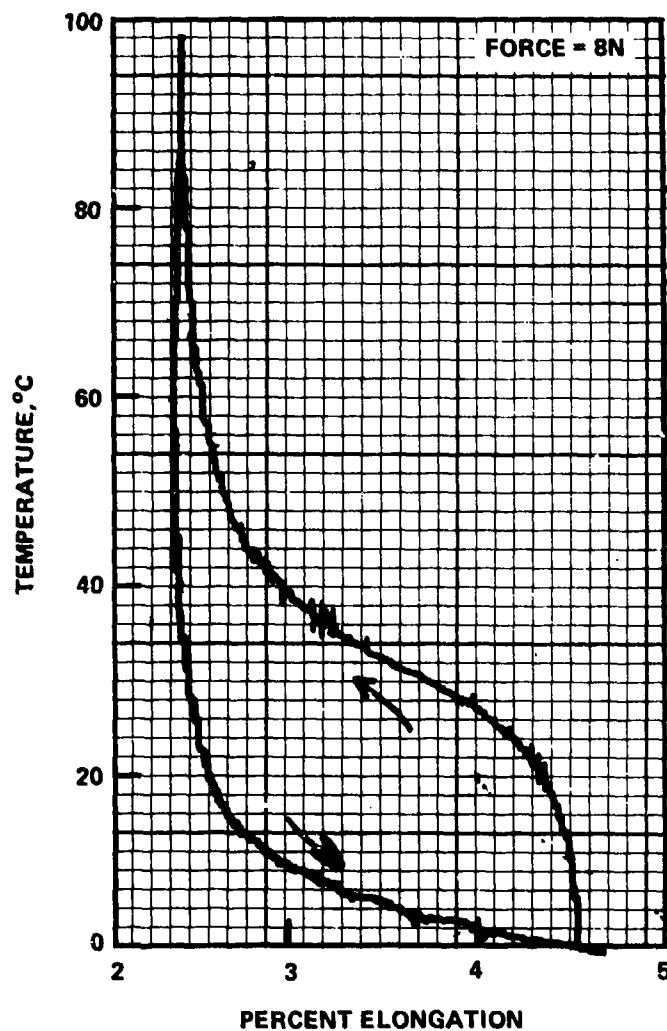HOT-FORCE CYCLE

LENGTH VS TEMPERATURE
AT CONSTANT FORCE

FIGURE 19

RAYMOND — TIMET WIRE 0.018" x 20"
AFTER CYCLING 21 TIMES IN LOW-
HOT-FORCE CYCLE
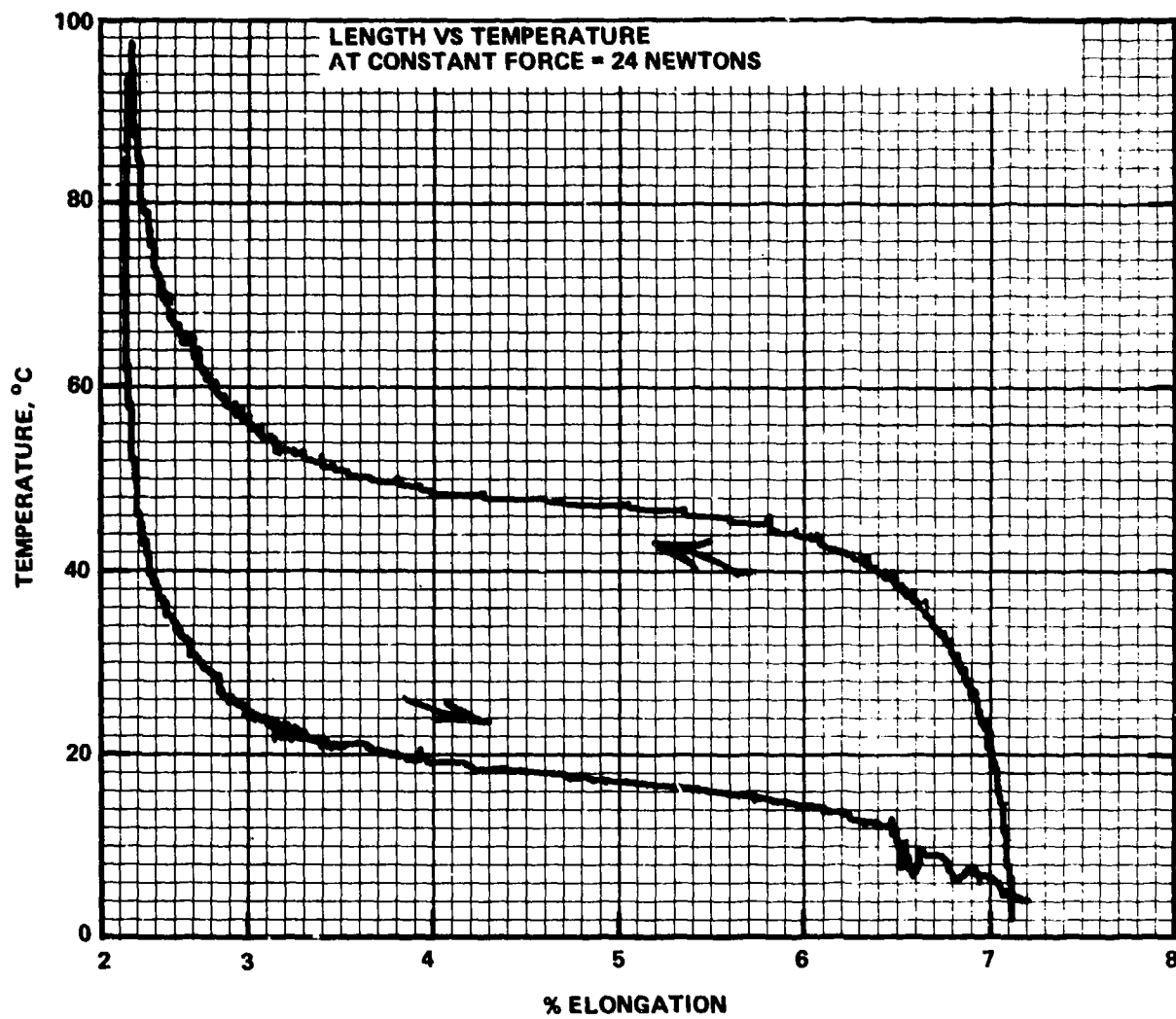

FIGURE 20

BIBLIOGRAPHY

H. P. Hernandez, R. M. Banks, D. Norgren, "NITINOL Test Bed Engine" Lawrence Berkeley Laboratory, Berkeley, CA, (1975).

J. S. Cory, "NITINOL Thermodynamic State Surfaces," Journal of Energy, Vol. II, No. 5, September-October 1978, pp. 257-258. Full report is National Technical Information Service #N78-31206, "Engineering Data and Correlations," Springfield, VA.

REPRESENTATION OF MARTENSITIC TRANSFORMATION IN SHAPE CHANGE SPACE, THE NATURE OF INTERNAL STRESS RETAINED DURING SM TRANSFORMATION, AND OPERATIONAL PERFORMANCE OF A SIMPLE NITINOL ENGINE

K.H.G. Ashbee and B. Cunningham
University of Bristol (England)
H.H. Wills Physics Laboratory

ABSTRACT

Martensitic transformations can be described geometrically in space defined by the principal strains. The condition for coherence between matrix and product phases, and details of microstructures can all be stated in geometrical terms. The case of transformation from cubic to orthorhombic or tetragon crystal structure features in most shape memory transformations and is described in detail. Retention of internal stress during transformation gives rise to features characteristic of shape memory behaviour. The nature of this internal stress, including differentiation between stress associated with elastic and that associated with plastic deformation, has been studied for one shape memory alloy by using Kossel X-ray diffraction in a scanning electron microscope. Operational experience, including measurements of power to weight ratio, is described for a simple NITINOL engine.

1. INTRODUCTION

For all known shape memory (SM) alloys, the transformation is from low crystal symmetry at low temperature to higher crystal symmetry above the transformation temperature range, the low symmetry phase consist of Laves pseudo-twins[1], and application of mechanical constraint at temperatures below the transformation is accommodated by redistribution of the relative proportions of the different twin orientations permitted by the crystal symmetry. After the deformed low temperature phase is heated, transformation to the high symmetry crystal structure first requires reversal of the redistribution of the relative proportions of different twin orientations. Recovery of the original shape, i.e., the shape memory phenomenon, accompanies this reversal. Martensitic transformations are conveniently analysed using the concept of shape change space. To illustrate one application of this concept, the commonly occurring shape memory cases of partial transformation of a cubic crystal to a crystal having orthohombic crystal structure and to a crystal having tetragonal crystal structure are presented here.

Internal stress is believed responsible for the reverse shape memory effect exhibited by some alloys and for the apparent dependence on sign of externally applied stress of changes in transformation temperature. Scanning electron microscopy with in situ Kossel X-ray

---

[1] Laves, F. Acta. Met. 14 (1966) 58.

diffraction offers a direct method for investigating elastic and plastic strain during stress and temperature cycling, and is used here to study a single crystal of Cu - 14.1 wt% Al - 3.0 wt% Ni.

Several inventors have exploited the SM effect to transform low grade heat into useful mechanical work. One of the simplest, built by Frank and Ashbee,[2] consists of an inch of leaf-spring, an inch of NiTi wire, a three-inch rod, another inch of NiTi wire, and another inch of leaf-spring in the same plane as the first and joined in a straight line. This assembly is bent into an S-shape and outer ends of the leaf-springs are fixed into slots in two pieces of metal mounted four inches apart on the axle. The axle rests across a dish of hot water. When either NiTi bend dips into the water, it stiffens and straightens a little. This increases the bend of the other and displaces the centre of gravity of the whole assembly, so that it rocks over and dips the cold NiTi bend into the water in its turn. The assembly rocks at about two strokes per second so long as the water is above the transformation temperature (~60°C). Various versions of this engine have been given a work load and measurements of work done are presented here.

2. TRANSFORMATION OF A SINGLE CRYSTAL BY A HOMOGENEOUS STRAIN

The martensites associated with shape memory are all cube-related martensites. For algebraic simplicity, we confine our attention to these, although the principles presented here are quite general and apply equally well to monoclinic martensites. Since the martensite is cube-related, the axes of the ellipsoid of deformaton are parallel to the crystal axes of the (orthorhombic or tetragonal) product phase.

2.1 THE CONDITION FOR COHERENCY

A sphere in the parent phase transforms to an ellipsoid in the product phase. The lines of intersection between these two figures are two non-planar closed loops (Figure 1). Radii from the origin to the loops represent directions of identical length in parent and product. In the general case no plane through the origin, and intersecting the loops, contains three non-parallel constant length directions. Hence, in general, there can be no plane of coherence between parent and product. To comply with the theorem that a plane of coherence (twinning plane in the case of orientation twins, habit plane in the case of transformation of austenite to martensite) contains three non-parallel constant length directions, it is necessary and sufficient for one principal strain to be zero. The lines of intersection between sphere and ellipsoid are then circles (Figure 2), and define two orientations for the plane of coherence.

In the general case, and in the special case of one principal strain equal to zero, the lines of intersection (non-planar loops and circles, respectively) define the orientations of constant length directions in the ellipsoid. These same constant length directions come from other radii in the sphere.

Rayleigh defined shear (meaning pure shear) as deformation at constant volume and with one principal strain equal to zero. For the sphere to ellipsoid transformation sketched in Figure 3 (a), the "no volume change" condition locates the constant length directions in the sphere; the two discs of radii, angle θ apart in the ellipsoid, were formerly the two discs of radii, angle ϕ apart in the sphere, $\phi = \theta$ and transformation between locations in the sphere and locations in the ellipsoid is by way of "scissors" action (Figure 3(b)), hence the name "shear." The martensite coherency criterion is evidently more general than the criterion for pure shear since $\phi \neq \theta$.

---

[2] Frank, F. C. and Ashbee, K. H. G. Spectrum 132 (1975) 1.

2.2 GEOMETRICAL REPRESENTATION OF MARTENSITIC TRANSFORMATION

This problem is conveniently analysed geometrically by using F.C. Frank's concept of shape change space[3,4], i.e., space defined by the principal strains ϵ_1, ϵ_2, ϵ_3. Consider the general case. The strain tensor can be rotated to the principal axes, giving rise to three principal strains and hence to 3!, i.e. six, different orientations for the shape change. Six points, each representing the state of strain coresponding to one of the six alternatives, define the apeces of a polygon. The polygon has cubic symmetry only if the unit cell diagonals for both parent (austenite) and product of transformation (martensite) are <110> directions.

Consider transformation of the cubic lattice parameters a_1, a_2, a_3 to the ortnohombic lattice parameters a, b, c. If a_1 transforms to a, a_2 can transform to either b or c and a_3 to either c or b. This gives rise to three different orientations for the product phase, i.e. to three different sets of lamellations. On the other hand, a_1 could transform to either b or c and, when the combinations for these alternatives are considered, six different orientations exist.

The principal strains corresponding to the transformation $a_1 \to a$, $a_2 \to b$, $a_3 \to c$ are

$$\epsilon_1 = \frac{a - a_c}{a_c}, \qquad \epsilon_2 = \frac{b - a_c}{a_c}, \qquad \epsilon_3 = \frac{c - a_c}{a_c}$$

where a_c ($=a_1 = a_2 = a_3$) is the lattice parameter of the parent cubic phase. Let these principal strains be denoted A B C after the lower case letters a b c in the respective numerators. The full complement of six sets of principal strains corresponding to the six different orientations is then

ABC, ACB, BCA, BAC, CAB, CBA

In $\epsilon_1 \epsilon_2 \epsilon_3$ - space, the points defined by these co-ordinates occur in pairs on a plane parallel to the (111) plane and are the apeces of a hexagon with trigonal symmetry, the orientation of which depends on whether one or two of the principal strains is positive (Figures 4(a) and (b)). The height of the hexagon above the origin is a measure of the volume change. If there is no volume change (the case of mechanical twinning) the hexagon passes through the origin.

The principal strain, $\epsilon_1 = \dfrac{a - a_c}{a_c} = \dfrac{a}{a_c} - 1$

$$\therefore 1 + \epsilon_1 = \frac{a}{a_c}$$

The corresponding true strain, $\epsilon = \displaystyle\int_{a_c}^{a} \frac{da}{a} = \log_e \frac{(a)}{(a_c)} = \epsilon_1$ since $\log_e (1+x) = x - \ldots$

---

[3] Frank, F. C. Rev. Geophys. 3 (1965) 485.

[4] Cunningham, B. and Ashbee, K. H. G. Acta. Met. 25 (1977) 1315.

The dilation Δ is the sum of the principal strains

$$\Delta = \epsilon_1 + \epsilon_2 + \epsilon_3 = \log_e \frac{(abc)}{(a_c^3)}$$ since the sum of the logarithms is equal to the logarithm of the product. This is the equation to a plane which F. C. Frank calls the Δ-plane. The net strain is defined by a vector $\underline{\epsilon}$ from the origin which just touches the Δ-plane. $\underline{\epsilon}$ completely describes the shape change

$$\underline{\epsilon} = \log_e (1 + \epsilon_1) + \text{Log}_e (1 + \epsilon_2) + \log_e (1 + \epsilon_3)$$

$$= \log_e (1 + \epsilon_1)(1 + \epsilon_2)(1 + \epsilon_3)$$

The volume change associated with the transformation is $\underline{\epsilon} \cdot e$, where $\underline{e}$ is unit vector $(1,1,1,)$.

Perfect shape memory behaviour demands that the transformation be truly elastic. Otherwise, accumulation of emissary dislocations accompanies repeated transformation, and this in turn eventually gives rise to fatigue. Truly elastic transformaton implies coherency between matrix (parent) and product. Although orientation twins of each other, the differently oriented alternatives the product phase are not twin-related to the matrix. However, the fact that by virtue of coherency they bear a special geometrical relationship with the matrix prompted Laves[1] to call them pseudo-twins.

Vectors to the corners of the hexagon in Figure 4 (a), for example, represent shape changes brought about by transformation to a single pseudo-twin. Vectors to points on any line connecting two apeces of the hexagon represent shape changes brought about by a combination of two pseudo-twin orientations, e.g. combinations of ABC and CBA for points on the line between these two corners. These two twins have identical principal strain parallel to the orthorhombic b - axis, i.e. they have the orthorhombic $(10 + 1)$ plane in common as sketched in Figure 5. One principal strain identical is the condition for so-called normal twinning, i.e. coincidence of composition plane and twinning plane. Note also the special points labelled of which there are three sets of four. For each such point, one principal strain equals zero, i.e. coherence exists with the parent. All points other than these special points represent shape changes for which no twin is coherent with the parent. For each principal strain equal to zero, two such special points give rise to the two alternative coherent microstructures sketched in Figure 6.

For some shape memory alloys, the transformation is from cubic to tetragonal. Transformation of the cubic lattice parameters a_1, a_2, a_3 to the tetragonal lattice parameters a_{1t}, a_{2t}, c can be accomplished in only three different ways. The triangle defined by the corresponding three sets of co-ordinates is, for $c > a_{1t} = a_{2t}$, differently oriented with respect to the Δ-triangle from the way it is for $c < a_{1t} = a_{2t}$ (Figure 7). By the same token, there are two cases for the special points (o).

In Figure 4 (a), again, for the two points labelled P one principal strain equals zero. Each may be realised by a combination of any two points labelled x and, since each of the latter is realised by a mixture of two special points (o), it follows that a point P represents a shape change achieved by a mixture of four pseudo-twins. Figure 8 sketches the resulting microstructure. Mixtures of all six pseudo-twins are also possible.

Finally, the origin in Figure 4 (a) represents the cubic parent phase. Points lying within the pyramid formed between the origin and the hexagon represent shape changes that involve mixtures of untransformed and transformed material.

---

[1] See footnote 1 on page 11-1.

3. . <u>NATURE OF THE TRANSFORMATION:</u>

<u>Application of scanning electron microscopy with in situ Kossel X-ray diffraction</u>

If the transformation is reversible, the effect of stress on transformation temperature

$$\frac{\partial T}{\partial \sigma} = \frac{\Delta \epsilon}{\Delta S} \qquad \dots\dots\dots\dots\dots\dots(1)$$

where $\Delta \epsilon$ and ΔS, respectively, are the associated strain and entropy changes. $\frac{\partial T}{\partial \sigma}$ is expected to be independent of sign of the applied stress. The fact that, for at least five alloys, $\frac{\partial T}{\partial \sigma}_{tensile} \neq \frac{\partial T}{\partial \sigma}_{compressive}$ (Table 1 in ref. 4) is cause for concern.

Another unexpected feature is the so-called reverse shape memory effect. Phenomenologically, the shape memory effect is characterised by the existence of a preferred shape above the transformation temperature. However, some alloys exhibit a preferred cold shape as well as a preferred hot shape, giving rise to reverse shape-memory behaviour. The preferred cold shape is attributed to retention of internal strain. If, for some microstructural reason, internal strain complements externally applied stress of one sign, it might also be possible to account for the anomalous difference between the effects on transformation temperature of tension and compression tests.

3.1 ELASTIC AND PLASTIC DEFORMATION DETECTED IN KOSSEL X-RAY DIFFRACTION PATTERNS

The SME in several alloys has been examined using a conventional scanning electron microsope, with situ Kossel X-ray diffraction facilities. The incident electron beam is focused onto the specimen and generates K_α X-radiation characteristic of the alloy. These are Bragg-reflected into a photographic plate positioned for back reflection. Intersection of the X-ray cones with the film results in Kossel lines shown schematically in Figure 9. Precision ball bearings located between the specimen and film cause sharp elliptical shadows to be cast on the film, intersection between the major axes of which defines the film centre after which only simple geometry is needed to determine the specimen-to-film distance.[5] Subsequent measurement of the co-ordinates of the Kossel lines permits lattice spacings to be calculated with an accuracy of 1 in 10^4. A homogeneous elastic strain, such as might be produced by thermal expansion, manifests itself as a change in lattice parameters and is readily detected if greater than 0.1%. Inhomogeneous elastic strain, such as that which would accompany a distribution of dislocations, amounts to the presence of local variations in lattice parameters anc causes broadening of Kossel lines.

Stress-induced martensitic transformation has been studied in a scanning electron microscope using a disc-shaped single crystal of Cu - 14.1 wt %, Al - 3.0 wt% Ni (character-istic temperatures $M_S \sim 3^oC$, $M_F \sim -11^oC$, $A_S \sim 15^oC$, $A_F \sim 20^oC$) stressed in situ by axially loading whilst supported at its rim. The sequence of Kossel photographs in Figure 10 shows the effect on the Kossel pattern of increasing the applied load. The numbers quoted for axial

---

[5]Biggin, S. and Dingley, D. J. <u>J. Appl. Cryst. 10</u> (1977) 376.

[4]See footnote 4 on page 11-3.

stress and strain corresponding to the known values of axial load were calculated using A.E.H. Love's formula[6] for deformation of an indented plate, and are strictly applicable only while the alloy is undergoing Hookean elastic deformation. When non-linearity (pseudoelasticity) sets in, the numbers are only a guide to the magnitudes of axial stress and strain. The sequence of five Kossel patterns clearly demonstrates the progressive break-up of a triple intersection between two $(110)_{Cu}$ and one $(200)_{Cu}$ diffraction lines. At 2% axial strain, the point of triple intersection has changed to three points of intersection. At 3% axial strain, the individual lines have obviously broadened. They disappear completely at 4% axial strain, and reappear as diffuse lines (not of cubic phase but of the product of transformation) at 6% strain. This sequence is interpreted as direct evidence of lowering of the crystal symmetry whilst accommodating elastic deformation in the range 02% axial strain, followed by generation of emissary dislocations the presence of which gives rise to the line broadening and subsequent masking of Bragg diffraction, and then partial recovery of low dislocation density crystal at the time of transformation. Figure 11 (a) and 11 (b) show scanning electron micrographs of the surface before and stressinduced martensitic transformation. When the stress is released (Figure 12), the crystal does not exactly revert to the original microstructure. Figure 13 is a Kossel pattern taken from the cubic phase after removing the stress. Some line broadening and therefore residual plastic strain is present. This residual strain is believed to be the origin of the reverse shape memory.

4. THE FRANK-ASHBEE ENGINE

Frank and Ashbee[2] demonstrated that the shape memory effect can be used to displace a rigid beam which, under the action of gravity, causes a useful mechanical displacement. That is reversed either as the result of a pendulum action in the case of a single element engine or as the consequence of an opposite displacement in the case of a two element engine. If an analogy can be drawn between this engine and the beam engine of Newcomen, efficiencies of about 2% are expected.

Several different variations of the basic rocking engine have been built. One incorporates a valve-less water pump and this has pumped 1.8 kg water per hour through a height of 5 cm, i.e. it does 0.88 joules of useful work per hour. The two strips of NITINOL working element in this engine weigh a total of 0.318 gm, so the power to weight ratio is 0.8 watts per kg. By mounting in bearings the common axle of a group of four basic engines, a rotary version has been developed which, when coupled to a generator, delivers sufficient electricity to barely illuminate a light emitting diode rated at 50 mA, 1.5V. The NITINOL elements of this engine weigh 13.51 gm and the power to weight ratio is a little under 9 watts per kg.

4.1 EFFICIENCIES

It is difficult to quote efficiencies. The Carnot efficiency is

$$\eta = \frac{A_f(\sigma) - M_f(\sigma \to o)}{A_f(\sigma)}$$

---

[6] Love, A. F. H. "The Mathematical Theory of Elasticity" 4th ed. Cambridge University Press (1959) 475.

[2] See footnote 2 on page 11-2.

where A_f and M_f, respectively, denote the temperatures for finish of transformation to the high temperature phase (austenite) and to the low temperature phase (martensite).

$$A_f (\sigma) = A_f (\sigma = 0) + \sigma \frac{dA_f}{d\sigma}$$

and re-writing Equation[1] using this new notation shows

$$\frac{dA_f}{d\sigma} = \frac{\Delta \varepsilon}{\Delta S}$$

$\Delta \varepsilon$ and ΔS are both measurable quantities. However, there exist the possibility of precursory effects and hence the possibility of smearing of experimental measurements. There is no possibility of precursory effects on $\Delta \varepsilon$ in the cubic phase. However, in say an orthohombic product phase, a range is possible of orthorhombic axial ratio, as might arise in a polygranular material from differently oriented crystals being differently stressed. Figure 14 sketches the anticipated axial ratio versus temperature relationship. ΔS precursories are possible in both phases.

In the absence of reliable $\Delta \varepsilon$ and ΔS data, it is necessary to resort to experimental measurement of the slopes of transformation temperature versus stress relationships. This has been done for several shape memory alloys and, taking cognizance of the fact that there is a maximum useful value of σ beyond which perfect shape memory behaviour is destroyed, Carnot efficiencies approaching 20% are predicted.[4]

The efficiency realized in practice is also difficult to measure. This is because the heat input is not known with any accuracy. The specific-heat anomaly associated with the transformation suffers from the same precursory effects described above for the entropy change. Superimposed on this, there appears to be a latent heat of transformation, i.e. shape memory behaviour appears to involve a combination of first and second order transformations.[7] Delaey[8] and co-workers claim to have reproducibly measured the thermodynamic parameters involved in the transformation of Cu - based alloys and find that the useful efficiency is about 3%.

4.2 OPERATIONAL CHARACTERISTICS

Since the axis of rotation is above the water level (hot source), the working elements spend more than half of the period (T) of oscillation (or rotation) cooling down. Forced cooling, by blowing cold air across the cooling elements, markedly reduces T. The use of oil

---

[4] See footnote 4 on page 11-3.

[7] Cunningham, B. Ph.D. Thesis. Univ. of Bristol (1979)

[8] loc. cit.

instead of water as the heat source increases T, presumably because evaporation no longer assists the cooling. Small increase in section of the working elements has little effect on T or, for that matter, on the output energy. All of these observations point to the importance of heat transfer.

The heating time (t) for a cross-section of wire is

$$t - \frac{r^2}{\alpha}$$

where r = radius of wire and α = thermal diffuscivity. α is given by:

$$\alpha = \frac{k}{\rho c}$$

where k = thermal inductivity, ρ = density and c = specific heat capacity. Inserting published values of the above parameters gives a heating time of ~½ second for NITINOL wire of 1 mm radius. One engine, a reciprocating version of the Frank-Ashbee engine, has been studied with slow motion replays of cine films taken whilst working under various operating conditions. A sequence of eight stills is reproduced in Figure 15, from which it is evident that a time lag of ~½ second exists between entry into the water bath and transformation of the heated element. Since t is proportional to r^2, consideration of heat transfer is evidently important when scaling up.

If the temperature of the water is above A_f (σ_{max}), the energy input will include heat absorbed by the high temperature (parent) phase over and above that absorbed by untransformed parent. It has not been possible to estimate either of these quantities.

Development of working models of the Frank-Ashbee engine has revealed the very large advantage of using roller bearings in preference to fixed bearings. It has also proved to be worth exploiting the fact that the basic engine rocks at its natural frequency.
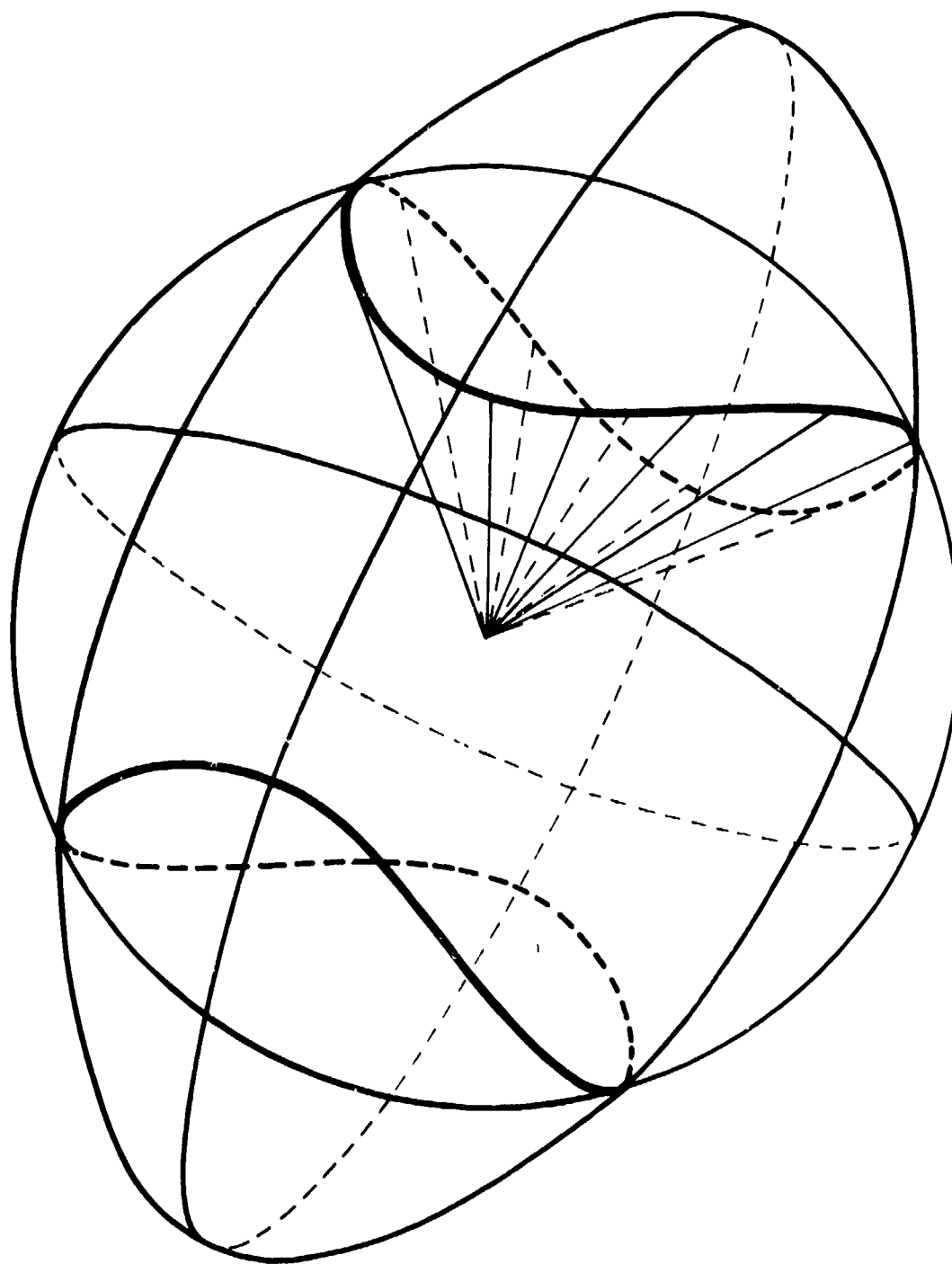
FIGURE 1   ILLUSTRATING THE GENERAL CASE OF NON-PLANAR LOOPS OF INTERSECTION
BETWEEN A SPHERE IN THE PARENT PHASE AND THE ELLIPSOID TO WHICH IT
TRANSFORMS IN THE MARTENSITE PHASE
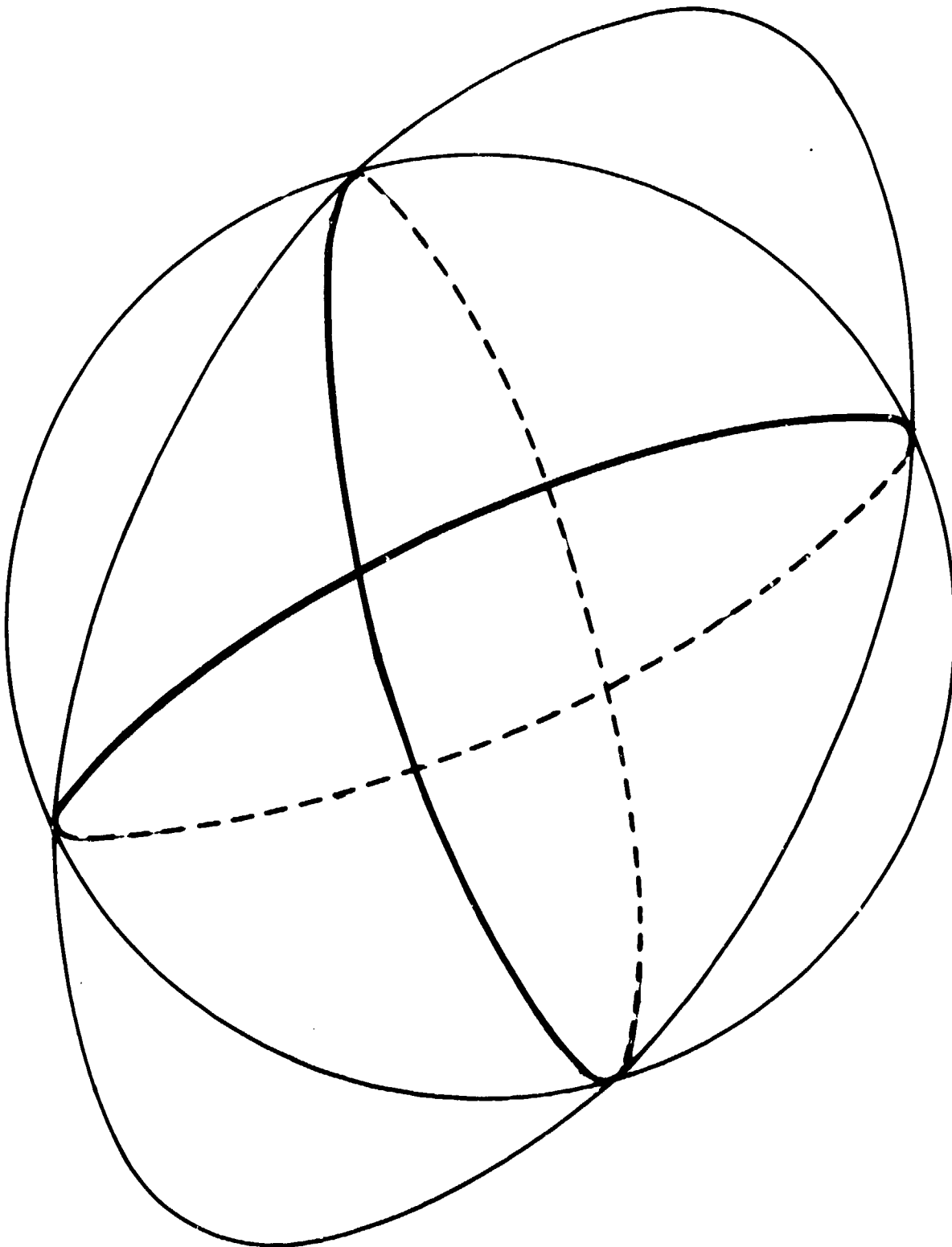
FIGURE 2   THE SPECIAL CASE OF FIGURE 1 CORRESPONDING TO ONE OF THE PRINCIPAL
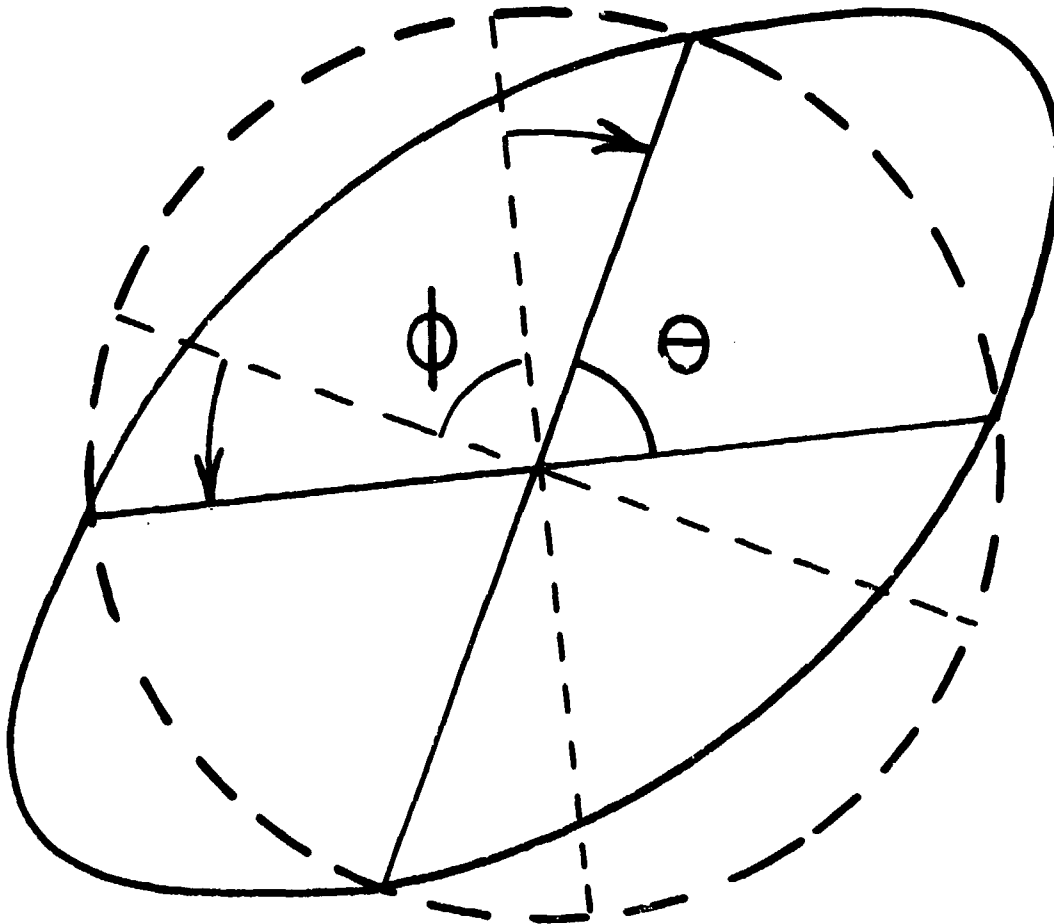STRAINS EQUALS ZERO
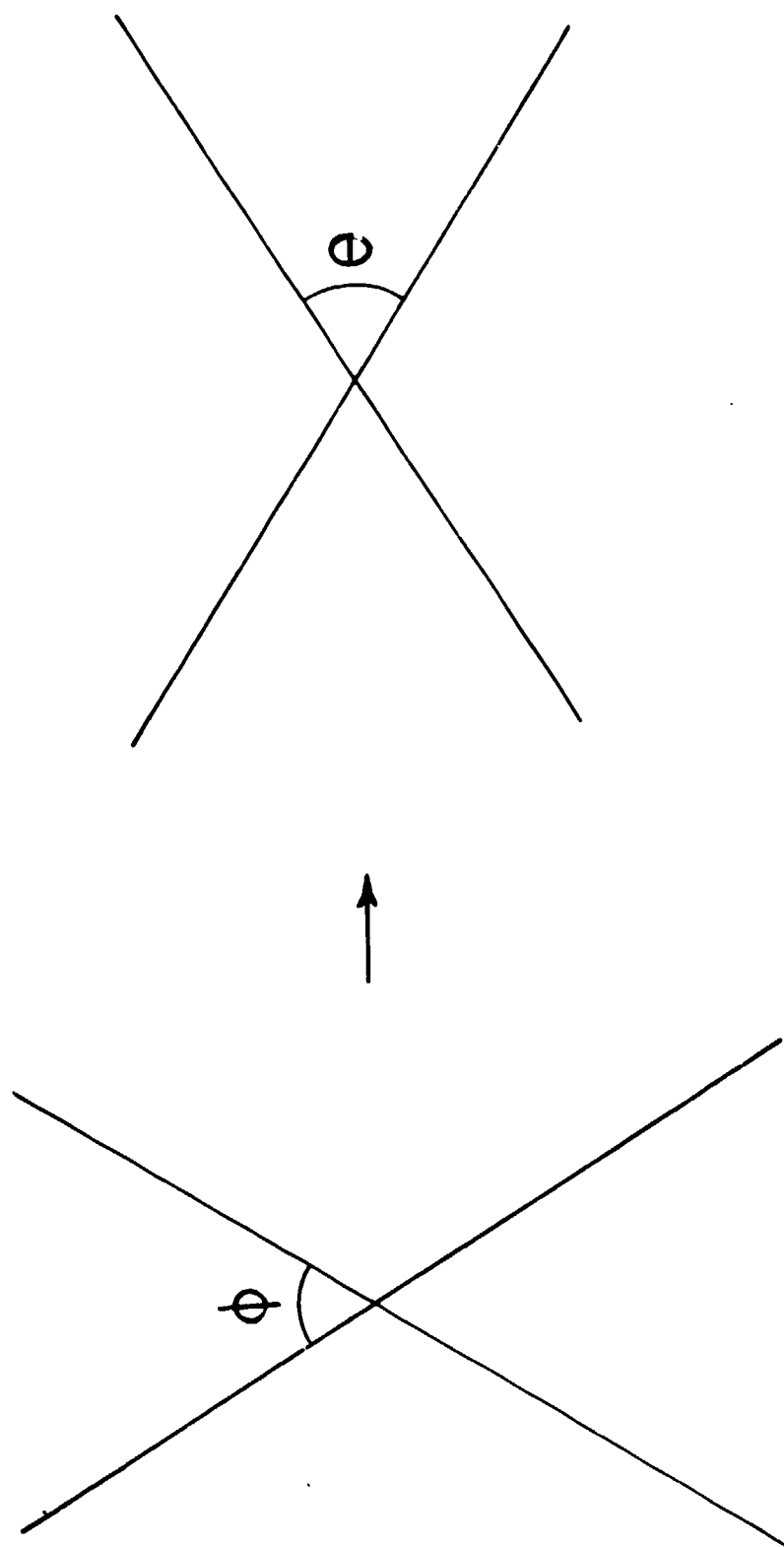
FIGURE 3 (A)   SPHERE TO ELLIPSOID TRANSFORMATION
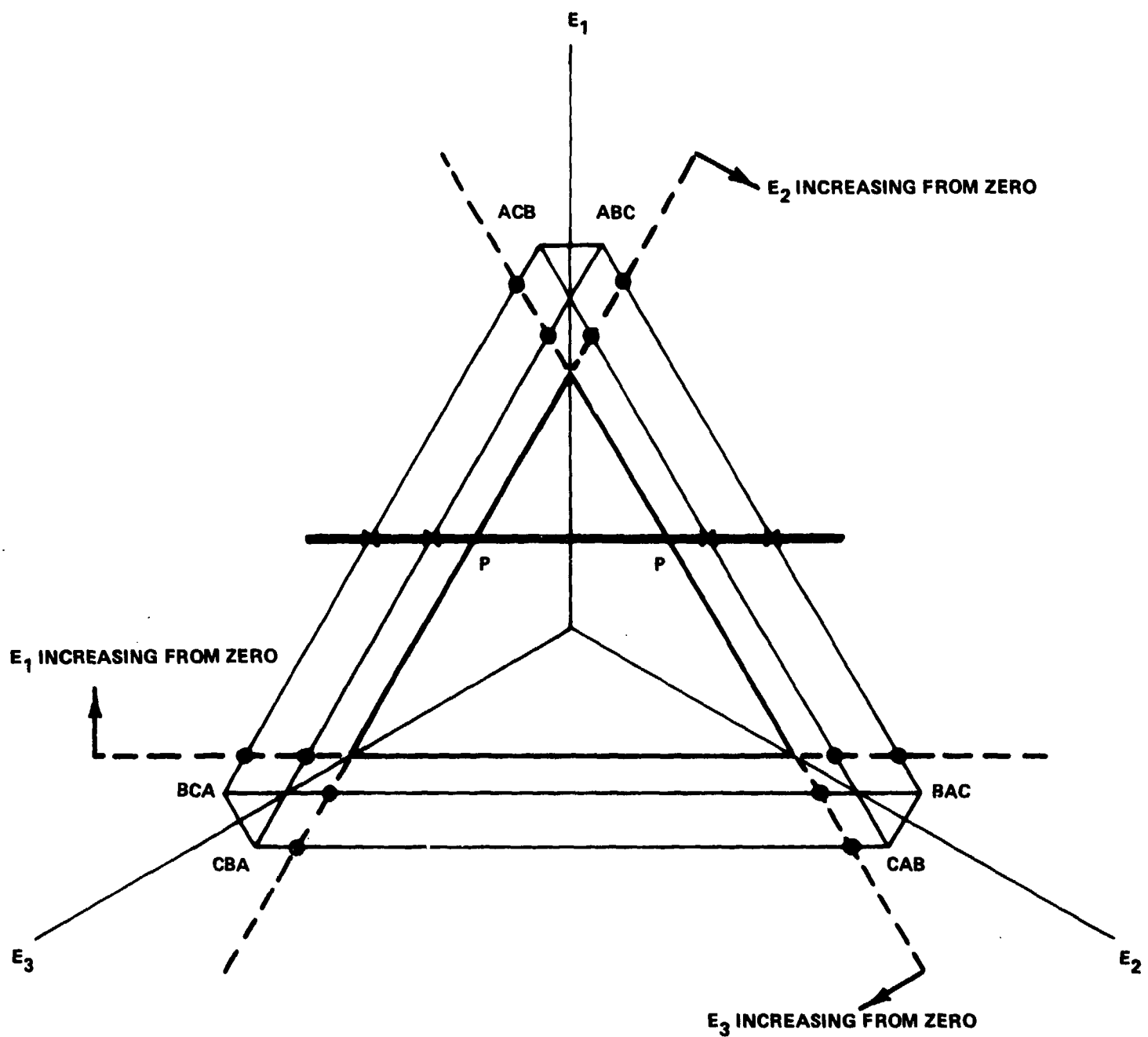
FIGURE 3(B) PURE SHEAR DEFORMATION

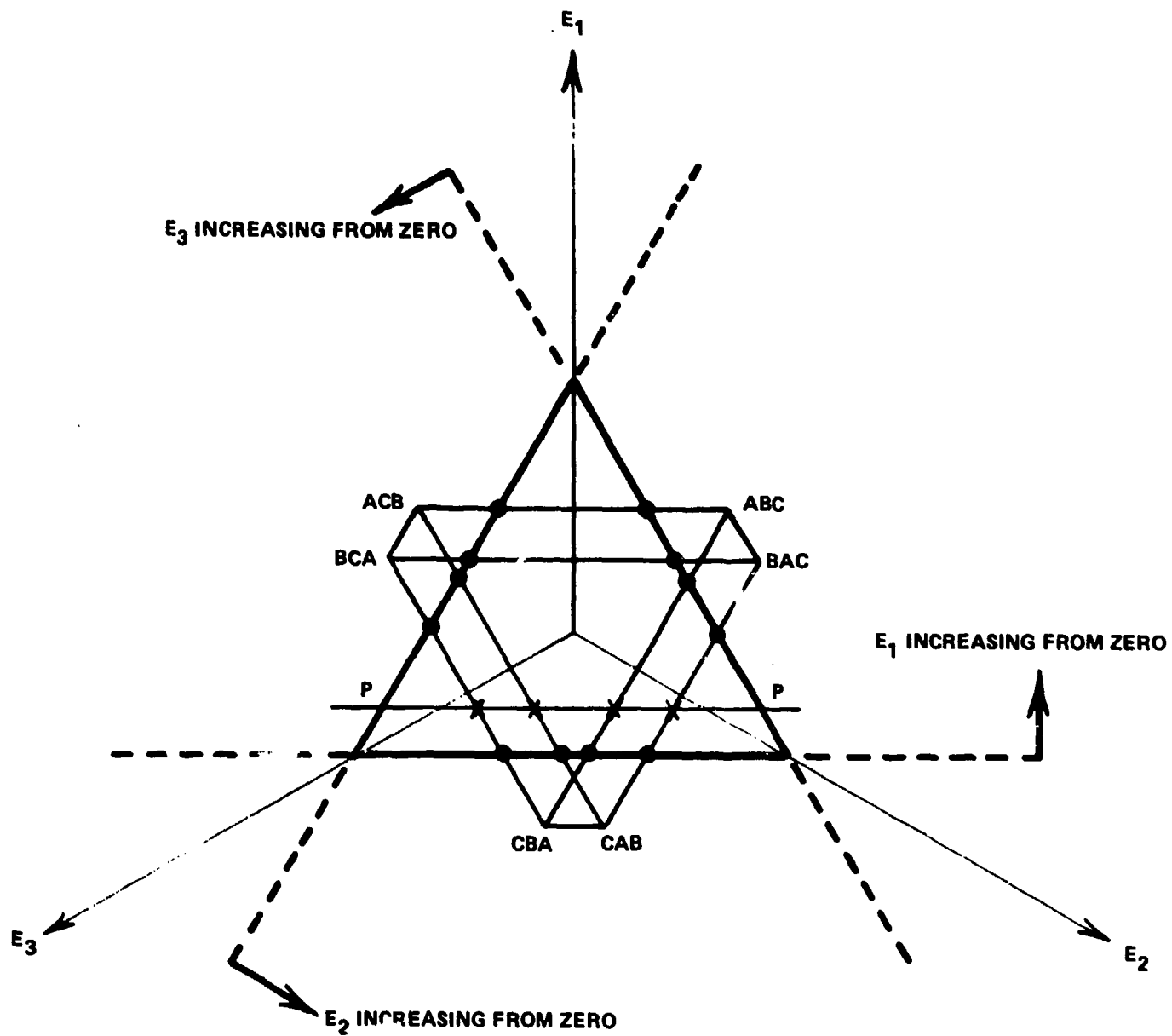FIGURE 4   SHAPE CHANGE SPACE REPRESENTATION OF MARTENSITIC TRANSFORMATION BETWEEN CUBIC AND ORTHORHOMBIC STRUCTURES (A) FOR ONE PRINCIPAL STRAIN POSITIVE

FIGURE 4   SHAPE CHANGE   .E REPRESENTATION OF MARTENSITIC TRANSFORMATION BETWEEN CUBIC AND ORTHORHOMBIC STRUCTURES (B) FOR TWO PRINCIPAL STRAIN POSITIVE
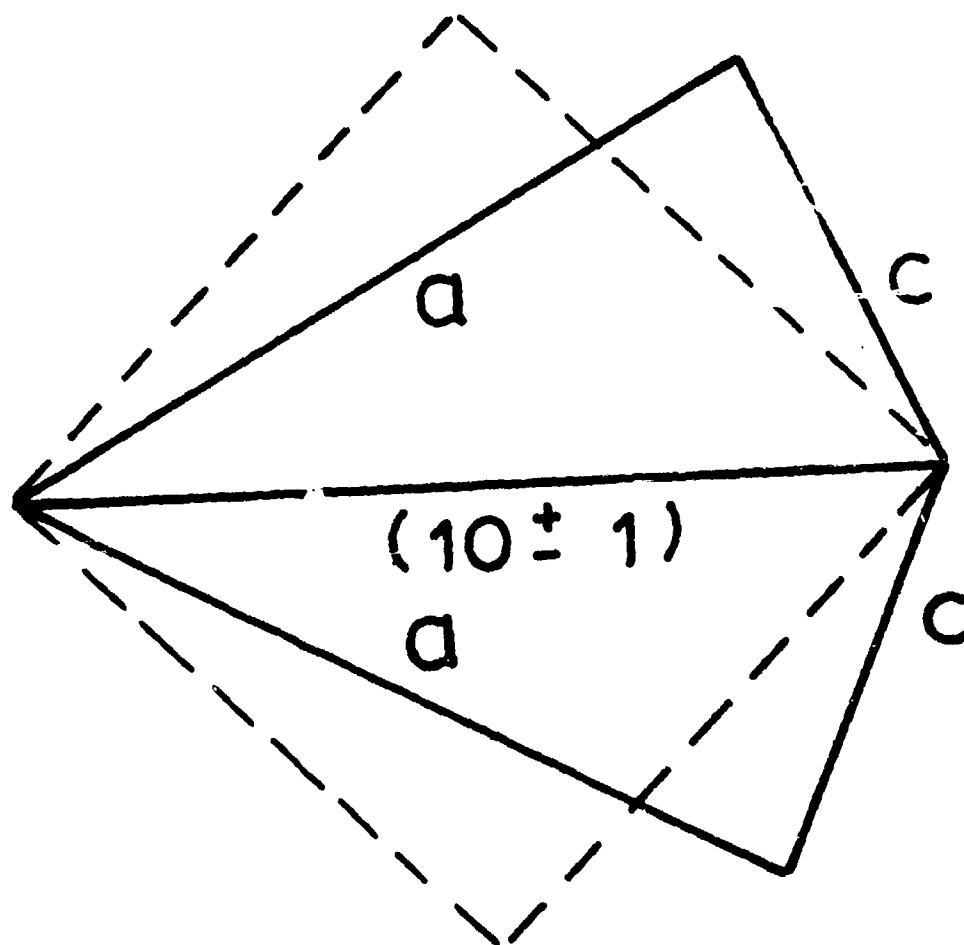
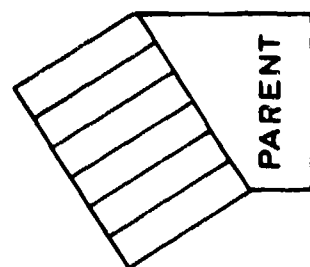FIGURE 5   SCHEMATIC REPRESENTATION OF TWO TWINS HAVING THE ORTHORHOMBIC (10 ± 1)
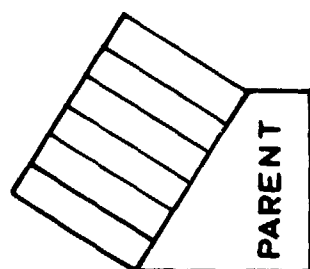PLANE IN COMMON

FIGURE 6   COHERENT MICROSTRUCTURES FOR THE PRINCIPAL STRAIN PERPENDICULAR TO THE PAPER EQUAL TO ZERO
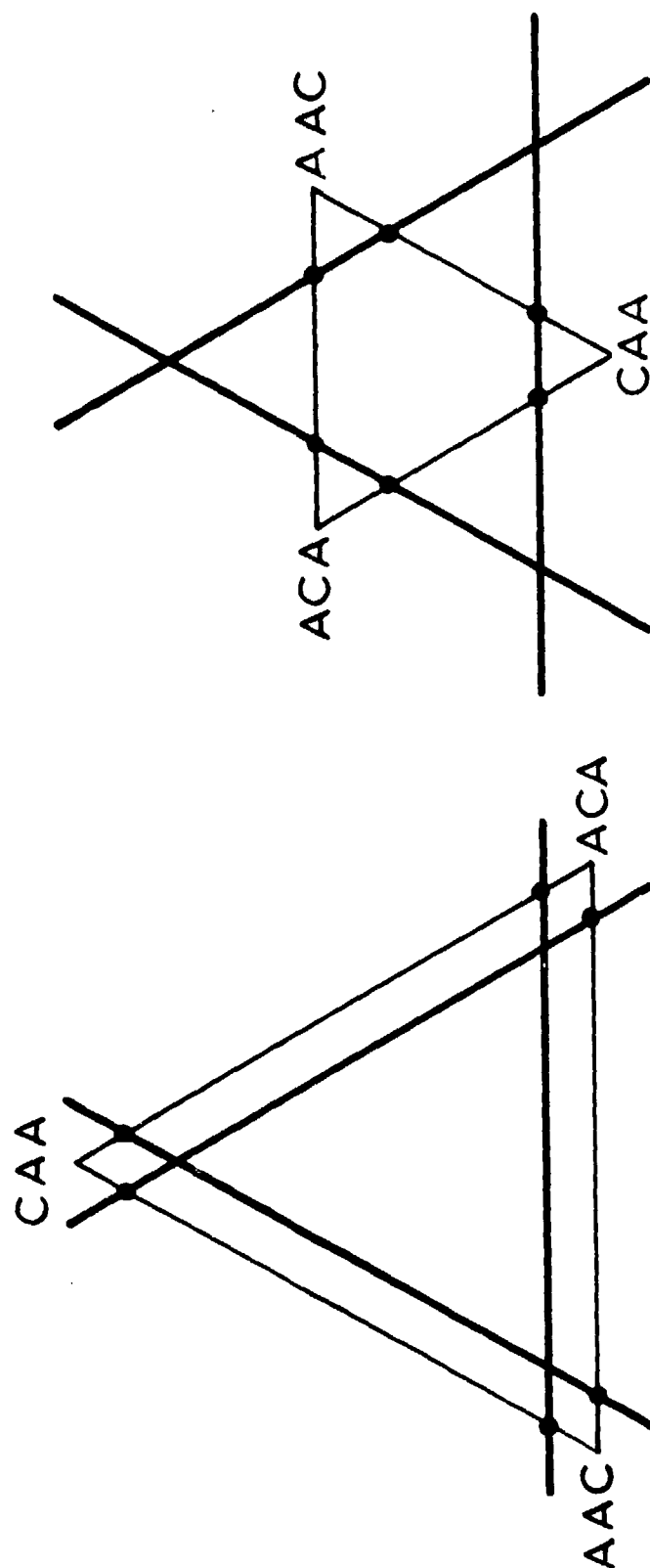
FIGURE 7   SHAPE CHANGE SPACE REPRESENTATION OF MARTENSITIC TRANSFORMATION BETWEEN CUBIC AND TETRAGONAL STRUCTURES FOR (A) $c > a_{1t} = a_{2t}$ (B) $c < a_{1t} = a_{2t}$
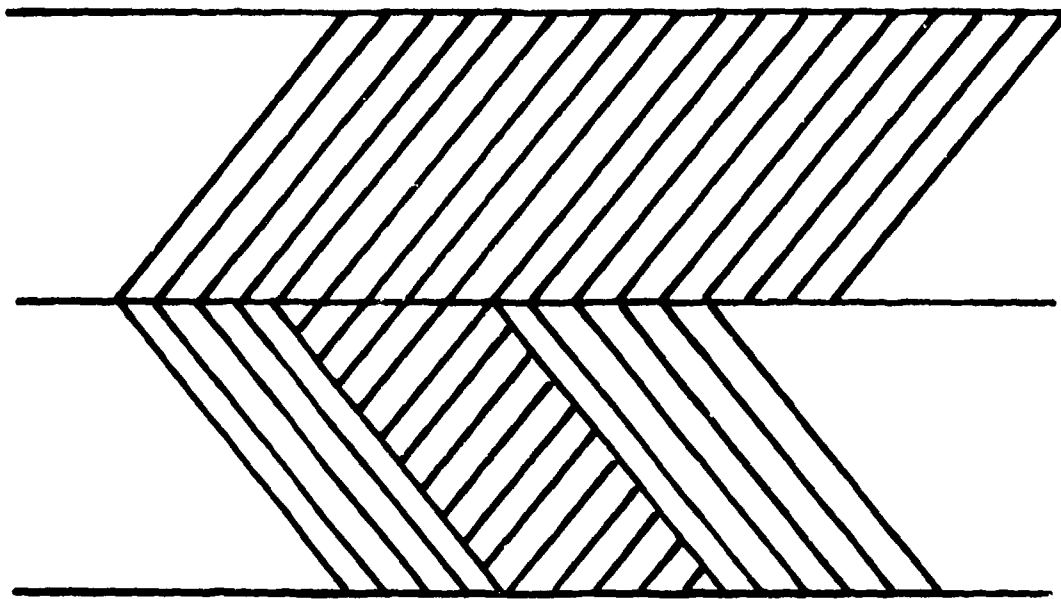
FIGURE 8   MICROSTRUCTURE RESULTING FROM A MIXTURE OF FOUR PSEUDO-TWINS

ELECTRON BEAM

RECORDING FILM

EXCESS CONE

SPECIMEN

DEFICIENCY CONE
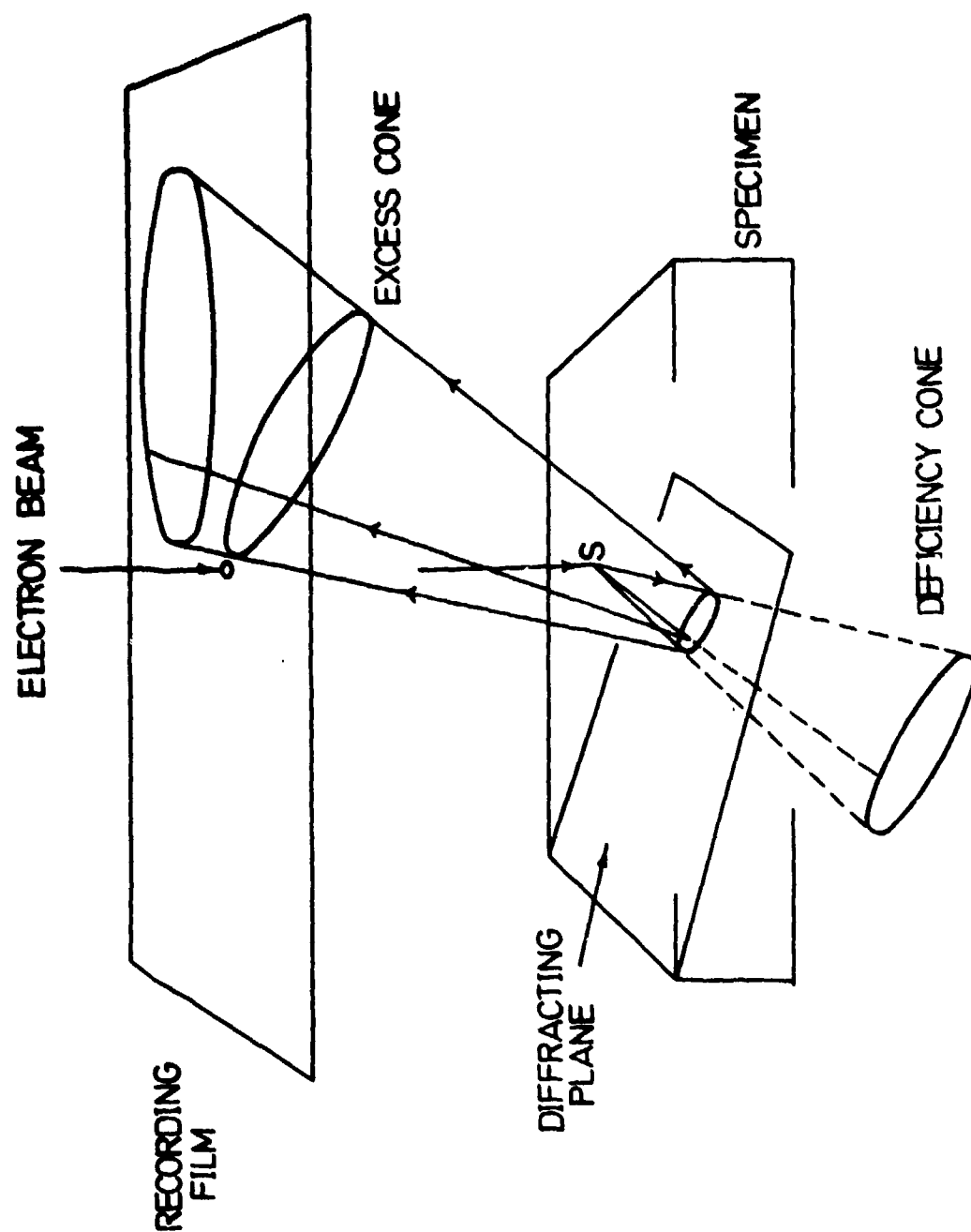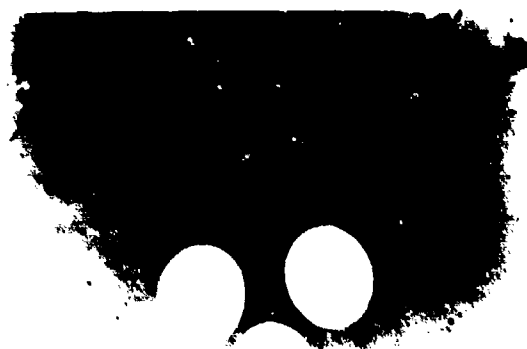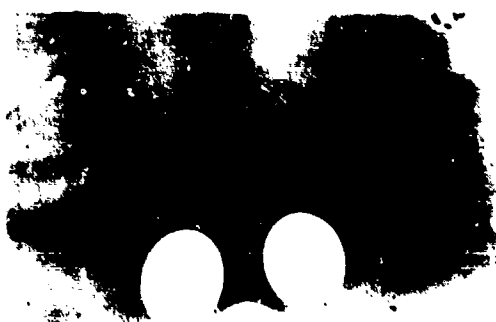
DIFFRACTING PLANE

O

S

FIGURE 9   REPRESENTATION OF GEOMETRICAL FORMATION OF KOSSEL CONICS IN BACK REFLECTION AND TRANSMISSION CASES
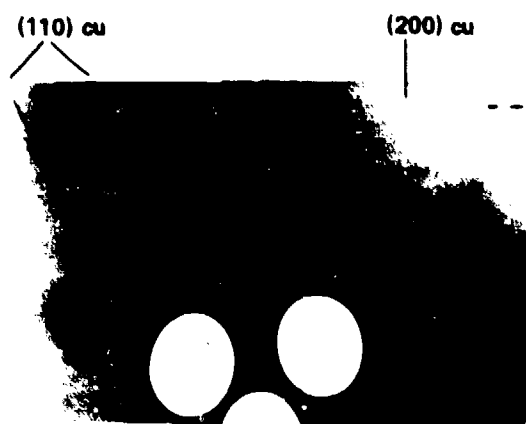
FIGURE 10   SEQUENCE OF KOSSEL PATTERNS SHOWING EFFECTS OF INCREASING STRESS

50μ

FIGURE 11   SCANNING ELECTRON MICROGRAPHS OF A Cu - 14.1 wt% A1 - 3.0 wt% Ni ALLOY
(A) BEFORE STRESS-INDUCED MARTENSITIC TRANSFORMATION

50μ

**FIGURE 11   SCANNING ELECTRON MICROGRAPHS OF A Cu - 14.1 wt% A1 - 3.0 wt% Ni ALLOY
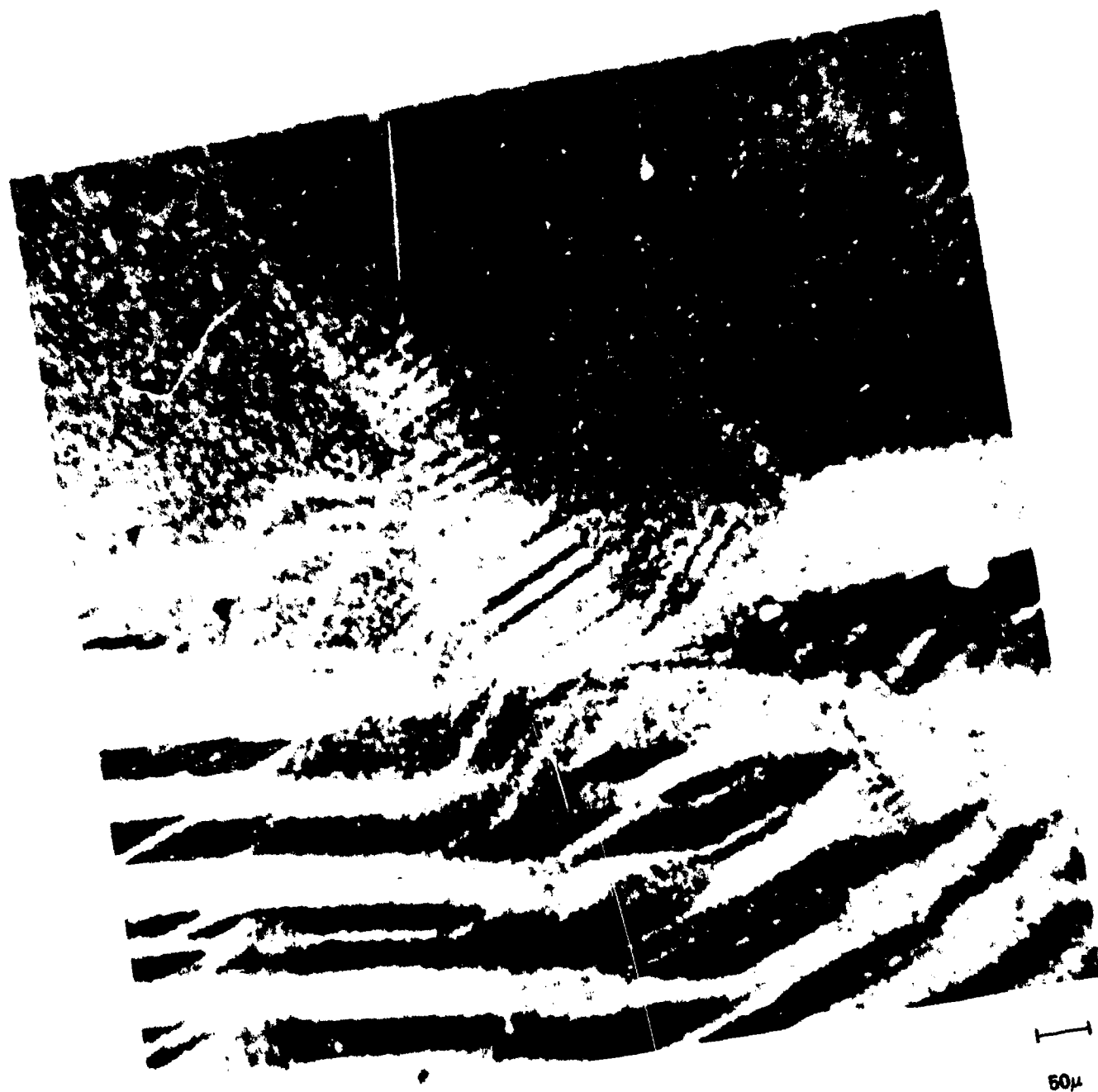(B) AFTER STRESS-INDUCED MARTENSITIC TRANSFORMATION**

50μ

FIGURE 12   SCANNING ELECTRON MICROGRAPH OF A Cu 14.1 wt% A1 - 3.0 wt% Ni AFTER RELEASING THE STRESS
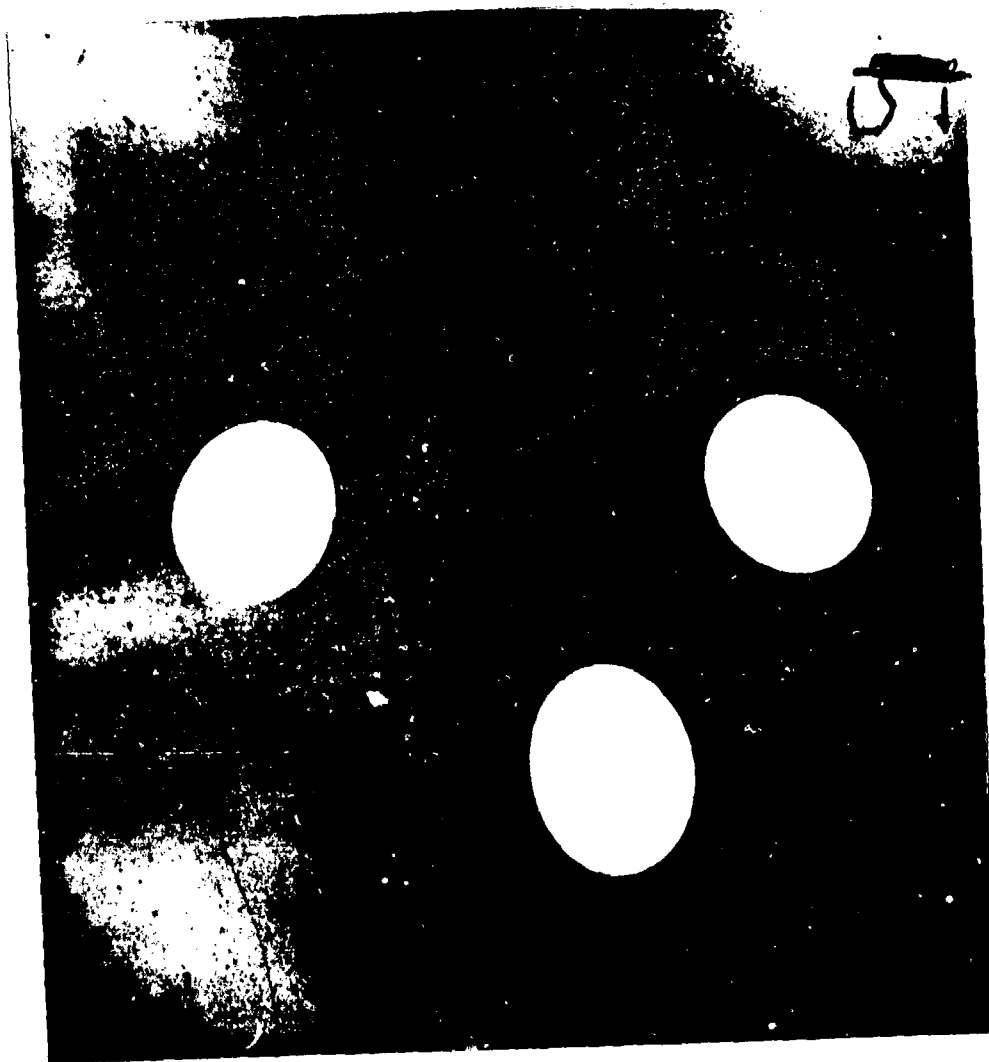
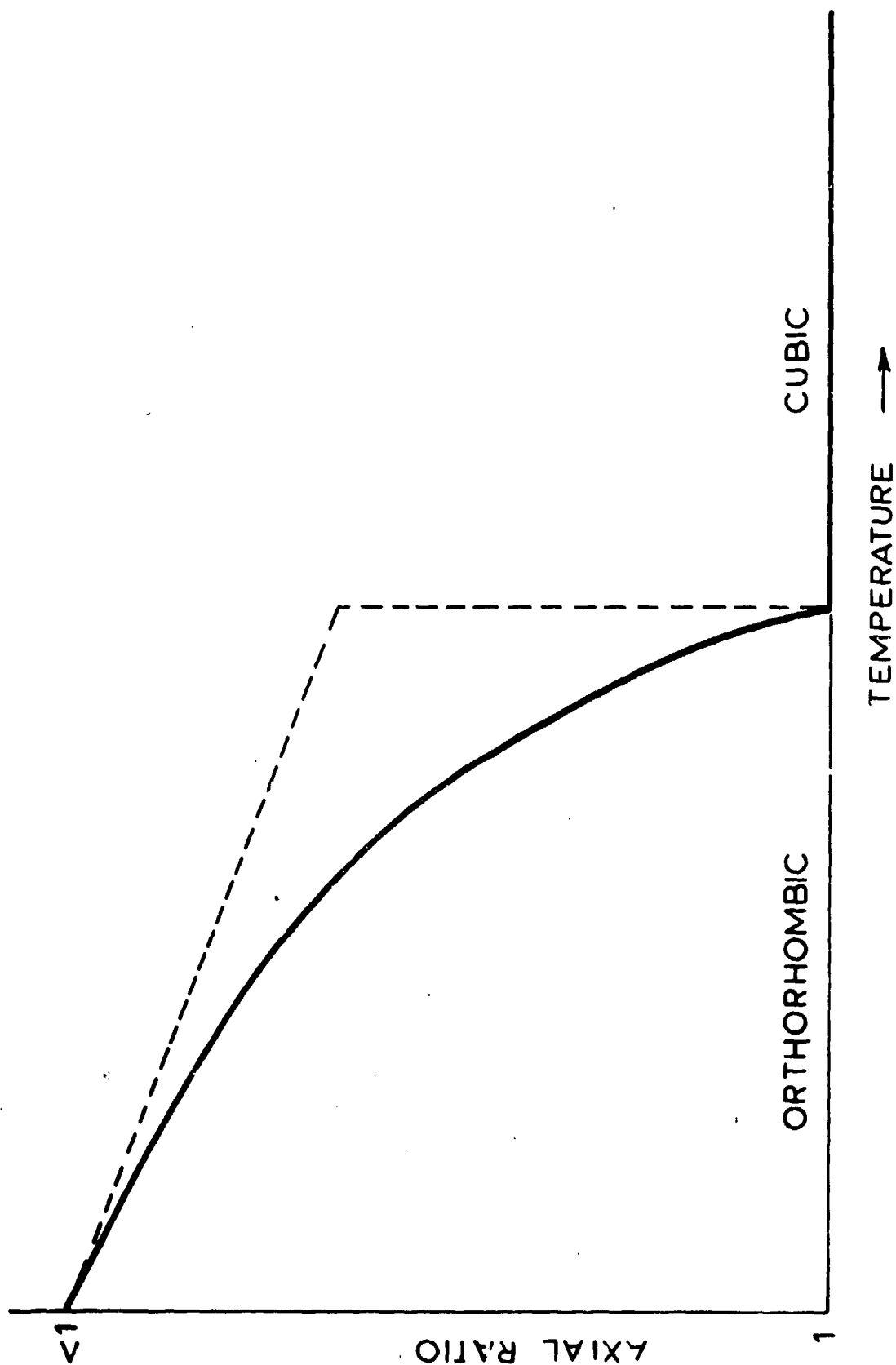FIGURE 13   KOSSEL PATTERN TAKEN FROM AREA SHOWN IN FIGURE 12

FIGURE 14   ANTICIPATED AXIAL RATIO VERSUS TEMPERATURE RELATIONSHIP FOR AN ORTHORHOMBIC PHASE
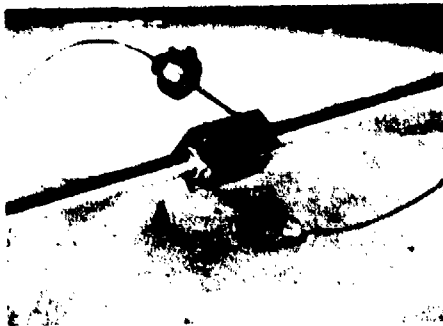
I
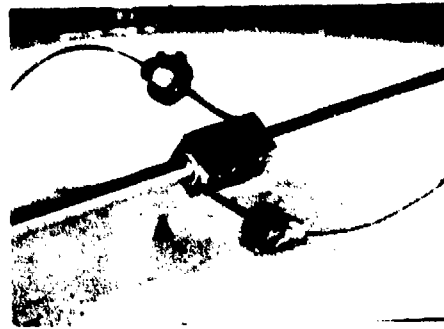
T+4f
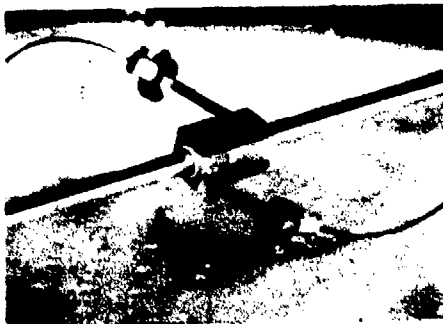
T+7f

T+11f

T+14f

T+20f
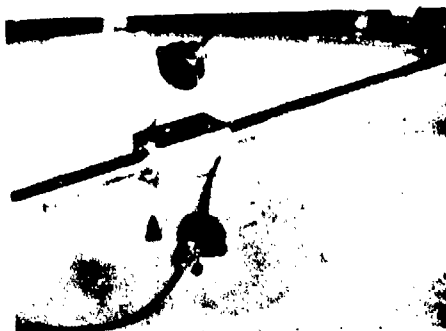
T+24f

T+26f

FIGURE 15   A SEQUENCE OF STILLS PRINTED FROM A CINE FILM TAKEN DURING HALF OF A
COMPLETE CYCLE OF THE ENGINE, FILM SPEED - 24 f.p.s.

References

(1) Laves, F. Acta. Met. 14 (1966) 58.

(2) Frank, F. C. and Ashbee, K. H. G. Spectrum 132 (1975) 1.

(3) Frank, F. C. Rev. Geophys. 3 (1965) 485.

(4) Cunningham, B. and Ashbee, K. H. G. Acta. Met. 25 (1977) 1315.

(5) Biggin, S. and Dingley, D. J. J. Appl. Cryst. 10 (1977) 376.

(6) Love, A. E. H. "The Mathematical Theory of Elasticity" 4th ed.
      Cambridge University Press (1959) 475.

(7) Cunningham, B. Ph.D. Thesis. Univ. of Bristol (1979)

(8) loc. cit.

HOT ISOSTATICALLY PRESSED POWDER METALLURGY NITINOL WIRE

M. T. Podob
Consolidated Metallurgical Industries
Farmington Hills, MI

W. A. Johnson
Special Metals Corporation
New Hartford, NY

S. H. Reichman
Special Metals Corporation
New Hartford, NY

INTRODUCTION

A range of compositions in the binary nickel-titanium alloy system possesses a rather unusual property -- shape memory. The series of alloys, discovered by the Naval Ordnance Laboratory (now Naval Surface Weapons Center) in the early 1960's, was designated NITINOL. Forming a sample of the alloys in the 55 weight percent nickel range--be they wire, rod, or sheet--into a desired shape above the martensitic transformation temperature, imparts the sample with a "memory" to return to that shape. If the sample is cooled and the configuration altered after cooling, reheating above the transition temperature will cause reversion to the "memorized" shape.

The temperature to which the material must be heated to cause shape transformation depends principally upon the alloy's composition. NITINOL demonstrates a shape memory response for compositions on the order of 53 to 57 weight percent nickel (the intermetallic compound compositional range). Transition temperature range varies from approximately -60°F (-50°C) to 300°F (166°C)[1]*, increasing with decreasing nickel content. During the material transformation, NITINOL experiences large deflections, which can be translated into mechanical forces.

One problem of NITINOL wire for any commercial application is the difficulty in producing a chemically homogeneous ingot for wire drawing, hence wire with a consistent, precise, and predictable shape memory response. It is felt that with the use of a powder metallurgical (P/M) approach towards NITINOL manufacture, a homogeneous ingot can be obtained by subsequently hot isostatically pressing (HIP'ing) prealloyed powders into billet and

---

[1] Jackson, C. M.; Wagner, H. J.; Wasilewski, R. J.: _55-NITINOL -- The Alloy With A Memory: Its Physical Metallurgy, Properties, and Applications_, NASA-SP5110, Battelle Memorial Institute, 1972.

*Editors' Note: 120°C is more commonly accepted today.

drawing into wire. This consolidated product will have the compositional uniformity necessary to tighten the broad transition temperature range to a narrow band and allow the development of a P/M NITINOL wire for a wide range of commercial applications, all incorporating the shape memory response. This report describes a series of experiments conducted to accomplish that goal.

EXPERIMENTAL PROCEDURE

ATOMIZATION. Inert (argon) gas atomization of all heats of material evaluated was accomplished in the Udimet Powder Division Research Center atomizer in Ann Arbor, Michigan. This unit is capable of a 200-pound conventional nickel-base superalloy pour. The furnace was modified to accommodate a graphite core, limiting its capacity to 40 pounds of NITINOL. All furnace parts and pour cups in contact with molten NITINOL were fabricated from ATJ Graphite.

Atomization is accomplished by pouring molten metal into a cup-tip-nozzle arrangement and allowing argon gas to impinge the molten stream, breaking the metal into fine droplets. Figure 1 is a schematic of a typical inert gas atomizer.

Two 40-pound NITINOL heats were atomized, the heats designated R78245-R78246. Charge for R78245 consisted of loose nickel shot (Ni-99) and titanium chips (Ti-99) with an aim chemistry of 55.5 wt % Ni. To provide better homogenization of the charge and minimze carbon pickup during melting, loose nickel shot and titanium chips were placed in a rolled and welded nickel-200 container and lid, with a nickel-200 evacuation tube TIG welded in place. The entire assembly was evacuated and the evacuation tube crimped and TIG welded closed. The can was then hot isostatically pressed (HIP'ed) at $1600^{\circ}F$ ($871^{\circ}C$)/15 Ksi (103 Mpa)/3 hours to allow for some diffusion bonding of the charge. Aim chemistry of this billet was 55.0% Ni. This was subsequently melted in the atomizer and atomized to powder.

Post-atomization processing consisted of transferring the powder from the collection vessel to a gloved dry box for screening. All powder handling was either under a vacuum or argon blanket to minimize oxidation. As-atomized product was screened to -40 mesh. Yield after screening was approximately 15-1/2 pounds of R78245 and 26 pounds of R78246.

POWDER CHARACTERIZATION. Microexamination of loose powder samples mounted in bakelite revealed most powder particles were homogeneous and single phased. Several random particles did show fine dispersion of a secondary phase which was light reflective, suggesting TiC.

Scanning electron microscope examination of the powder (Figure 2) revealed spherical powder with relatively little flake present. Few satellite particles were observed. In general, the appearance of the as-atomized NITINOL powder was typical of nickel-base superalloy product atomized in the Ann Arbor facility.

SCREEN ANALYSIS AND DENSITY. Screen analysis (Table I) of 100 gram samples of powder revealed R78245 was coarser than R78246. The corresponding apparent and tap densities of R78245 were greater than its counterpart. These somewhat unusual results suggest sampling rather than a materials problem.

CHEMISTRY. Difficulty exists in the precise analytical technique for major element determination of NITINOL. For a nominal NITINOL composition of 55 weight percent nickel, the literature indicates[1] a compositional measurement uncertainty of $\pm$ 0.3 weight percent titanium. Table II chemically analyzes heats R78245 and R78246 performed in Princeton using atomic absorption. Wet chemical analysis was not performed.

HIP CONSOLIDATION. Six 0.75 inch (0.905 cm) O.D. X 0.049 inch (0.124 cm) wall 304L stainless steel tubes were cleaned utilizing Scotchbrite and acetone, crimped on one end, and TIG welded closed. Three tubes were filled with powder from heats R78245 and R78246. Five additional tubes were similarly filled. Table III gives can filling data.

All containerized materials (including melt stock) were HIP'ed in the HIP unit at the Udimet Powder Division in Ann Arbor. This unit, designed and built by Autoclave Engineering, Erie, PA, has a graphite element furnace. Working zone, temperature, and pressure capability of the unit are 9.5 inches (24.1 cm) outside diameter by 18 inches in height; 2300°F (1260°C), and 15,000 psi (103 MPa), respectively. Argon gas is the pressurizing medium.

Microstructural examination of consolidated material samples revealed a uniform, single phase, recrystallized structure, interspersed with grain boundary and matrix carbonitrides and nickel-titanium oxides (Figure 3). Grain size was on the order of ASTM 9-10, with no evidence of prior powder particle boundaries. The overall microstructure is accicular, the basket-weave structure being more pronounced than the typical hot swaged NITINOL alloy.

WIRE DRAWING. Cylinders 1/4-inch (0.64cm) in diameter were machined from samples of each heat and submitted to the Naval Surface Weapons Center for wire drawing. The samples were hot swaged at 1560°F (850°C) to a finished diameter of 1/8 inch (0.318 cm). Observed reductions were on the order of 10% per pass. Attempts to draw the swaged rods into wire at room temperature resulted in brittle failure. Visual and SEM examination of the fracture surfaces revealed no evidence of cracking through prior particle boundaries.

Microexamination of longitudinal and transverse sections from the swaged rods revealed a fine grained microstructure, interspersed with carbonitrides and oxide particles (Figures 4 and 5).

SUMMARY AND DISCUSSION

The preliminary experimental results are encouraging. This program demonstrated that NITINOL can be successfully atomized and the resulting powder HIP consolidated into billet. Subsequent experiments revealed that the billet can be hot swaged into a useful shape which demonstrated 100 percent shape recall. Microstructural analysis of samples from this product showed a uniform structure free from the gross segregation present in conventionally fabricated material. Results, and the literature, indicate that when the transition temperature of the two heats is greater than 20°C (room temperature), wire drawing can be accomplished utilizing existing NITINOL wire production technology. An experiment was conducted by Naval Research Laboratory to determine whether P/M NITINOL wire behaves differently from material cast from the same composition. A sample of heat R78245 was HIP consolidated and then vacuum arc remelted by the Navy. The button produced was then hot swaged. Attempts

---

[1] See footnote 1 on page 12-1.

to draw the swaged rod into wire failed; resistivity measurements on the bar revealed it had a transition temperature similar to the original HIP'ed P/M NITINOL of the same composition. Microstructural analysis (Figures 6 and 7) of the recast bar revealed that, with the exception of a slightly larger grain size, the microstructure was similar to the HIP P/M bar, indicating the key reason for the low transition temperatures lies with the composition of the material, not the process which produced it.

CONCLUSIONS

1. NITINOL can be successfully inert gas (argon) atomized into a spherical powder.

2. Conventional canning, outgassing, and HIP'ing techniques can be utilized to compact NITINOL powder into a fully dense material.

3. HIP P/M NITINOL is uniform in composition and relatively free from the segregation present in conventional NITINOL composition billets utilized for wire drawing.

4. The HIP product can be hot swaged into bars which demonstrate a 100 percent shape memory response. The chemistry of the heats utilized for the experiments produced shape memory transition temperatures below room temperature, preventing the drawing of the HIP NITINOL billets into wire.

FUTURE PLANS

Experimental results reveal that a powder metallurgical approach towards NITINOL wire fabrication is a practical technique to produce a homogeneous material. Conclusion--P/M NITINOL behaves no differently from cast NITINOL. Fabrication of wire with a precise narrow band of shape memory transition temperature will require greater chemistry control and chemistry predictability. This goal will be accomplished by atomizing four heats of powder. Nickel contents of the powders will be 56.0 weight percent nickel.

An incremental approach is undertaken to produce a powder with a usable transition temperature range. A second task will be to study the use of double-VAR forged material for atomization stock. The use of a fairly homogeneous, low carbon starting material should enhance the cleanliness of the powder metallurgy product.
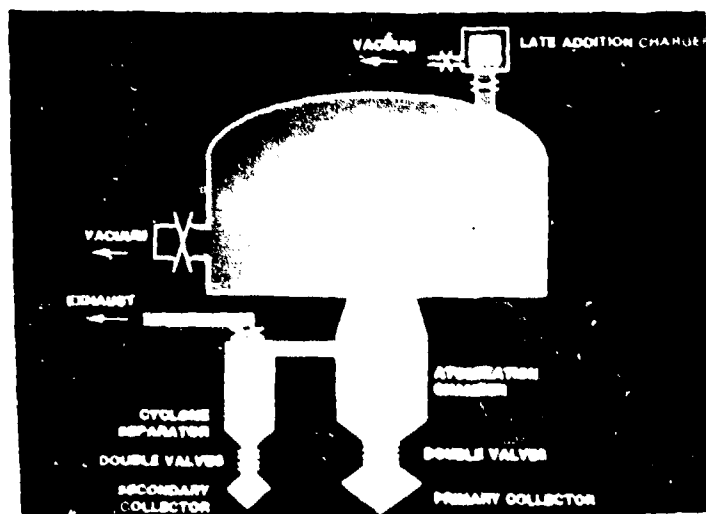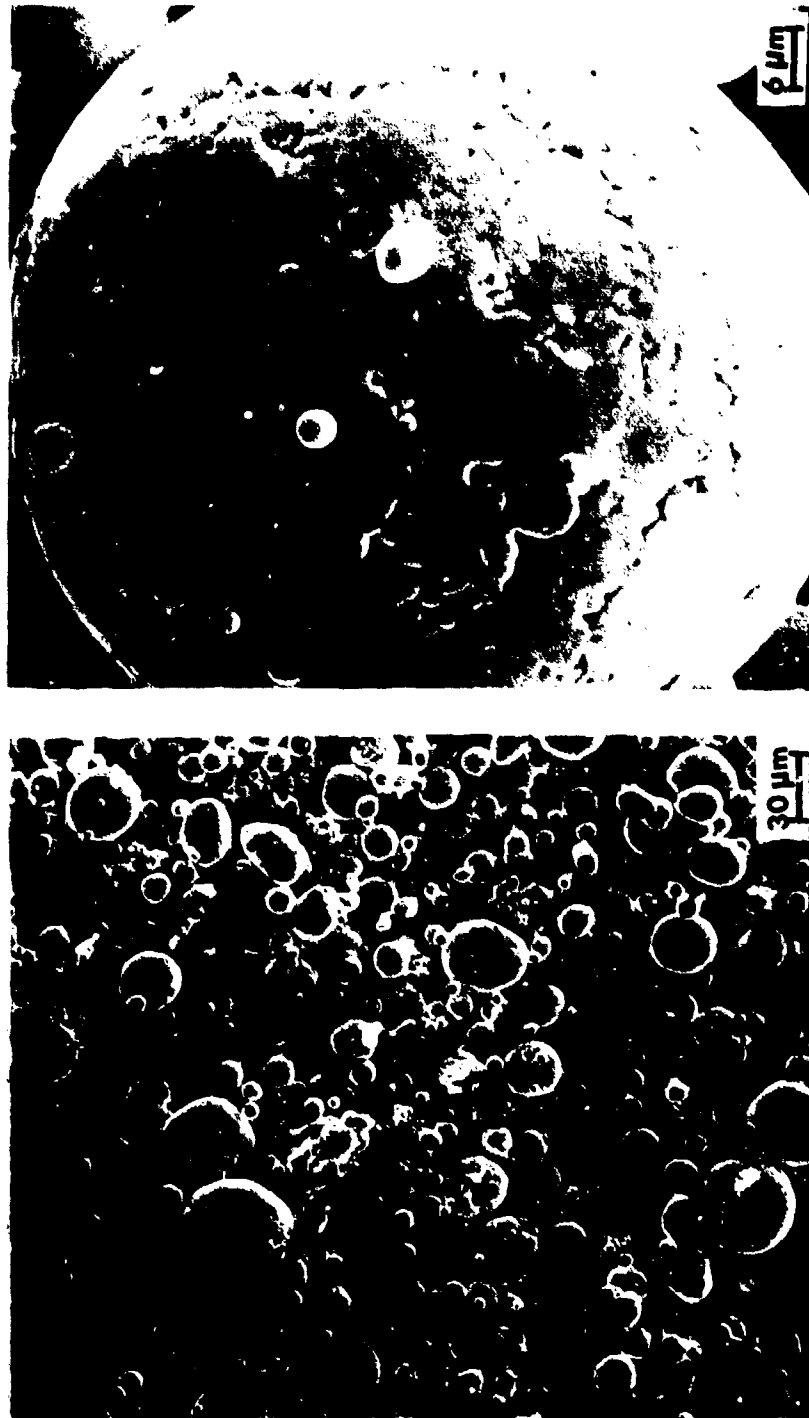
FIGURE 1. Schematic of inert gas atomizer

FIGURE 2. Scanning electron micrographs of Nitinol as-atomized powder, heat R78245 (55.5 Wt.% Ni – 44.5 Wt.% Ti).
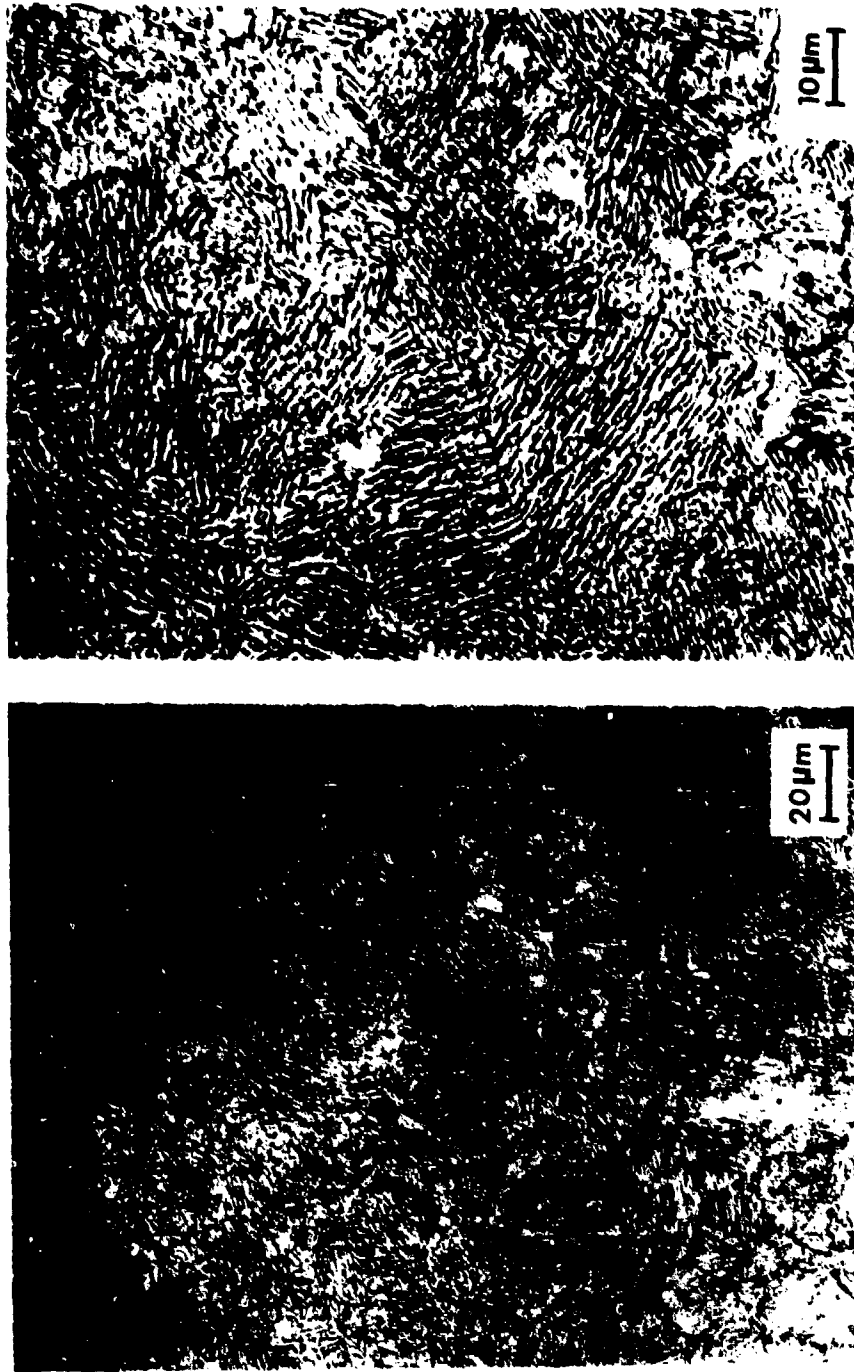
Mag: 300X, Left
1600X, Right

FIGURE 3. Photomicrographs of P/M Nitinol after consolidation by HIP at 1600°F (871°C)/15,000 psi (103MPa)/3 hours.
Etchant: 1% HF, 12% HNO$_3$

Mag: 500X, Left
1000X, Right
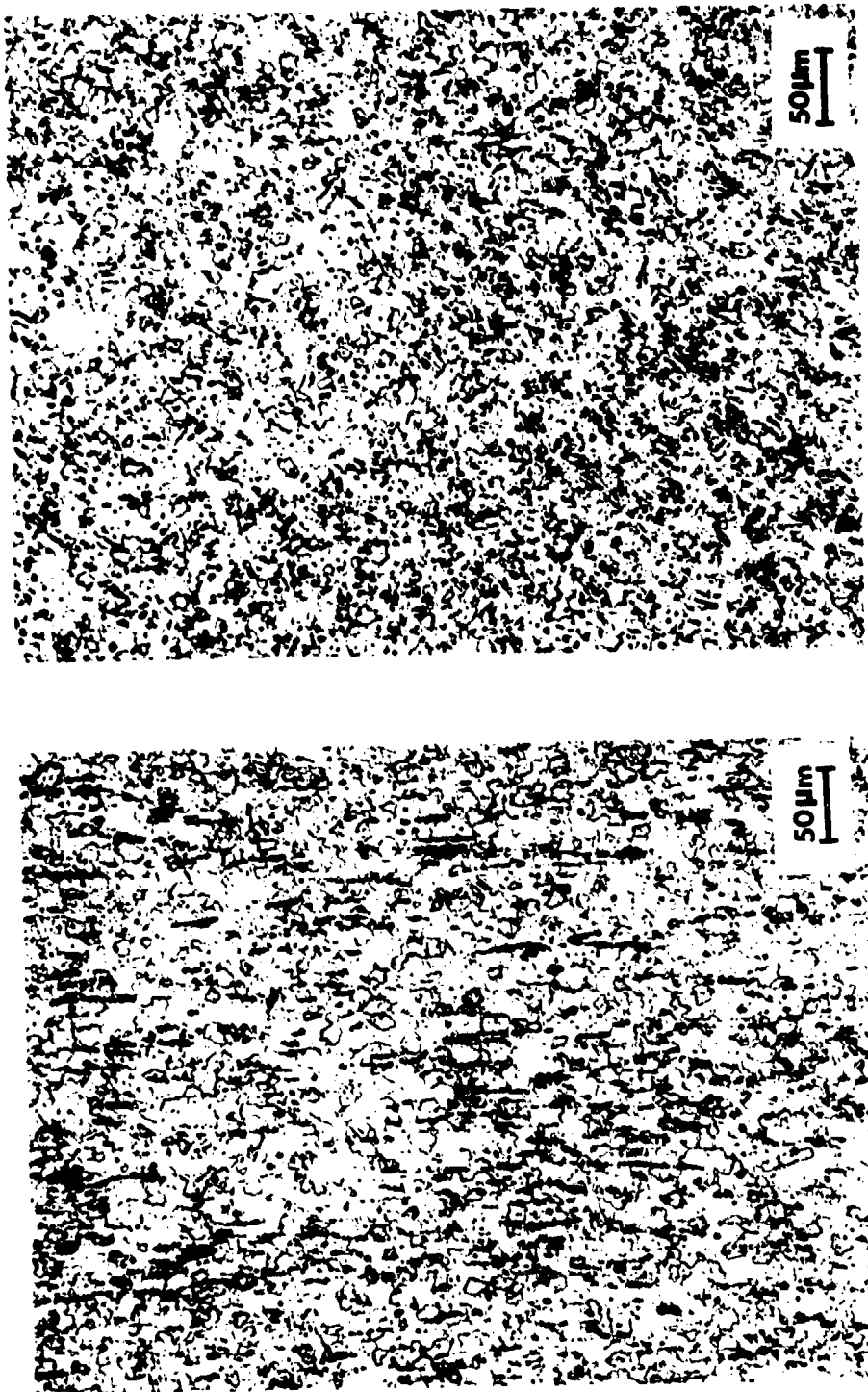
FIGURE 4. Photomicrographs of longitudinal (left) and transverse section (right) of P/M Nitinol wire made from heat R78245 (55.5 Wt.% Ni – 44.5 Wt.% Ti). Powder was hot isostatically pressed and subsequently swaged into rod. Etchant: 1% HF, 12% HNO$_3$

Mag: 200X

FIGURE 5. High magnification micrograph of P/M Nitinol
rod showing fine dispersion of oxides and/or
carbides.
Etchant: 1% HF, 12% HNO$_3$

Mag: 1500X

FIGURE 6. Photomicrographs of longitudinal section (left) and transverse section (right) of Nitinol rods made by recasting powder from heat R78245 (55.5 Wt. % Ni – 44.5 Wt. % Ti).
Etchant: 1% HF, 12% HNO$_3$

Mag: 200X
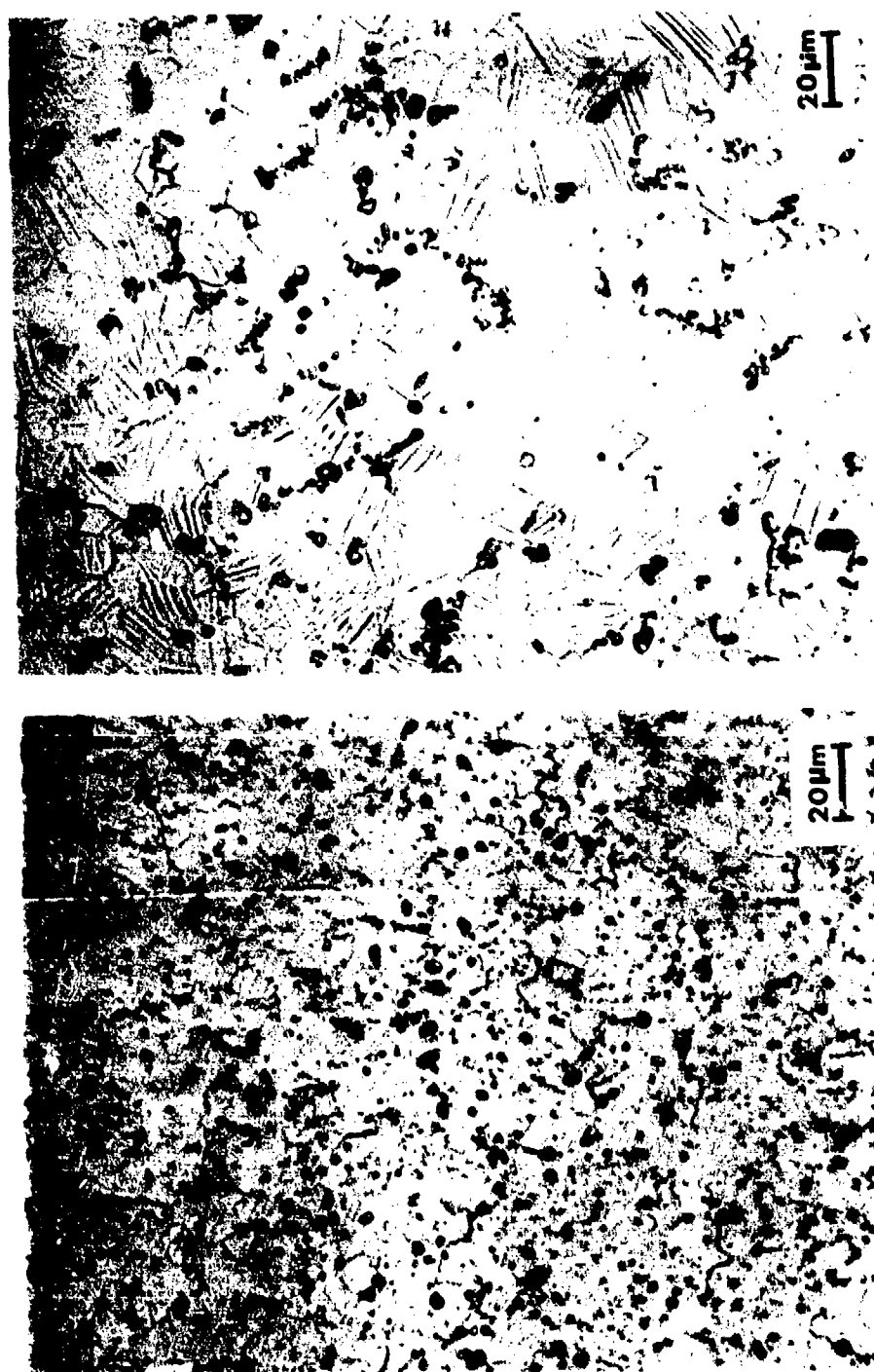
FIGURE 7. Photomicrographs of transverse section areas of HIP + drawn wire (left) compared with recast powder + swaged rod (right). Note finer grain size of HIP material.
Etchant: 1% HF, 12% HNO_3

Mag: 500X

TABLE 1 SCREEN ANALYSIS AND DENSITY
RESULTS FOR NITINOL HEATS R78245 AND R78246

Mesh	Percent Retained in Screen R78245	R78246
+40	0	0
-40+60	15.2	4.7
-60+80	13.0	6.7
-80+100	8.3	4.6
-100+120	6.4	5.4
-120+140	7.3	5.7
-140+170	7.2	7.1
-170+200	6.9	7.3
-200+230	3.9	4.8
-230+270	4.6	5.8
-270+325	7.0	12.2
-325+400	3.2	4.2
-400+500	7.4	14.2
-500 (Pan)	9.5	17.3
Apparent Density	3.1 g/cc	3.9 g/cc
Tap Density	4.2 g/cc	4.7 g/cc
Theoretical Density[2]	(Consolidated) ----	6.47 g/cc

DISTRIBUTION

<u>Copies</u>

Library of Congress
Attn: Gift & Exchange Division   4
Washington, DC 20540

Defense Documentation Center
Cameron Station
Alexandria, VA. 22314   12

Office of Advanced Conservation
    Technologies
Attn: Mr. Marvin Gunn   1
Department of Energy
1000 Independence Ave. S.W.
Washington, DC 20585

Naval Civil Engineering Laboratory
Naval Construction Battallion Center
Attn: Dr. Larry W. Hallanger   1
Port Hueneme, CA 93043

Attn: X-10
P.O. Box X
Building 4500 North
Attn: H. Arnold   1
Oak Ridge National Laboratory
Oak Ridge, TN 37830

Attn: Y-12
P.O. Box Y
c/o Building 9204-1
Attn: J. Michel   1
Oak Ridge National Laboratory
Oak Ridge, TN 37830

Library
Oak Ridge National Laboratory
Oak Ridge, TN 37830   1

TABLE 2 CHEMICAL ANALYSIS
OF NITINOL HEATS R78245 AND R78246

ELEMENT	R78245 (Wt.%)	R78246 (Wt.%)
Ni	56.5	56.4
Ti	43.8	44.4
C	0.06	0.09
O_2	858ppm	848ppm
N_2	7ppm	14ppm

TABLE 3 CAN FILLING DATA FOR NITINOL SAMPLES

Serial Number	Heat Number	Filling Pressure (microns)	Vacuum After Transfer (microns)	Static Pressure (microns)	Leak Up Rate (microns/3 min.)
1	R78245	8	200	3×10^{-6}	1
2	R78245	7	120	4×10^{-6}	4.5
3	R78245	5	250	4×10^{-6}	3.5
4	R78246	10	200	4×10^{-6}	8
5	R78246	8	400	4×10^{-6}	2.5
6	R78246	7	300	4×10^{-6}	1
2A	R78245	9	80	Unavailable	
3A	R78245	9	200	Unavailable	
4A	R78246	8	250	Unavailable	
5A	R78246	5	35	Unavailable	
6A	R78246	5	85	Unavailable	
UPD Standard Practice:		<10	<500	$<1 \times 10^{-5}$	<9

BIBLIOGRAPHY

Jackson, C. M.; Wagner, H. J.; Wasilewski, R. J.: 55-NITINOL -- The Alloy With A Memory: Its Physical Metallurgy, Properties, and Applications, NASA-SP5110, Battelle Memorial Institute, 1972.